Characterising natural genetic variation in dynamic photosynthesis and photoprotection in Sorghum

Richard Lee Vath

St Edmund's College

University of Cambridge

This thesis is submitted for the degree of

Doctor of Philosophy

July 2023

Declaration

This thesis is the result of my own work and includes nothing which is the outcome of work done in collaboration except as declared in the preface and specified in the text. It is not substantially the same as any work that has already been submitted before for any degree or other qualification except as declared in the preface and specified in the text. It does not exceed the prescribed word limit for the School of Biological Sciences Degree Committee.

Richard Vath
Department of Plant Sciences
St Edmund's College
University of Cambridge
July 2023

Abstract

Characterising natural genetic variation in dynamic photosynthesis and photoprotection in Sorghum

Richard Lee Vath

Non-photochemical quenching (NPQ) photoprotective processes are key for protecting photosynthetic machinery from excess light energy. Improving the regulation of NPQ in leaves during dynamic light conditions has been identified as a potential route toward increasing photosynthetic efficiency in the world's most important crops. Prior studies have revealed intraspecific variability in other photosynthetic efficiency-related traits, but variation in photoprotective capacity within crop species, particularly those utilizing the C_4 photosynthetic pathway, is not yet well-characterized. The aim of this research project was to determine the genetic underpinnings of photoprotective traits in *Sorghum bicolor* and improve understanding of the balance between photosynthesis and photoprotection in dynamic light conditions.

Utilising a high-throughput chlorophyll fluorescence technique, a panel of 869 field-grown sorghum accessions was screened for multiple traits related to NPQ kinetics over two growing seasons. An ensemble approach combining genome and transcriptome-wide association studies was used to characterise the genetic architecture of NPQ in sorghum, and several high-confidence loci correlated with the observed variation were identified. These results were validated via re-screening of NPQ kinetics of selected sorghum accessions displaying contrasting genotypes at two of these loci. Sorghum's photoprotective response was also compared and contrasted with that of three other C_4 crops and one C_4 model species, in order to contextualise photoprotection in sorghum within a broader C_4 photosynthetic phylogeny.

Subsequently, two sorghum accessions with strongly contrasting NPQ phenotypes were used to investigate the effect of photoinhibition on the coordination between the C_4 carbon concentrating mechanism and Calvin-Benson-Bassham cycle CO_2 fixation. Imbalances between these cycles during stress conditions likely represent a loss of photosynthetic efficiency in the field, potentially resulting in decreased

productivity, but there presently exists minimal knowledge of the effect of photoinhibition on coordination of mesophyll/bundle-sheath cell carboxylation activity. A combined carbon isotope/leaf-level gas exchange system was developed and utilised for real-time measurement of carbon isotope discrimination during photosynthesis in high-intensity steady-state and fluctuating light conditions, to investigate the effects of high-light treatments on bundle sheath leakiness– an indicator of loss-of-coordination between cell types. The results suggest that the C_4 photosynthetic apparatus is robust under both fluctuating and steady-state high light conditions and that NPQ capacity may partially explain susceptibility to photoinhibition.

This project has identified genetic loci underlying key photoprotective traits in sorghum and improved understanding of the interplay of photosynthesis and photoprotection under dynamic light conditions. The resulting knowledge of the genetic basis and physiological implications of variation in photoprotection will help guide crop improvement via both traditional breeding and biotechnology-based approaches.

Acknowledgements

This work was facilitated and vastly improved by the contributions of several collaborators. At the University of Illinois, Carl Bernacchi hosted and provided resources for 2021 field trials, and provided storage for sorghum seeds for experiments in Cambridge. Taylor Pederson managed the sorghum panel planting in all field seasons, organised and shipped sorghum seeds, and assisted in field sampling during 2020 and 2021 field trials, and Erin Fisher and Scott Swanson assisted in field sampling and NPQ assays during the 2020 field season. Samuel Fernandes (University of Arkansas) modelled NPQ trait BLUPs and performed genome-wide analyses on 2017/2019 NPQ trial data. Katarzyna Głowacka (University of Nebraska-Lincoln) and Johannes Kromdijk (University of Cambridge) sampled sorghum panel leaf material during the 2017 field season. Additionally, Johannes Kromdijk conceived the sorghum genome-wide NPQ variation study design, sampled sampled sorghum panel leaf material along with me during the 2019 field season, designed the chlorophyll fluorescence imaging routine for high-throughput NPQ measurements, and processed 2017 and 2019 raw fluorescence imaging data. Brandon Monier (Cornell University) performed transcriptome-wide analyses on 2017/2019 NPQ trial data, and John Ferguson (University of Essex) provided advice on follow-up experiments from genome-wide analysis results.

More generally, a hearty thank-you goes out to the many people who supported me during my time at Cambridge. First, to Wanne, whose generosity with time and resources I tremendously appreciate. His willingness to answer questions, provide advice, and review an absurd number of drafts has been immensely helpful, and his well-distributed balance of patience and occasional impatience have complemented my scepticism in what seems to have been a productive way. His guidance and and leadership have certainly helped me become a better scientist and writer.

Thanks as well to all the folks in my lab, particularly the "early few"– Emmanuel, Lucía, Julia. I don't know that I'll miss our pre-Covid labbook meetings, but certainly will miss our loud conversations at the associated semi-obligatory post-meeting pub trips, and our Thanksgiving dinners. Thanks as well to Cris, a wonderful friend and coworker, and to Georgia, for having a fantastic sense of humour and for helping me deal with Howard on Portugal trips. To Angie and Matt Burnett, who've been wonderful friends and have facilitated what are likely the most

entertaining conversations I've had during this PhD, over dinners. Thanks to Jessica, whose patience and understanding in lab management is much appreciated as well. Finally, thanks to the rest of the lab– Alice, Katie, Lee, Elizabeth, Ali, Mariela, Rohan, Weng Yik, who have been a lot of fun to work with over the years.

Outside of the immediate lab: thanks to Conor Simpson for advice and discussion about GWAS and the mysterious world of quantitative genetics. It's nice to know someone else finds these things as occasionally bewildering as I do. Thank you as well to Tally Wright for the sage advice on field trial design. Down in the Department basement, thanks to Simon, Ben, and Steve for letting me borrow tools and for carting plants to-and-fro. Jason Hupp and Doug Lynch from LI-COR deserve a big thanks as well– in additional to being excellent friends, their support in getting instruments to play well together has vastly improved my experiments, and taught me a lot.

Thanks as well to Chris Davies for being a phenomenal friend, always ready to commiserate on the general state of things. And thanks to Martin and Jan Davies– I don't know that many landlords are acknowledged in theses, but if any are deserving of such note it would be them, for always being understanding, flexible, and generous!

Thanks to my parents for raising and always supporting me, and particularly for storing my belongings and dogs while I've been in Cambridge.

Finally, thanks to my dear sweet wife, Emma, for dealing with me during this PhD. It has required an immense amount of patience and a great sense of humour, and I very, very much appreciate the support throughout the last few years.

Contents

List of Figures

List of Tables

List of Abbreviations and Units

. . . . . Abbreviations and units for chapter five are listed within the chapter

3L . . . . . Third-leaf tissue

$\boldsymbol{A_{net}}$ . . . . . Net rate of CO_2 assimilation (μmol m^{-2} s^{-1})

$\boldsymbol{A_{max}}$ . . . . . Light-saturated rate of CO_2 assimilation (μmol m^{-2} s^{-1})

$\boldsymbol{A/Q_{inc}}$ . . . . Response curve of CO_2 assimilation to incident light intensity

$\boldsymbol{a_{NPQi}}$ . . . . . Initial value of NPQ induction

$\boldsymbol{a_{NPQr}}$ . . . . . Initial value of NPQ relaxation during the dark period

$\boldsymbol{a_{\Phi PSII}}$ . . . . . Initial value of $\Phi PSII$ recovery during the dark period

BSC . . . . . Bundle sheath cell

C_3 . . . . . Three-carbon photosynthesis

C_4 . . . . . Four-carbon photosynthesis

DI . . . . . Deionised water

FCT . . . . . Fisher's combined (permutation) test

FHL . . . . . Fluctuating high-light treatment

$\boldsymbol{Fv/Fm}$ . . . . Maximum photosystem II quantum efficiency

$\boldsymbol{Fv'/Fm'}$ . . . Maximum photosystem II quantum efficiency at a given light intensity

GxE . . . . . Genotype-by-environment interaction

GP . . . . . Growing-point tissue

GWAS . . . . . Genome-wide association study

$\boldsymbol{H^2}$ . . . . . Generalised heritability

$\boldsymbol{k}$ . . . . . Reaction rate constant (min^{-1})

$\boldsymbol{k_{Ind}}$ . . . . . Rate constant of NPQ induction (min^{-1})

$\boldsymbol{k_{Rel}}$ . . . . . Rate constant of NPQ relaxation (min^{-1})

$\boldsymbol{k_{Rec}}$	Rate constant of recovery of photosystem II quantum efficiency (min^{-1})
LD	Linkage disequilibrium
MC	Mesophyll cell
MDA	Malondialdehyde (nmol g^{-1} dry leaf mass)
NAD-ME	NAD-malic enzyme
NADP-ME	NADP-malic enzyme
NPQ	Nonphotochemical quenching
PC	Principle component
PEER	Probabilistic estimation of expression residual
PI	Photoprotection index, the proportion of drop in Fv/Fm after a high-light treatment that is attributable to the quickly-relaxing component of NPQ
P. glaucum	*Pennisetum glaucum*
P. miliaceum	*Panicum miliaceum*
PSI	Photosystem I
PSII	Photosystem II
PPFD	Photosynthetic photon flux density (μmol m^{-2} s^{-1})
$\boldsymbol{\Phi CO_2}$	Maximum quantum efficiency of CO_2 assimilation (mol mol^{-1})
$\boldsymbol{\Phi PSII}$	Photosystem II quantum efficiency at a given operating light intensity
$\boldsymbol{Q_{inc}}$	Incident light intensity (μmol m^{-2} s^{-1})
QTL	Quantitative trait loci
$\boldsymbol{RH_d}$	Relative humidity, daytime (%)
$\boldsymbol{RH_n}$	Relative humidity, night-time (%)
Ri	Relative injury measured via electrolyte leakage assay (%)
$\boldsymbol{R_d}$	Total non-photorespiratory CO_2 respiration in the light (μmol m^{-2} s^{-1})
ROS	Reactive oxygen species
S. viridis	*Setaria viridis*
S. bicolor	*Sorghum bicolor*
SIFT	Sorting intolerant from tolerant

SHL . . . . . Steady-state high-light treatment

SNP . . . . . Single-nucleotide polymorphism

TBA . . . . . Thiobarbituric acid

TBARS . . . . Thiobarbituric acid reactive substances assay

$\boldsymbol{T_0}$ . . . . . Conductivity of deionised water (μS m^{-2} s^{-1})

$\boldsymbol{T_1}$ . . . . . Initial conductivity of leaf disc solution (μS m^{-2} s^{-1})

$\boldsymbol{T_2}$ . . . . . Final conductivity of incubated leaf disc solution (μS m^{-2} s^{-1})

$\boldsymbol{T_d}$ . . . . . Temperature, daytime (^{o}C)

$\boldsymbol{T_n}$ . . . . . Temperature, night-time (^{o}C)

TWAS . . . . . Transcriptome-wide association study

$\boldsymbol{\lambda}$ . . . . . Wavelength (nm)

$\boldsymbol{\theta}$ . . . . . Curvature factor of photosynthetic light response curve

Z. mays . . . *Zea mays*

1 Introduction

1.1 A brief history of dynamic photoprotection

Human interest in plants' response to light dates back at least as long as written records, with Greek philosophers noting plants' morphological plasticity in light response well before there was an understanding of how, or why (Whippo and Hangarter, 2006). Centuries later, after the Ages of Discovery and Reason brought new ways of thinking about natural phenomena, Charles Darwin's hypotheses on phototropism (Darwin, 1880) effectively founded the modern-day study of plant environmental responses as we know it (Holland et al., 2009). In the 1930s, researchers observed that xanthophyll pigments responded to changes in light quantity and quality and appeared able to dissipate light energy (Burkholder, 1936), but the underlying mechanisms were not yet understood. The 1960s and 1970s brought rapid advances in flash photometry and chlorophyll fluorescence measurement technology, and with them an increased understanding of the dual-photosystem electron transport chain found in higher plants (Franck and Rosenberg, 1964; Witt et al., 1963; Wraight and Crofts, 1970) and photoinhibition of electron transport centres resulting from excess light (Kok et al., 1965). Nonphotochemical quenching (NPQ) as energy-dependent quenching (qE) was first described (Wraight and Crofts, 1970).

Eventually, the role of carotenoids in photoprotection of photosynthetic apparatuses began to be elucidated (Oquist et al., 1980), leading rapidly to early mechanistic understanding of pH-gradient dependent energy dissipation by the xanthophyll cycle (Demmig et al., 1987; Rees et al., 1989) and redox regulation of photosynthetic activity (Foyer, Furbank, et al., 1990) in the 1980s and early into the 1990s. It was beginning to be understood that the complex organisation of chloroplastic pigments participating in photosynthetic electron transport conferred immense flexibility in the ability to respond to changes in light conditions.

During the 1990s, the structural organisation and individual components of photosynthetic light harvesting apparatuses began to be revealed (Bassi et al., 1993; Gómez et al., 1998) and the role of protonatable residues and zeaxanthin binding to photosystem II (PSII) antennae in qE was uncovered (Walters et al., 1994). The 2000s brought discovery of the role of PSII small subunit protein *S* (PsbS) in regulation of PSII light harvesting and qE (Li, Björkman, et al., 2000), and since then substantial progress has been made in understanding the molecular components, mechanisms, regulatory pathways which underlie NPQ and photosynthetic response to dynamic light. New sites and quenchers (Nicol et al., 2019) and NPQ components such as zeaxanthin-dependent (qZ, Nilkens et al., 2010) and sustained nonphotoinhibitory quenching (qH, Malnoë, 2018) continue to be described, and it is now clear that dynamic photoprotection plays a crucial role in photosynthetic efficiency and plant productivity (Murchie and Ruban, 2020).

1.2 Sorghum as a model for C_4 photosynthesis

The genus *Sorghum*, within the family *Poaceae*, is a diverse group of mostly weedy grasses with a cosmopolitan distribution, generally considered split into five subgenera. The subgenus *Eusorghum* contains three species– *S. halepense* (Johnson grass) and *S. propinquum*, both of which are rhizomatous perennials, and *S. bicolor*, a crop with a long history of cultivation by humans (Office of the Gene Technology Regulator, 2017). *S. bicolor* is further divided into three subspecies (de Wet, 1978;

Ejeta and Grenier, 2005), with the species *Sorghum bicolor bicolor* (L.) Moench (sorghum, Figure 1.1) the experimental subject of this dissertation. Sorghum is extremely diverse in growth habit, with the subspecies further divided into five races based on panicle morphology (Office of the Gene Technology Regulator, 2017). This diversity has allowed sorghum to rise to global importance, being grown worldwide as a source of food, fuel, and fodder (Hao et al., 2021; Mundia et al., 2019).

Sorghum utilises the C_4 photosynthetic pathway and is considered one of the most water use efficient major crops (Bhattarai et al., 2019), a crucial trait in the face of climate change and the expected warmer and dryer climate of many regions. C_4 photosynthesis in sorghum, an NADP-ME species (Hatch, Kagawa, et al., 1975), involves hydration of CO_2 by carbonic anhydrase to bicarbonate, which is then fixed by phosphoenolpyruvate carboxylase into oxaloacetate, which is then reduced to malate within mesophyll cells (MC). Malate is then transported into bundle sheath cells (BSC) for subsequent decarboxylation by NADP malic enzyme, resulting in an above-ambient concentration of CO_2 around Ribulose-1,5-bisphosphate carboxylase/oxygenase, which fixes CO_2 into downstream photosynthetic products (Hatch and Slack, 1966; Leegood, 2002). Sorghum bundle sheath chloroplasts are depleted in PSII (Meierhoff and Westhoff, 1993), as the NADPH needed for bundle sheath CO_2 fixation is provided via the malate shuttle.

Resource and water efficient millets such as sorghum are now acknowledged as critically important future-smart crops, as evidenced by 2023 being recently declared "International Year of Millets" by the United Nations (`https://www.fao.org/millets-2023`). The widely available genomic resources, stress resilience, and genetic similarity to other important crops such as maize and sugarcane make sorghum an excellent system for studying photosynthetic efficiency under dynamic environmental conditions (Hao et al., 2021).

Figure 1.1: A field of biomass sorghum growing in Illinois

1.3 Genetic variation in dynamic photoprotection

Modern agriculture's rush to increase crop yields and decrease production costs through large-scale monoculture has led to substantially diminished genetic diversity in today's crops, often at the expense of disease, pest, and stress resilience (Khoury et al., 2022). Exploiting or "unlocking" natural genetic variation in agronomically important traits within crop species is a topic of particular interest to plant scientists and crop breeders, offering the potential to improve crop yield, stress resilience, and biodiversity, without reliance on transgenic modifications (Fernie et al., 2006; Liang et al., 2021; Martínez-Fortún et al., 2022).

Vast improvements in genotyping scale and resolution have provided tools for fine-mapping phenotypic trait variation across entire crop genomes, and combining this data with increased phenotyping capacity has led to greater understanding of nat-

ural genetic variants underlying complex crop traits (Flood et al., 2011; Lawson et al., 2012; van Bezouw et al., 2019). This knowledge is being used to inform genome editing and marker assisted breeding for traits contributing to crop quality, yield, and climate resilience. These non-transgenic methods of crop genetic improvement shorten cultivar release cycles and are considered more palatable to transgene-weary societies (Pixley et al., 2022; Springer and Schmitz, 2017).

Natural genetic variation in photosynthetic traits, including NPQ, exists within crop and non-crop germplasm (Ortiz et al., 2017; Sahay et al., 2023; van Rooijen et al., 2017). Previous studies have successfully identified genes involved in NPQ regulation in model species via molecular and reverse genetics-based approaches (Bru et al., 2020; Kasajima et al., 2011; Li, Björkman, et al., 2000), but larger-scale screening of NPQ, particularly under dynamic light conditions, is a relatively recent pursuit. NPQ screens have been undertaken in Arabidopsis (Rungrat et al., 2019), rice (Wang, Zhao, et al., 2017), soybean (Herritt et al., 2016), and maize (Sahay et al., 2023), revealing genomic diversity and identifying previously unknown genes associated with photoprotection.

Cultivated sorghum is exceptional to many crops in the immense diversity contained within its relatively small diploid genome (Boyles et al., 2019). However, phenotypic diversity in photoprotective capacity is not yet well-understood in sorghum. The presence of natural genetic variation in heritable photoprotective traits within the sorghum genome would allow for identification of genomic regions associated with photoprotection, providing a starting point for photosynthetic efficiency improvement via optimisation of photoprotection using genome-editing or marker-assisted breeding in sorghum, and potentially inform such improvements in other closely related C_4 crops.

1.4 C_4 photosynthesis in dynamic light

Research on C_4 photosynthetic efficiency during dynamic light conditions is still in its infancy, and many questions remain as to what conditions are more or less

favourable for increased photosynthetic efficiency (Slattery et al., 2018). C_4 photosynthesis in dynamic light is a complicated balancing act, as the proportioning of energy in the form of ATP and NADPH between MC and BSC must be tightly regulated– the connections required for metabolite transport between MC and BSC also permit CO_2 to retrodiffuse back out of BSC (bundle sheath leakiness, or ϕ – Farquhar, 1983; von Caemmerer, 2000), in conditions where MC decarboxylation and CO_2 fixation are insufficiently matched with the rate of BSC carboxylation. This results in a loss of photosynthetic efficiency as ATP is unnecessarily utilised for carboxylation without useful downstream fixation.

The role of photoprotection in C_4 photosynthetic efficiency and ϕ during dynamic light conditions is not well-characterised. ϕ increases under suboptimal light conditions (Cousins et al., 2006; Henderson et al., 1992; Kromdijk, Griffiths, et al., 2010; Kromdijk, Schepers, et al., 2008; Kromdijk, Ubierna, et al., 2014; Tazoe et al., 2008). Transient increases in ϕ have also been noted during photosynthetic induction (Wang, Stutz, et al., 2022), suggesting energy-use incoordination during the low-to-high portion of dynamic light fluctuation, though this incoordination could potentially be buffered in field conditions due to existing metabolite gradients (Cubas et al., 2023; Stitt and Zhu, 2014).

In sorghum and other NADP-ME species, the lack of PSII in BSC compared to MC may conceivably result in heightened MC photoinhibition and photodamage in comparison to BSC, during fluctuating light conditions. If this is the case, MC/BSC metabolic coordination would likely be disrupted, potentially manifesting as impaired photosynthesis and increases in ϕ during or after periods of high and fluctuating light.

1.5 Research objectives

Based on the exceptional stress tolerance of sorghum, and the fact that excess light can be a potent abiotic stress factor, it could be reasoned that the photoprotection and photoinhibition characteristics of sorghum would also be outlier relative

to other C_4 species. In order to make generalisations about C_4 photosynthesis in dynamic light based on observations of sorghum, it is important to understand sorghum's photoprotective capacity relative to that of other C_4 species of interest. In chapter two, the objective was therefore to compare and contrast sorghum's susceptibility to photoinhibition under dynamic and steady-state light conditions with several other C_4 species. Chapter two provides an in-depth introduction to the mechanisms and consequences of photoinhibition and photodamage and their importance to photosynthetic efficiency, and details the development of high-throughput assays to measure photodamage in C_4 species. This study provides a basis for understanding C_4 photoinhibitory responses to dynamic and steady-state light treatments and contextualises sorghum within a broader range of C_4 species.

The work in chapter three aimed to uncover the level of variation in dynamic photosynthetic traits within the sorghum phenome, and tie that variation to underlying genetic variation. Chapter three provides an introduction to high throughput phenotyping of photoprotective kinetics, quantitative genetic methods, and the value of natural genetic variation in crop genome improvement. The chapter reports on the results of a large-scale multi-year field trial, which involved screening of more than 800 sorghum accessions for variation in NPQ kinetic traits. This variation was correlated with genetic variation in order to determine candidate regions underlying photoprotective traits in sorghum.

Work in chapter four aimed to validate the mapping results in chapter three. To do so, a smaller-scale field trial was conducted, utilising a selection of accessions which contained contrasting alleles for two SNPs identified as significant correlates with photoprotective traits in chapter three. The genetically-contrasting accessions were re-screened for dynamic NPQ traits, in order to confirm that the previously-observed phenotypic variation was a result of underlying genetic variation.

Finally, work in chapter five aimed to investigate the putative link between NPQ amplitude and coordination of C_3 and C_4 cycle activity in response to high light

stress. To achieve this aim, a detailed investigation into the physiological mechanisms underlying photosynthetic efficiency in dynamic light conditions was undertaken, in sorghum. C_4 photosynthetic and metabolic response under dynamic light is introduced in detail, followed by presentation of the results of a study designed to: 1) uncover the sensitivity of C_4 photosynthesis to steady and fluctuating high-light conditions, and 2) investigate whether sorghum with improved photoprotective capacity is more resilient to the potentially damaging effects of high-intensity light conditions. A mechanistic understanding of C_4 photosynthetic response under changing light conditions will provide the foundation for future targeted improvements in photosynthetic efficiency in C_4 crop species.

These studies provide an integrated picture of sorghum's photosynthetic and photoprotective response to dynamic light conditions. The characterisation of variation in photoprotection within the sorghum genome shows that heritable variation exists in traits integral to photosynthetic efficiency and identifies sorghum genomic regions associated with photoprotection, providing valuable information for future genetic gains via breeding and genome editing. Further, the improved mechanistic understanding of sorghum's photoprotective and photosynthetic response to dynamic light conditions, contextualised within a group of related, important C_4 species, can be used to guide research efforts toward improving C_4 photosynthesis in dynamic light, allowing us to more efficiently feed and fuel a rapidly changing world.

2

Photoprotection and photodamage of C_4 grasses under dynamic light

2.1 Introduction

Feeding a global human population expected to reach nearly 9.8 billion by 2050 (UN Department of Economic and Social Affairs, 2019) will require substantial increases in agricultural productivity (Ray et al., 2013), and increased photosynthetic efficiency has been identified as a potential route toward crop productivity improvement. One promising solution to boost photosynthetic efficiency involves breeding or modifying crops to better take advantage of their prevailing light environments (Zhu, Long, et al., 2010). Plant leaves are often exposed to variable-length periods of high light, absorbing energy in excess of what's needed for downstream photosynthetic processes. This imbalance of energy supply and demand is particularly prominent during periods of abiotic and biotic stress. The energy surplus caused by excess light absorption drives a series of reactions which damage components integral to photosynthetic light harvesting and electron transport; the resulting sustained down-regulation of energy transport capacity is termed photoinhibition (Murata et al., 2007).

Plants have evolved a variety of energy quenching mechanisms that work in concert to prevent photoinhibition and instead dissipate surplus energy as heat (Demmig-Adams, 1990; Li, Björkman, et al., 2000; reviewed in Ruban and Wilson, 2021). Together these photoprotective mechanisms serve to regulate use of absorbed light energy in a controlled manner and are collectively termed nonphotochemical quenching (NPQ). NPQ involves light-triggered aggregation of light harvesting complexes (LHCs) and conversion of the xanthophyll violaxanthin into zeaxanthin, resulting in an energy-quenching photoprotective state (Ruban and Wilson, 2021). Improvements in the induction and relaxation rates of NPQ provide a promising opportunity for enhancements in crop photosynthetic efficiency (Zhu, Long, et al., 2010), by reducing photoinhibition during shade-to-sun transitions and diminishing energy lost via "overprotective" NPQ during sun-to-shade transitions (De Souza et al., 2022; Kromdijk, Głowacka, Leonelli, et al., 2016; Ruban, 2017; Zhu, Ort, et al., 2004).

2.1.1 Photosynthesis in dynamic light

Leaves of field-grown crops experience frequent fluctuations in light availability due to canopy structure, wind movement, and cloud conditions (Pearcy, 1990). Photosynthesis research, with the goal of improving light use efficiency, must include such dynamic light conditions to be relevant for improvement of the field-grown crops which feed the majority of the world's human population (Pearcy, 1990; Slattery et al., 2018; Stitt and Zhu, 2014; Walter and Kromdijk, 2021). Plants up- and down-regulate NPQ in these dynamic light conditions to take advantage of available light while maintaining photosynthetic activity. The balance between steady and fluctuating light conditions changes dramatically with variation in weather, growth location, and even between canopy levels (Murchie and Burgess, 2022; Pearcy, 1990). Though photoprotective regulation of light harvesting is one of the most extensively studied areas of photosynthesis research (Ruban and Wilson, 2021), it is not yet clear to what extent *photoinhibition* is differentially manifested during

these variable light conditions. Improving our understanding of this balance will impact the manner in which we study and attempt to improve crop photosynthesis.

Photosynthetic responses to steady versus fluctuating light and to light transitions have been shown to vary between species and photosynthetic subtypes (Chazdon and Pearcy, 1991; Kubásek et al., 2013; Lee et al., 2022; McAusland et al., 2016; Yamori, Masumoto, et al., 2012) but we are still lacking detailed information about response to contrasting light profiles in several widely-grown crop species. Past evidence on the degree of correlation between photoinhibition, photodamage, and photoprotective mechanisms during different light and growth regimes has also been mixed (Demmig-Adams, Adams, et al., 1996; Lambrev et al., 2012; Plumb et al., 2018; Sarvikas et al., 2006). Recent work suggests that increases in the rate of NPQ induction and relaxation kinetics can improve photosynthetic efficiency and increase biomass and yield (De Souza et al., 2022; Kromdijk, Głowacka, Leonelli, et al., 2016) (but see also Garcia-Molina and Leister (2020) and Lehretz et al. (2022)); however, inducing variation in the enzymes and carotenoids involved in NPQ kinetics may also affect susceptibility to oxidative damage to the photosynthetic light harvesting apparatus, causing photoinhibition or photodamage (Wang, Fang, et al., 2008), as carotenoids also play diverse roles as energy quenchers and antioxidants (Sandmann, 2019).

2.1.2 Photoinhibition and photodamage

In photosystem II (PSII), oversupply of light energy can lead to formation of triplet-state chlorophyll. Left unquenched, triplet-state chlorophyll can react with triplet ground state $^3O_2$ to produce the reactive oxygen species (ROS) singlet oxygen ($^1O_2$) (Krieger-Liszkay, 2004). Additionally, stepwise reduction of O_2 through the electron transport chain can lead to superoxide (O_2^-) production, resulting in accumulation of dihydrogen peroxide (H_2O_2) and hydroxyl radicals ($\bullet OH$). These ROS, particularly H_2O_2, have important roles in signalling and messaging and are produced in a controlled manner in unstressed conditions, balanced via a myriad of scavenging mechanisms (Baxter et al., 2014; Chan et al., 2016; Sharma et al., 2012;

Yan et al., 2007). However, in stress conditions the energy demand of CO_2 fixation is reduced, light energy supply can become excessive, and the resulting ROS production can overwhelm scavenging mechanisms. In this situation, the especially reactive $^1O_2$ and $\bullet OH$ damage cellular components including pigment-protein complexes, PSII reaction centres and repair mechanisms (Murata et al., 2007; Ohnishi et al., 2005), and membrane lipids (Krieger-Liszkay, 2004; Sharma et al., 2012; Trebst et al., 2002), leading to photoinhibition.

There are methods available to quantify damage incurred by ROS. Oxidative breakdown of chlorophyll due to high-light induced ROS damage (photobleaching, Velitchkova and Picorel, 2004) can be quantified spectroscopically. Additionally, the reaction of ROS with organellar and cellular membrane lipids (lipid peroxidation) causes changes in membrane fluidity and loss of stability, leading to loss of turgor pressure and even cellular collapse. One of the end-products of lipid peroxidation is malondialdehyde (MDA), which is a reactive compound that can further peroxidise lipids and take part in "runaway" ROS damage (Heath and Packer, 1968). MDA in leaf material can be quantified, allowing for a relative measure of the extent of lipid peroxidation that has occurred in a leaf (Du and Bramlage, 1992). Another result of reduced membrane stability is the loss of potassium ions from cells (Demidchik et al., 2014), which can be quantified via measurement of changes in electrical conductivity of leaves in solution.

2.1.3 *Sorghum bicolor* as an experimental model

This chapter sets out to compare the photoinhibitory response of sorghum [*Sorghum bicolor* (L.) Moench] to dynamic and steady-state high-light conditions. Sorghum, originally domesticated in arid northeast Africa, is a staple food crop for millions of people in Africa and Asia. Sorghum is also an essential source of animal feed and biofuel substrate throughout the world (Mundia et al., 2019; Silva et al., 2021). Sorghum's high potential productivity and outstanding water use efficiency have led to renewed interest in breeding for food and fuel in the context of global climate change (Hariprasanna and Rakshit, 2016). Additionally, the sorghum genome

is known to harbour considerable variation in photosynthetic traits (Ortiz et al., 2017; Salas Fernandez et al., 2015), but there is a lack of existing work examining photoprotection and photoinhibition in sorghum, in comparison to other major crops. The diversity of economic uses of sorghum and its tolerance to drought and heat stress suggest it could potentially supplant or replace other related crops such as maize (*Zea mays*) or sugarcane (*Saccharum sp.*) in the face of climate change (Allen et al., 2011; Assefa et al., 2010; Craufurd and Peacock, 1993; Nagy et al., 1995; Nguyen et al., 2013; Silva et al., 2021; Singh and Singh, 1995). In areas where sorghum is already grown, climatic warming will also require improvements in abiotic stress tolerance of the sorghum germplasm (Tack et al., 2017). To help contextualise the photoprotective and photoinhibitory response of sorghum, this work also directly compares the results with those of the globally significant C_4 crops *Z. mays*, *Panicum miliaceum*, *Pennisetum glaucum*, and model C_4 species *Setaria viridis*.

2.1.4 Chapter objectives

The objectives of the study were: 1) To develop an unbiased, high-throughput method to impose and measure the effect of light-stress treatments on leaf samples of several species; 2) To contrast the photoprotective and photoinhibitory responses of sorghum with other C_4 grasses; and 3) To further our understanding of the differences in photodamage caused by steady versus fluctuating high-light treatments. The results presented will help improve our understanding of photosynthesis in dynamic light conditions and help us contrast *S. bicolor's* photoprotective characteristics with the photoprotective responses of related C_4 species. By understanding and improving photosynthetic efficiency in sorghum, we can further breed and adapt the crop to fit global food and economic needs.

2.2 Materials and Methods

2.2.1 Plant growth

Seeds of *Zea mays* 'B73' and *Setaria viridis* 'A10' were acquired from Professor Julian Hibberd (University of Cambridge). Seeds of *Sorghum bicolor* 'Tx430' were provided by Dr Katarzyna Głowacka (University of Nebraska-Lincoln). Seeds of *Pennisetum glaucum* 'GB8735' were supplied by Dr Stéphanie Swarbreck (NIAB, Cambridge, UK). Seeds of *Panicum miliaceum* 'white millet' were donated by Cotswold Seeds (Moreton-in-Marsh, UK).

Plants for fluctuating (FHL) and steady-state high-light (SHL) experiments were grown in an unshaded glasshouse at the National Institute of Agricultural Botany Park Farm research facility in Histon, Cambridgeshire, UK. Supplementary lighting from overhead high-pressure sodium fixtures (600 W Papillion 270, Lights Interaction Agro, Eindhoven, Netherlands) provided approximately 150 μmol m^{-2} s^{-1} photosynthetic photon flux density (PPFD) at bench level (values varied from 90–230 μmol m^{-2} s^{-1} across bench) as measured using a light sensor (LI-190, LI-COR, Nebraska, USA). Supplemental lighting was provided when outdoor light intensity dropped below approximately 230 μmol m^{-2} s^{-1} PPFD, maintaining a 14–16 hour daylength. Temperature was controlled at 24–26/18–20 °C day/night.

Summary records of outside light intensity and indoor temperature and humidity can be found in Supplementary table 7.1.

Seeds of all species were germinated in potting soil (FHL experiments: Levington Advance Pot & Bedding M2, ICL Horticulture, Ipswich, UK; all other experiments: Levington Advance Pot & Bedding M3) in 9 cm pots. Seedlings were transferred to 5 litre pots with a custom soil mix (80% peat, 20% 0-8 mm bark, plus Osmocote 13-13-13 +TE) 3-4 weeks after emergence. Pots were placed on absorptive growth mats on benches and watered daily from below to ensure soil water content remained at field capacity. One hundred ml of chelated Fe solution (0.16% w/v) was applied bi-weekly directly into each pot.

FHL experiment plants were grown in a randomised augmented block design in three separate sets. Set one contained five plants each of *Z. mays*, *P. miliaceum*, and *P. glaucum*. The second set consisted of five plants each of *S. viridis* and *P. glaucum*. The third set consisted of *S. bicolor* and *P. glaucum*. SHL experiment plants were grown in a single set with five plants of each species. Within each growth set pots were moved sequentially thrice per week to negate effects of heterogeneous lighting. Sets were planted consecutively, with approximate emergence dates noted in Table 2.1.

Plants used for light response curves and fluorescence traces were grown in a walk-in growth room at the University of Cambridge Plant Growth Facilities (see Table 2.1 for dates). Lighting was provided by LEDs and at the bench level was approximately 500 μmol m^{-2} s^{-1} PPFD, with a 14 hour daylength. Room temperature was controlled at 28–32/20–22 °C day/night. Seeds of all species were germinated in Levington M3 potting soil in 9 cm pots, then transferred to 5 litre pots of Levington M3 soil 3–4 weeks after emergence. Plants were hand watered 3–4 times per week to ensure soil water content remained at field capacity. Pots were moved sequentially thrice weekly to negate effects of heterogeneous lighting.

Table 2.1: Emergence and sampling dates for experimental plants, day of year (year)

Growth set	Emergence date	Sampling date	Experiment
1	151-152 (2020)	181-188 (2020)	Fluctuating
2	264-271 (2020)	318-328 (2020)	Fluctuating
3	316-323 (2020)	54-58 (2021)	Fluctuating
4	20-22 (2021)	82-85, 89-93 (2021)	Steady-state
5	276-277 (2021)	314-322 (2021)	Light response and fluorescence

2.2.2 Development of high-throughput photodamage assays

Due to the large quantity of samples used in these experiments and later in this thesis, it was essential to develop a high-throughput method to impose and quantify the effects of high-light treatments on a substantial amount of diverse leaf material. The methods used to quantify photodamage (as mentioned in the introduction) follow; more information about specific method development can be found in results section 2.3.1.

Leaf sampling for photodamage assays

Leaves were sampled by cutting 6 mm diameter leaf discs with a hole punch. Discs were cut at the midlength of leaves, avoiding the midrib and leaf edge. Leaf discs were placed into transparent flat-bottom 96-well plates (Thermo Fisher Nunc clear) with the adaxial side of the leaf facing the plate bottom. Discs for measurement of pigment and MDA content were held in place by pieces of damp sponge, and discs used for electrolyte leakage were held in place by short segments of polyethylene tubing backed by damp paper towels, to avoid contact of the disc with wet surfaces that could transfer electrolytes. Each plant was sampled for every treatment time point; this repeated-measures design was accounted for in the results analysis. Disc placement in well plates was grouped by sampling time point and randomised by species to prevent biases due to uneven lighting during treatments.

Sample plates were wrapped in aluminium foil for 1 to 2 hours to prevent light intrusion and buffer temperature changes while being transported to the University of Cambridge Department of Plant Sciences for light treatments.

Light treatment

High-light treatments utilised a three-colour (RGB) LED light panel (SL 3500-C, Photon Systems Instruments, Drásov, Czech Republic). FHL treatments consisted of six hour cycling of five minutes of 2,960 μmol m^{-2} s^{-1} PPFD followed by one minute in <10 μmol m^{-2} s^{-1} PPFD light. The SHL treatment entailed six hours at

2,470 μmol m^{-2} s^{-1} PPFD, thus both treatments provided approximately equivalent total photon loads over six hours (light intensities were measured at the centre of 96-well plates). The light composition from the LED panels was as follows: 36% green (533 nm peak λ), 33% red (633 nm peak λ), 31% blue (446 nm peak λ).

The 96-well plates were placed under the LED panels upside-down, thus the adaxial side of the leaf discs faced upward toward the light source during treatment (Fig. 2.1). Individual, discrete discs were removed from the well plate for sampling after two, four, and six hours of treatment time.

A water bath with layer of water approximately 5 cm deep was placed between the light source and well plates to prevent excessive heating of leaf discs. During light treatments, temperature near the leaf discs reached approximately 35°C as measured with a standard glass immersion thermometer lying next to the plate.

Untreated control leaf discs were kept in a separate 96-well plate in dim light, sampled at the beginning of the light treatment to provide starting values for all assays. Another set of discs was kept in this plate and sampled after six hours, to check for the presence of "control drift" caused by time spent in the plate and not caused by the light treatment. In a few assays slight drift was observed, but the magnitude was minimal compared to light treatment time course effects, and was inconsistent in direction between species. See Supplement (7.1) for associated plots and ANOVA tables.

Chlorophyll and carotenoid content

Chlorophyll and carotenoid content of leaf discs was determined spectroscopically. Discs were removed from the 96-well plate and, under dim lighting, snap-frozen in liquid nitrogen then homogenised in microtubes containing a 95% ethanol solution. The resulting whole-leaf extract was incubated in the 95% ethanol solution at 4°C in darkness for 72 hours, before centrifuging at 3,000 g for 10 minutes. Absorbance of the supernatant was measured (UV300, Spectronic Unicam, Cambridge, UK) and pigment contents and ratios were determined using the equations of Lichtenthaler (1987).

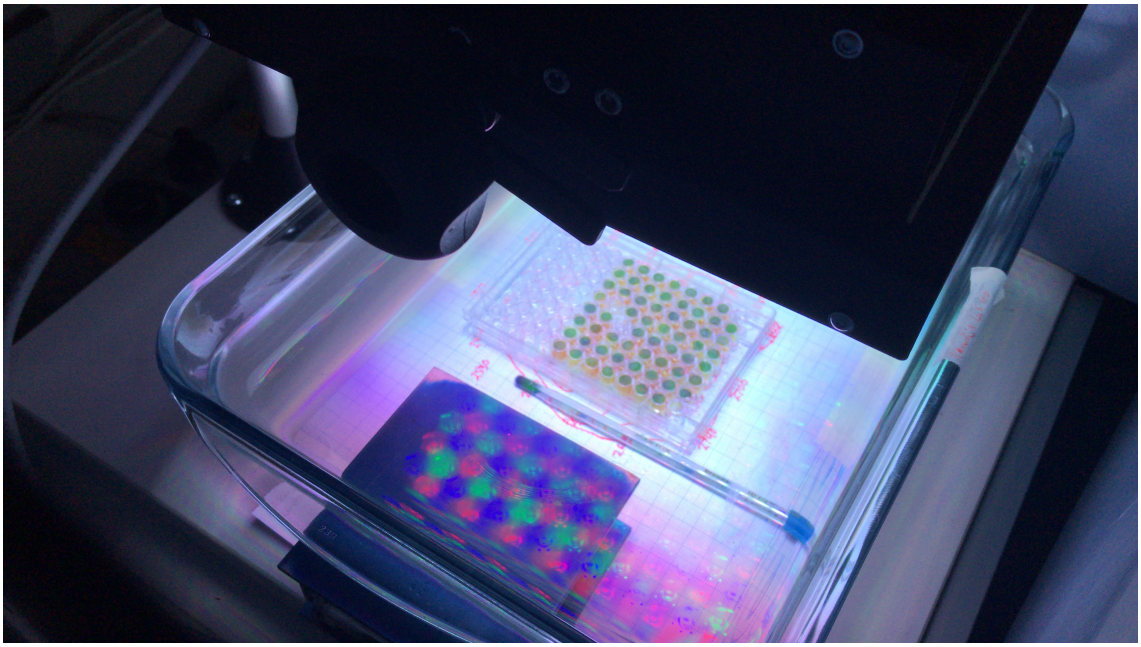

Figure 2.1: Leaf discs under LED panel during high-light treatment

Malondialdehyde abundance

Photodamage and changes in membrane stability were assessed via measurement of MDA abundance, using the thiobarbituric acid (TBA) reactive substances assay (TBARS), in accordance with the methods of Du and Bramlage (1992) and Hodges et al. (1999). Homogenisation and incubation of leaf discs was performed as noted for pigment content measurement, using 80% instead of 95% ethanol. After centrifuging at 3,000 g for 10 minutes, 550 μl of supernatant from individual samples was split into microtubes containing 550 μl of either a "+TBA" (0.045 M [0.65% w/v] TBA and 4.54 x 10^{-4} M [0.01% w/v] butylated hydroxytoluene, in 1.224 M [20% w/v] trichloroacetic acid) or "-TBA" (same as "+TBA", except without TBA) solution. Tubes were then vortexed, heated at 95°C for 25 minutes, then plunged into an ice bath for 10 minutes to halt the TBARS reaction. Tubes were then centrifuged at 3,000 g for 10 minutes and absorbance of the supernatant was measured. MDA equivalents were calculated on a dry-mass basis using the equations of Hodges et al. (1999), accounting for an error noted by Landi (2017).

Electrolyte leakage

Electrolyte leakage was expressed as percent relative injury (Ri) based on the methods of Warren et al. (1996) and Qu et al. (2014), with modifications. After cutting, leaf discs were floated on deionised (DI) water in individual microtubes for 30 to 45 minutes with periodic gentle agitation, to wash the disc edges. This wash time was determined through prior testing of change in solution conductivity over time (Supplementary figure 7.2). Leaf discs were then placed into 96-well plates for light treatment. The sponges used to hold leaf discs in the other assays were found to interfere with the conductivity measurement and thus were replaced here by short pieces of polyethylene tubing backed by a damp paper towel, to allow air to reach the disc without drying. After high-light treatment, discs were placed into individual microtubes with fresh DI water and allowed to incubate for 18 to 20 hours in darkness at room temperature. The tubes were then gently shaken on a rotary shaker for 15 minutes, and the initial electrical conductivity of the leaf solution (T_1) was measured using a handheld electrical conductivity meter (LAQUAtwin EC-11, Horiba, Kyoto, Japan). Tubes were then heated at 99°C for three hours to release remaining electrolytes. The tubes were then allowed to cool to room temperature, shaken for 15 minutes, and conductivity was re-measured (T_2). Ri was calculated as

$$Ri = ((T_1 - T_0)/(T_2 - T_0)) * 100 \tag{2.1}$$

where T_0 represents the conductivity of the DI water used.

2.2.3 Chlorophyll fluorescence traces

Photoprotective kinetics of the five species were compared via NPQ traces using plants grown in the Plant Growth Facility walk-in growth room, using a high-throughput method similar to that implemented in Gotarkar et al. (2022). Leaves were sampled by cutting 6 mm diameter leaf discs with a hole punch in a similar manner to the photodamage assay sampling, using a damp sponge to hold the discs

in place. Each plant was sampled twice from the same area of the youngest fully expanded leaf (as indicated by ligule emergence).

The sample plate was wrapped in aluminium foil to prevent light intrusion and buffer temperature changes, then transported to the University of Cambridge Department of Plant Sciences. The plate was stored for two hours, allowing the leaf discs to dark-adapt before chlorophyll fluorescence screening. Leaf discs were imaged using a fluorescence imaging cabinet (CFImager, Technologica, Colchester, UK). In a dimly lit room, the foil was removed from the plate immediately before imaging, and the plate placed into the imaging cabinet. The imaging routine consisted of a dark-adapted measurement of maximum PSII quantum efficiency (Fv/Fm) followed by periodic fluorescence measurements over 10 minutes at 2,000 μmol m^{-2} s^{-1} PPFD, followed by measurements over 12 minutes of darkness. During the NPQ induction period, fluorescence was measured every 20 seconds for the first minute, then every minute for the remainder of the light period. During the NPQ relaxation period, fluorescence was measured every 20 seconds for the first minute, then every minute for the next three minutes, then every three minutes for the duration of the dark period.

Image thresholding and segmentation were performed in MatLab (MATLAB, 2020). Fluorescence values for each disc were taken as the median pixel value of the disc. The distribution of Fv/Fm values for the discs was examined to discern any obvious outlier leaf samples. Sample Fv/Fm values showed a slightly left-skewed distribution ranging from 0.67 to 0.79; one *Z. mays* disc with a value of 0.60 was filtered away. Traces of the two technical replicates for all other leaves were averaged. Exponential models were fit to the NPQ light induction and dark relaxation periods separately, to allow quantitative comparison of NPQ induction (Eq. (3.1)) and relaxation (Eq. (3.2)) rates, as well as the PSII operating efficiency ($\Phi PSII$) dark recovery rate (Eq. (3.3)), using the *minpack.lm* package in R (Elzhov et al., 2016):

$$y = a_{NPQi}(1 - e^{-k_{Ind}t}) \tag{2.2}$$

$$y = a_{NPQr}(e^{-k_{Rel}t}) + b \tag{2.3}$$

$$y = a_{\Phi PSII}(1 - e^{-k_{Rec}t}) + b \tag{2.4}$$

where a_{NPQi}, a_{NPQr} and $a_{\Phi PSII}$ are the initial values of NPQ induction, relaxation, and $\Phi PSII$ recovery during the dark period, respectively; k_{Ind}, k_{Rel}, and k_{Rec} the rate constants of NPQ induction and relaxation and $\Phi PSII$ recovery, respectively (thus a larger number indicates faster kinetics), t is the measurement time point, and b an offset to account for a non-zero y-intercept term at the beginning of the dark relaxation/recovery period.

Additionally extracted from the NPQ traces were the maximum NPQ reached during the trace, initial linear slopes of NPQ induction/relaxation, and photoprotection index (PI, Kromdijk, Głowacka, Leonelli, et al., 2016; Ruban and Murchie, 2012), the ratio between observed Fv'/Fm' (maximum PSII quantum efficiency at a given PPFD) and the calculated Fv'/Fm'_f based on the predictable decrease due to NPQ, during the dark period. $PI \geq 1$ suggests that the reduction in Fv'/Fm' relative to initial Fv/Fm can be attributed to NPQ, while values lower than one suggest a portion of the drop is attributable to photoinhibition. PI was calculated as follows

$$PI = \frac{\frac{Fv}{Fm}_f}{1 - \left[(1 - \frac{Fv}{Fm})/\left(\frac{Fv}{Fm} + [(1 - \frac{Fv}{Fm})/\frac{1}{1+NPQ_f}]\right)\right]/\frac{1}{1+NPQ_f}} \tag{2.5}$$

modifying the "$pNPQ$" approach of Ruban and Murchie (2012), where Fv'/Fm'_f and NPQ_f are Fv'/Fm' and NPQ, respectively, at the final dark time point.

2.2.4 Light response curves

The photosynthetic response to a range of incident light intensities (A/Q_{inc} response) for each species was examined using a leaf-level gas exchange system (LI-6800, LI-COR, NE, USA). Light response was measured prior to chlorophyll fluo-

rescence sampling, on the same plants grown in the Plant Growth Facility walk-in growth room. On each of the plants the leaf was placed in the instrument gas exchange chamber (6800-01A, LI-COR) at 1,000 μmol m^{-2} s^{-1} PPFD (90% red light, up to a maximum 40 μmol m^{-2} s^{-1} PPFD blue light) and allowed to acclimate for five minutes, then light level was set to 1,800 μmol m^{-2} s^{-1} PPFD and leaves allowed to fully acclimate. Leaf temperature was controlled at 32°C, flow to sample chamber at 280 μmol s^{-1}, sample [CO_2] at 410 ppm, and leaf-air vapour pressure deficit at 1.5 kPa. Chamber light intensity was stepped down from 1,800 to 1,500, 1,200, 900, 750, 600, 500, 400, 300, 200, 120, 60, and 20 μmol m^{-2} s^{-1} PPFD. CO_2 assimilation was measured at each light intensity step once the CO_2 assimilation rate was stable, with a maximum wait time of 120 s. The instruments were range-matched prior to starting the experiment and point-matched before starting each curve. A non-rectangular hyperbolic model (Marshall and Biscoe, 1980; Ögren and Evans, 1993) was fit to the light response points of each replicate via the *photosynthesis* R package (Stinziano et al., 2020).

2.2.5 Correlation analyses

Pearson's correlation coefficient was calculated for pairwise interactions between photodamage, photoprotection (NPQ induction/relaxation traits), and A/Q_{inc} response traits, using R package "psych" (Revelle, 2022) and R Corrplot (Wei and Simko, 2021) packages. Probability values were multiple-test adjusted using the Holm method (Holm, 1979). Species estimated marginal means for each trait were used (n = 4–5 plants per species), with values for photodamage traits taken as the absolute change from the zero-hour control to two-hour time point. Principle component analysis (PCA) on the species estimated marginal means was performed using the R FactoMineR package (Lê et al., 2008).

2.2.6 Statistical analyses

Statistical analyses were performed using R v4.2.0 (R Core Team, 2022). High-light treatment response, NPQ kinetics, and A/Q_{inc} data were checked for normality us-

ing a Shapiro-Wilk test via the *dlookr* package (Ryu, 2021). Homoscedasticity was checked via the native R *stats* Bartlett test. Data was also visually assessed via qq plots, histograms, Cook's distance plots, and scale-location plots. Outlier data points (as judged by Cook's distance threshold) were filtered out for photodamage assays, and data which did not reasonably conform to assumptions of statistical tests (fewer than 5% of samples) were not analysed further. For high-light treatments, linear mixed-effects models (R package *lme4*, Bates et al., 2015) were fit by residual maximum likelihood to light treatment response data with species and treatment time (nested within treatment type) as fixed effects. Individual plant and growth set were fitted as random effects, to account for repeated measures and the augmented-block experimental design. *t*-tests utilised Satterthwaite's degrees of freedom correction method for unequal replication rate. Contrasts between estimated marginal means of treatment time points and 0-hour (control) measurements were calculated utilising the Kenward-Roger degrees of freedom correction (Lenth, 2021). Significance values were adjusted via Bonferroni correction to account for multiple comparisons.

Estimated marginal means of NPQ kinetic trace-derived traits which conformed to linear model / ANOVA assumptions were tested for pairwise species differences via Tukey's HSD (Lenth, 2021). Light response curve data was checked and tested using mixed-effects modelling as above, except that *species* was fitted as a fixed effect and day-of-measurement fitted as a random effect. Pairwise comparisons between species were conducted via Tukey's HSD.

2.3 Results

2.3.1 Development of high-throughput light stress treatments and photodamage assays

The protocols for pigment content, MDA abundance, and electrolyte leakage assays used in this project are based on descriptions from prior use in peer-reviewed literature. These descriptions seldom include thorough protocol-style instructions neces-

sary to faithfully repeat the measurements. Thus they required further (sometimes extensive) testing and development to provide consistent results on the specific plant material used. Consequently, thorough testing was required to render each procedure as efficient, consistent, and high-throughput as possible. Summaries of the variability of these protocols in the literature, along with summary tables describing the various tests performed to optimise protocols for the current work, are presented in this section.

Pigment content

In the case of pigment content quantification, spectrophotometric methods are well-developed to perform these assays, but fine-tuning related to sample/solvent concentrations and homogenisation strategies was needed to create a protocol fitting the experimental needs. Measurements of chlorophyll and carotenoid content have been foundational to a vast number of studies in plant biology, and there have been an accordingly large number of protocols in peer-reviewed literature describing how to best quantify these pigments (Arnon, 1949; Lichtenthaler, 1987; Porra et al., 1989). The most common, lower cost methods involve homogenisation of leaf material followed by a period of pigment extraction in ethanol, methanol, acetone, or similar solvents, followed by measurement of the light absorption of the extracted leaf solution at wavelengths at which pigments are strongly absorptive. However, as Ritchie (2006) points out, several of the most common protocol references offer different absorption coefficients when using the same solvents for extraction. Choosing the correct method requires consideration of the efficacy, safety, and availability of extraction solvents, the physical strength and relative pigment content of the leaf material to be measured, and availability of equipment, among others.

The C_4 monocot species studied in this project tend to have "tough" leaves, which are more challenging to homogenise than that of many dicots. Additionally, the Kranz anatomy and corresponding high chlorophyll a:b ratios (compared to C_3 species) appears to be less amenable to complete pigment extraction when using more dilute solvents. Presumably for those reasons, full extraction of pigment

required a longer incubation time than what is often reported in the literature for C_3 dicots. The tests outlined in Table 2.2 provide an overview of protocol optimisation for this work.

Table 2.2: Description of the variables, specific tests, and results of optimisation tests for pigment content assays

Variable	Test	Result
Appropriate leaf material solution concentration	Compared spectrophotometric absorbance of homogenised *Z. mays* between different numbers of discs and solvent volumes.	Determined that a single disc in 1.5-1.8 ml of 90% methanol yields absorbance values in an appropriate range for further interpretation.
Appropriate extraction time	Using the same leaf material and homogenisation method, incubated solutions for various lengths of time, sampling periodically. Completeness of extraction was judged by absorptance values and apparent "whiteness" of pellet.	Determined that chlorophyll appears fully extracted after 72 hours; incubation at 4^oC should help limit pigment degradation and conversion.
Homogenisation method	Tested: Cutting leaf material into small pieces; grinding with mortar and pestle; grinding in microtube followed by multiple centrifuge spins; including silica sand in tube to aid grinding. Judged efficacy by "whiteness" of pellet after incubation at 4^oC.	Determined that homogenising in a microtube under liquid N_2 followed by three-day incubation was effective in fully extracting samples and best fit throughput needs.

Malondialdehyde abundance

One of the end-products of the peroxidation of membrane lipids is MDA (Heath and Packer, 1968). When MDA is reacted with TBA, a chromophore is formed which absorbs strongly at 532 nm (Janero, 1990). By comparing the absorbance at 532 nm of leaf solution from stressed and unstressed samples, the extent of ROS-induced damage due to stress conditions can be proximally quantified. This method, called the TBARS assay, has been used widely in medical, animal, and plant biology, to assess stress response and cellular damage.

With this widespread use there exist myriad different off-the-shelf solutions and protocols designed to perform the TBARS assay. Compared to human and animal samples, measurements on plant material require different considerations, particularly regarding the high sugar content (Du and Bramlage, 1992) and content of other compounds that absorb at 532 nm (Hodges et al., 1999) of many plant cells. For these reasons, off-the-shelf TBARS kits do not appear to be applicable for most plant work. The methods commonly cited in peer-reviewed plant biology literature typically refer the work of Du and Bramlage (1992) and Hodges et al. (1999), but errors and variability in the actual implementation of the assay and especially in reporting of results seem to infest the literature. As a brief example, the method in Hodges et al. (1999), which has been cited over 3,400 times as of May 2022 (Google Scholar), contains an arithmetic error in the equation used to calculate MDA abundance. This appears to have not been formally addressed until a 2017 commentary by Landi (2017). Additionally, though expression of MDA abundance on a *nmol per fresh mass* basis is implemented in the previously mentioned methods, there seems to be little agreement on the appropriate units in the wider literature. In some cases, peer-reviewed literature reports MDA abundance values hundreds of fold higher (Moussa and Abdel-Aziz, 2008) or lower (Huang et al., 2021) than that of the current, or comparable studies, suggesting confusion and errors as to calculating and reporting MDA content. The choice of extracting solution and concentration also varies, though nearly every publication uses the same absorption coefficients and wavelength. This may not be appropriate, as

the peak wavelength and absorption coefficient of compounds in solution changes based on the solvent (a matter which led to the proliferation of coefficients for chlorophyll and carotenoid content measurements). For these reasons, and the concerns noted for homogenisation in the "pigment quantification" section, substantial testing and optimisation was required before consistent and sensible results were observed in this work (Table 2.3).

Table 2.3: Description of the variables, specific tests, and results of optimisation tests for the malondialdehyde abundance content assay

Variable	Test	Result
Appropriate leaf material solution concentration	Compared spectrophotometric absorbance of homogenised *Z. mays* between different numbers of discs and solvent volumes.	Determined that four leaf discs in 1.8 ml of 80% ethanol allows consistent TBARS reaction and appropriate absorbance values
Appropriate acid mixes (storage, mixing, etc.)	Compared measurements made on separately mixed +/- TBA solutions stored over several weeks with solutions mixed fresh before reacting, with TBA added to an identical -TBA solution.	Found that using fresh solution from a single batch of acid solution helped yield much more consistent MDA abundance results.
Appropriate sample treatment	Compared measurements made on separately homogenised samples versus single, larger aliquots split into two different aliquots.	Determined that utilising split single aliquots reduced variability in results and reduced overall preparation time.
Appropriate containers	Performed heating steps using either pop-top microtubes, microtubes with holes in caps, or threaded cap microtubes.	Found threaded cap microtubes could withstand pressure build-up from heating reaction without loss of solution.

Electrolyte leakage

Electrolyte leakage has been well-characterised as a relatively simple measurement of cell damage due to plant stressors. ROS production during stress conditions can lead to peroxidation of lipids in organelle and cellular membranes, reducing membrane stability. The resulting efflux of electrolytes out of cells can be measured by incubating leaf material in water and measuring the total electrical conductivity of the leaf/water solution.

The conductivity of the leaf solution will increase as the amount of damage due to stressors increases, allowing for a proximal measurement of *Ri* between samples exposed to different stress conditions. Conductivity measurements are normalised to the maximum possible conductivity of the sample after heating (releasing all electrolytes into solution), allowing comparison of *Ri* between leaf material with different initial electrolyte contents. A number of groups have implemented the method: Bajji et al. (2002) utilised the assay to measure *Ri* in wheat under different levels of water stress, Campos et al. (2003) used the technique to characterise sensitivity of *Coffea sp.* to cold stress, Correia et al. (2018) measured response of *Eucalyptus globulus* to drought and heat stress, and Qu et al. (2014) investigated the response of *Z. mays* to heat and CO_2 stress. However, electrolyte leakage has not been applied widely to evaluate the effects of short-term high light treatments. The description of the electrolyte leakage protocols in these papers typically includes only the incubation time and heating time and temperature chosen, without indicating the rationale for these choices. Incubation times range from 16 to 24 hours, and heating times from a few minutes boiling to an hour or more at lower temperature. Additionally, it is expected that leaf discs will be washed before being placed into the incubation solution in order to remove electrolytes from the "cut" region of the disc. The time and number of washes required is typically only loosely described, ranging from "two to three brief rinses" to 30 minutes floating on DI water, before being transferred to the incubation water. In Bajji et al. (2002), the authors performed a test of the efficacy of different wash times in order to avoid choosing arbitrarily based on other literature.

The rationale for this level of method-and-plant specific testing is well supported by results from Prášil and Zámečník (1998), who concluded that the size and shape of leaf segments, amount and nature of leaf material, and different incubation times, can have a substantial effect on measured *Ri*. Thus, characterisation of these parameters should be performed on the specific plants of interest with consideration given to the experimental design and available resources to ensure consistent, valid data is collected. Additionally, the lack of past work using the assay for high-light treatment in C_4 species meant that the level of *Ri* that might be observed during treatments was unknown. Until testing began there was little frame of reference available to understand "how bright" and "how long" light treatment might be before a measurable response in *Ri* was observed. Table 2.4 lists various parameters and tests involved in optimising the assay for this work.

Table 2.4: Description of the variables, specific tests, and results of optimisation tests for the electrolyte leakage assay

Variable	Test	Result
Appropriate ratio of water : leaf material required	Compared conductivity values measured after incubation between samples with three different amounts of leaf material, and two different volumes of water.	Determined a single leaf disc in 1 ml of deionised water provides a high enough conductivity to resolve sample differences using the chosen conductivity meter.
Appropriate sample containers and heating apparatus	Tried heating protocol with glass vials, microtubes with holes in caps, and threaded cap microtubes, in lab oven and heating block.	Determined threaded cap microtubes heated in block could withstand pressure build-up during heating and were appropriate to prevent solution loss or melting.
Appropriate heating time	Measure samples after successive hours of heating, cooling and measuring conductivity after each time period.	Determined 3 hours at 99^{o}C is adequate-second conductivity value does not increase appreciably with further heating.
Appropriate wash time	Measured conductivity of leaf discs immediately after cutting, every 15-30 minutes for two hours to quantify "new electrolytes" in solution.	Approximately 75% of electrolyte leakage that occurs in the first two hours happens within the first 30 minutes.
Appropriate incubation time	Sampled conductivity of leaf solution over 24 hours.	Determined 16-18 hours is adequate, and conductivity change between 16 and 20 hours was less than 15% for untreated samples.

Table 2.4: Description of the variables, specific tests, and results of optimisation tests for the electrolyte leakage assay *(continued)*

Variable	Test	Result
Appropriate backing material for discs in well plate	Using leaf discs in well plate backed by small pieces of sponge, measured conductivity of discs alone, discs with sponges, and standalone sponges. Left discs and sponges in well plates for different periods of time. Repeated this test procedure using polyethylene tubing backed by moist paper instead of sponges, to hold discs in place.	Determined that sponges appear to add/remove electrolytes to wet discs, significantly skewing conductivity measurements, with effects exacerbated by time spent in well plate. No interaction was observed when discs were backed by tubing and moist paper towel, and conductivity values agreed with those measured on leaf discs that never were in a well plate.

2.3.2 Photodamage during fluctuating and steady-state high-light treatments

Chlorophyll and carotenoid content, MDA abundance, and electrolyte leakage of the five species were measured during separate FHL and SHL treatments, in an effort to understand interspecies variation in photodamage response. In particular, experiments were conducted to test whether the susceptibility to photodamage of *S. bicolor* is different from that of the other species.

Pigment degradation is more substantial under fluctuating high-light

Total chlorophyll content tended to decrease in all species during both light treatments, with a more deleterious response after six hours to FHL (mean decrease of 5.85 mg g^{-1}) than to SHL (mean decrease of 3.07 mg g^{-1}, $p < 0.001$, linear mixed-effect model, Fig. 2.2, A and Supplementary table 7.8). Species-specific responses to treatment time in either high-light regime were not substantially different from one another ($p = 0.2$, linear mixed-effect model), though it is notable that during both treatments *Z. mays* exhibited negligible further chlorophyll breakdown after the four hour time point, and *S. viridis* behaved similarly during the SHL treatment. During the SHL treatment *S. bicolor* experienced a somewhat more dramatic decrease in chlorophyll content (4.91 mg g^{-1} after six hours) than the other species.

Similar to cholorophyll content, the decrease in total carotenoid content was much more pronounced in response to the FHL treatment (species' mean decrease of 0.82 $mg\ g^{-1}$ after six hours) compared to SHL (mean decrease of 0.42 $mg\ g^{-1}$, $p < 0.001$, linear mixed-effect model, Fig. 2.2, B and Supplementary table 7.9), with the only exception being *Z. mays* which again seemed to reach maximum pigment breakdown after four hours followed by an increase at the six hour time point, in both treatments. The carotenoid content response to treatment time did not vary much between species ($p = 0.12$, linear mixed-effect model) in either light regime. The response over time of *S. bicolor* to either treatment type was not substantially different than that of the other species.

During the FHL treatment there was a strongly divergent species response in chlorophyll a:b ratio, with *Z. mays* and *S. bicolor* increasing over six hours by 0.6 and 0.23, respectively, while the other three species' a:b ratios decreased over six hours (mean of -0.64, $p = 0.001$, linear mixed-effect model, Fig. 2.2, C and Supplementary table 7.10). This species-specific contrast was not seen during the SHL treatment, during which all species showed a drop in chlorophyll a:b ratio over the time course (mean decrease of 0.69); as a whole the SHL treatment caused a notably larger drop than the FHL treatment ($p < 0.001$, linear mixed-effect model).

The change over time in the ratio of total chlorophyll : total carotenoids varied considerably between species (p <0.001, linear mixed-effect model, Fig. 2.2, D and Supplementary table 7.11), with *Z. mays* exhibiting the sharpest decline in both treatments (-1.2 in FHL and -0.46 in SHL, after six hours) while after six hours *S. bicolor* decreased least (-0.19) in FHL and *P. glaucum* the least in SHL (-0.06). During the SHL treatment, species-specific differences in chlorophyll : carotenoid ratio were less pronounced than in FHL. The SHL treatment species' mean decrease of 0.32 was smaller than that of the FHL treatment (-0.58, $p < 0.001$, linear mixed-effect model, for the difference between treatments).

Lipid peroxidation is increased under fluctuating high-light, compared to steady-state high-light conditions

Malondialdehyde abundance in leaf samples can provide a relative measure of the extent of lipid peroxidation caused by reactive oxygen species-induced stress. During the high light treatments all species showed sizeable differences in the magnitude of response to the different treatment types ($p < 0.001$, linear mixed-effect model, Fig. 2.3 and Supplementary table 7.12); the species mean increase over the control during the FHL treatment was 95.7 nmol g^{-1} while the SHL species mean MDA decreased by 31 nmol g^{-1}.

There were also substantial interspecies differences in MDA content in response to treatment time ($p < 0.001$, linear mixed-effect model). During the FHL treatment, after six hours *S. viridis* increased to 177.21 nmol g^{-1} while *P. miliaceum*

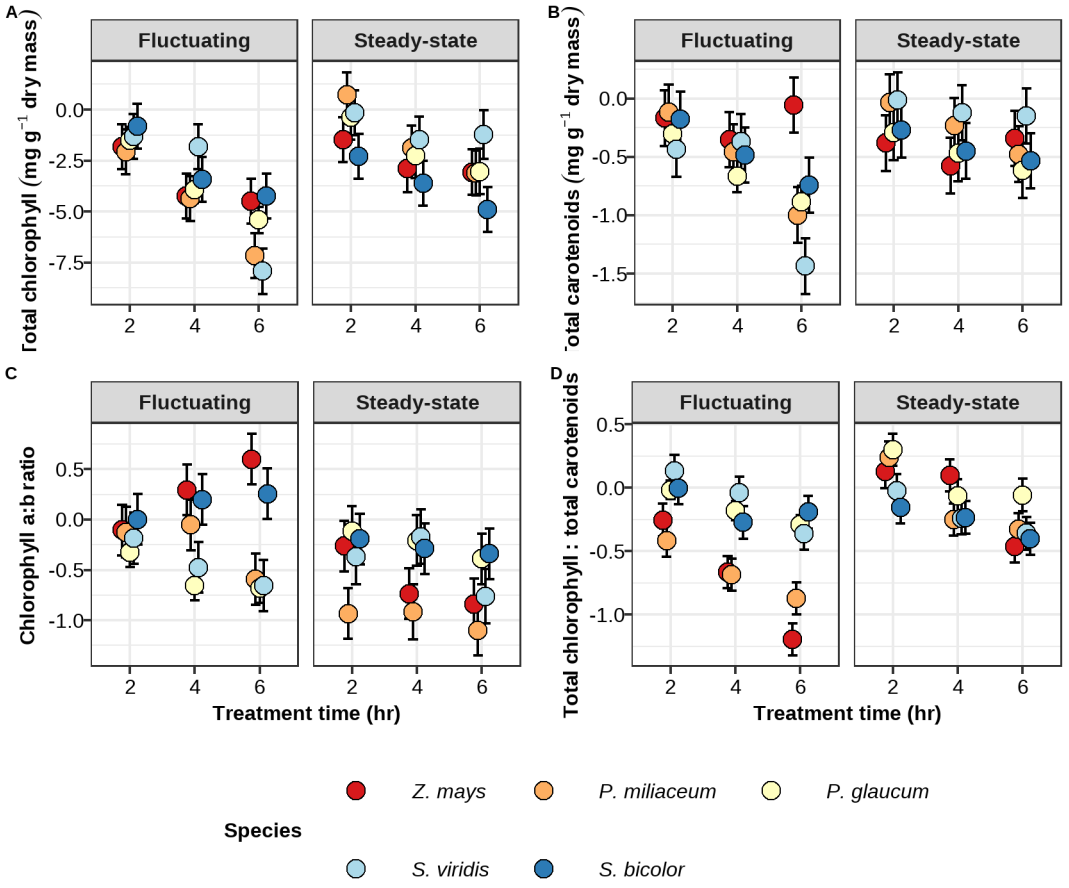

Figure 2.2: Photoinhibitory response to steady-state and fluctuating high-light treatments in five C_4 species. **A**, Total chlorophyll content. **B**, Total carotenoid content. **C**, Chlorophyll a:b ratio. **D**, Ratio of total chlorophylls to total carotenoids. Discrete leaf disc samples were exposed to either 2,470 μmol m^{-2} s^{-1} PPFD steady-state RGB light or 2,960 μmol m^{-2} s^{-1} PPFD fluctuating (five minutes high, one minute at <10 μmol m^{-2} s^{-1} PPFD) RGB light. Data are estimated marginal means (EMM) relative to untreated control absolute values. Error bars indicate standard error of EMM (n = 4–5 plants per species).

only increased to 44.44 nmol g^{-1} with the other species falling between. All species showed an increase in MDA after two hours, but *P. miliaceum* slowly declined after that and *Z. mays* decreased after the four-hour peak. The other three species increased over six hours.

In the SHL treatment, due to high 0-hour control values, MDA in *Z. mays* dropped strongly from the control level over the course of six hours (-268.69 nmol g^{-1}); the reason for the initially elevated level of MDA is unclear, but it was consistent

among separate maize plants. *P. glaucum* and *S. bicolor* showed small reductions in MDA content during the treatment (mean decrease of 9.31 nmol g^{-1}), and *P. miliaceum* and *S. viridis* increased to 84.72 and 47.40 nmol g^{-1}, respectively. All species showed a decrease in MDA after the four-hour time point.

Fluctuating high-light causes more extensive electrolyte leakage than does steady-state high-light

Electrolyte leakage (percent *Ri*) was measured in the five species in response to the FHL and SHL treatments and used as a proxy for cellular and organellar membrane damage. Species-specific variability in response to treatment time and type was observed ($p = 0.004$, linear mixed-effect model, Fig. 2.4, F and Table 7.13). In the FHL treatment, *Z. mays* had the highest increase in calculated percent *Ri* over the control value after six hours (24.5%) while *S. bicolor* showed the smallest increase at 4.9%. However, all species except *P. glaucum* peaked in *Ri* at the four-hour time point, followed by a decrease at six hours, in the FHL treatment. *P. glaucum* steadily increased to 12.4% *Ri* over the six hour period.

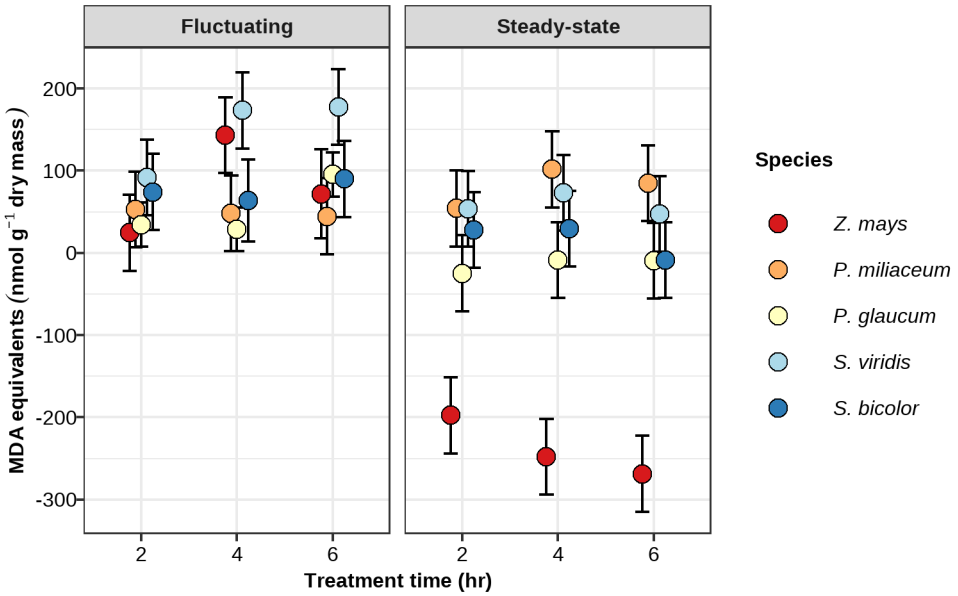

Figure 2.3: Malondialdehyde (MDA) abundance under fluctuating and steady-state high-light treatments. Data are estimated marginal means (EMM) relative to untreated controls. Error bars indicate standard error of EMM (n = 4–5 plants per species).

Compared to FHL, SHL treatment response of *Ri* over time was much less pronounced (six-hour species' mean increase over control of 4.8% compared to 11.4% in FHL, $p < 0.001$, linear mixed-effect model). Generally there was negligible increase in *Ri* in the SHL treatment compared to the control value; however, *S. bicolor* was an outlier in that the SHL four and six-hour *Ri* value increased to 35.4% and 21.5%, respectively, over the control value. This was the most extreme *Ri* response of any species in either treatment type.

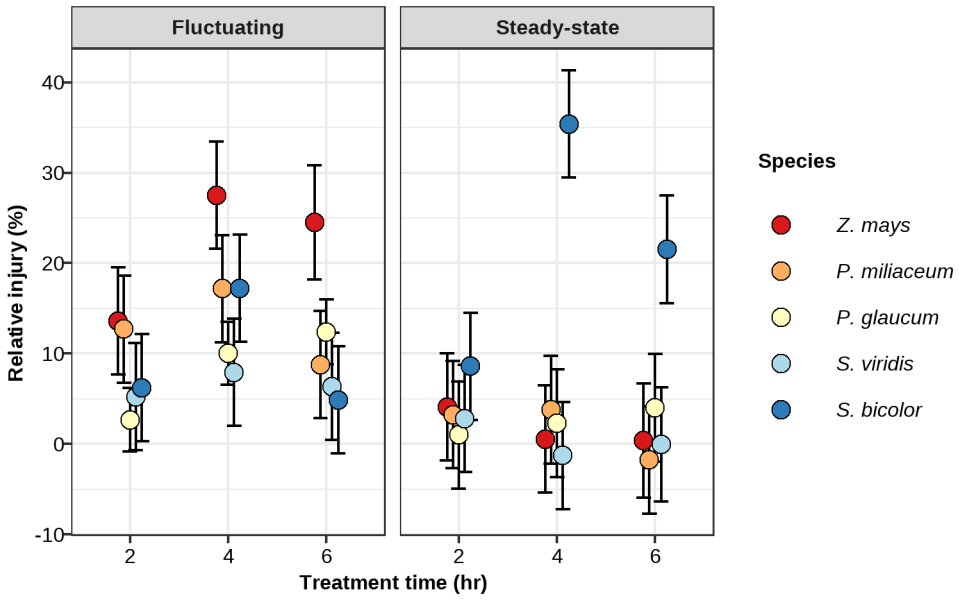

Figure 2.4: Relative injury measured via electrolyte leakage, under fluctuating and steady-state high-light treatments. Data are estimated marginal means (EMM) relative to untreated controls. Error bars indicate standard error of EMM (n = 4–5 plants per species).

2.3.3 Downregulation of light harvesting during a brief period of high light

The kinetics of NPQ induction and relaxation of the five species were investigated via measurement of chlorophyll fluorescence during a short-term high light treatment followed by a dark relaxation period (Fig. 2.5, A). *Z. mays* exhibited both the fastest NPQ induction and relaxation rate constants (k). The NPQ relaxation k differed between species, ranging from 3.51 to 6.09 min^{-1} ($p = 0.025$, ANOVA). NPQ induction k ranged from 0.34 to 0.61 min^{-1} (it did not meet assumptions of the statistical test). *P. glaucum* showed the slowest NPQ induction k but second-fastest NPQ relaxation k. *P. miliaceum* had the lowest NPQ relaxation k. The other species fell between. Maximum NPQ reached during the trace also varied strongly between species ($p = 0.002$, ANOVA), with *Z. mays* reaching the highest and *S. viridis* the lowest maximum NPQ during the treatment at 3.39 and 2.45, respectively, and the other species intermediate. The PSII quantum efficiency ($\Phi PSII$) recovery k during the dark period varied strongly between species as well ($p = 0.0014$, Fig. 2.5, B), with *S. viridis* and *P. glaucum* the fastest and *P. miliaceum* the slowest rate constants. Mean PI varied considerably between the species ($p < 0.001$, ANOVA), highest in *Z. mays* at 1.03 and lowest in *P. miliaceum* at 0.91. $PI \geq 1$ suggests that the reduction in Fv'/Fm' relative to initial Fv/Fm can be attributed to NPQ, while values lower than one suggest a portion of the drop is attributable to photoinhibition. This suggests that the drop in $\Phi PSII$ from initial Fv/Fm (Fig. 2.5, B) in *Z. mays* after a period of dark recovery may have been attributable to a slower-relaxing NPQ component such as qZ or qH, rather than to photoinhibition. In the other species PI values were below 1, indicating that NPQ did not explain the full decline in $\Phi PSII$, which may thus be attributed to photoinhibition. Species means for traits are provided in Table 2.5 and ANOVA results in the Supplementary materials 7.1. Pairwise p-value comparisons between species, for selected traits, are plotted in Supplementary figure 7.16.

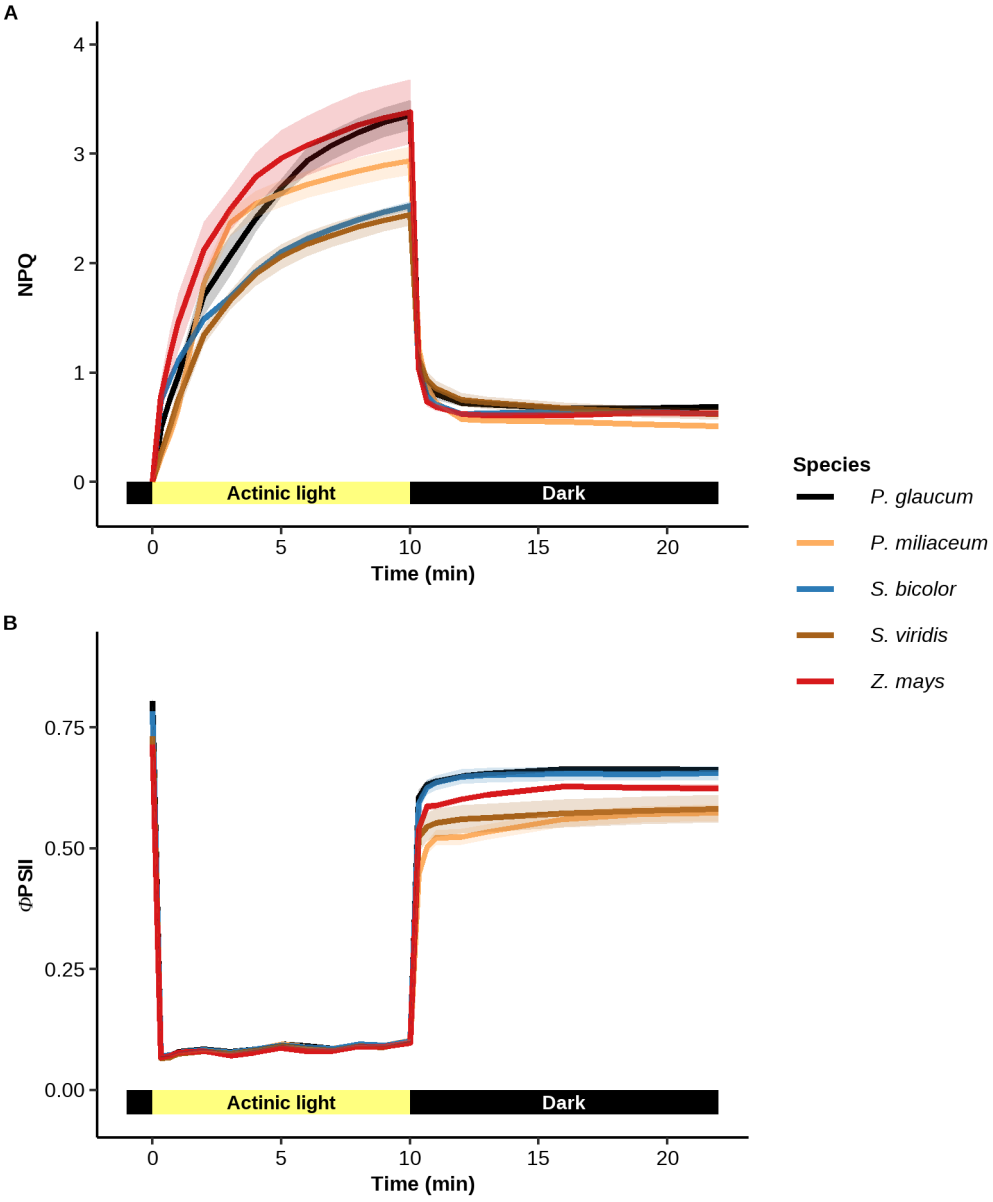

Figure 2.5: Chlorophyll fluorescence traces of five C_4 species during a short term high light treatment, followed by a dark period. **A**, Nonphotochemical quenching (NPQ). **B**, Photosystem II operating quantum efficiency ($\Phi PSII$). Lines are species means and shading is +/- SE of the mean. $n = 4$.

Table 2.5: Estimated marginal means of NPQ kinetic trace parameters for five C_4 species

Species	Fv/Fm	NPQ induction k (min^{-1})	Maximum NPQ	NPQ relaxation k (min^{-1})	$\Phi PSII$ recovery k (min^{-1})	PI
Z. mays	0.71 ± 0.01	0.61 ± 0.07	3.39 ± 0.16	6.09 ± 0.62	5.85 ± 0.48	1.03 ± 0.01
P. miliaceum	0.72 ± 0.01	0.41 ± 0.07	2.94 ± 0.16	3.51 ± 0.62	4.10 ± 0.48	0.91 ± 0.01
P. glaucum	0.80 ± 0.01	0.34 ± 0.07	3.36 ± 0.16	6.04 ± 0.62	7.46 ± 0.48	0.93 ± 0.01
S. viridis	0.73 ± 0.01	0.38 ± 0.07	2.45 ± 0.16	3.94 ± 0.62	7.00 ± 0.48	0.93 ± 0.01
S. bicolor	0.78 ± 0.01	0.54 ± 0.07	2.53 ± 0.16	4.28 ± 0.62	6.81 ± 0.48	0.95 ± 0.01

Note:
Means shown +/- pooled standard error of the mean. $n = 4$. See Supplementary table 7.14 and Supplementary figure 7.16 for ANOVAs and pairwise comparisons of selected traits. k is the rate constant of respective trait, PI is Photoprotection index: see Equations (3.1)-(3.4).

2.3.4 Light use during photosynthesis

Net CO_2 assimilation response to incident light (A/Q_{inc}) was measured for each of the species (Fig. 2.6), to help interpret the results of photodamage assays, described in (Section 2.3.2). A non-rectangular hyberbolic model (Marshall and Biscoe, 1980) was fit to the light response data to derive maximum light saturated rate of CO_2 assimilation (A_{sat}) rate, maximum quantum efficiency of CO_2 assimilation (ΦCO_2), total non-photorespiratory CO_2 respiration in the light (R_d), and model curvature factor (θ). The hyperbolic model generally fit the CO_2 assimilation data well with a low RMSE and R^2 of >0.99 (Fig. 2.7). Some variation in response was apparent; *P. miliaceum* appeared to have the highest photosynthetic capacity and transitioned from the light-limited portion to biochemical-limited portion of the response curve (curve saturation at higher light intensities) at a higher incident light intensity than the other species.

P. glaucum showed the opposite, with the transition from light-limitation happening at a low light intensity, suggesting substantial biochemical limitations to net photosynthesis. The other species fell between these extremes. A_{sat} differed strongly but not significantly between species ($p = 0.13$, linear mixed-effect model), with *P. miliaceum* (27.44 μmol m^{-2} s^{-1}) and *S. viridis* (26.80 μmol m^{-2} s^{-1}) being the highest, *P. glaucum* (13.70 μmol m^{-2} s^{-1}) being the lowest, and *Z. mays* (17.58 μmol m^{-2} s^{-1}) and *S. bicolor* (19.03 μmol m^{-2} s^{-1}) falling between. Small differences were also present in ΦCO_2, R, and θ (Table 2.6), but none of the parameters were significantly different between species at $\alpha = 0.05$ (Supplementary table 7.15).

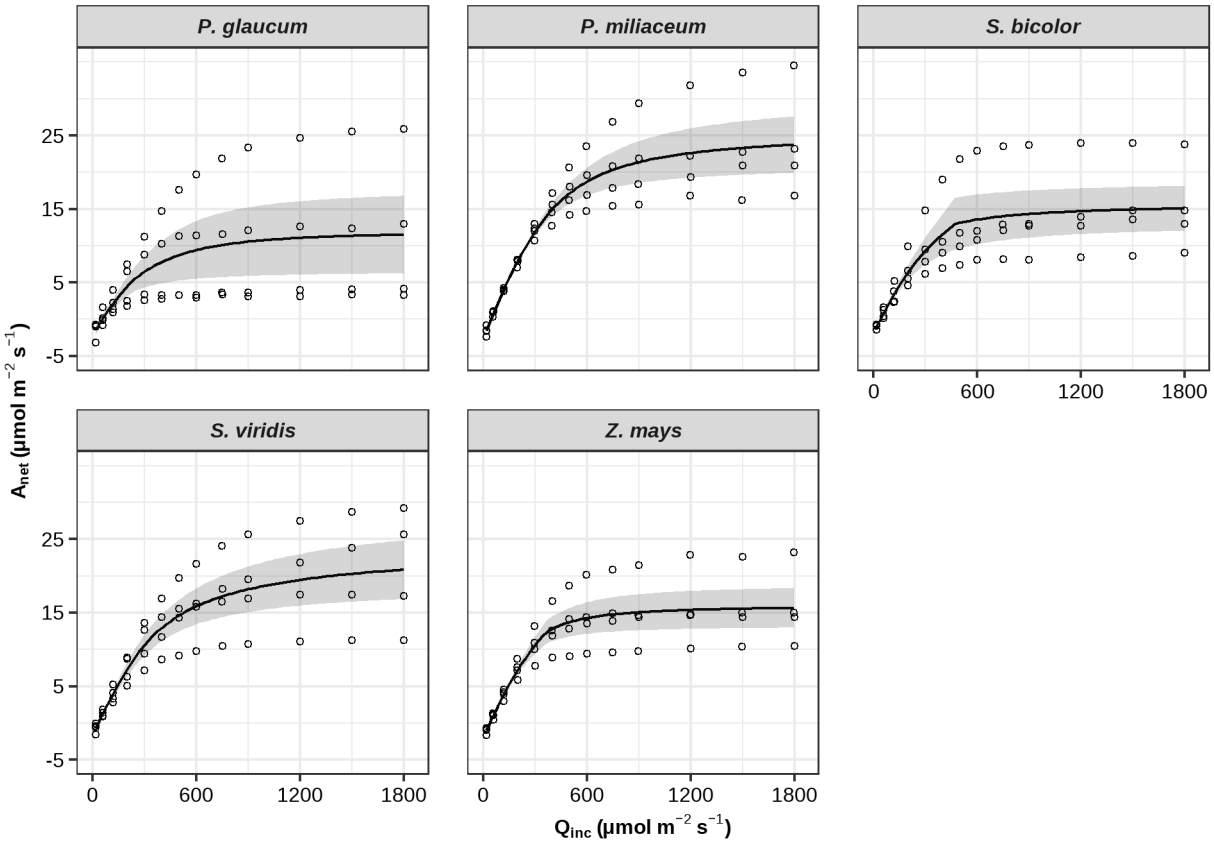

Figure 2.6: Steady-state response of net CO_2 assimilation (A_{net}) to incident photosynthetic photon flux density (Q_{inc}) at ~410 ppm CO_2 concentration, of five C_4 species. Points are raw data from individual plants. Lines are the mean modelled fits of four replicates (n). Error shading is standard error of the mean modelled fits. Species are indicated in panel titles.

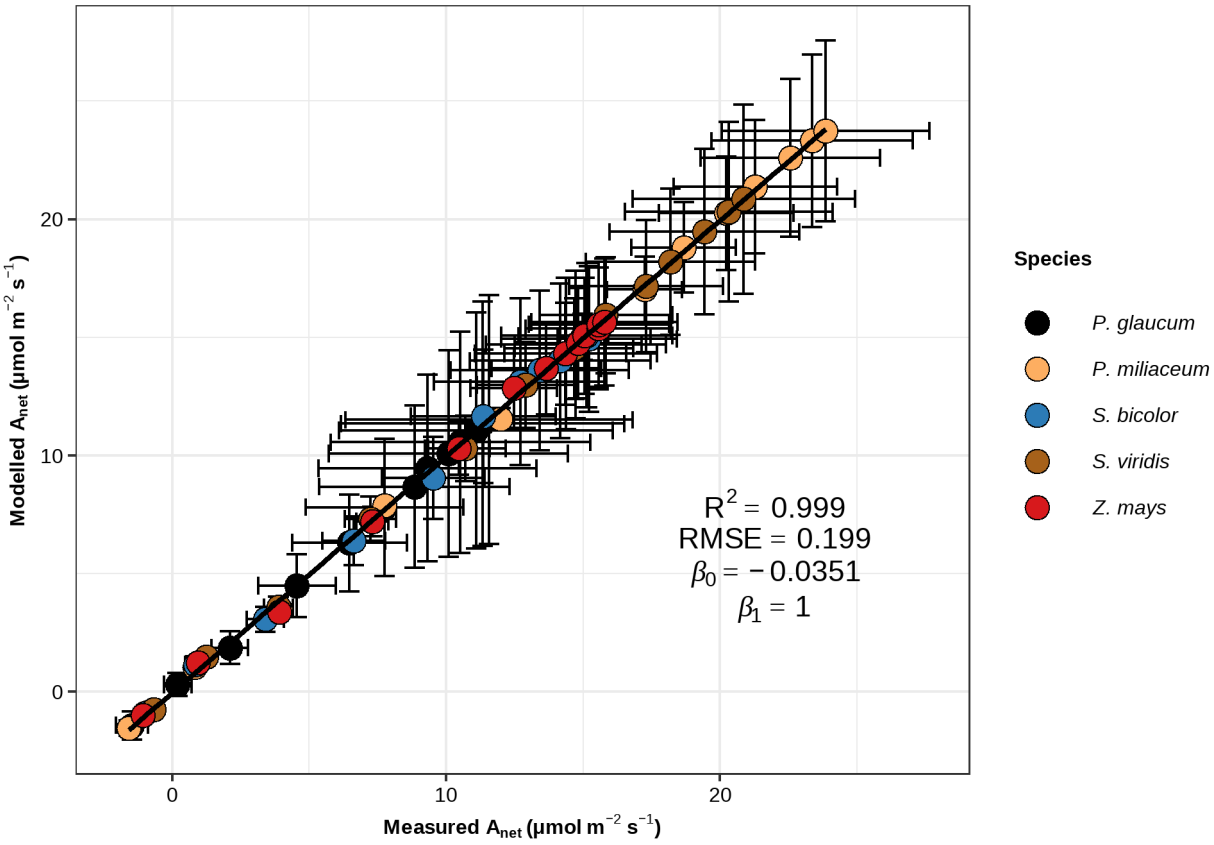

Figure 2.7: Modelled vs measured steady-state net CO_2 assimilation (A_{net}) of five C_4 species. Non-rectangular hyperbolic models were fit to the response of A_{net} to incident photosynthetic photon flux density (Q_{inc}) at ~410 ppm CO_2 concentration. Points are means of measured values and modelled fits of four replicates (n), at 13 Q_{inc} levels. Error bars are standard error of the mean modelled and measured values.

Table 2.6: Estimated marginal means of modelled A/Q_{inc} response curve parameters for five C_4 species

Species	A_{sat} ($\mu mol\ m^{-2}s^{-1}$)	ΦCO_2 ($mol\ mol^{-1}$)	R ($\mu mol\ m^{-2}s^{-1}$)	θ
Z. mays	17.58 ± 5.11	0.05 ± 0.01	2.00 ± 0.45	0.90 ± 0.10
P. miliaceum	27.44 ± 5.11	0.06 ± 0.01	2.71 ± 0.45	0.82 ± 0.10
P. glaucum	13.70 ± 5.11	0.04 ± 0.01	2.24 ± 0.45	0.73 ± 0.10
S. viridis	26.80 ± 5.11	0.05 ± 0.01	1.78 ± 0.45	0.72 ± 0.10
S. bicolor	19.03 ± 5.11	0.05 ± 0.01	1.89 ± 0.45	0.77 ± 0.10

Note:
Means shown +/- pooled standard error of the mean. $n = 4$. No parameters were statistically significantly different between species at $\alpha = 0.05$ (see ANOVA table, Supplementary table 7.15).

2.3.5 Correlations between photoinhibition, photoprotection, and light response traits

An analysis of the Pearson coefficients from a correlation analysis of the photodamage traits (the absolute change in trait value from zero to two hours of treatment), photoprotection traits from the NPQ traces, and A/Q_{inc} response traits revealed a small number of strongly associated variables (Fig. 2.8).

The only photodamage experiment variables which were significantly ($p < 0.05$) related to each other were the change in chlorophyll A:B ratio in the FHL treatment and change in Ri in the SHL treatment, which were strongly positively associated (r = 0.92). SHL chlorophyll a:b ratio was positively correlated with $\Phi PSII$ recovery k (r = 0.91) and negatively with Φ CO_2 (r = -0.89). $\Phi PSII$ recovery k and Φ CO_2 were correlated as well (r = -0.89). Other significant correlations included FHL Ri, which was positively correlated with θ (r = 0.92), and maximum NPQ, which was negatively correlated with FHL MDA (r = -0.98). PI was correlated with SHL MDA (r = -0.93), and A_{sat} was positively correlated with SHL total carotenoids (r = 0.91) and negatively with NPQ relaxation k (r = -0.89).

Full pairwise correlation scatterplots for traits with significant Pearson correlations are shown in Supplementary figure 7.17.

A principle component analysis (PCA) was performed on species means of these traits (Figure 2.9). PCs 1 and 2 accounted for 35.6% and 32.3% percent of the observed variation, respectively. The first component primarily consisted of A/Q_{inc} curve traits and featured large positive effects from θ, Φ CO_2, A_{sat}, and R, as well as FHL Ri, and strong negative effects of $\Phi PSII$ recovery k, SHL chlorophyll a:b ratio, and FHL chlorophyll:carotenoid ratio. The second component primarily constituted NPQ trace traits and was positively influenced by NPQ relaxation and induction k's, maximum NPQ, and PI, and negatively affected by MDA (both light regimes), SHL total carotenoids, and A_{sat}. While the photoprotection (NPQ trace) and light response traits tended to group on PCA axes, the photodamage traits did not appear to show strongly grouped patterns.

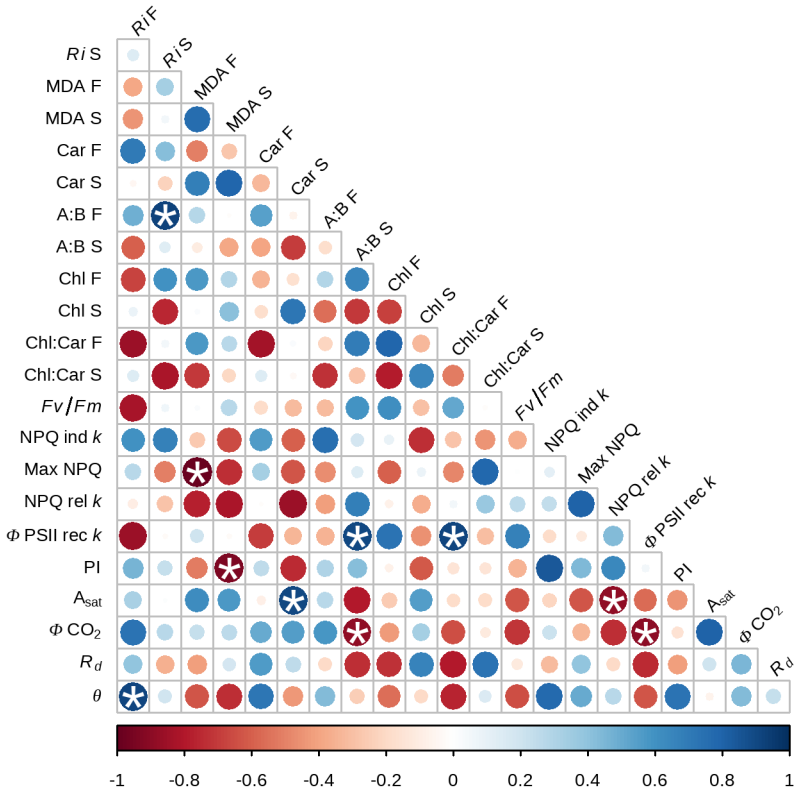

Figure 2.8: Correlogram demonstrating Pearson correlations of photodamage traits, photoprotection (NPQ trace) traits, and light response (A/Q_{inc}) curve parameters. The colour of each circle represents the correlation coefficient of the pairwise interaction. Circles marked with an asterisk denote Holm-method corrected p-values < 0.05. Photodamage traits represent the change in absolute value of the measured parameter from the zero-hour control to two-hour time point and are appended by *S* (steady-state high-light) or *F* (fluctuating high-light). *Ri*, percent relative injury; *MDA*, malondialdehyde abundance; *Car*, total carotenoid content; *A:B*, chlorophyll a:b ratio; *Chl*, total chlorophyll content; *Chl:car*, ratio of total chlorophyll to carotenoids. Traits extracted from NPQ traces include: *Fv/Fm*, maximum PSII quantum efficiency; *NPQ ind k* and *rel k*, rate constants of nonphotochemical quenching (NPQ) induction and relaxation, respectively; *Max NPQ*, maximum NPQ reached during trace; $\Phi PSII$ *rec k*, rate constant of $\Phi PSII$ recovery; and *PI*, photoprotection index. Traits extracted from A/Q_{inc} curves include: A_{sat}, maximum CO_2 assimilation under saturating light; ΦCO_2, quantum efficiency of CO_2 assimilation; R_d, total non-photorespiratory CO_2 respiration in the light; and θ, model curvature factor.

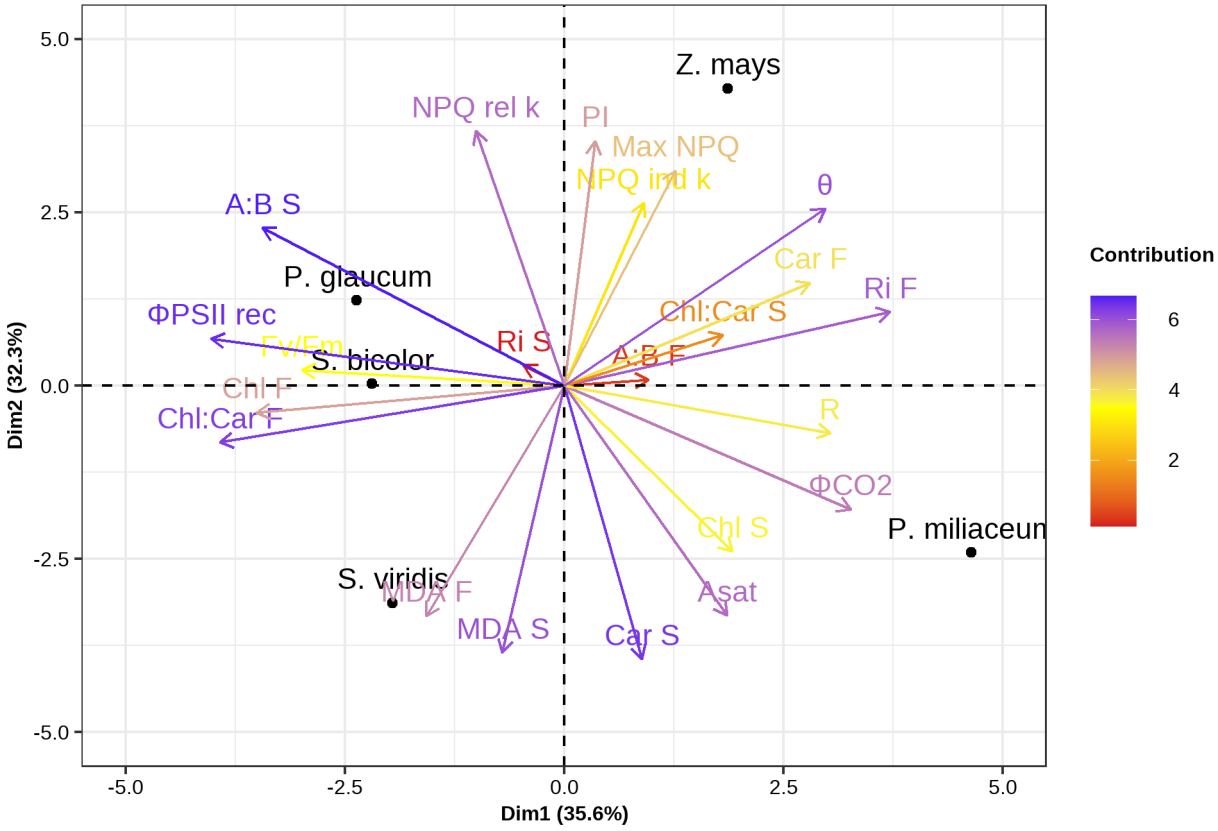

Figure 2.9: Combined principle component analysis biplot and trait factor map for photodamage, photoprotection, and A/Q_{inc} response traits for five C_4 species. Traits are described in the caption of Figure 2.8.

2.4 Discussion

The objectives of this study were to determine whether or not *S. bicolor*'s response to dynamic high light treatments is notably different than that of other C_4 grasses and to enhance our understanding of the differential photoprotective responses of C_4 species to steady-state vs. fluctuating high intensity light. To facilitate meeting those objectives, high-throughput methods were developed to expose leaf samples to variable light treatments and measure the subsequent photodamage responses. The results suggest that in most cases, the high-light response of *Sorghum bicolor* lies between that of the other tested C_4 grasses *Zea mays*, *Setaria viridis*, *Pennisetum glaucum*, and *Panicum miliaceum*. Additionally, it appears FHL treatments cause higher levels of photoinhibition/damage than do SHL treatments, even when the total flux of light incident upon leaves over a given period is equivalent.

2.4.1 High-intensity fluctuating light conditions cause increased photodamage, compared to steady-state high-light treatments

Changes in pigment composition due to the high light treatments were evident in all five species. Substantial reductions in both chlorophyll (Fig. 2.2, A) and carotenoid content (Fig. 2.2, B) were observed during both light regimes over the six-hour treatment period. In both cases, FHL appeared to be more damaging.

There is existing evidence that fluctuating light is less efficient for plant growth and photosynthesis than steady-state light, which could in part be due to increased photoinhibition in fluctuating light conditions. Over five hours of fluctuation between 200 and 1,500 μ mol m^{-2} s^{-1} PPFD, Yamori, Kusumi, et al. (2020) observed substantial drops in CO_2 assimilation, stomatal conductance, and P700 maximum oxidation state in rice, but did not see the same magnitude of effect in a paired steady-state light (1,500 μ mol m^{-2} s^{-1} PPFD) treatment. Additionally, Kubásek et al. (2013) reported lower photosynthetic performance in two C_4 species grown in dynamic light conditions, compared to the same species grown in steady-state light.

However, in their case the reduction in photosynthetic performance was due to sustained dynamic light growth conditions and likely represented acclimatory effects. In the current study, plants were grown in steady-state conditions before being exposed to several-hour long periods of extremely high irradiance, which would suggest short-term photoinhibitory response is at play, rather than sustained acclimatory response. Due to the destructive nature of the assays used in this study it is unclear whether the long term effects of this photoinhibition and photodamage would have manifested as a sustained or permanent drop in photosynthetic efficiency, but long-term effects of short-term extreme light treatment would be interesting to investigate in future studies– there appears to be a dearth of research in this area (discussed in Morales and Kaiser, 2020). Such research may prove relevant to crops, especially under short-term extreme weather conditions (such as drought or heat stress) where the incident light level in excess of that required for photochemistry gets depressed by the compounding abiotic stresses.

MDA abundance during the light treatments corresponded loosely with the observed reduction in chlorophyll and carotenoid contents. As MDA is a product of lipid peroxidation, it is expected to increase concurrently with build-up of ROS. Indeed the MDA response appears consistent with this, and was observed for both light treatments. The only exception was the response of *Z. mays* and *P. glaucum*, which exhibited decreases in MDA over the SHL time course (quite substantially, in the case of *Z. mays*). *Z. mays*, though, started the SHL treatment with a surprisingly high zero-hour control MDA value (which was consistent among biological replicates). Consequently the large drop in MDA between the control and two-hour time point in *Z. mays* may reflect an unintended stress inflicted upon the leaves during sampling or measurement, as the change from two through six hours is not substantially different from that of the other species. In fact, during the SHL treatment the other species appear to have reached maximum MDA accumulation after four hours, which may either reflect somewhat "complete" peroxidation or perhaps indicate a balance reached between production and scavenging processes. This could also be indicative of MDA forming adducts with DNA (Basu, O'Hara,

et al., 1988; Stone et al., 1990), which may reduce absorbance at the measurement wavelength, or of MDA becoming incorporated into fatty acids in a lipid repair cycle (Schmid-Siegert et al., 2016).

Similar results occurred during the FHL treatment; though the species in general exhibited a higher build-up of MDA over control values, only *P. glaucum* showed a fairly large increase after the four hour time point. Similar to the pigment assays, *S. viridis* appeared to be most damaged by FHL compared to the other species.

Ri sustained during the FHL treatment was fairly similar between species, and was higher than during the SHL treatment. *S. bicolor* was in this case a notable outlier, exhibiting large increases in SHL *Ri* after four and six hours, compared to the other species. Some of the variation observed in the FHL photodamage assays could be assigned to differences in growth light and temperature as the plants were grown in a glasshouse over different seasons (Table 2.1); however, this variance should have been minimised by accounting for growth set (period of growth) in the mixed-effect models used to test for differences.

Taken together the five C_4 species generally were more adversely affected by the FHL treatment than the SHL regime with the same total photon load, over the same amount of time. The extent of the aforementioned deleterious effects of fluctuating light to photosynthetic efficiency vary by species, growth environment, and period and intensity of fluctuations (Chazdon and Pearcy, 1991; Pearcy, 1990). The current study demonstrates that in light-adapted C_4 leaves, dynamic high light conditions cause more extreme photodamage (as judged by common ROS damage assays) than do steady-state high-light conditions. Possibly, due to the steady-state light growth environment, photosynthetic machinery of these leaves was not pre-primed for rapid and sustained photoprotection and thus was unable to cope with the frequent changes in energy supply proffered during the FHL treatment. Development under steady-state light may have resulted in leaves with lower levels of photoconvertible violaxanthin (violaxanthin involved in the photoprotective xanthophyll cycle), resulting in subsequent zeaxanthin levels which were inadequate to protect PSII under sudden unfamiliar dynamic light conditions. Plants adapted to

dynamic light conditions tend to have a higher capacity for photoprotection, or an NPQ "memory" (Chazdon and Pearcy, 1991; Demmig-Adams, Winter, et al., 1989; Murchie, Pinto, et al., 2009), the extent of which likely depends on the relative balance of shaded and unshaded intervals, and light intensities experienced during those times. NPQ memory (or lack of) in the steady-light grown plants in this study may have led to inadequate photoprotection, with these plants accordingly showing increased photodamage during the FHL treatment.

2.4.2 Photodamage susceptibility varies between species

In the majority of instances during this study, *S. bicolor* did not appear to be substantially more or less sensitive to several hours of high light than the other species studied, as judged by several common assays used to determine the extent of photoinhibition and photodamage.

Generally pigment loss continued steadily over the entire course of the high-light treatments, though notably *Z. mays* appeared to reach maximum pigment breakdown after four hours, a pattern seen throughout the other photodamage assays as well. This may suggest that *Z. mays* is more sensitive than other C_4 species to photoinhibition and damage, but as *Z. mays* did not exhibit the greatest loss of chlorophyll or carotenoids over the six-hour treatments it could instead reflect a capacity to quickly rebalance light harvesting and repair processes and respond to damaging high-light faster than the other species.

Photosynthetic subtype may play a role in the observed species-level differences. *P miliaceum* is an NAD-ME species, while the other four species feature the NADP-ME C_4 pathway (Brutnell et al., 2010). Biochemical and anatomical differences attributed to distinct C_4 subtypes differentially affect photosynthetic efficiency (Edwards and Walker, 1983; Ehleringer and Pearcy, 1983; Hatch, 1987) and thus could explain photoinhibitory response variation between C_4 species. It also appears that chloroplast light avoidance behaviour may vary between C_4 subtypes, which certainly could differentially affect photoinhibition (Maai et al., 2020; Yamada et al.,

2009). NADP-ME species typically have a higher chlorophyll a:b ratio and ΦCO_2 than NAD-ME species due to differences in ratios of PSII/photosystem I (PSI) content (PSII and PSI have chlorophyll a:b ratios of ~1.2 and 3, respectively: Lichtenthaler and Buschmann, 2001). NAD-ME species show increased bundle-sheath chloroplast PSII content and grana stacking resulting in lower chlorophyll a:b ratios (Edwards and Walker, 1983; Hatch, 1987; Pfündel and Neubohn, 1999). This was reflected in the FHL NAD-ME *P. miliaceum* exhibiting the lowest control-level chlorophyll a:b ratio, though this was not the case for SHL *P. miliaceum*. The other species used in this study are generally considered NADP-ME hence it is unlikely that the atypical photodamage response shown by *Z. mays* in this work could be explained by C_4 subtype alone. *S. bicolor* exhibited the largest drop in total chlorophyll content during the SHL treatment, but otherwise was not notably different from other species in the pigment content assays.

Higher chlorophyll a:b ratio has previously been positively correlated with the amount of convertible violaxanthin in *S. bicolor* and *Z. mays* (Brugnoli et al., 1998). In the current work it does not appear that control-level a:b ratios and the previously demonstrated relationship to the xanthophyll cycle would explain susceptibility to photodamage as *S. bicolor* and *Z.mays* both had initial chlorophyll a:b ratios intermediate of the other species for the FHL treatment (Supplementary fig. 7.12), but showed contrasting photodamage responses to those of the other species. Why the change during treatment in chlorophyll a:b ratios varies between species but not consistently between C_4 subtypes is not immediately clear. The decrease in chlorophyll a:b ratio in *P. miliaceum*, *P. glaucum*, and *S. viridis* during the FHL treatment may suggest more profound damage to reaction centres and proteins rather than LHCs, which would fit with hypotheses and studies suggesting that photoinhibition is generally manifested as damage to protein synthesis and repair processes (Nishiyama et al., 2011; Vass, 2012) rather than directly damaging light harvesting apparatuses, due to carotenoid quenching in LHCs (Frank and Cogdell, 1996). This could also be evidence of damage specific to (the higher chlorophyll a:b ratio) PSI. Damage to PSI is likely exacerbated in fluctuating light

conditions due to an overload of electron transport from PSII before downstream carbon metabolism has acclimated to the immediate light environment (Takagi, Amako, et al., 2017; Takagi, Takumi, et al., 2016; Yamori, Makino, et al., 2016; Yang, Ding, et al., 2019).

Reduction in total carotenoid content during a light treatment time course can also indicate oxidative damage to light harvesting apparatuses, as carotenoids make up a functional component of LHCs (Balevičius et al., 2017; Ort and Yocum, 1996) which are destroyed when acting in a protective capacity (Ridley, 1977). The bulk carotenoid measurement employed in the current work does not allow for distinguishing between different xanthophyll epoxidation states, but the resulting loss of carotenoids should be indicative of a loss of photoprotective capacity. Indeed four of the species experienced a decline in carotenoid content over both light treatments over six hours; however, *Z. mays* stood out, being the only species to *increase* in total carotenoids in both light treatments. It is unclear what might have caused this result, but it is unlikely to be a measurement artefact as both SHL and FHL measurements, using plants grown entirely separately, showed the same result. This may be a further example of *Z. mays* having alternative capacity to re-balance light harvesting, photoprotection, and repair processes when presented with a stressful light environment.

P. miliaceum and *S. viridis* appear to be outliers in total carotenoid content response, showing the strongest decrease compared to the other species over six hours of FHL treatment. Notably, these species also had the highest A_{sat} and ΦCO_2 in the light response curves. These results could indicate species-specific differences in convertibility and fluidity of the carotenoid pool. Perhaps, the high photosynthetic capacity and efficiency of *P. miliaceum* and *S. viridis* is in part due to the light harvesting capacity conferred by their xanthophylls, but due to species differences in LHC composition or binding properties these xanthophylls are more susceptible to ROS damage over extremely stressful periods. Distinct structural and conformational states of carotenoids in LHCs exist for varying levels of light harvesting and photoprotection (Liguori et al., 2017), and it is reasonable to think

there is species-specific variability in these traits, considering the species' ranges of photosynthetic capacities and general leaf structures. These two species also had relatively low maximum NPQ and the slowest NPQ relaxation rate constants during the chlorophyll fluorescence assay, possibly suggesting that some amount of photoprotective or ROS scavenging capacity during stress conditions could be a trade-off with photosynthetic capacity under non-stress conditions.

In common with the other assays, *Ri* varied between species as well. The four-hour "maximum effect" phenomena mentioned previously for the MDA assay was observed in all species except *P. glaucum*. It is unclear why electrolyte leakage would be lower after further light treatment, as presumably the leaf samples could not re-uptake electrolytes in the period of time studied, though this apparent response to stress over time is not unprecedented– Travassos-Lins et al. (2021) observed lower electrolyte leakage after seven hours than after only one hour in a *S. viridis* accession subjected to drought stress, though potentially the between-treatment rehydration period allowed for some recovery. The same group noted a similarly small decrease in electrolyte leakage after seven, compared to five, hours of water deficit treatment in de Souza Rodrigues et al. (2019), but did not suggest an explanation. In the current work, the discrete leaf samples measured at different time points could have been exposed to slightly different light conditions due to their location in the well plate, as groups of leaf discs from all species were grouped in randomised positions based on sampling time point, to facilitate comparisons between species at a given time point. During the FHL treatment, *Z. mays* appeared to be most damaged as indicated by *Ri* increase, contrasting with the MDA assay results. Because the electrolyte leakage assay is not solute-specific, it is possible that changes in relative injury are not solely due to membrane damage (for instance, ammonium accumulation due to chloroplast breakdown could be at play, Rolny et al., 2011). Variation in internal leaf structure could play a role in leakage and explain some of the differences measured between species. *S. bicolor* stood out among the other species during the SHL treatment, with an increase in *Ri* notably higher than the other species (which otherwise responded quite similarly to the

treatment). The only other instance in which *S. bicolor* appeared to have notably different response during SHL was in the total chlorophyll content assay, where *S. bicolor* exhibited the largest decrease during the time course in comparison to the other species. The reason for this is unclear.

While few direct comparisons between these species' stress response exist, Stefanov et al. (2021) observed *S. bicolor* to be less damaged than *Z. mays* by a salt stress treatment; in that study the larger increases in MDA and electrolyte leakage in *Z. mays* were attributed to differences in cyclic electron transport (CET) between the species, with *S. bicolor* apparently being better photoprotected due to increased CET around PSI and potentially more efficient antioxidant activity.

2.4.3 The photoprotective response of *Sorghum bicolor* is not appreciably different than that of other C_4 species

Investigation of NPQ and $\Phi PSII$ kinetics (Section 2.3.3) during a light/dark cycle was used to characterise *S. bicolor*'s capacity for efficient photoprotection in dynamic light conditions, relative to that of other related C_4 grasses. It is worth noting that PSI fluorescence, which is unaccounted for in the measurements here, contributes a non-negligible signal to the measured "PSII" fluorescence values. This is particularly prominent in NADP-ME C_4 species which generally maintain a higher PSI/PSII ratio than C_3 species (Pfündel, 1998), and likely played a part in the depressed Fv/Fm values measured at the beginning of the NPQ traces (Table 2.5).

While *S. bicolor* displayed a fairly low maximum NPQ reached during light induction, its rate constants of NPQ induction, NPQ relaxation and $\Phi PSII$ recovery fell between those of the other species. Brugnoli et al. (1998) observed nearly identical levels of NPQ in fully light-adapted sun leaves of *S. bicolor* and *Z. mays* (approximately 3.5), and only slight differences between shade leaves of the same species with *Z. mays* being slightly lower. The PI parameter calculated based on the drop and subsequent recovery of $\Phi PSII$ is indicative of the relative balance between photoprotective and photoinhibitory NPQ during the trace, and *S. bicolor* fell neatly in the middle of the species' PI values as well.

2.4.4 *Sorghum bicolor* assimilates CO_2 under a range of incident light intensities in a comparable manner to other C_4 species

The light responses of the five species were compared to determine if any obvious differences in CO_2 assimilation response to variation in light level might explain observed variation in the photodamage assay results (Section 2.3.4). Response to increasing levels of incident radiation (Q_{inc}) was shallower and saturating CO_2 assimilation rate (A_{sat}) was lower than expected for *Z. mays*, *S. bicolor*, and *P. glaucum*. Lee et al. (2022) observed higher A_{sat}, ΦCO_2, and total non-photorespiratory CO_2 respiration in the light (R_d), and lower curvature factor (θ) for glasshouse-grown *Z. mays* than were observed for the growth-room grown *Z. mays* in this study. Similar results were seen in Collison et al. (2020), for field-grown *Z. mays*. This is likely due to difference in growth light conditions (Boardman, 1977; D'Odorico et al., 2019) with this study's plants being adapted to a lower growth light level. In the case of Collison et al. (2020), who used a high-yield modern hybrid, this may also reflect accession-related differences. Similarly, (Jaikumar et al., 2021) found higher values of A_{sat} and ΦCO_2 in field-grown *S. bicolor* , even in shade leaves, than those for *S. bicolor* in this study.

P. miliaceum and *S. viridis* exhibited the highest A_{sat} and ΦCO_2 values in this work, but in general did not stand out consistently as more-or-less susceptible to damage during the photodamage assays, suggesting assimilatory response to varying light levels may not be indicative of vulnerability to photodamage. *S. bicolor* did not appear to be an outlier in light use characteristics as judged by the parameters extracted from the A/Q_{inc} curves.

2.4.5 Increased photoprotection during a short period of high light may indicate reduced susceptibilty to longer-term photodamage

Trait values from the photoprotection (NPQ trace), photodamage (MDA, *Ri*, pigment content) and A/Q_{inc} (light response curve) experiments were compared via

Pearson's correlation and principle component analysis to quantitatively examine relationships between the separate experiments. The absolute change in photodamage trait values between the zero-hour control and two-hour time point were used in the correlation analyses, to most closely align with the time frame represented during the photoprotection traces. The positive correlation between θ and FHL Ri suggests that the species here which reach their A_{max} at lower light levels were also more susceptible to increased ROS damage (proxied by electrolyte leakage).

The species with the highest maximum NPQ measured during the chlorophyll fluorescence traces tended to have the lowest initial build-up of MDA during the FHL treatment, which could suggest that photoprotection indeed protected against ROS increase and subsequent damage during a high-light treatment. This is also supported by the strong negative correlation of SHL MDA with PI; species with a higher proportion of Fv/Fm decline explained by photoinhibitory damage, rather than photoprotective NPQ, tended to have a larger increase in MDA of the initial two hours of high-light treatment. That the θ-Ri and NPQ-MDA correlations were not significant and had a lower R^2 for the SHL treatment is consistent with the plants having generally responded less deleteriously to the SHL treatment compared to the FHL treatment.

A_{sat} values were strongly negatively correlated with the NPQ relaxation k. This relationship is not necessarily indicative of faster or slower NPQ kinetics having an effect on assimilatory capacity as the NPQ rate constants are a measure of dynamic response, while A_{sat} was modelled from a series of steady-state light responses. The related fairly strong (though not significant) negative correlation between A_{sat} and max NPQ may suggest that plants with lower capacity for photochemical quenching need to develop a higher capacity for NPQ to get rid of excess excitation energy. These results are in line with the well-established trade-off between photochemistry and photoprotection (Kromdijk, Głowacka, Leonelli, et al., 2016; Murchie and Ruban, 2020). Maximum NPQ also correlated positively with NPQ relaxation rate (though not statistically significantly); thus, a negative correlation between relaxation rate and A_{sat} is unlikely to represent a direct causal relationship.

These correlations are seen in the PCA groupings (2.9) as well. That the photodamage traits don't group together in the PCA confirms that these assays are not measuring the same components of photodamage-related processes in leaves. Their relationship with photoprotection and assimilatory response to light intensity does suggest, though, that at least MDA and *Ri* assays may be representative measurements of the damaging effects of lessened photoprotective capacity. As well, it suggests that several parameters from the chlorophyll fluorescence assay are indicative of susceptibility to photodamage, serving as proof-of-concept for the utility of using this assay in a large-scale screen of chlorophyll fluorescence in a sorghum population (presented in Chapter 3), to identify genetic loci underlying important photoprotection traits.

2.4.6 Conclusion

High-throughput protocols were developed to measure several common photoinhibition phenotypes during high-light treatments for *Panicum miliaceum*, *Pennisetum glaucum*, *Setaria viridis*, *Sorghum bicolor*, and *Zea mays*. The species exhibited often consistent but occasionally contrasting responses to imposed extremely high-intensity fluctuating and steady-state light treatments. It is clear that fluctuating high-light was more damaging to these species than steady-state high-light conditions, which may suggest that dynamic light conditions caused an imbalance in light energy utilisation between photosystems leading to photodamage and reduced photosynthetic efficiency; crop leaves in sunfleck and cloudfleck conditions may suffer reduced productivity because of this. As part of this larger work examining genetic variation in photosynthesis and photoprotection in *S. bicolor*, it is important to understand how photoprotective traits of *S.bicolor* compare to those of other widely grown and studied C_4 species, particularly as the high productivity and water-use efficiency of *S. bicolor* confer the potential to supplant other established crops in a predicted warmer, drier future climate. This work provides evidence that max NPQ, PI and NPQ kinetic traits derived from a short term chlorophyll fluorescence screen under dynamic light are representative of photodamage susceptibility, and

that in general, *S. bicolor* is not an outlier in photoprotective capacity, suggesting knowledge gathered from the NPQ phenotype screen discussed later in this work may be applicable to other closely related species.

3

Revealing the genetic architecture of NPQ in sorghum through a high-throughput screen of dynamic photoprotection

3.1 Introduction

Growth in global agricultural productivity is likely to be substantially diminished by projected increases in climatic variability (Lewis and King, 2017; Pendergrass et al., 2017; Rahman et al., 2022; Rosenzweig et al., 2014), while demand for food, feed, and biofuel in 2050 is projected to require a 50% increase in agricultural productivity over 2012 levels (Food and Agriculture Organization of the United Nations, 2017). Improvement in crop photosynthetic efficiency offers a potential mitigating solution to help sustain productivity in a changing climate (Zhu, Long, et al., 2010). Nonphotochemical quenching (NPQ), a leaf physiological process which dissipates excess absorbed light energy (photoprotection), is an important determinant of photosynthetic efficiency, and enhancements in the efficiency of photoprotective NPQ have been shown to increase yield and biomass in crops under field conditions (De Souza et al., 2022; Kromdijk, Głowacka, Leonelli, et al., 2016). Natural genetic variation in photosynthetic traits, including NPQ, exists within

crop and non-crop germplasm (Ortiz et al., 2017; Sahay et al., 2023; van Rooijen et al., 2017). An understanding of the extent of naturally occurring variation in photoprotection, and identification of the genes underlying this variation could facilitate germplasm improvement via breeding, genomic editing, and transgenic approaches (Flood et al., 2011; Lawson et al., 2012; van Bezouw et al., 2019).
Genome- and transcriptome-wide association studies (GWAS and TWAS, respectively) can be used to identify quantitative trait loci (QTL) which underlie highly polygenic photosynthetic traits (Gui et al., 2023; Tam et al., 2019; Tibbs Cortes et al., 2021), by correlating genomic marker and transcript expression variation with trait phenotype variation; these loci might otherwise be difficult or impossible to identify via traditional mutant studies. Despite their demonstrated usefulness, both methods are complicated by the need to set an appropriate threshold for significance, which needs to maintain sufficient stringency to account for the multitude of parallel tests while keeping the rate of false negatives low. However, since the occurrence of false negatives and positives between both methods can be assumed independent, combining GWAS and TWAS has recently been demonstrated to be a powerful new approach to detecting higher-confidence QTL associated with complex crop physiological traits (Ferguson et al., 2021; Kremling et al., 2019; Lin et al., 2022; Pignon, Fernandes, et al., 2021).

Molecular and reverse genetics-based approaches have successfully identified genes involved in NPQ regulation in model species (Bru et al., 2020; Kasajima et al., 2011; Li, Björkman, et al., 2000), but larger-scale screening of NPQ is a relatively recent pursuit. GWAS have been successful in identifying QTL associated with NPQ in Arabidopsis, rice, soybean, and maize, both in controlled (Rungrat et al., 2019) and field (Herritt et al., 2016; Sahay et al., 2023; Wang, Zhao, et al., 2017) conditions. Screening of NPQ kinetics on field-grown plants can be cumbersome and challenging to accomplish in a manner which is high-throughput enough for the large number of accessions required to discern small-effect loci via GWAS and TWAS. As a result, our understanding of the genes behind natural variation in NPQ under the most relevant conditions is still very limited for several of the world's most important

crops, particularly those with C_4 photosynthetic metabolism, such as *Zea mays* (maize), *Saccharum officinarum* (sugarcane), and *Sorghum bicolor* (sorghum).

Sorghum is grown extensively throughout the world as a food and feed crop (Visarada and Aruna, 2019) and offers high potential as a bioenergy stock (Erickson et al., 2012; Rodrigues Castro et al., 2015). Its high water use efficiency and resiliency to stressors (Hadebe et al., 2017; Maman et al., 2003) makes sorghum an attractive option to potentially supplement or replace other crops in increasingly uncertain climate conditions. Sorghum's adaptability, relatively small diploid genome (~730 Mb), and extensive genetic diversity facilitate highly tractable variant studies to be conducted in diverse climates. These traits, combined with the the available high quality reference genome (McCormick et al., 2018), make an sorghum an attractive resource for understanding genotype-by-environment (GxE) interactions in key C_4 crop traits (Boyles et al., 2019). Uncovering the extent of variability in photoprotective capacity and identifying genes underlying NPQ will prove useful in advancing breeding efforts toward improvement of photosynthetic efficiency in sorghum.

The current study utilises a recently-developed high-throughput method (Gotarkar et al., 2022) to characterize and quantify rates of NPQ induction and relaxation in field-grown plants of 861 biomass sorghum accessions across two years. Most of the measured traits showed moderate broad-sense heritability and their observed variation was underpinned by a complex architecture of many significant small-effect loci. Combined GWAS and TWAS analyses uncovered 110 unique high-confidence candidate genes, which may be used to improve understanding of NPQ regulatory regions in sorghum– thus constituting a valuable asset for efforts toward photosynthetic efficiency improvement in sorghum through breeding and targeted genome editing. The outcomes may also inform genetic gains via similar or transgenic approaches in other closely-related C_4 crops such as maize and sugarcane, given their high degree of genomic synteny (Grivet and Arruda, 2002; Schnable and Freeling, 2011).

3.2 Materials and Methods

3.2.1 Germplasm and field trial design

A sorghum panel composed of 869 genetically diverse biomass accessions (described previously in Dos Santos et al. (2020)) was grown in 2017 and 2019 at the University of Illinois Maxwell Farm (2017) and Energy Farm (2019) Research Sites near Urbana, IL, USA. Accessions were planted in an augmented block design with 960 four-row plots (3 m row length) arranged into 40 columns and 24 rows, in 16 blocks. The incomplete blocks were connected through six common *S. bicolor* check accessions to account for block effects during statistical analysis of phenotyped traits. This study utilised data from 855 and 846 accessions in 2017 and 2019, respectively, after filtering for availability of marker data. 839 accessions were common to both years, with three check accessions (Pacesetter, PI276801, and PI148089) common between years. The panel was planted during on May 31 of both years, with five plots replanted on June 10, 2019 due to poor germination. Temperature, precipitation, and incident light data for the growing periods are available in Figure 3.1.

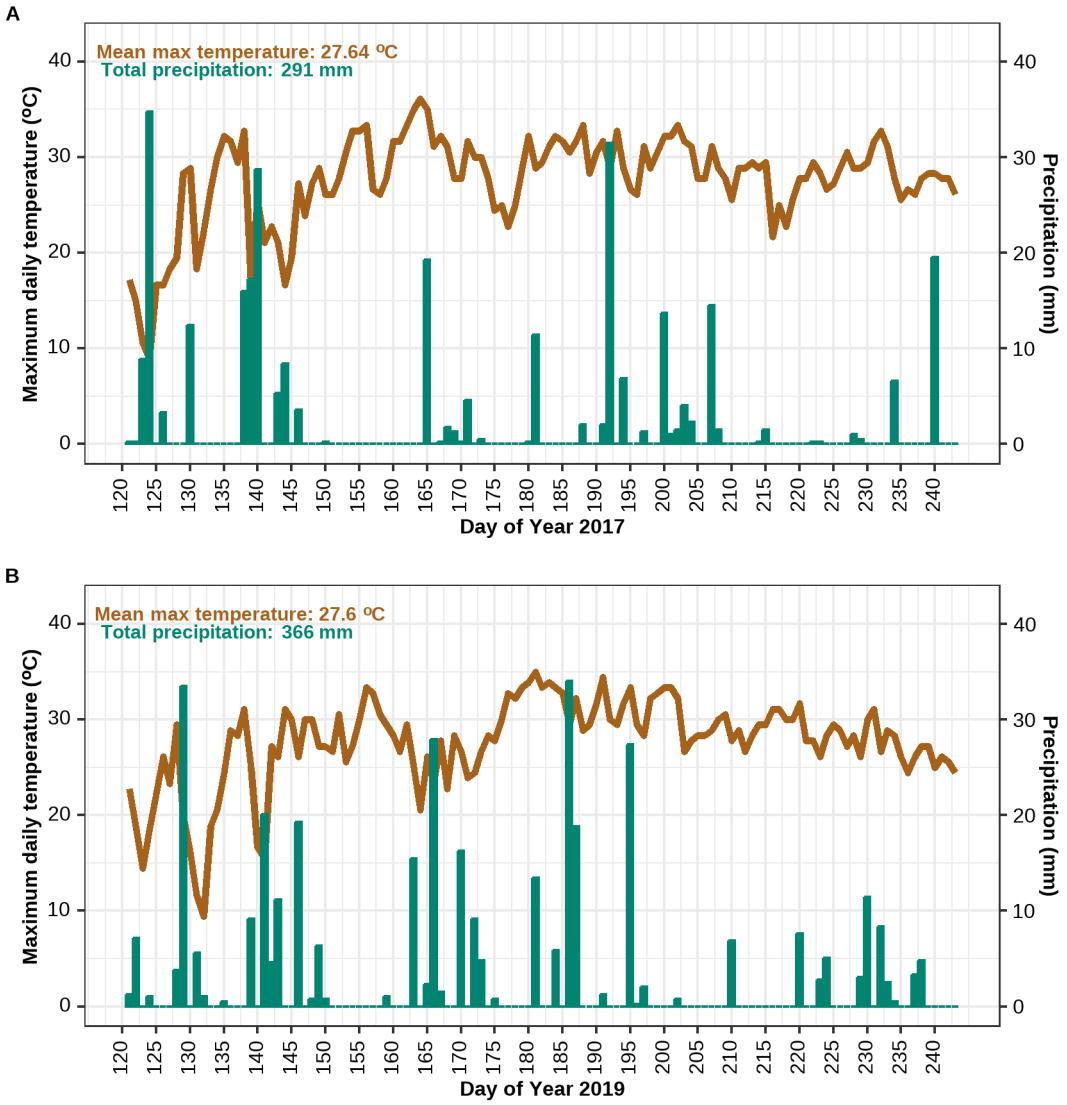

Figure 3.1: Plots of maximum daily temperature (brown lines) and total daily precipitation (green columns) recorded at the Willard Airport weather station (Savoy, IL, USA) during the 2017 (**A**) and 2019 (**B**) sorghum panel growing seasons. Seasonal totals calculated from May 05 through August 31. Planting date: 151. Sampling dates: 206-216 (2017); 203-212 (2019). Data retrieved from www.ncdc.noaa.gov (Station ID GHCND:USW00094870; 3.1 km from Maxwell Farm and 6.73 km from Energy Farm).

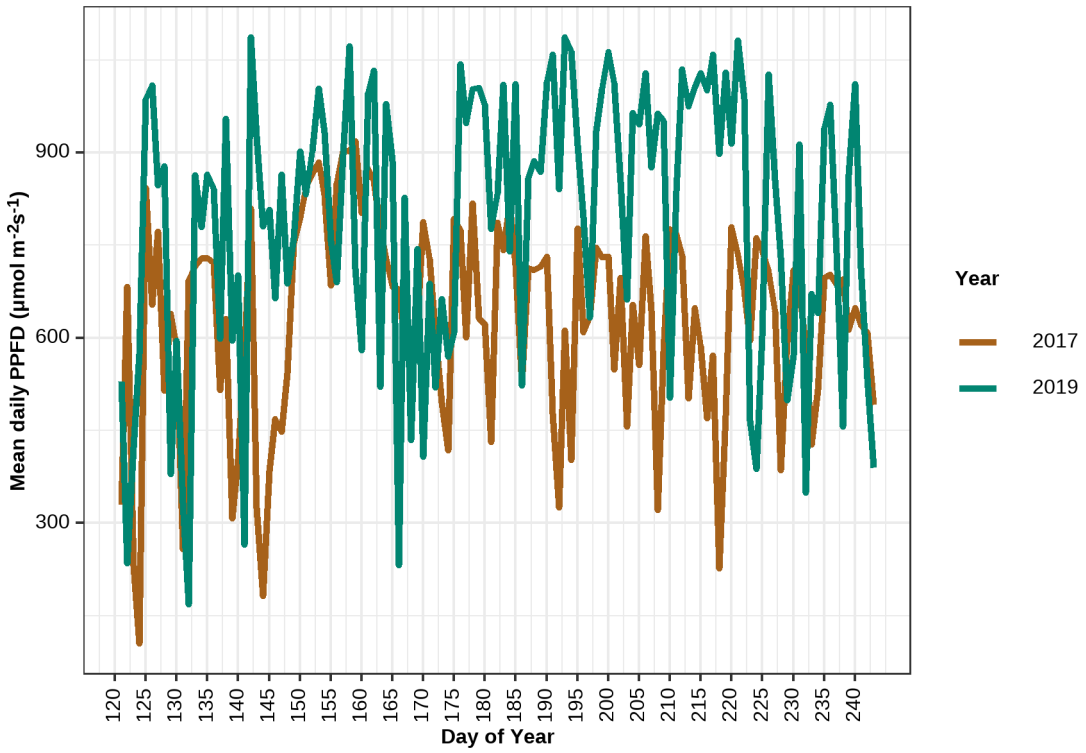

Figure 3.2: Incident light intensity at University of Illinois Energy Farm (Urbana, IL) during 2017 and 2019 growing seasons. Daily means calculated from half-hourly averages of incoming photosynthetically active radiation, for all time periods with photosynthetic photon flux density above five μmol m^{-2} s^{-1}. Planting date: 151. Sampling dates: 206-216 (2017); 203-212 (2019).

3.2.2 Field sampling

Sorghum accessions were screened for photoprotective traits in 2017 by Johannes Kromdijk (University of Cambridge) and Katarzyna Głowacka (University of Nebraska-Lincoln) and in 2019 by Richard Vath and Johannes Kromdijk. Sampling and screening was accomplished via the 96-well plate method detailed in Gotarkar et al. (2022) and Sahay et al. (2023). Plants were sampled by cutting 6 mm diameter leaf discs with a hole punch from the youngest fully expanded leaf as indicated by ligule emergence at time of measurement. Two samples from separate plants in the middle of an inner row from each plot were taken before moving to the next plot. Discs were cut at the midlength of leaves, avoiding the midrib and leaf edge, then placed into clear flat-bottom 96-well plates (Thermo Fisher Nunc clear) with the adaxial side of the leaf facing the plate bottom. A piece of moistened sponge was inserted behind the leaf disc to prevent sample drying. Upon completion of the day's entire set of plots, the process was repeated with samples being taken from plants in the remaining unsampled inner row of each block, providing a total of four biological replicates per accession. Sample plates were wrapped in aluminium foil to prevent light intrusion and buffer temperature changes, then stored in a cooled polystyrene container while further sampling was completed. Four replicates of 128 accessions were sampled per day, between 14:30 and 18:30 local time. After all daily sampling was completed, plates were stored overnight at approximately 20°C in a temperature-controlled lab. Sampling took place in 2017 from July 25 to 28 and August 1 to 4, and in 2019 from July 22 to 25 and July 28 to 31.

3.2.3 Chlorophyll fluorescence screening of photoprotective traits

Discs were imaged on the morning proceeding sampling using a fluorescence imaging cabinet (CFImager, Technologica, Colchester, UK) at the Carl R. Woese Institute for Genomic Biology (Urbana, IL, USA). The 96-well plates were imaged in the order in which they were sampled the previous afternoon, to mitigate temporal bias.

In a dimly lit room, foil was removed from each plate immediately before imaging, and the plate placed into the imaging cabinet. The imaging routine consisted of a dark-adapted measurement of maximum photosystem II (PSII) quantum efficiency (Fv/Fm) followed by periodic fluorescence measurements over 10 minutes at 2,000 μmol m^{-2} s^{-1} photosynthetic photon flux density (PPFD), followed by measurements over 12 minutes of darkness. During the NPQ induction period, fluorescence was measured every 20 seconds for the first minute, then every minute for the remainder of the light period. During the NPQ relaxation period, fluorescence was measured every 20 seconds for the first minute, then every minute for the next three minutes, then every three minutes for the duration of the dark period. Image thresholding and segmentation were performed in MatLab (MATLAB, 2020). Fluorescence values for each disc were taken as the median pixel value of the disc. The distribution of Fv/Fm values for the discs was examined to discern outlier leaf samples. Discs with Fv/Fm values lower than 0.65 were excluded from further analyses.

Using MatLab, exponential models were fit to the NPQ traces of light induction and dark relaxation periods separately, to allow quantitative comparison of NPQ induction (Eq. (3.1)) and relaxation (Eq. (3.2)) rates, as well as the dark recovery of PSII operating efficiency ($\Phi PSII$) (Eq. (3.3)):

$$y = a_{NPQi}(1 - e^{-k_{Ind}t}) \tag{3.1}$$

$$y = a_{NPQr}(e^{-k_{Rel}t}) + b \tag{3.2}$$

$$y = a_{\Phi PSII}(1 - e^{-k_{Rec}t}) + b \tag{3.3}$$

where a_{NPQi}, a_{NPQr} and $a_{\Phi PSII}$ are the initial values of NPQ induction, relaxation, and $\Phi PSII$ recovery during the dark period, respectively; k_{Ind}, k_{Rel}, and k_{Rec} the rate constants of NPQ induction and relaxation and $\Phi PSII$ recovery, respectively (thus a larger number indicates faster kinetics), t is the measurement time point,

and b an offset to account for a non-zero y-intercept term at the beginning of the dark relaxation/recovery period. Modelled curve fits were visually examined for goodness-of-fit, with all traits of non-conforming discs excluded from further analyses. Fig. 3.3 provides a stylised depiction of NPQ trace parameters.

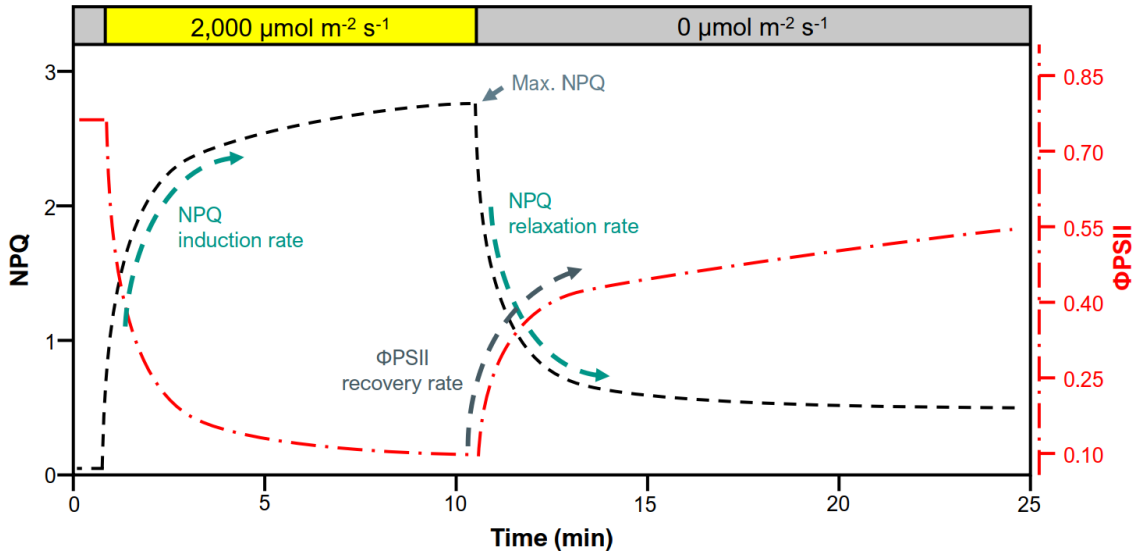

Figure 3.3: Illustrative plot of NPQ induction during a high-light treatment followed by NPQ relaxation and $\Phi PSII$ recovery during a subsequent period of low light (styled after Kaiser et al. (2017)).

Additionally extracted from the NPQ traces were the maximum NPQ reached during the light period and the initial linear slopes of NPQ induction/relaxation. Photoprotection index (PI) was calculated based on the method described by Ruban and Murchie (2012) and implemented in Kromdijk, Głowacka, Leonelli, et al. (2016). Briefly, PI is the ratio between observed Fv'/Fm' (maximum PSII quantum efficiency at a given PPFD) and the calculated Fv'/Fm'_f based on the predictable decrease due to NPQ, during the dark period. The fast-relaxing component of NPQ, qE, was assumed to be relaxed by the end of the 12 minute dark period. Fm' and Fo', the non-dark adapted PSII maximum and minimum fluorescence, respectively, were measured at the final point time point in the dark and compared with Fv'/Fm' to determine the effect of NPQ on Fo', as in Ruban and Murchie (2012). $PI \geq 1$ suggests that the entire reduction in Fv'/Fm' relative to initial Fv/Fm can be attributed to NPQ, while values progressively lower than one suggest a portion of the drop is attributable to photoinhibition (sustained depression of Fv'/Fm'_f due to reaction centre damage). PI was calculated as follows:

$$PI = \frac{\frac{Fv}{Fm_f}}{1 - \left[(1 - \frac{Fv}{Fm})/\left(\frac{Fv}{Fm} + [(1 - \frac{Fv}{Fm})/\frac{1}{1+NPQ_f}]\right)\right]/\frac{1}{1+NPQ_f}} \tag{3.4}$$

where Fv'/Fm'_f and NPQ_f are Fv'/Fm' and NPQ, respectively, at the final dark time point.

3.2.4 Statistical modeling and heritability

For each trait/year combination a restricted maximum likelihood model was fit to each trait using ASReml for R [Butler et al. (2017); this was done by collaborator Samuel Fernandes at the University of Arkansas]:

$$y = 1\mu + Z_1 g + Z_2 s + Z_3 b + e \tag{3.5}$$

where y is the vector of phenotypes; $\mathbf{1}$ (n x 1) is a vector of ones; μ is the trait mean; Z_1 is the incidence matrix associated with the vector of random genotype (accession) effects g, with $g \sim N(0, \sigma_g^2)$ where σ_g^2 is the genetic variance; Z_2 is the incidence matrix associated with the vector of random effect set s, with $s \sim N(0, \sigma_s^2)$ where σ_s^2 is the variance of set; Z_3 is the incidence matrix associated with the vector of random effect block within set b, with $b \sim N(0, \sigma_b^2)$ where σ_b^2 is the variance of block within set; and e is the vector of residuals, with $e \sim N(0, \sigma^2_{AR1xAR1})$ where $\sigma^2_{AR1xAR1}$ is the residual variance with a first-order auto-regressive structure applied to row and column for spatial correction.

Additionally, the two years' data were analysed in a joint model:

$$y = 1\mu + Xt + Z_1 g + Z_2 s + Z_3 b + Z_4 gt + e \tag{3.6}$$

where y is the vector of phenotypes for j environments; $\mathbf{1}$ (n x 1) is a vector of ones; μ is the trait mean; X is the incidence matrix associated with the vector of fixed effect environments t (j x 1); Z_1 is the incidence matrix associated with the vector of random genotype effects within environment g, with $g \sim N(0, \sigma_g^2)$ where σ_g^2 is the genetic variance; Z_2 is the incidence matrix associated with the vector of random effect of set within environment s, with $s \sim N(0, \sigma_s^2)$ where σ_s^2 is the variance of set within environment; Z_3 is the incidence matrix associated with the vector of

random effect block within set within environment b, with $b \sim N(0, \sigma_b^2)$, where σ_b^2 is the variance of block within set within environment; Z_4 is the incidence matrix associated with the vector of random effect genotype interacting with environment gt, with $b \sim N(0, \sigma_{gt}^2)$, where σ_{gt}^2 is the variance of genotype with environment; and e is the vector of residuals, with $e \sim N(0, \sigma_{AR1xAR1}^2)$ where $\sigma_{AR1xAR1}^2$ is the residual variance with a first-order auto-regressive structure applied to row and column for spatial correction. The most appropriate variance-covariance structure to model the residuals was selected based on the Akaike information criterion. Outliers were filtered out based on method two of Bernal-Vasquez et al. (2016).

Best linear unbiased predictions (BLUPs) were obtained separately for each genotype for 2017, 2019, and the combined model, resulting in data for 861 accessions to be used for genomic analysis. Generalised heritability (analogous to broad-sense heritability) for each trait was calculated as

$$H^2 = 1 - \overline{SED}^2 / 2\sigma_g^2 \tag{3.7}$$

where SED is the standard error of the difference in phenotype means (used due to the complex variance structure– see Cullis et al. (2006); Piepho and Möhring (2007)) and σ_g is genetic variance.

Correlations between BLUPs were calculated and visualised with R packages *psych* (Revelle, 2022) and *ggcorrplot2* (Cai et al., 2022).

3.2.5 Genome-wide association

The genotype data set utilized in this study was previously published by Ferguson et al. (2021). GWAS mapping was performed by Samuel Fernandes. Briefly, 100,435 genotyping by sequencing single nucleotide polymorphisms (SNPs) available for 869 individuals (Dos Santos et al., 2020) were imputed using a whole genome re-sequencing panel with 5,512,653 SNPs and 229 accessions from Valluru et al. (2019). Imputation was done with Beagle 4.1 (Browning and Browning, 2016) after filtering out SNPs with a minor allele count less than 20 and pruning SNPs in high LD

($r^2 > 0.9$), using Plink (Purcell et al., 2007) with options "–indep-pairwise 50 10 0.9". The resulting data sets had 450,074 (2017), 450,449 (2019), and 454,087 (joint analysis) SNPs that were used for GWAS. The SNP dataset was used in TASSEL 5 (Bradbury et al., 2007) to obtain the kinship matrix and five principal components (PCs). In both cases, the default options were used. Univariate and multivariate GWAS were conducted in GEMMA (Zhou and Stephens, 2012) using the Q+K model for each trait/year combination. The best number of principal components was decided based on the Bayesian information criterion.

For multitrait GWAS, the following trait combinations (CT) were evaluated:

- CT1: Max NPQ, NPQ induction amplitude, NPQ induction k, NPQ relaxation k
- CT2: NPQ induction amplitude, NPQ induction k, NPQ relaxation k
- CT3: Max NPQ, NPQ induction k, NPQ relaxation k
- CT4: PI, $\Phi PSII$ recovery amplitude, $\Phi PSII$ recovery k

The unpruned dataset was used to calculate pairwise linkage disequilibrium (LD), only including SNPs with an r^2 above 0.2, and using a sliding window maximum size of 500kb and 99,999 SNPs with Plink options "–blocks no-pheno-req no-small-max-span, –blocks-max-kb 500, –blocks-min-maf 0.001.

LD blocks were calculated as proposed in Gabriel et al. (2002). SNPs were considered to be in strong LD if the bottom 90% D-prime confidence interval was greater than 0.70, and the top of the confidence interval was at least 0.98, for a total of 45,311 LD blocks (see Supplementary Table S1) with a median size of 1.178kb containing a median 11 SNPs.

Manhattan plots for visualisation of SNP mapping were based on the "myManhattan" function (`https://github.com/alfonsosaera/myManhattan`) with modifications.

3.2.6 Transcriptome-wide association

Gene expression data (described in Ferguson et al., 2021) from the controlled environment-grown 229 accessions of Valluru et al. (2019) was used to analyse covariance of transcript abundance with photoprotection traits, with the following mapping conducted by Brandon Monier (Cornell University). Transcripts abundance from tissue at the shoot growing point (GP) and base of the third-leaf (3L) was analysed separately for each photoprotection trait/year combination.

Before mapping, ten hidden factors were calculated using probabilistic estimation of expression residual (PEER) factors for each tissue (Stegle et al., 2012). Five PCs were also calculated from prior genotype data. Finally, genes expressed in less than half of the individual lines were removed from each tissue set. After covariate calculation and filtering, a general linear model was fit individually for each NPQ trait and gene expression value using prior PEER factors and PCs as covariates. In addition to mapping each NPQ trait, a multitrait approach was also performed by combining several traits using methods mentioned in the prior section. Mapping was conducted in the R environment (v4.2.2, R Core Team, 2022) using *rTASSEL* (v0.9.28, Monier et al., 2022).

3.2.7 Combined genome and transcriptome-wide analysis

Fisher's combined test (FCT) was performed (by Brandon Monier) utilising the GWAS and TWAS results to generate a fuller picture of the analysis, as GWAS results alone may not represent functionally expressed phenotype variation. The likelihood of true functional genetic variation increases dramatically when multiple types of analyses are performed and co-analysed (Kremling et al., 2019). For each trait/year combination, the nearest gene (by physical location) was assigned to the top 10% of GWAS SNPs by p-value. FCT was then run on the combined top GWAS and all TWAS transcripts using the *metap* package for R (Dewey, 2022).

3.2.8 Candidate gene selection and investigation

Candidate genes (Supplementary Table S8) were selected utilising an ensemble approach (Kremling et al., 2019) which increases the statistical power available for determining genes associated with likely highly polygenic leaf physiological traits. Genes within LD blocks of the top 0.05% of GWAS SNPs (Supplementary Table S3) and the top 1% of genes from each TWAS (Supplementary Table S4) and FCT analysis (Supplementary Table S5), by p-value, were classified as "top genes". Fifteen total analyses were performed for each trait, comprising of 2017, 2019, and joint models for GWAS and 2017, 2019, and joint models for both TWAS and FCT based on GP and 3L tissue.

Top sorghum genes were considered candidates for photoprotection based on: 1), overlapping eight or more individual analyses for a given trait, and 2) overlapping as a top gene in 10 or more separate traits (Supplementary Table S6). Several top sorghum genes were also considered candidates based on manual investigation via direct searches for the sorghum gene ID in Google Scholar and based on their corresponding *Arabidopsis thaliana* (Arabidopsis) orthologue being annotated in TAIR (Berardini et al., 2015) for light response and photoprotection related traits (such as xanthophyll synthesis or nonphotochemical quenching).

Arabidopsis orthologues of sorghum genes which overlapped in more than three separate analyses were identified using *gProfiler2* R package (Kolberg et al., 2020). Panther (`http://pantherdb.org/`) statistical over-representation analysis for biological function was performed on the Arabidopsis gene list against the Arabidopsis reference genome via the *rbioapi* (Rezwani et al., 2022) R package (Supplementary Table S7).

Sorting intolerant from tolerant (SIFT) analysis (Ng and Henikoff, 2003) was performed to investigate the likelihood of coding-region SNPs' contribution to variation in protein function, utilising SIFT scores from a sorghum panel containing 286 of the accessions used in this study (Lozano et al., 2021). Upset plots (Lex

et al., 2014) were produced using the *UpSetR* package (Conway et al., 2014) to aid in visualisation of top gene set overlaps for individual traits.

3.3 Results

3.3.1 Genetically diverse sorghum harbours substantial variation in photoprotection traits

A high-throughput chlorophyll fluorescence screening method was employed to characterise photoprotective trait diversity in a field-grown sorghum panel. NPQ induction and relaxation kinetics were measured in each sorghum accession via the application of a high-light treatment followed by a dark period, allowing for a quantitative comparison of photoprotective capacity across a genetically diverse sorghum population. Substantial variation was observed among sorghum accessions in NPQ traits. The percentage difference between the lowest and highest accessions in maximum NPQ, NPQ induction rate constant, NPQ relaxation rate constant, and rate constant of $\Phi PSII$ recovery were 24%, 115%, 87%, and 63%, respectively, for joint model BLUPs of each trait (Table 3.1 and Figure 3.4).

Table 3.1: Descriptive statistics of photoprotection traits for joint adjusted means (BLUPs) of 861 sorghum accessions

Trait	Description	Mean	Min	Max	H^2
Max NPQ	Maximum NPQ level reached during fluorescence trace	2.80	2.50	3.10	0.52
NPQ ind. slope	Initial linear slope of NPQ induction (min^{-1})	1.29	0.92	1.72	0.58
NPQ rel. slope	Initial linear slope of NPQ relaxation in dark (min^{-1})	-2.68	-3.20	-2.19	0.67
NPQ ind. k	Exponential rate constant of NPQ induction (min^{-1})	0.58	0.39	0.84	0.67
NPQ rel. k	Exponential rate constant of NPQ relaxation in dark (min^{-1})	5.09	3.68	6.87	0.44
NPQ_f	NPQ at final dark time point	0.89	0.69	1.12	0.47
$\Phi PSII$ rec. k	Exponential rate constant of $\Phi PSII$ recovery in dark (min^{-1})	5.08	3.97	6.48	0.43
PI	Photoprotection index	0.82	0.76	0.85	0.36
Fv/Fm	Maximum $PSII$ quantum efficiency	0.75	0.73	0.77	0.30

Note:
Trait calculations detailed in section 3.2.3 and illustrated in Fig. 3.3. H^2 is heritability.

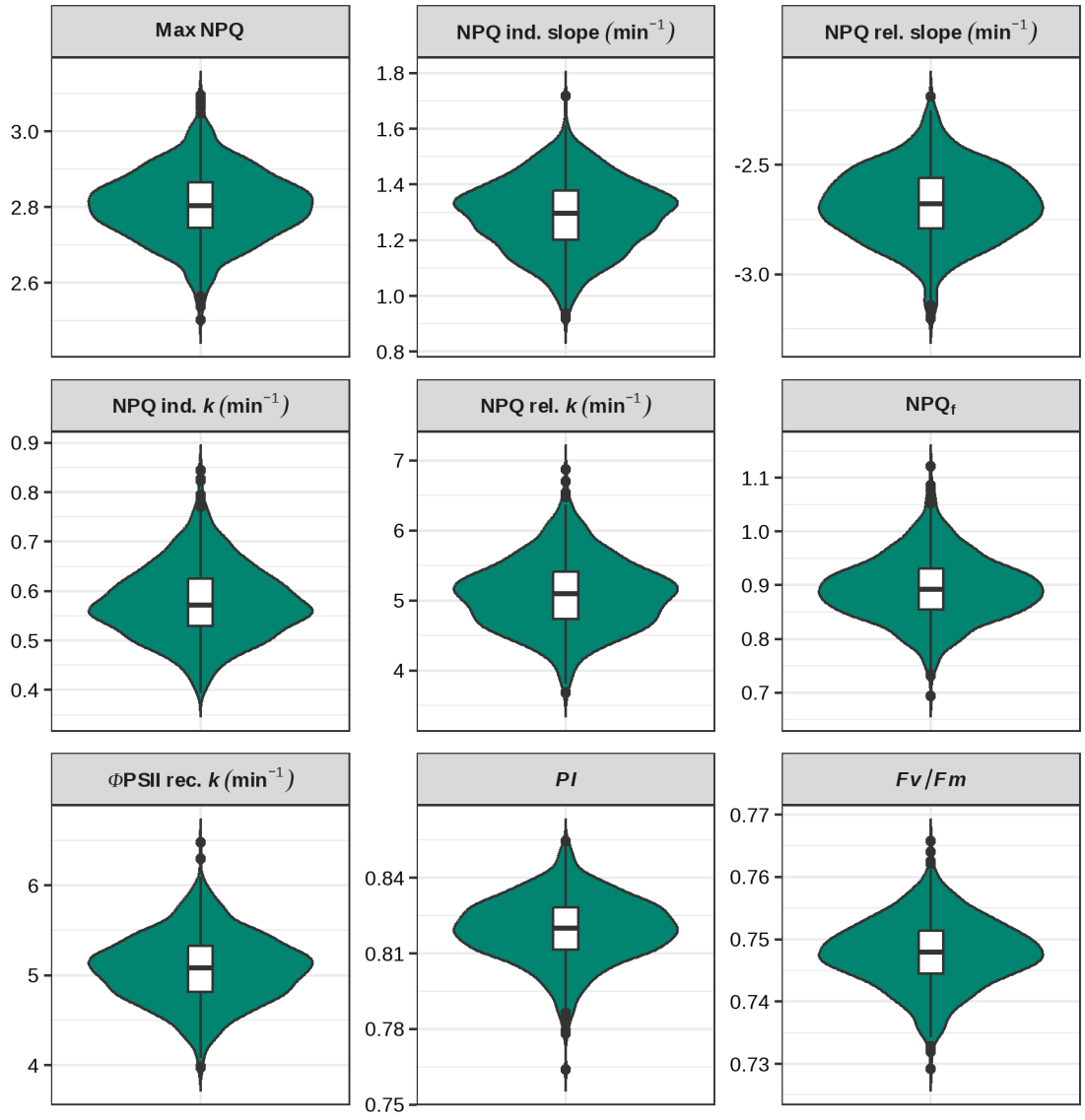

Figure 3.4: Violin plots of variation in adjusted genotype means of NPQ trace parameters for the joint model. Internal box plot edges represent first and third quartiles. Points represent outliers beyond 1.5 times the interquartile range. The solid line within the boxes indicates the median.

While the range of maximum NPQ remained similar in both 2017 and 2019, NPQ kinetic and light-use efficiency traits varied considerably over the two years (Fig. 3.5), potentially due to weather differences between both years (Figures 3.1 and 3.2). NPQ induction in 2019 was slower across the panel, with a slope of 1.19 min^{-1} and k of 0.53 min^{-1}, compared to a slope of 1.41 min^{-1} and k of 0.62 min^{-1} in 2017. NPQ relaxation was faster in 2019, with a median slope of -2.91 min^{-1} and k of

6.19 min^{-1}, compared to a slope of -2.44 min^{-1} and k of 3.97 min^{-1} in 2017. The rate of $\Phi PSII$ recovery was also faster in 2019, with a median value of 5.66 min^{-1} compared to 4.47 min^{-1} in 2017. These differences may relate to inter-year variation in susceptibility to photoinhibition during the light treatment, as the median PI in 2019 was 0.85 compared to 0.79 in 2017. Pairwise scatterplots of 2017 and 2019 BLUPs are shown in Figure 3.12. Accession values for all traits were weakly to moderately correlated between years with Pearson's r values ranging between 0.21 and 0.45, but correlations were strongly significant in all cases, suggesting that accession ranks were generally maintained despite fairly high genotype-environment interaction effects on photoprotective traits.

Heritability (H^2) of NPQ traits was moderate to moderately high (Figure 3.11), with joint model H^2 for maximum NPQ at 0.52, NPQ induction and relaxation slopes at 0.58 and 0.67, respectively, and NPQ induction and relaxation k at 0.67 and 0.44, respectively. Light use efficiency traits and PI were less heritable, with joint BLUP H^2 values of 0.43 and 0.30 for $\Phi PSII$ recovery k and Fv/Fm, respectively, and 0.36 for PI. Values of H^2 for 2017 and 2019 models were consistent across years for most traits, excepting PI and Fv/Fm which were notably higher in 2019 (0.60 for PI and 0.45 for Fv/Fm) than in 2017 (0.47 for PI and 0.37 for Fv/Fm).

Correlations between traits were consistent between years (Figure 3.7) and thus are effectively represented by correlations between joint model BLUPs (Fig. 3.6). Maximum NPQ tended to correlate with slower NPQ induction and faster relaxation kinetics– significant ($p < 0.05$) correlations were observed between joint BLUP max NPQ and NPQ induction k (Pearson's r = -0.33), initial relaxation slope (r = -0.74), and relaxation k (r = 0.13). NPQ relaxation k was also strongly positively correlated with ΦPSII recovery k (r = 0.85), suggesting the short high light treatment did not cause substantial reaction centre damage which might otherwise disrupt the expected strong relationship between ΦPSII and NPQ. Initial slopes of NPQ induction and relaxation were significantly correlated with their corresponding rate constants k, at r = 0.88 for induction and r = -0.48 for relaxation. Intriguingly,

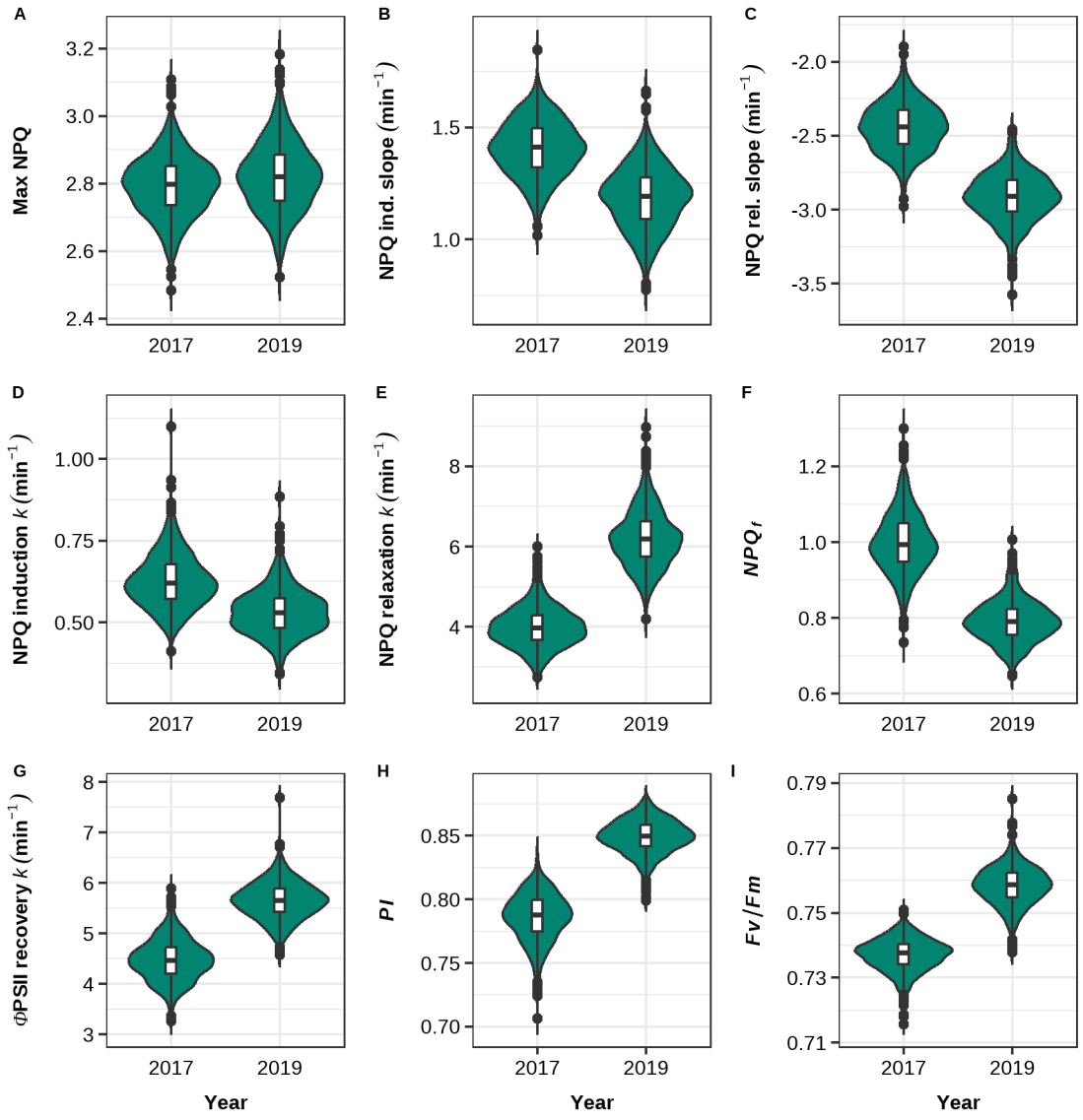

Figure 3.5: Violin plots of variation in adjusted genotype means of NPQ trace parameters for 2017 and 2019 field seasons. Internal box plot edges represent first and third quartiles. Points represent outliers beyond 1.5 times the interquartile range. The solid line within the boxes indicates the median. A, maximum NPQ level reached during the trace; B, linear slope of NPQ induction; C, linear slope of NPQ relaxation; D, rate constant k of NPQ induction; E, rate constant k of NPQ relaxation; F, residual NPQ at end of dark relaxation period; G, rate constant k of $\Phi PSII$ recovery; H, photoprotection index; I, Fv/Fm.

accessions with a higher NPQ induction k tended to have a slower (less negative) initial relaxation slope ($r = 0.25$). Accessions with lower PI (more photoinhibited) tended to exhibit a higher NPQ_f (r = -0.72), suggesting the PI calculation is indeed representative of the degree of photoinhibition sustained during the light

treatment.

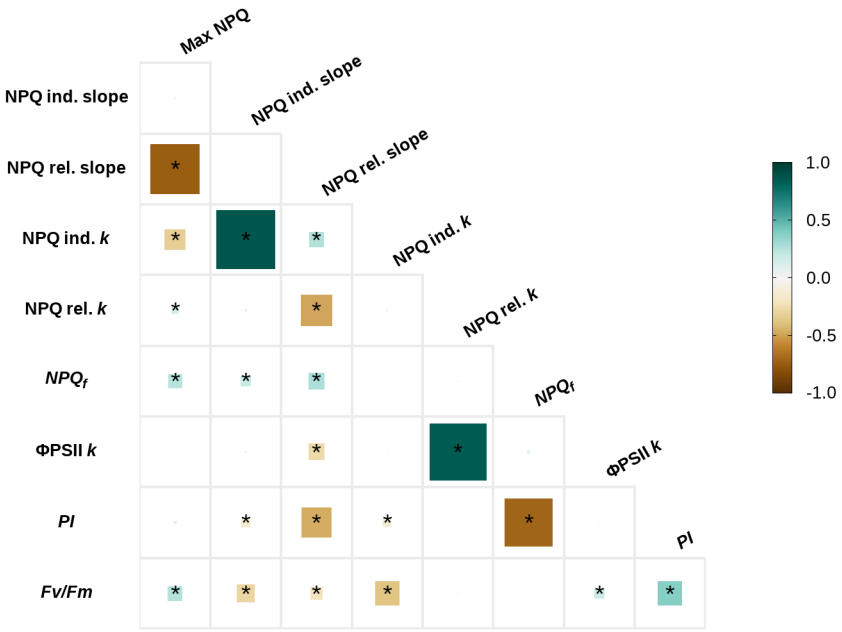

Figure 3.6: Correlogram demonstrating Pearson correlations between joint model BLUPs of photoprotection traits of 839 sorghum accessions. The colour and size of each square represent the correlation coefficient of the pairwise interaction. Squares marked with an asterisk denote Holm-method corrected p-values < 0.05. Traits are described in Table 3.1.

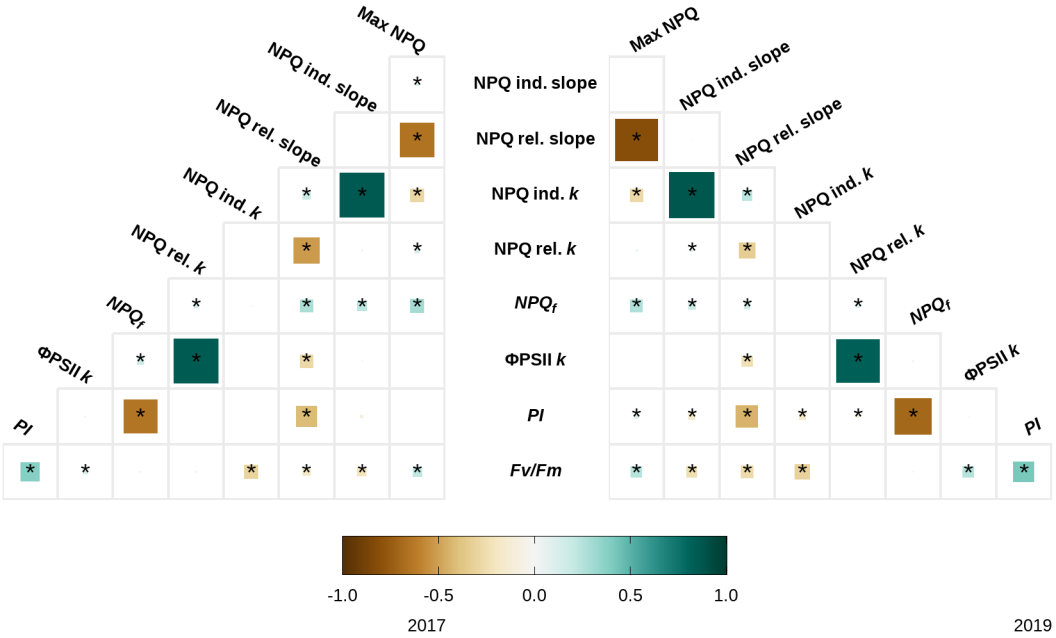

Figure 3.7: Correlogram demonstrating Pearson correlations of photoprotection trait BLUPs of 839 sorghum accessions, measured in 2017 and 2019. The colour and size of each square represent the correlation coefficient of the pairwise interaction. Squares marked with an asterisk denote Holm-method corrected p-values < 0.05. Max NPQ, maximum NPQ level reached during the trace; NPQ ind./rel. slopes, initial linear slopes of NPQ induction and relaxation, respectively; NPQ ind./ rel. k, exponential rate constants of NPQ light induction and dark relaxation, respectively; NPQ_f, NPQ at final dark time point; $\Phi PSII$ rec. k, Exponential rate constant of $\Phi PSII$ recovery in dark; PI, photoprotective index; Fv/Fm, Maximum $PSII$ quantum efficiency.

3.3.2 Genome- and transcriptome-wide analyses uncover genes associated with photoprotection

Marker-trait association (MTA) analyses were performed using the BLUPs from 2017, 2019, and combined year (joint) models, to identify sorghum genomic regions associated with variation in photoprotective traits. For each model/year

combination, MTA analyses were conducted using the sorghum SNP set (GWAS) and transcript expression data (TWAS). Genes in LD with the top 0.05% of GWAS SNPs (Supplementary Table S3), and the top 1% of TWAS genes (Supplementary Table S4) were brought forward as "top" genes. Additionally, genes in LD with the top 10% of GWAS SNPs (as ranked by Bonferroni-adjusted p-value) and their corresponding transcript expression levels were analysed for covariance with the NPQ traits via Fisher's Combined Test (FCT), with the top 1% of genes by Bonferroni-adjusted p-value brought forward as top FCT results (Supplementary Table S5).

Arabidopsis orthologues were identified for the collated top gene results (Supplementary Table S6); GO term-enrichment was run on orthologues of sorghum genes which overlapped in three or more analyses (1,035 unique Arabidopsis genes) to determine whether specific GO biological functions were non-randomly associated with sorghum NPQ traits (Supplementary Table S7). Significantly (greater than two-fold of expected) enriched biological processes from the Arabidopsis GO analysis were not obviously related to photoprotective processes. The highest-fold GO enrichment process (4.04) was *response to sucrose* (GO:0009744) with 11 Arabidopsis orthologues appearing in top sorghum genes. *Alpha-amino acid biosynthetic process* (GO:1901607) and *small molecule catabolic processes* (GO:0044282) were next highest with 2.87 fold enrichment/19 genes and 2.40 fold enrichment/23 genes, respectively. Of the 52 unique sorghum genes overlapping more than three analyses and orthologous to Arabidopsis genes in significantly enriched GO bins, four were implicated in response to light stimulus, one in response to light intensity, one in photosynthesis, one in blue light response, and one to absence of light (TAIR, Berardini et al., 2015).

An intersection-based approach was used to produce a list of sorghum photoprotection candidate genes (Figure 3.8). As an example for a single trait, maximum NPQ may be reasonably representative of an accession's photoprotective capacity, particularly as it tended to correlate significantly with both NPQ induction and relaxation k. The joint max NPQ GWAS indicted four SNPs with an FDR-adjusted p-value below 0.05, spanning a region of less than 20 kilobases within two LD

blocks containing 74 genes (Figure 3.9 **A**), with a SNP at this locus investigated further in chapter four. When combined with TWAS results (Figure 3.9 **B&C**) for the joint analysis, the FCT tests in both GP and 3L tissues (Figure 3.9 **D&E**) strengthened this association with several genes in the same locus comprising some of the highest-confidence genes in the analysis. This region was also substantially enriched in the joint FCT of CT 1, the multivariate analysed combination of max NPQ, NPQ induction amplitude, and NPQ induction and relaxation k. A number of top genes overlapped in multiple joint-model max NPQ analyses (Figure 3.10), with five genes overlapping in three separate analyses and 93 genes overlapping in two separate analyses.

Manhattan and Upset plots of all MTAs are available in the supplementary materials.

Seventy genes overlapped in eight or more model analyses for individual traits, considered progressively higher-confidence based on total number of overlaps. The 16 genes overlapping in nine or more analyses are summarised in Table 3.2.

Many top genes were common to multiple traits, with nearly 30% of top genes overlapping three or more trait top gene lists. The 37 genes which overlapped 10 or more traits were considered candidates; Table 3.3 summarises the highest-confidence portion of those. The multi-model/single trait and multitrait overlap thresholds together resulted in 104 unique candidates (Supplementary Table S8). An additional six unique genes were recorded as candidates based on overlapping three or more traits and being either annotated in TAIR for light-response related function or noted as a carotenoid biosynthesis prior in Ortiz et al. (2017).

Several candidates are orthologous to Arabidopsis genes which feasibly contribute directly or indirectly to photosynthetic efficiency and photoprotective traits in dynamic light conditions. Sobic.006G152000 overlapped in 11 separate analyses for NPQ induction slope and k, eight analyses for CT3 (max NPQ, NPQ induction k, and NPQ relaxation k) and several analyses for the other combined traits. The Arabidopsis orthologue (*LCD1*) of this gene is involved in palisade mesophyll cell

density (Barth and Conklin, 2003). Sobic.003G418000, which overlapped 11 analyses for the NPQ relaxation intercept term, has been suggested to alter strigolactone biosynthesis in response to parasite stress in sorghum (Bellis et al., 2020), and is orthologous to Arabidopsis LBO1, involved in strigolactone biosynthesis (Brewer et al., 2016). Similarly, Sobic.006G060100 (overlaps nine analyses for NPQ induction k) is orthologous to Arabidopsis AT5G58530, a glutaredoxin (GRX)-like protein.

Sobic.009G187300, with 10 overlaps for NPQ relaxation rate constant and the correlated $\Phi PSII$ recovery rate constant, is an orthologue of Arabidopsis AT3G59840, an allyl alcohol dehydrogenase-like protein has been implicated in regulation of ATP synthase activation/deactivation kinetics (Gong et al., 2006). Sobic.001G185600, overlapping nine analyses for NPQ_f, is orthologues to a MATE efflux family protein in Arabidopsis (AT1G11670), which has been implicated in transcriptional regulation of light induction.

Of the multiple-trait overlap candidates, Sobic.005G154850 was a top gene in 14 traits analysed, and is orthologous to AT1G79750 (NADP-ME4). Sobic.001G189300, orthologous to an AMP-dependent synthase and ligase family protein, overlaps 13 top gene sets. This jasmonic acid precursor has been implicated in stress response in Arabidopsis (Bonsegna et al., 2005). Notably, Sobic.006G128300 overlapped as a top gene in seven separate analyses and has been included in the candidate gene priors due to its orthology with the Arabidopsis *NPQ6* gene, a YCF-20 family gene involved in energy-dependent quenching (Jung and Niyogi, 2010). Additionally, Sobic.008G021000 was found to overlap four top gene analyses for both NPQ relaxation k and $\Phi PSII$ recovery k; this gene was annotated in Ortiz et al. (2017) as PIF4, a carotenoid biosynthesis protein.

SIFT analyses of coding sequence SNPs within candidate genes was performed to uncover potential causal SNPs which may play a part in photoprotective regulation (Supplementary Table S9). Of the 110 candidate genes, 99 contained at least one predicted nonsynonymous substitution (encodes a different amino acid than the reference allele), further increasing confidence in these genes as causal actors in sorghum photoprotection.

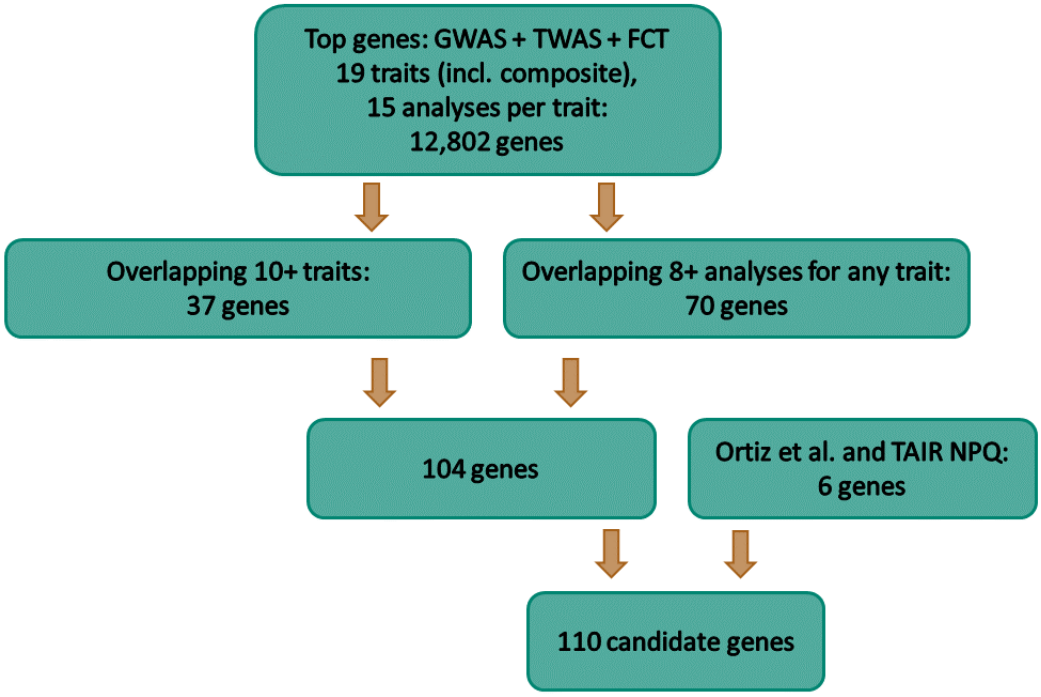

Figure 3.8: Workflow of sorghum candidate gene selection based on top 0.05% of GWAS and top 1% of TWAS and FCT genes overlapping multiple traits and analyses, and based on manual investigation.

Table 3.2: Top sorghum genes overlapping in nine or more analyses for various NPQ kinetic traits

Analyses overlapped	Gene	Traits	Arabidopsis description
11	Sobic.001G255300	Fv/Fm	
	Sobic.003G418000	NPQ rel. intercept term	2-oxoglutarate (2OG) and Fe(II)-dependent oxygenase superfamily protein
	Sobic.006G152000	NPQ ind. k & NPQ ind. slope	reticulata-like protein, putative (DUF3411)
	Sobic.008G142400	NPQ ind. slope	
10	Sobic.002G277900	$\Phi PSII$ rec. amplitude	PLC-like phosphodiesterases superfamily protein
	Sobic.009G187300	$\Phi PSII$ rec. k & NPQ rel. k	allyl alcohol dehydrogenase-like protein
	Sobic.010G093800	NPQ ind. k	
10 & 9	Sobic.004G161800	NPQ ind. slope & NPQ ind. k	
9	Sobic.001G185600	NPQ_f	MATE efflux family protein
	Sobic.001G269000	NPQ ind. slope	Glycosyl hydrolase family 38 protein
	Sobic.001G496900	NPQ ind. amplitude	DNAse I-like superfamily protein
	Sobic.002G021900	$\Phi PSII$ rec. k & NPQ rel. k	wall associated kinase-like 6
	Sobic.004G250300	NPQ rel. amplitude	Eukaryotic aspartyl protease family protein
	Sobic.006G060100	NPQ ind. k	Glutaredoxin family protein
	Sobic.009G054900	NPQ rel. amplitude	Ca2+-activated RelA/spot-like protein
	Sobic.009G187100	NPQ rel. k	

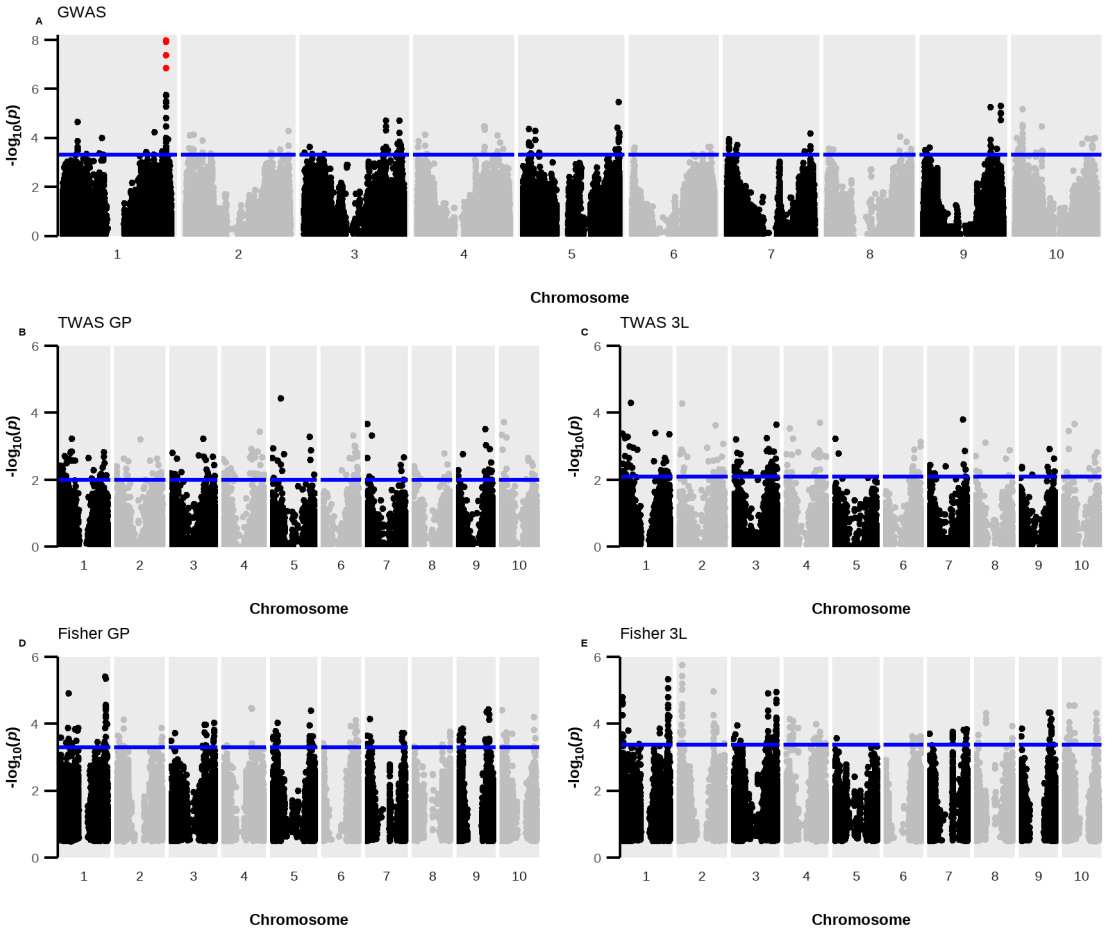

Figure 3.9: Chromosome mapping (physical location) for SNPs and genes associated with maximum NPQ combined 2017/2019 adjusted means. **A**, GWAS; **B**, TWAS in GP tissue; **C**, TWAS in 3L tissue ; **D**, Fishers combined test from GP tissue; **E**, Fishers combined test from 3L tissue; Blue lines indicate threshold of SNPs in top 0.05% (**A**) or genes in top 1% (**B-E**) of -$\log_{10}$ p values. SNPs in plot **A** with an FDR-adjusted p-value <0.05 are highlighted in red. TWAS and FCT gene positions plotted as midpoint of each gene.

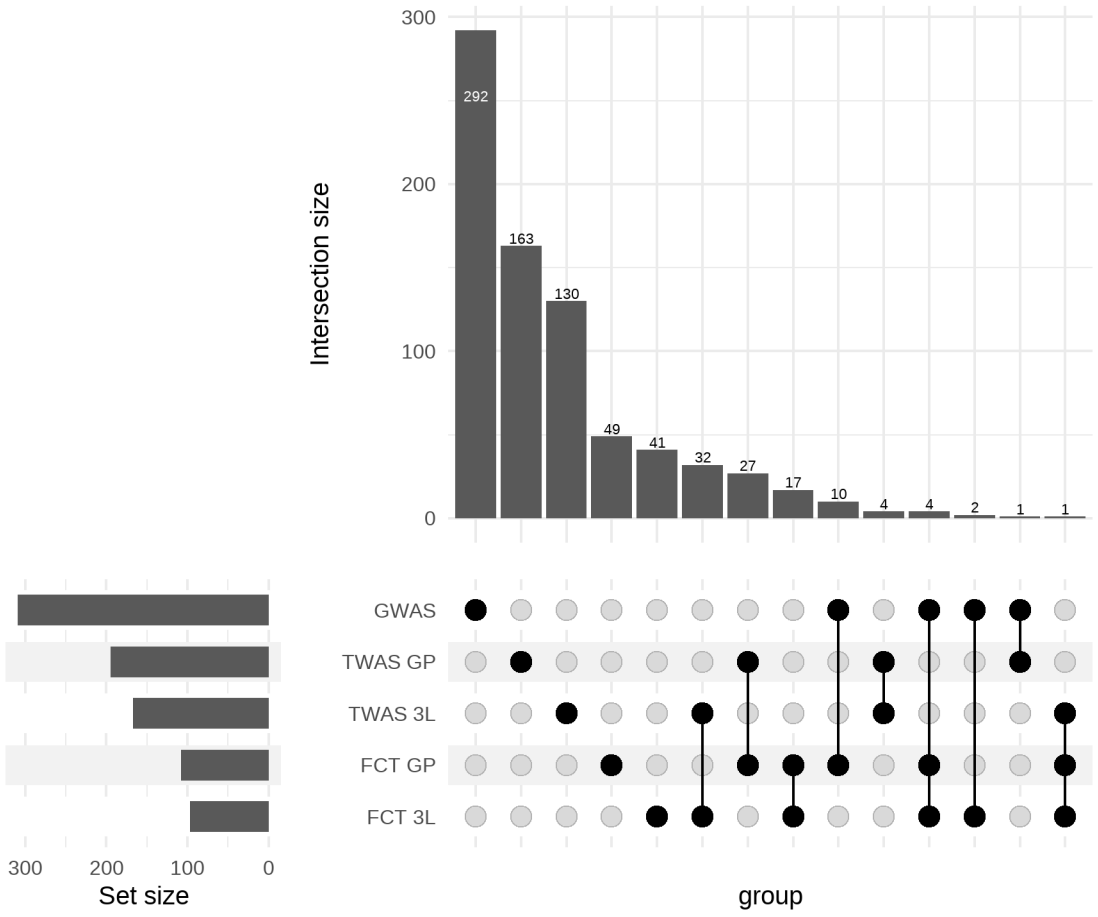

Figure 3.10: Upset plot showing number of overlapping genes between top 1% of hits in FCT 3L and GP, TWAS 3L and GP, and top 0.05% of hits in GWAS analysis, for maximum NPQ (joint model).

Table 3.3: Genes in top 0.05% of GWAS and top 1% of TWAS and FCT analyses overlapping 11 or more traits

Traits overlapped	Gene	Arabidopsis description
14	Sobic.005G154850	NADP-malic enzyme 4
13	Sobic.001G189300	AMP-dependent synthetase and ligase family protein
	Sobic.001G385400	guanyl-nucleotide exchange factors;GTPase binding;GTP binding protein
12	Sobic.001G308100	
	Sobic.009G187900	basic helix-loop-helix (bHLH) DNA-binding superfamily protein
	Sobic.002G057400	HAUS augmin-like complex subunit
	Sobic.005G200800	
	Sobic.004G150200	centrosomal protein
	Sobic.001G494400	myosin-binding protein (Protein of unknown function, DUF593)
	Sobic.003G287000	
11	Sobic.001G139100	
	Sobic.006G188100	
	Sobic.002G007800	Transcription factor jumonji (jmj) family protein / zinc finger (C5HC2 type) family protein
	Sobic.004G172100	Protein kinase superfamily protein

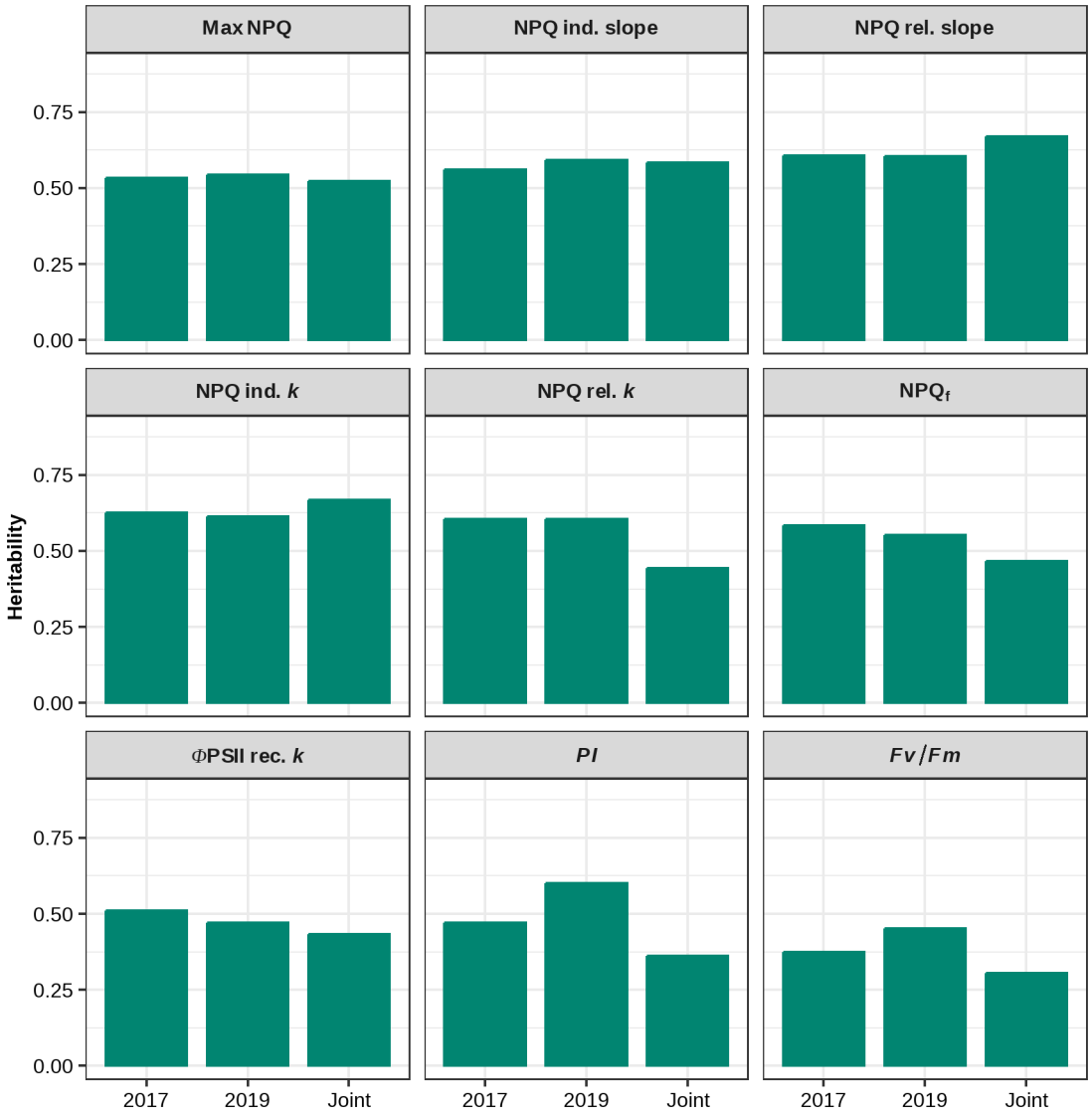

Figure 3.11: Bar plots of heritabilities of photoprotective traits calculated from 2017, 2019, and joint analysis BLUPs. Max NPQ, maximum NPQ level reached during the trace; NPQ ind. / rel. slopes, initial linear slopes of NPQ induction and relaxation, respectively; NPQ ind./ rel. k, exponential rate constants of NPQ light induction and dark relaxation, respectively; NPQ_f, NPQ at final dark time point; $\Phi PSII$ rec. k, Exponential rate constant of $\Phi PSII$ recovery in dark; PI, photoprotective index; Fv/Fm, Maximum PSII quantum efficiency.

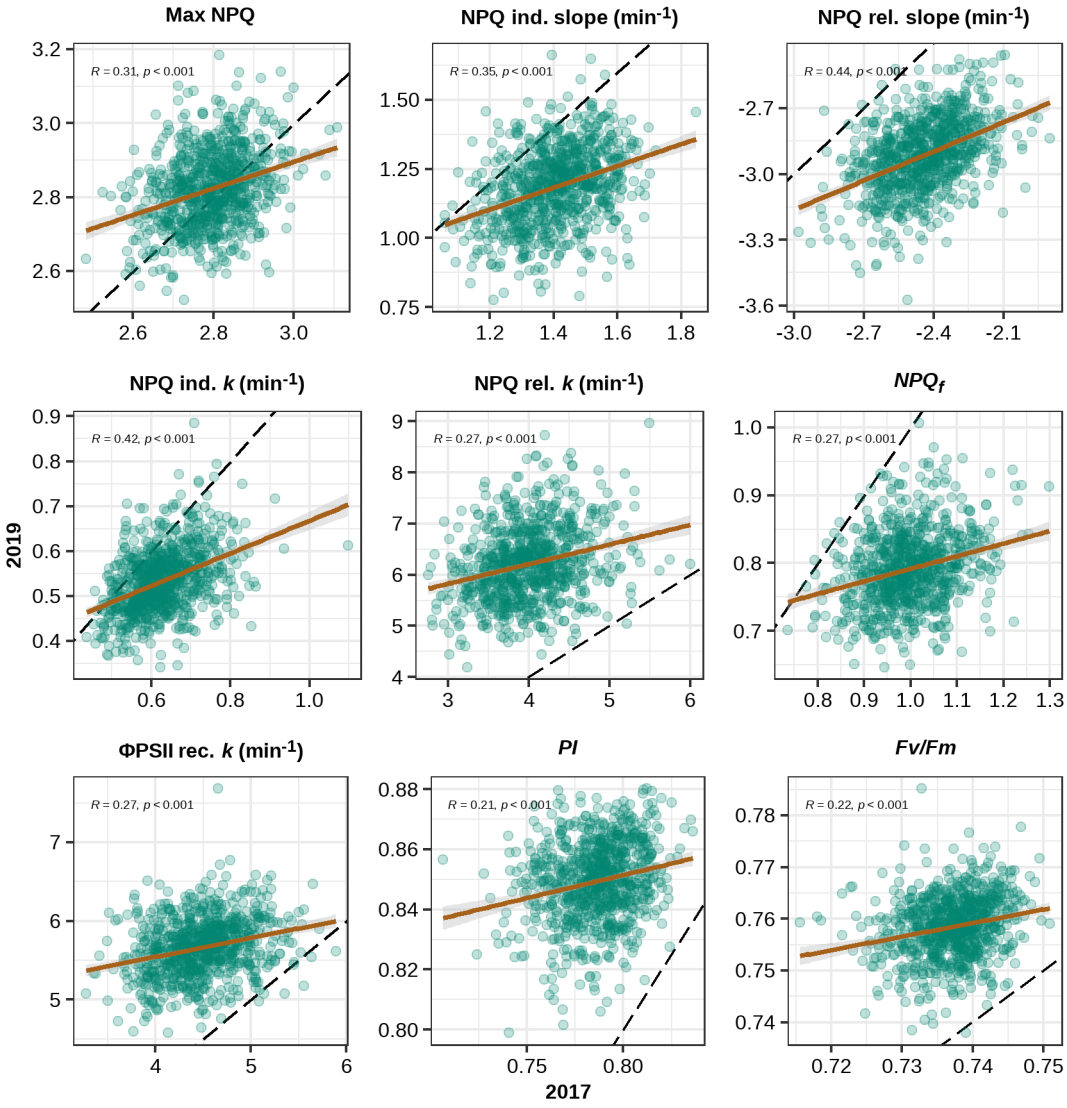

Figure 3.12: Relationships of 2017 and 2019 BLUPs including Pearson's r and p-value. Best fit linear regression line shown in brown. Dashed black line is 1:1 line.

3.4 Discussion

Fine-tuning photoprotection to better match prevailing light conditions could be a key step toward improvement in photosynthetic efficiency in the crops that feed and fuel the world (Zhu, Long, et al., 2010). This study has revealed existence of a substantial amount of heritable variation in NPQ within the sorghum genome via high-throughput chlorophyll fluorescence screening. Subsequent genome- and transcriptome-wide analyses identified a number of high-confidence candidate loci underlying genetic control of NPQ.

The resulting understanding of the genetic basis of photoprotective capacity in sorghum, one of the world's most widely-grown crops, may facilitate germplasm improvement via genomic selection and provide opportunity for improvements in photosynthetic efficiency via transgene-free genome editing in sorghum as well as in related, agronomically important C_4 crops.

3.4.1 Implications of natural diversity in NPQ and heritability of photoprotective traits

Variation in NPQ within species is not yet well-characterised, with only a few species examined at a genome-wide scale. The variation in photoprotective traits observed within this sorghum population confirms the presence of significant intraspecies variability in photoprotective capacity in a C_4 crop both within and between environments. BLUPs of maximum NPQ measured during the 10-minute high light treatment varied from just above 2.4 up to more than 3.2, a greater range than that found in a large rice collection investigated by Wang, Zhao, et al. (2017). That study reported mean NPQ values of 2.36 to 2.98 in panel of 529 diverse rice accessions, measured in the field after imposition of five minutes of 1,000 μmol m^{-2} s^{-1} PPFD. Quero et al. (2021) also noted genetic variation in the quantum yield of NPQ, and Wei, Liu, et al. (2022) in NPQ_t (a simplified NPQ measurement), in rice diversity panels. Herritt et al. (2016) reported variable NPQ within a diverse soybean panel, derived via measurements of photochemical reflectance index. Rungrat

et al. (2019) found NPQ ranging from approximately 1.5 to nearly 4 (non-averaged values) in Arabidopsis after eight minutes at 1,000 μmol m^{-2} s^{-1} PPFD– in comparison, quality-filtered unaveraged sorghum NPQ values in the current study ranged from below 1 up to nearly 4.3. While actinic light intensities and treatment timing differ between these studies, it is clear that variation in NPQ exists within single species, including economically important crops.

NPQ, like many photosynthetic traits, is quite developmentally and environmentally plastic. Accordingly, the distribution of several trait values in this study shifted between 2017 and 2019 (Figure 3.5), though notably maximum NPQ was more correlated between environments than several of the other NPQ parameters. The faster NPQ induction and slower NPQ relaxation rates, and higher residual NPQ_f in 2017 compared to 2019 suggest a "more protected" state in 2017. As mean daily incoming light intensity was similar during the early part of the growing season in both years and higher in 2019 during weeks preceding sampling (Figure 3.2), the 2017 result may be due to less frequent and lower total precipitation (Figure 3.1) during the early part of the 2017 growing season prior to sampling. The resulting reduction in water availability may have reduced downstream photosynthetic capacity, leading to a need for more persistent NPQ. Nonetheless, the depressed PI and Fv/Fm values measured in 2017 suggest a higher level of photoinhibition, even with more sustained NPQ capacity.

The previously mentioned studies in soybean, rice, and Arabidopsis similarly noted shifts in mean NPQ over separate growing seasons or environments, confirming plasticity in other species as well. Despite this plasticity, the medium-to-high levels of heritability found for max NPQ and induction and relaxation rate constants in this study (Figure 3.11), the high level of heritability reported in PRI in soybean (0.69, Herritt et al., 2016), and the clear intraspecies trait variation reported in all of these studies, facilitate the use of GWAS and TWAS to determine underlying causal genes and suggest photoprotective traits can be targeted for genetic manipulation or selective breeding.

The strong positive correlation observed here between NPQ relaxation k and ΦPSII recovery k indicates that accessions with faster NPQ relaxation likely suffered less photoinhibition during the light treatment, supported also by a slight positive, significant correlation between PI and ΦPSII recovery in 2017. Considering also the significant negative correlations between induction kinetics and PI, it appears accessions which were slower to engage NPQ suffered more photoinhibition. Arabidopsis mutants with faster NPQ kinetics during a similar length of treatment show similar results (Li, Müller-Moulé, et al., 2002), though the particularly high max NPQ reached by mutants in that work may also have played a role in photoinhibition avoidance. In the current study maximum NPQ reached was not correlated with PI, suggesting that during this short-term high light treatment, NPQ kinetics were a larger determinant of potential photoinhibition than the actual level of sustained NPQ reachable by a given accession.

The apparent high level of GxE in most NPQ traits, evidenced by the low to moderate correlation between same-trait BLUPs between years (Figure 3.12) may be representative of developmental plasticity in photosynthetic light use, due to different incoming light conditions between growth years. It appears likely that plants developing in the higher light and potentially slightly more water-limited environment of 2017, with evident higher rates of NPQ induction and slower relaxation, may have been developmentally conditioned to maintain more sustained NPQ in dynamic light conditions.

3.4.2 Genes underlying NPQ in sorghum identified by combined analyses

This study identified several high-confidence loci with genes that likely play a role in controlling photoprotection in sorghum, by utilising an ensemble approach combining GWAS, TWAS, and FCT analyses. Arabidopsis orthologues of top genes in these analyses were identified, and a GO enrichment analysis performed to uncover non-randomly enriched biological process categories in which the sorghum genes might function. Genes which overlapped in eight or more analyses for a

given trait, or were top genes for 11 or more traits, were considered candidates. By including multiple environments with different growing conditions, this study has shown that several dynamic photoprotective traits are stably heritable and may be viable targets for improvement via genomic editing approaches in sorghum. Further, candidate genes which overlap in multiple analyses, particularly over multiple years' analyses, are more likely stable (not adaptive) QTL providing more confidence in genetic enhancement efforts.

Several of the candidate are orthologous to Arabidopsis genes annotated for light use/photosynthesis related processes. The Arabidopsis *LCD1* gene, similar to Sobic.006G152000, is involved in palisade mesophyll cell density, and mutant phenotypes exhibit sensitivity to growth light conditions, though without an apparent response to short-term high-light stress (Barth and Conklin, 2003). Structural genetic variation in developmental response to light conditions in sorghum could indicate that this gene is indirectly (but strongly) associated with photoprotection; potentially, if the gene has a similar role in sorghum, modulation of cell density may affect light absorption, reflected in fluorescence measurements. Sobic.003G418000 is involved in strigolactone biosynthesis (Bellis et al., 2020). Strigolactones regulate plant growth responses to suboptimal conditions and share a biosynthesis pathway with carotenoids involved in photoprotection and antioxidant defence (Hirschberg, 2001). Recently, Thula et al. (2022) observed a direct role of strigolactones in influencing high light tolerance in Arabidopsis via modulation of photosynthetic pathways. Similarly, Sobic.006G060100 likely encodes a GRX-like protein. GRXs are involved in abiotic stress response via redox regulation and antioxidant capacity (Rouhier et al., 2008). Redox metabolism and antioxidant scavenging are deeply intertwined with both short and longer-term photoprotective processes (Foyer, Neukermans, et al., 2012; Müller-Moulé et al., 2002), sharing mechanisms and precursor molecules, and variability in dynamic photoprotective response due to underlying variation these processes may be manifested here as a GRX gene underlying NPQ in sorghum.

Sobic.009G187300, orthologous to an allyl alcohol dehydrogenase-like protein, may play a role in activation and deactivation of ATP synthase (Gong et al., 2006). Variation in sorghum accessions' ATP activation kinetics may have affected the balance of nonphotochemical and photochemical quenching, reflected during the fluorescence measurement trace– another indirect contributor to NPQ kinetics. Possibly, a gene which affects ATP activation could also play a fairly direct role in NPQ modulation via effects on the chloroplast stroma/thylakoid lumen pH gradient, given the role of lumenal pH on PsbS and xanthophyll cycle-dependent NPQ (Li, Björkman, et al., 2000). Sobic.001G269000, orthologue of Arabidopsis AT5G66150, overlapped nine analyses for NPQ induction slope. The gene is linked to N-glycosylation modification in Arabidopsis (Strasser et al., 2006); though N-glycosylation ubiquitously affects protein biogenesis and function in plants (Strasser, 2022), mutants in N-glycosylation have shown impairment in NPQ capacity and quantum efficiency (Jiao et al., 2020). These genes also overlapped multiple, but fewer than eight, analyses in other traits.

Of the genes overlapping a high number of traits, Sobic.005G154850 is an interesting candidate, orthologous to Arabidopsis NADP-ME4. This fatty-acid oxidation pathway NADP-ME is associated with photomorphogenesis in the ancestral C_3 (Ma et al., 2002), and variability in this enzyme could conceivably be responsible for developmental plasticity in light harvesting and photoprotective capacity. Sobic.005G154850 is a truncated protein with a large mis-sense section at the 3' end, but it is unclear if this is the same NADP-ME gene directly involved in the C_4 decarboxylation cycle. Sobic.001G189300 is orthologous to a jasmonic acid precursor and overlapped 13 top gene lists. Jasmonic acid (JA) and its precursors have a well-defined role in antioxidant stress response (Munné-Bosch, 2005; Yamauchi and Matsushita, 1979); within-population variance in JA production and activity could quite reasonably underlie variability in the photoprotection traits measured here.

Genes orthologous to Arabidopsis genes previously associated with photoprotection were top genes in several traits, as well. An orthologue to Arabidopsis chloroplast lipocalin LCNP (Sobic.006G222700) overlaps six analyses in three separate traits

including the NPQ relaxation slope and NPQ_f. This gene has been found to be involved in sustained non-photodamage quenching (qH, Malnoë et al., 2017), and its association with residual NPQ after light treatment in this study suggests it may function similarly in sorghum. Another prior, Sobic.006G128300, overlapped seven trait top gene list, and is predicted to contain two tolerated (non-deleterious) nonsynonymous SNPs. The Arabidopsis orthologue At5g43050 is a chloroplast-encoded YCF20 gene sharing 70% sequence similarity (Berardini et al., 2015); a single base pair deletion within this gene (mutant *NPQ6*) exhibits reduced NPQ (Jung and Niyogi, 2010). The previously discussed genes are mostly novel, high-confidence candidates associated with variation in sorghum photosynthetic efficiency in dynamic light conditions. While large-scale quantitative genomic studies like this are not causal evidence for functional regulation, they shed light on genomic regions that have strong associations with the traits of interest, providing a valuable resource for future validation study.

A coupled analysis of likelihood of causal variation (SIFT) of SNPs within coding regions of candidate genes showed that most identified candidates were predicted to contain nonsynonymous substitutions, which suggests one potential mechanism which could give rise to the observed phenotypic variation. The high percentage of nonsynonymous substitutions in photoprotection-associated genes couples well with the apparent high-level of genetically controlled diversity in photoprotection within this diverse sorghum population. Given the diversity of origin environments of the panel (Ferguson et al., 2021), this lack of conservation in candidate gene sequences may reflect strong environmental adaptation. This diversity and the measured trait heritability also suggests that informed genomic selection or selective breeding could effect meaningful changes in NPQ phenotypes in sorghum. While the presented loci provide valuable information about the genetic architecture of sorghum photoprotection, functional validation will be needed to uncover mechanistic photoprotective relationships for these candidate genes. For genes identified through GWAS, quantification of candidate gene transcript expression between

accessions with contrasting photoprotective traits would provide a further verification of gene causality. Sorghum or Arabidopsis candidate gene mutants may also provide a platform for future causal confirmation, similar to the approach taken in Sahay et al. (2023), who used a complementation of Arabidopsis mutants to verify a selection of their maize NPQ candidate genes.

3.4.3 Conclusion

This work confirms the existence and characterises the extent of variation in photoprotective traits in the sorghum genome, and highlights the complexity of genetic control of photoprotection in a C_4 species. Additionally, several novel loci have been identified as high-confidence candidates associated with genetic control of photosynthetic and photoprotective traits in dynamic light conditions in sorghum. This information can be used to inform further, targeted experiments via mutant or genetic modification studies to manipulate NPQ in sorghum, and potentially if combined with appropriate marker development could be used in marker or genomics-assisted breeding for photosynthetic efficiency in sorghum and related C_4 crops.

4

Toward the confirmation of causal genomic variants via genotype-based selection

4.1 Introduction

Genome-wide association studies (GWAS) have proven useful in identifying genetic loci underlying a variety of plant photosynthetic traits (Ferguson et al., 2021; Ortiz et al., 2017; Pignon, Fernandes, et al., 2021), including nonphotochemical quenching (NPQ, Herritt et al., 2016; Rungrat et al., 2019; Sahay et al., 2023; Wang, Zhao, et al., 2017). Genomic regions uncovered through GWAS, or layered studies which combined multiple levels of -omics (such as presented in chapter three) provide associations, but not causal proof (Mohammadi et al., 2020). GWAS can provide a wealth of information about non-random variation of traits within genomes, but these large quantitative studies have weaknesses (discussed in Bazakos et al., 2017; Mohammadi et al., 2020), including poor ability to identify small-effect loci, confounding effects due to population structure, and general inability to detect rare alleles. Although control methods to alleviate some of these shortcomings have been and are being actively developed (Devlin and Roeder, 1999; Lipka et

al., 2015; Zhang et al., 2016), GWAS are sensitive to spurious results and quantitative trait loci (QTL) associations derived from these studies are therefore in need of further verification.

Several steps can be taken based on GWAS results to improve confidence in candidate loci. Commonly this involves further investigation based on genotypes displaying contrasting alleles to verify if these result in different phenotypes for the traits of interest. Using contrasting genotypes, methods such as transcript sequence investigation in candidate loci (Yang, Zhu, et al., 2021), differential expression analysis (Basu, Bajaj, et al., 2019), or screening of QTL mutants for expected phenotypic variation in studied or model species (Sahay et al., 2023) can be used to improve QTL confidence. These methods can be implemented relatively quickly and easily as validations before investing the time and money required for molecular functional validation via gene editing (overexpression and silencing). This is particularly valuable when working in species with more complex genomes such as wheat (Li, Ye, et al., 2012), or species such as *Sorghum bicolor* (sorghum), which tends to be relatively recalcitrant to transformation (Parikh et al., 2021)– though rapid improvements are occurring, which should facilitate more rapid direct functional validation in the near future (Massel et al., 2022; Wang, Riaz, et al., 2018).

The work presented in this chapter attempted to validate two QTL which were significantly associated with NPQ kinetic parameters in the sorghum GWAS field trial presented in chapter three– single nucleotide polymorphism (SNP) Chr01_67331530, associated with photoprotection index (PI) and Combined Trait 1 (Section 3.2.5), and SNP Chr01_76704821, associated with maximum NPQ (max NPQ). We hypothesised that a subset of sorghum accessions which have contrasting allele values at these SNPs, randomly chosen out of the broader panel, would show phenotypic divergence in those traits when re-screened in a separate field trial. The results provide an additional line of evidence for genetic control of NPQ in sorghum and suggest that the QTL containing the two SNPs are likely causal variants worthy of functional validation.

4.2 Materials and Methods

4.2.1 Variant and genotype selection

Sorghum genotypes were selected based on allele values at two SNPs of interest. SNP Chr01_67331530 was chosen due to its significant GWAS association with both *PI* and Combination trait 1 (CT1, max NPQ, NPQ relaxation amplitude, NPQ relaxation rate constant *k*, NPQ induction rate constant *k*) and due to its nearest gene (Sobic.001G385900) being orthologous to *Arabidopsis thaliana* (Arabidopsis) AT2G39050, a hydroxyproline-rich glycoprotein family protein implicated in stress response. SNP Chr01_76704821 was chosen due to its high-confidence GWAS association with max NPQ in both the 2017 and joint (2017/2019) models, resulting in the lowest FDR-adjusted *p*-value in any analysis, as well as due to it being collocated within 20 kB of three other SNPs significant for max NPQ. The nearest genes to SNPs at this locus are orthologous to AT2G37440, a DNAse I-like superfamily protein and AT1G05460 (SDE3), a protein-encoding gene involved in gene silencing.

SNP allele values for the sorghum panel were acquired from Dr Samuel Fernandes (University of Arkansas). The VCF file of ~2.3 million markers was converted to GDS and pruned to 480,032 snps using the snpgdsLDpruning function of R package *SNPRelate* (Zheng et al., 2012) ("corr" method, correlation coefficient >0.975, window size 50k BP), to closely match the pruning used for GWAS analyses . Major and minor homozygous alleles were designated "0/0" and "1/1", respectively. Principle component analysis (PCA) was run on the pruned SNP set (snpgdsPCA, *SNPRelate*, default options), then accessions were segregated by their homozygous allele value at either SNP (Figures 4.1 and 4.2). For each SNP, eight sorghum accessions representing each allele group were chosen at random, after filtering for accessions which were closely clustered in the PCA to avoid potential genetic-distance bias. K-means clustering was also performed on the SNP matrix with 10 clusters chosen based on the elbow method; the chosen accessions were confirmed to be collocated within the same clusters.

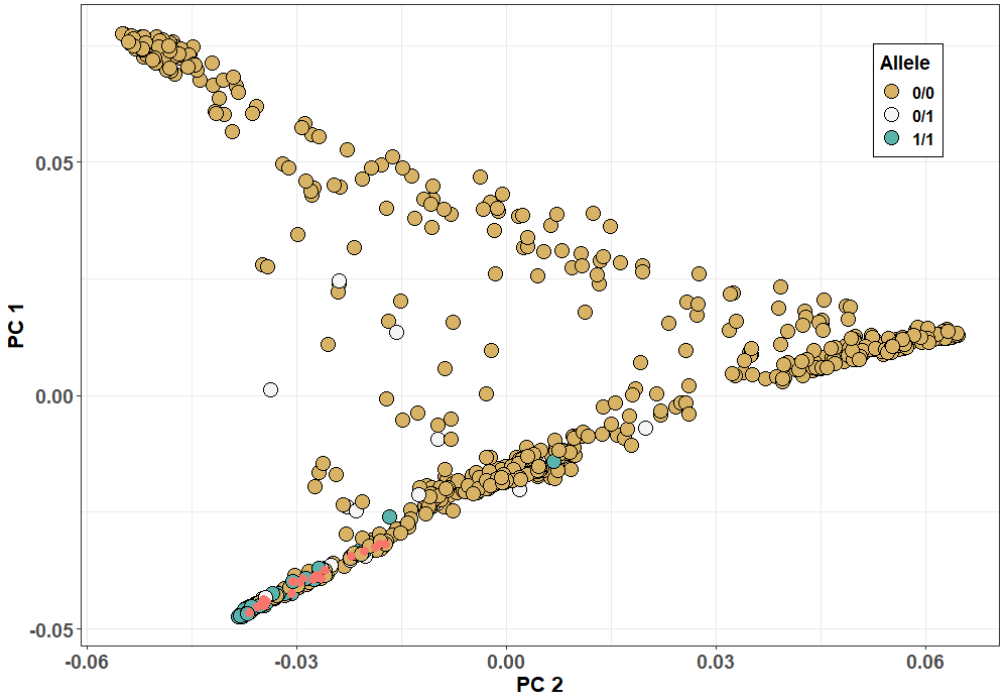

Figure 4.1: Principle component biplot of sorghum panel SNP dataset (panel information available in GWAS chapter reference). Accessions are coloured by allele value at locus Chr01_67331530. Red dots mark the 16 accessions selected for the current study.

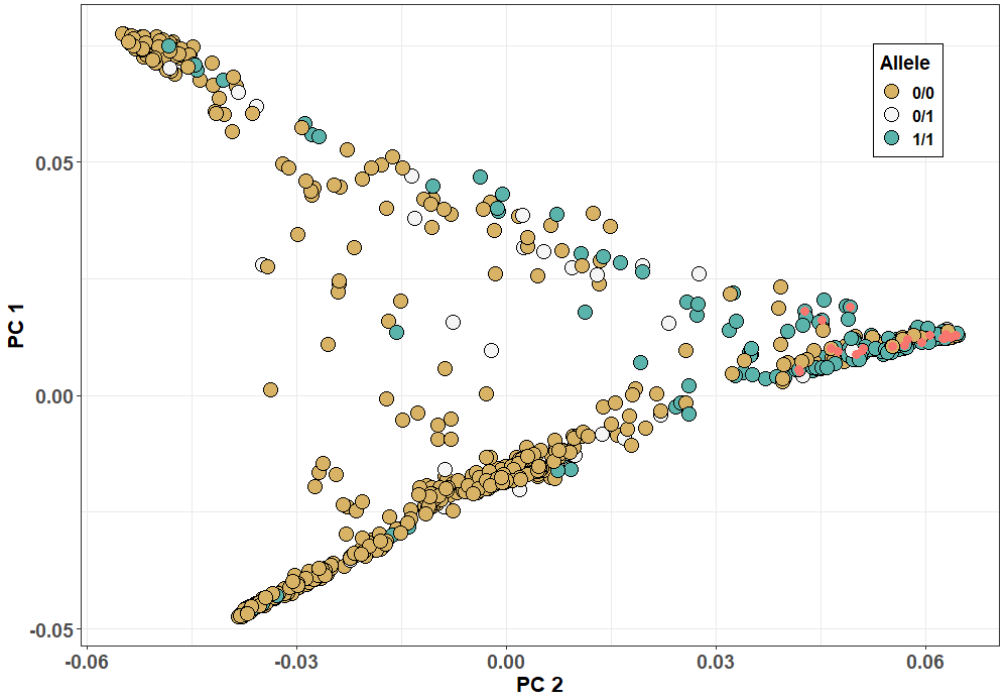

Figure 4.2: Principle component biplot of sorghum panel SNP dataset (panel information available in GWAS chapter reference). Accessions are coloured by allele value at locus Chr01_76704821. Red dots mark the 16 accessions selected for the current study.

4.2.2 Field trial design and growth

The sorghum accessions were grown at the University of Illinois Energy Farm research site near Urbana, IL, USA in 2021 in four-row plots (3 m rows). The field was planted on May 27, 2021 in a randomised block/subblock design, with the 16 accessions from each SNP group arranged in physically separate blocking structures with two replicates, for a total of 64 plots in an 8x8 square (Figure 4.3). For each SNP group, two complete replicated blocks were subblocked into two groups of eight accessions, composed of four accessions of each allele group randomised within the subblock, to better control for spatial variation in the trial.

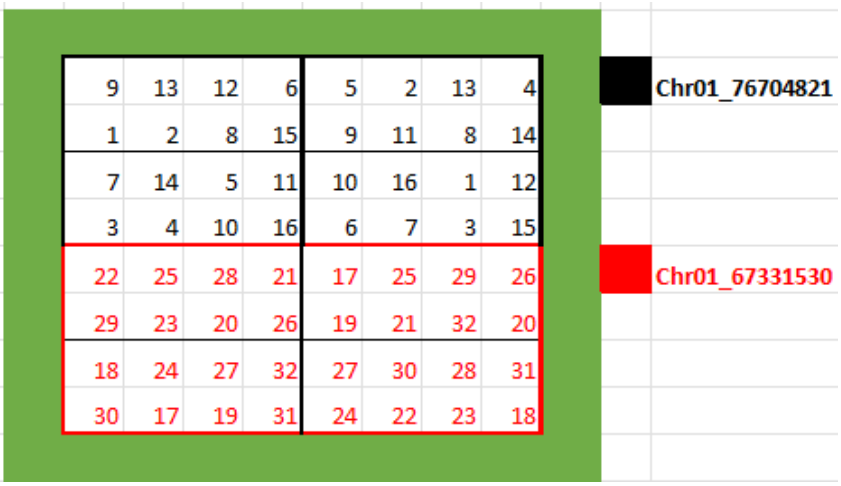

Figure 4.3: Blocking structure of sorghum field trial. Plot numbers 1-16 (black) consist of eight accessions of 0/0 and eight accessions of 1/1 allele at locus Chr01_76704821. Plot numbers 17-32 (red) consist of eight accessions of 0/0 and eight accessions of 1/1 allele at locus Chr01_67331530. Separately for each locus, each complete replicate (4x4 block) is subdivided into two 4x2 subblocks containing four randomised accessions from each allele group.

4.2.3 NPQ screen

Sorghum accessions were screened for NPQ kinetics using the high throughput chlorophyll fluorescence sampling method detailed in Chapter three (3.2.3); NPQ traces can be viewed in Figures 4.4 and 4.5. Discs of Chr01_76704821 accessions were sampled on the afternoons of July 29-31 2021 and discs of Chr01_67331530 accessions were sampled on 02, 03, and 05 August 2021. 48 discs from individual plants were sampled for each plot, for a total of 96 biological replicates per accession (excepting accession NSL55230 [Chr01_76704821 1/1], which provided ~35 plants after poor germination). Plants from the middle two rows of plots were sampled preferentially; plants in the outside rows and row-ends were only sampled when there were not enough plants in the middle rows to reach the desired sample number. All 32 plots from a single SNP experiment were sampled eight times per day (in eight plates) by two samplers (four plates each) collecting two samples from a plot before moving on to the next, then repeating the circuit. Disc placement in well-plates and sampling route through field was structured in advance such that samples of each accession were located in different wells in each plate on different sampling days to avoid both spatial bias within the well-plate during imaging and temporal bias during sampling. Sample routes were staggered through the field to avoid temporal bias and well-plates assigned to individual sampler for later model accounting.

4.2.4 Data analysis

Chlorophyll fluorescence traces were processed and analysed as in GWAS chapter reference, with modification. Based on the distribution of maximum photosystem II quantum efficiency (Fv/Fm), discs with spuriously low values (below 0.68, less than 6% of samples) were excluded from further analysis. Models of NPQ kinetics (Section 3.2.3) were implemented and fit using R package Minpack.lm (Elzhov et al., 2016). The resulting modelled values of maximum NPQ, NPQ induction k,

NPQ relaxation k, and PI were tested between allele groups using linear mixed-effects models fit by residual maximum likelihood, using R packages *lme4* (Bates et al., 2015) and lmerTest (Kuznetsova et al., 2017). For each NPQ trait phenotype, allele group was fit as a fixed effect with random effects of accession, sampler, day of measurement, well-plate, replicate, and subblock nested within replicate:

$$
\begin{aligned}
\mathrm{y}_i &\sim N\left(\alpha_{j[i],k[i],l[i],m[i],n[i],o[i]}, \sigma^2\right) \\
\alpha_j &\sim N\left(\mu_{\alpha_j}, \sigma^2_{\alpha_j}\right), \text{ for plate j} = 1,\ldots,\mathrm{J} \\
\alpha_k &\sim N\left(\gamma^\alpha_0 + \gamma^\alpha_1(\text{allele\_value}_{1/1}), \sigma^2_{\alpha_k}\right), \text{ for accession k} = 1,\ldots,\mathrm{K} \\
\alpha_l &\sim N\left(\mu_{\alpha_l}, \sigma^2_{\alpha_l}\right), \text{ for replicate:subblock l} = 1,\ldots,\mathrm{L} \\
\alpha_m &\sim N\left(\mu_{\alpha_m}, \sigma^2_{\alpha_m}\right), \text{ for day m} = 1,\ldots,\mathrm{M} \\
\alpha_n &\sim N\left(\mu_{\alpha_n}, \sigma^2_{\alpha_n}\right), \text{ for sampler n} = 1,\ldots,\mathrm{N} \\
\alpha_o &\sim N\left(\mu_{\alpha_o}, \sigma^2_{\alpha_o}\right), \text{ for replicate o} = 1,\ldots,\mathrm{O}
\end{aligned}
\tag{4.1}
$$

where y is the vector of phenotypes; α the random intercept for plate j, accession k, subblock nested within replicate l, day m, sample n, and replicate o, with $\alpha_k \sim N\left(\gamma^\alpha_0 + \gamma^\alpha_1(\text{allele\_value}_{1/1}), \sigma^2_{\alpha_k}\right)$ a regression for the random intercept α_k on allele value and a regression for phenotype y, $\alpha \sim N(0, \sigma^2_\alpha)$ where μ_α is the mean and σ^2_α the variance for the given component.

Models were run in full then reduced by stepwise elimination based on AIC using the R Stats "step" function. Estimated marginal means (emmeans, Lenth, 2021) of traits were calculated for each allele group to include shrinkage based on remaining random effects.

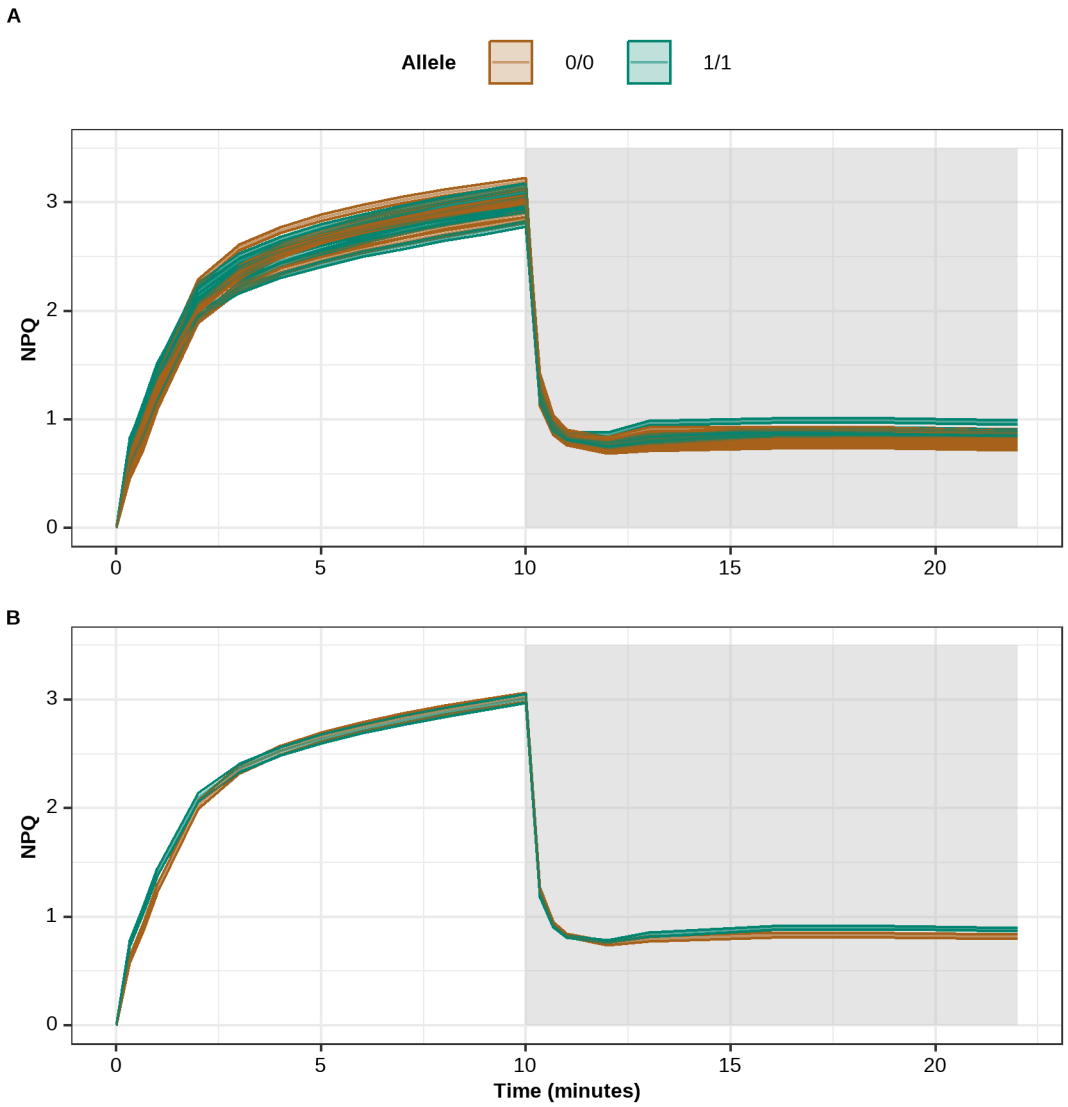

Figure 4.4: Nonphotochemical quenching (NPQ) kinetic traces of 16 *S. bicolor* accessions during a 10 minute high-light treatment, followed by 12 minutes in darkness (shaded region). Traces are coloured by allele value at SNP locus Chr01_67331530. **A**, lines are means of single accessions, shading +/- SE of the mean (n = 93-96). **B**, lines are means of all accessions in allele group, shading +/- SE of the mean (n = 8).

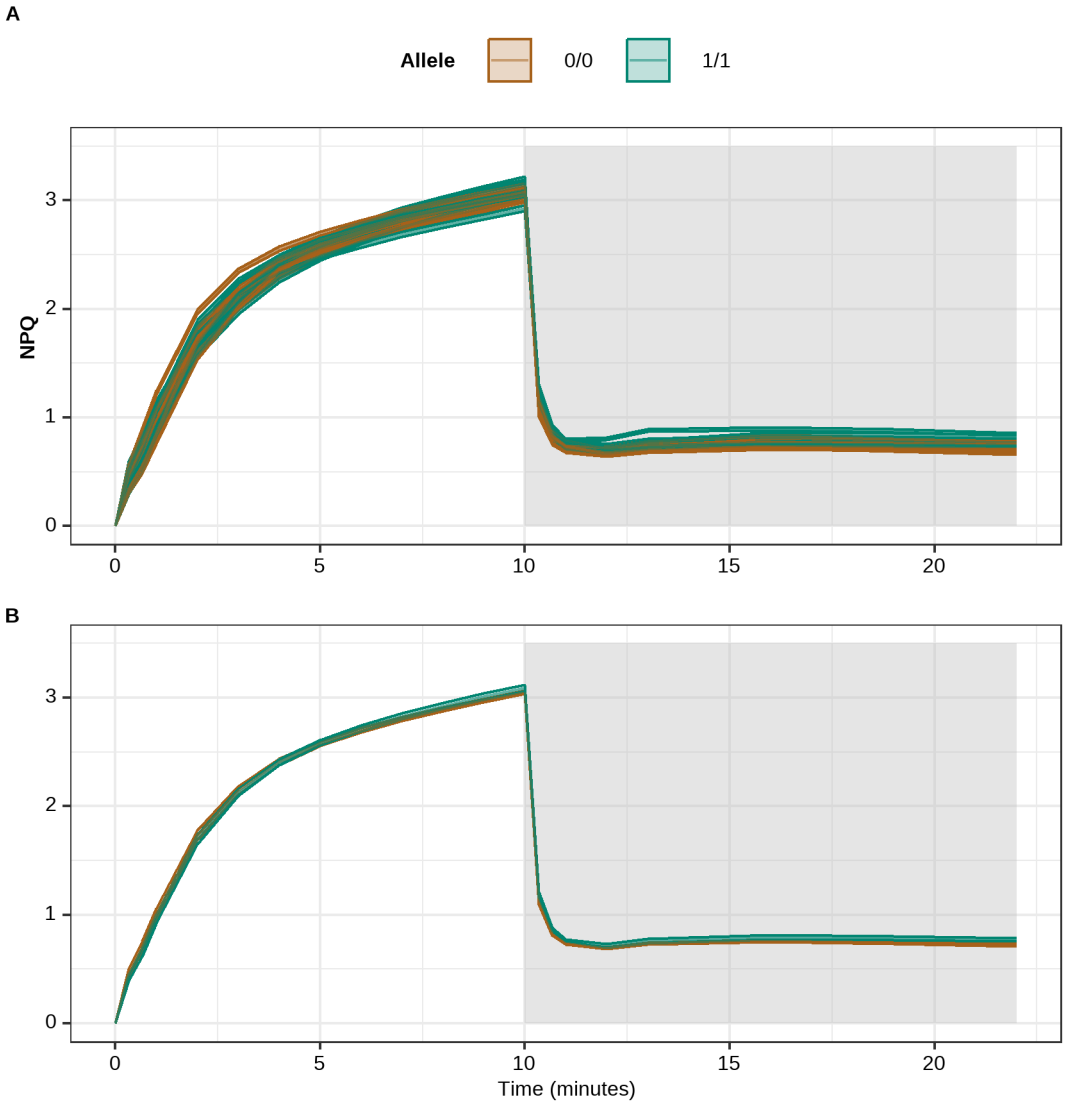

Figure 4.5: Nonphotochemical quenching (NPQ) kinetic traces of 16 *S. bicolor* accessions during a 10 minute high-light treatment, followed by 12 minutes in darkness (shaded region). Traces are coloured by allele value at SNP locus Chr01_76704821. **A**, lines are means of single accessions, shading +/- SE of the mean (n = 91-95, excepting accession "NSL55230"– n = 31). **B**, lines are means of all accessions in allele group, shading +/- SE of the mean (n = 8).

4.3 Results

4.3.1 Phenotypic segregation confirms trait associations at SNP Chr01_67331530

Sorghum accessions with contrasting alleles at SNP Chr01_67331530 were expected to segregate phenotypically for maximum NPQ, PI, NPQ induction k, and NPQ relaxation k, based on the SNP's significant associations with those traits in the joint model GWAS analyses. The accession groups segregated strongly by allele group for both NPQ induction k and NPQ relaxation k. Mean (estimated marginal mean) NPQ induction k for allele group 0/0 was 0.60 min^{-1}, compared to 0.71 min^{-1} for allele group 1/1 (linear mixed effect model, $p = 0.002$, Figure 4.6 **C**). Mean NPQ relaxation k for allele group 0/0 was 5.07 min^{-1}, compared to 5.67 min^{-1} for allele group 1/1 (linear mixed effect model, $p = 0.015$, Figure 4.6 **D**).

The accessions did not contrast notably for max NPQ, with mean NPQ for allele group 0/0 reaching 3.03 and 1/1 reaching 3.01 (linear mixed effect model, $p = 0.804$, Figure 4.6 **A**). Notably, the direction of relationship between allele groups matched that observed in the 2017/2019 field trial joint BLUPs, where median max NPQ for allele 0/0 was 2.81 and for 1/1 was 2.77 (Figure 4.8 **A**). There was no substantial difference in PI in the current study– the mean value for both allele groups was 0.88 (linear mixed effect model, $p = 0.993$, Figure 4.6 **B**).

Sorghum accessions with contrasting alleles at SNP Chr01_76704821 were expected to segregate phenotypically for maximum NPQ based on the SNP's significant association with that trait in the 2017/2019 GWAS analyses. However, in this validation experiment the accessions did not show large contrasts between allele groups for any trait. Mean max NPQ for allele 0/0 was 3.05, compared to 3.08 for allele 1/1 (linear mixed effect model, $p = 0.319$, Figure 4.7 **A**). Mean PI for both allele groups was 0.88 (linear mixed effect model, $p = 0.614$, Figure 4.7 **B**). Mean NPQ induction k for allele 0/0 was 0.42 min^{-1}, compared to 0.39 min^{-1} for allele 1/1 (linear mixed effect model, $p = 0.368$, Figure 4.7 **C**). Mean NPQ relaxation k

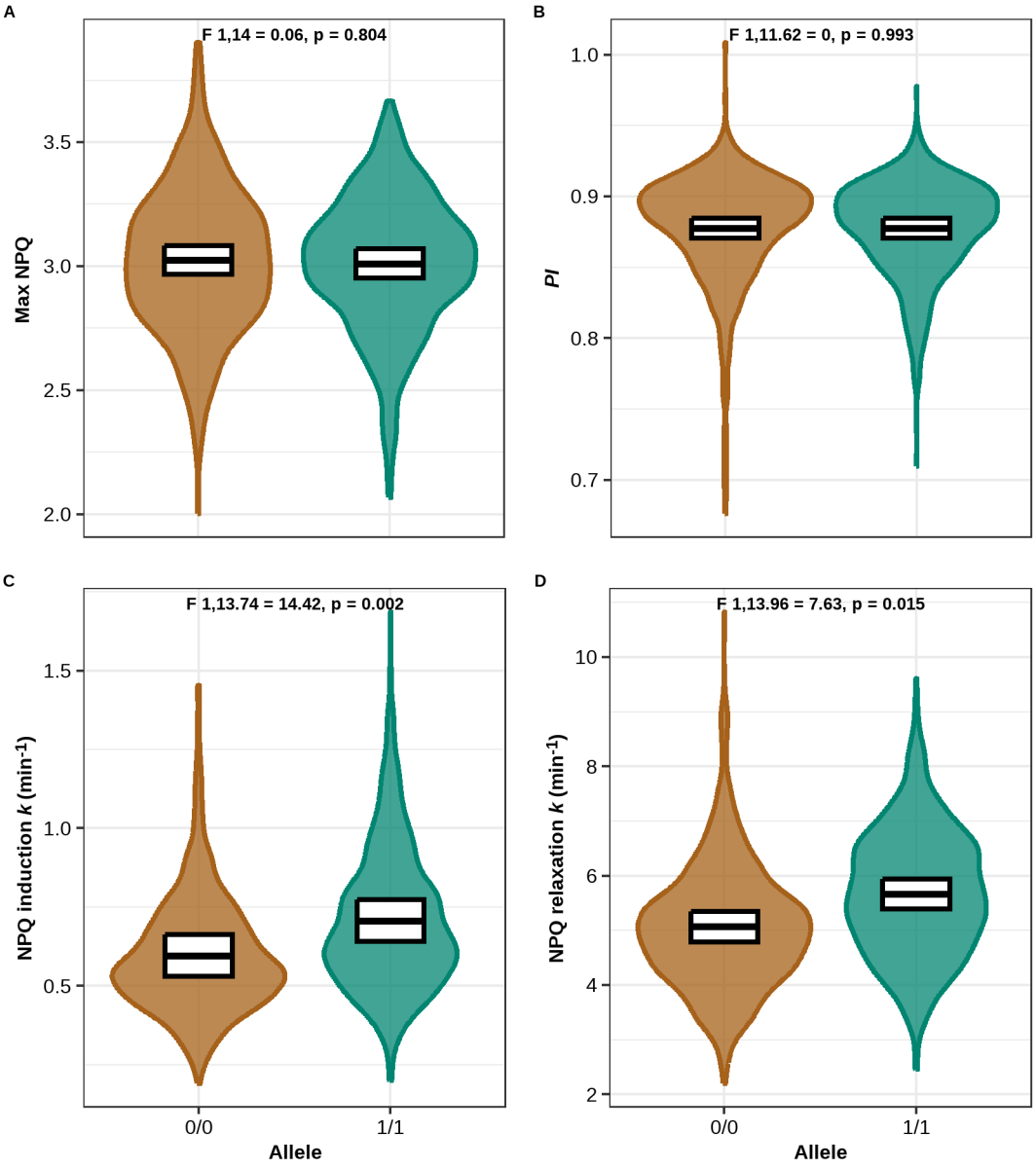

Figure 4.6: Violin plots of NPQ trace parameters for 16 sorghum accessions with contrasting alleles at SNP Chr01_67331530. Internal crossbar boxes represent the estimated marginal mean +/- standard error of the mean ($n = 8$) based on linear mixed effect models (Tables 7.17, 7.18, 7.19, 7.20). **A**, maximum NPQ level reached during the trace; **B**, photoprotection index; **C**, rate constant k of NPQ induction; **D**, rate constant k of NPQ relaxation.

for allele 0/0 was 5.54 min^{-1}, compared to 5.34 min^{-1} for allele 1/1 (linear mixed effect model, $p = 0.487$, Figure 4.7 **D**).

It is noteworthy that both max NPQ and NPQ induction k exhibited a similar

directional relationship to that seen in the 2017/2019 field trial BLUPs, both in the chosen accessions and in the larger panel, which suggests that Chr01_76704821 may still associate as a causal locus for photoprotective capacity. In the larger panel, median max NPQ for allele 0/0 was 2.79 and for 1/1 was 2.85 (Figure 4.9 **A**). Median NPQ induction k of 2017/2019 joint model BLUPs was 0.58 min^{-1} for allele 0/0, but 0.55 min^{-1} for allele 1/1 (Figure 4.9 **C**). The relationship between the current study's accessions and those of the 2017/2019 BLUPs was not maintained for NPQ relaxation k; median whole panel values of 2017/2019 BLUPs were 5.03 and 5.26 for alleles 0/0 and 1/1, respectively (Figure 4.9 **D**).

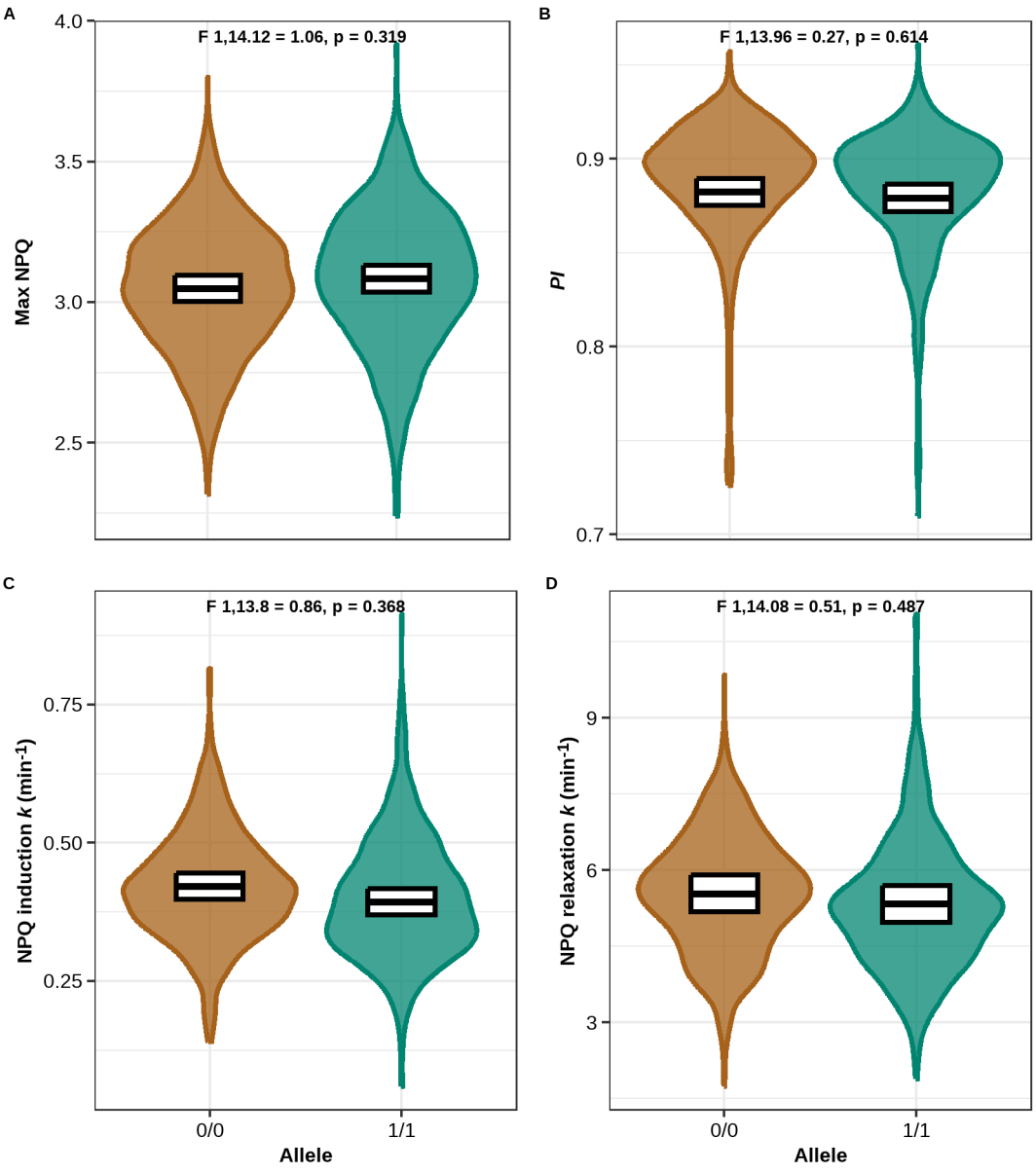

Figure 4.7: Violin plots of NPQ trace parameters for 16 sorghum accessions with contrasting alleles at SNP Chr01_76704821. Internal crossbar boxes represent the estimated marginal mean +/- standard error of the mean ($n = 8$) based on linear mixed effect models (Tables 7.21, 7.22, 7.23, 7.24). **A**, maximum NPQ level reached during the trace; **B**, photoprotection index; **C**, rate constant k of NPQ induction; **D**, rate constant k of NPQ relaxation.

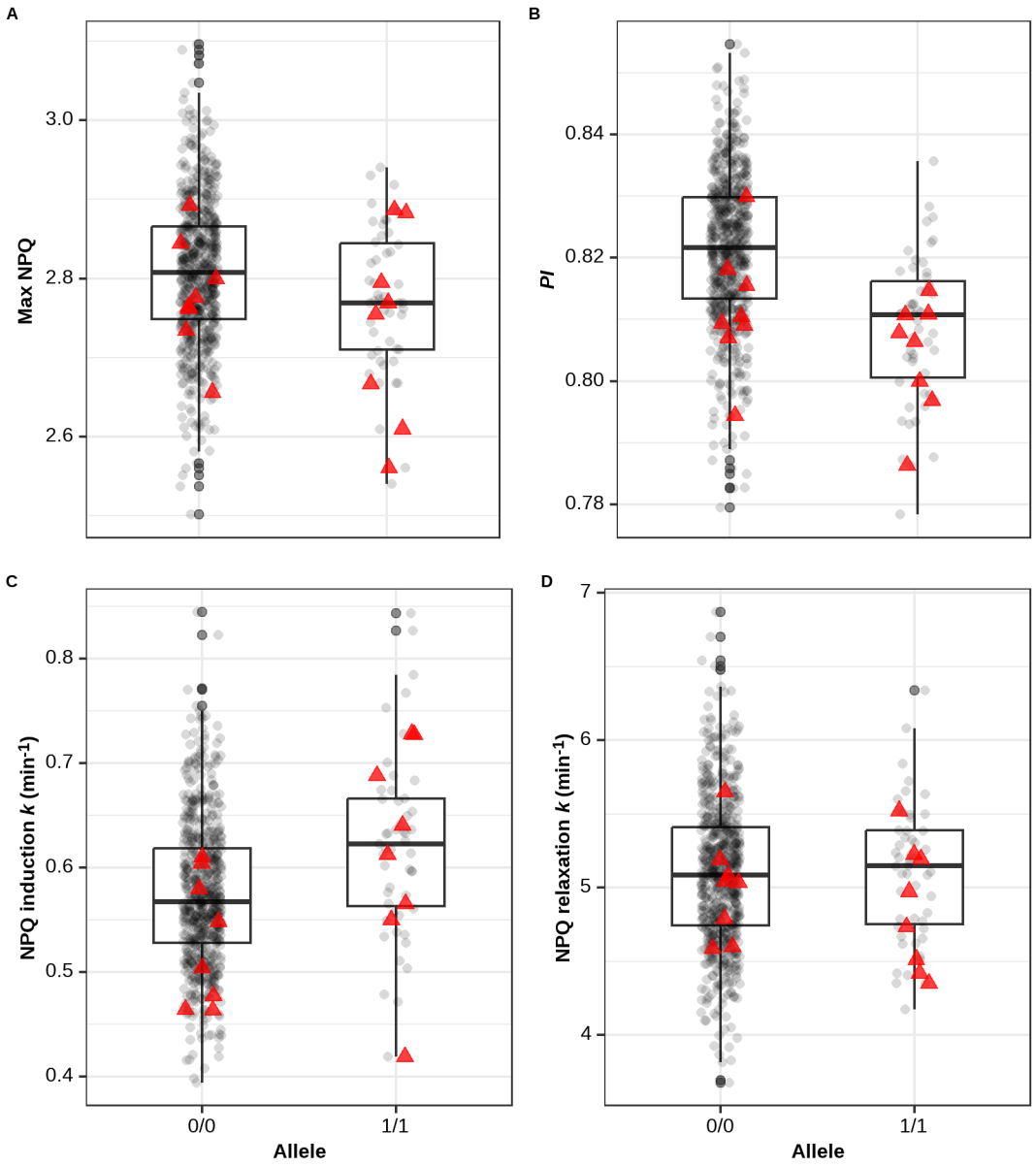

Figure 4.8: NPQ trait best linear unbiased predictions (BLUPs) from joint 2017/2019 model NPQ screen results (3.3.1) , by allele value at SNP Chr01_67331530. **A**, maximum NPQ level reached during the trace; **B**, photoprotection index; **C**, rate constant k of NPQ induction; **D**, rate constant k of NPQ relaxation. Red triangles denote values for accessions used in this study. Black points are accession BLUPs. Internal box plot edges represent first and third quartiles. Box endpoints represent outliers beyond 1.5 times the interquartile range. The solid line within the boxes indicates the median.

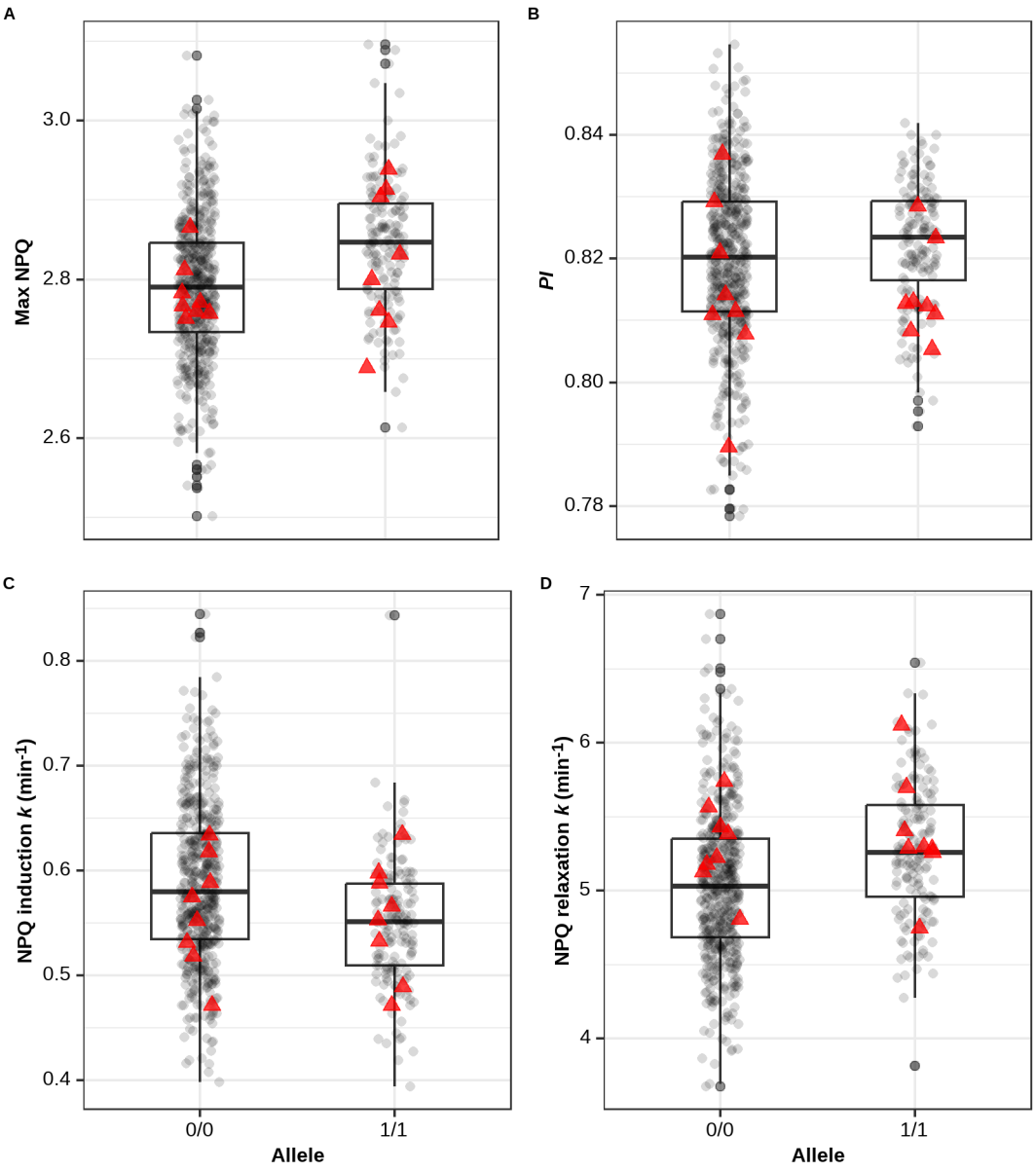

Figure 4.9: NPQ trait best linear unbiased predictions (BLUPs) from joint 2017/2019 model NPQ screen results (3.3.1) , by allele value at SNP Chr01_76704821. **A**, maximum NPQ level reached during the trace; **B**, photoprotection index; **C**, rate constant k of NPQ induction; **D**, rate constant k of NPQ relaxation. Red triangles denote values for accessions used in this study. Black points are accession BLUPs. Internal box plot edges represent first and third quartiles. Box endpoints represent outliers beyond 1.5 times the interquartile range. The solid line within the boxes indicates the median.

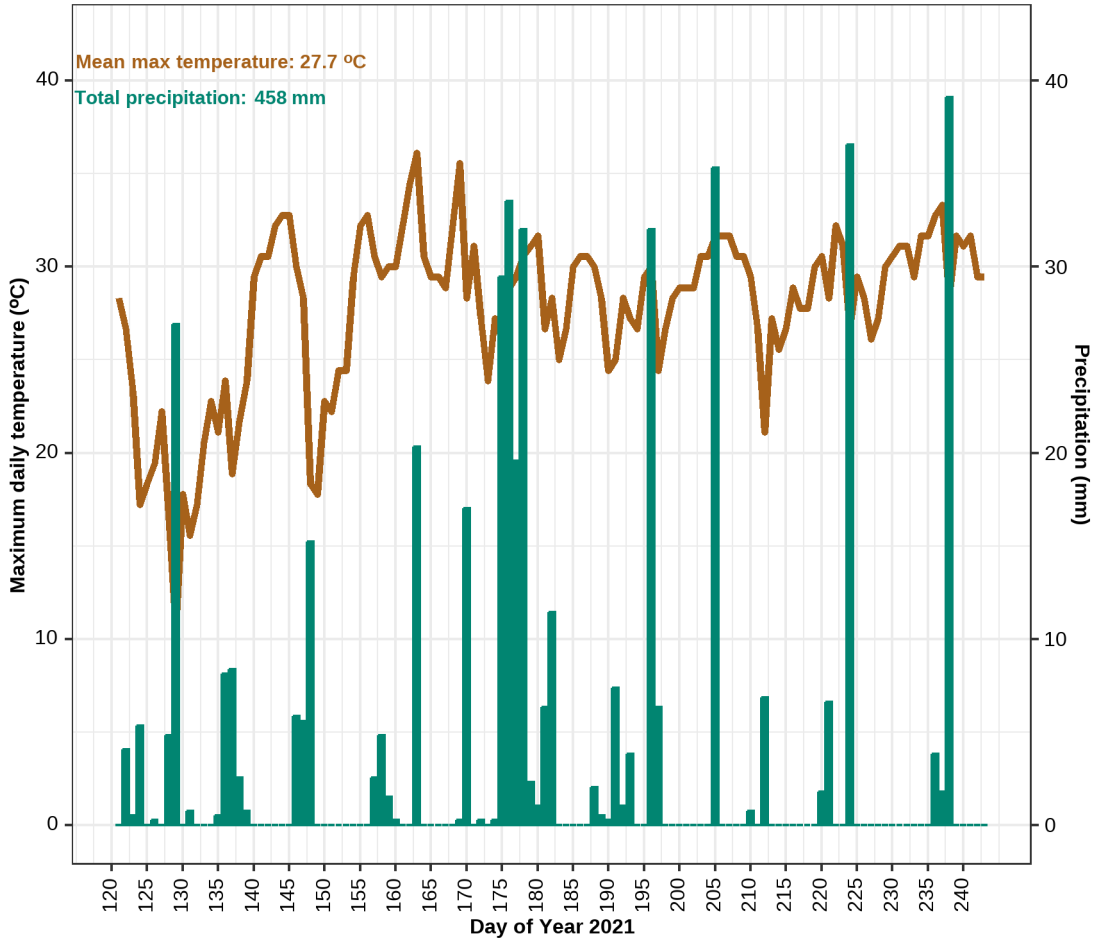

Figure 4.10: Plot of maximum daily temperature (brown line) and total daily precipitation (green columns) recorded at the Willard Airport weather station (Savoy, IL, USA) during the 2021 sorghum trial growing season. Seasonal totals calculated from May 05 through August 31. Planting date: 147. Sampling dates: 210-217. Data retrieved from www.ncdc.noaa.gov (Station ID GHCND:USW00094870, 6.73 km from Energy Farm).

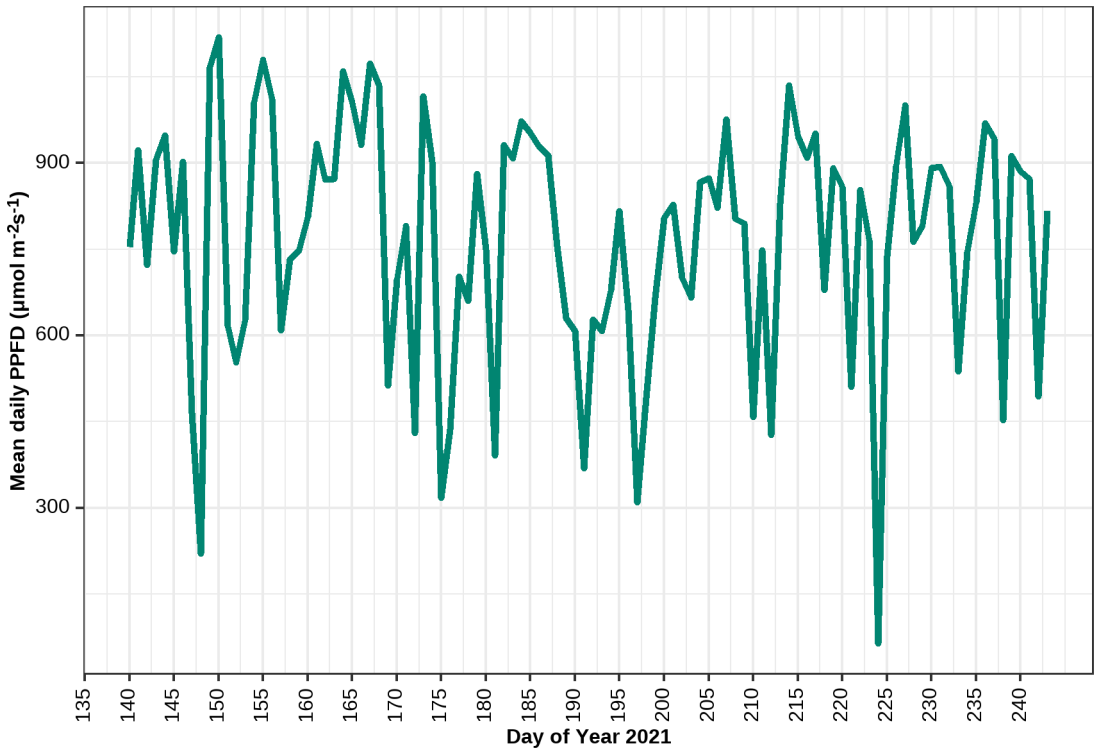

Figure 4.11: Incident light intensity at University of Illinois Energy Farm (Urbana, IL) during the 2021 growing season. Daily means calculated from half-hourly averages of incoming photosynthetically active radiation, for all time periods with photosynthetic photon flux density above five μmol m^{-2} s^{-1}. Planting date: 147. Sampling dates: 210-217.

4.4 Discussion

GWAS are important early-pipeline quantitative tools which provide the ability to uncover genomic regions associated with trait phenotypes in crops. Results from GWAS serve as an informative starting point for QTL functional validation, as trait associations are not in themselves direct evidence of mechanistic molecular regulation. Here, we performed NPQ kinetic screening on two groups of randomly selected sorghum genotypes which display contrasting alleles at two candidate QTL previously identified through a GWAS for NPQ traits (chapter reference), hypothesising that NPQ trait phenotypes would segregate between the accession groups. If confirmed, this would provide stronger evidence of a potential causal role of the QTL and increase confidence generally in the GWAS results.

4.4.1 Comparison with 2017/2019 field trial results

The re-screened accessions, grown in 2021 in the same field as used for the 2019 GWAS, exhibited minor shifts in max NPQ and PI compared to the whole-panel BLUPs, but NPQ kinetic traits spanned the range of variation observed in the 2017/2019 screen results. In general, the accessions selected here by genotype were either representative of the median BLUP values or reasonably spanned the range of BLUP values for their allele groups in 2017/2019 (Figures 4.8 and 4.9). Thus, the random selection of accessions for 2021 appears well-representative of the allele groups as a whole. Mean max NPQ of re-screened accessions was higher (above 3) than that observed in the GWAS trial panel (~2.8). PI was also higher in this study, at a consistent 0.88 (Figures 4.6 **B** and 4.7 **B**) compared to 0.79 (2017) and 0.85 (2019) (Figure 3.5) observed in the panel. These results suggest 2021 presented a more stressful light environment leading to increased photoprotective capacity (higher max NPQ), compared to 2017 and 2019, while the higher PI in this study than in 2017 suggests that the increased photoprotective capacity may have manifested in plants that were less sensitive to photoinhibition during the light treatment. PI in this study was more similar to that observed in 2019, perhaps as a

result of similar trends in mean incoming light intensity (Figures 4.11 and 3.2), both generally higher than that of 2017. These results are supported by the somewhat higher temperatures early in the growing season and a generally slightly higher maximum temperature throughout the growing season (Figure 4.10), compared to 2017 and 2019 (Figure 3.1). However, rates of NPQ induction k spanned a broader range in the 2021 re-screen (0.39 to 0.71 min^{-1}, Figures 4.6 **C** and 4.7 **C**) than the 2017 and 2019 BLUPs (0.53 to 0.62 min^{-1}, Figure 3.5 **D**). NPQ relaxation k in 2021 was intermediate of that observed in the broader panel (5.07 to 5.67 min^{-1} in 2021 (Figures 4.6 **D** and 4.7 **D**), compared to 3.97 to 6.19 in the panel (Figure 3.5 **E**).

4.4.2 NPQ variation between allele groups

The experimental groups chosen for SNP Chr01_67331530 diverged strongly between alleles for both NPQ induction k ($p = 0.002$, Figure 4.6 **C**) and NPQ relaxation k ($p = 0.015$, Figure 4.6 **D**) allowing for rejection of the null hypothesis, and were directionally consistent in max NPQ with the 2017/2019 panel results, a strong indication that this locus is indeed associated with genetic variation in photoprotective capacity. SNP Chr01_67331530 was significant in the joint model GWAS for CT1 (a multitrait composite of max NPQ, NPQ induction k, NPQ relaxation k, and NPQ relaxation amplitude) as well as joint model PI. That PI was not variable between allele groups in 2021 may be indicate a high level of genotype x environment effect in PI. This tendency is supported by the fairly low heritability observed in joint-model GWAS PI (0.36, Figure 3.11) and low correlation between 2017 and 2019 results (Pearson $r = 0.21$, Figure 3.12).

Sobic.001G385900, the nearest gene and only gene within the same LD block to Chr01_67331530, is a hydroxyproline-rich glycoprotein orthologous to an Euonymus related lectin (EUL) protein coding gene in rice (LOC_Os07g48460, OsEULD2). Lectins are carbohydrate-binding proteins and EULs are a unique group specifically found in plants (Fouquaert et al., 2009). The sorghum gene has been noted as likely to be chloroplast, cytoplasm, or extracellularly targeted and associated with cold stress tolerance and stay-green in sorghum, with another nearby gene

model (Sobic.001G386500) appearing to have a single insertion mutation separating it from other lectins and a single binding domain, suggesting a specialised functionality in splicing or gene expression (Osman et al., 2022). De Schutter et al. (2017) characterised OsEULD2 as a putatively expressed lectin, significantly upregulated in response to drought and osmotic stress. OsEULD2 likely binds to α-D-mannose (Man), α-1,2-dimannoside (Man1,2Man), and N-acetyl-D-lactosamine (LacNAc) (De Schutter et al., 2017). While the monosaccharide mannose and glycoprotein latosamine are not clearly directly related to photoprotection, variation in the presence of mannose-derived complex carbohydrates and glycoproteins, which play a role in membranes as cellular structural carbohydrates and in signaling mechanisms (Léonard et al., 2002; Liepman et al., 2007; Meier and Reid, 1982; Stefanowicz et al., 2012), could influence chloroplast structure and potentially affect the distribution and stability of carotenoids and potentially indirectly affect photoprotection. EULs have been implicated in abiotic and biotic stress sensing response in rice (Al Atalah et al., 2014), flax (Levchuk et al., 2013), and Arabidopsis (via stomatal regulation, Van Hove et al., 2015). Given the apparent overlap in sensing and regulatory mechanisms of both stomata and NPQ (Busch, 2014; Głowacka et al., 2018; Kromdijk, Głowacka, and Long, 2019; Talbott et al., 2003), this provides additional credit towards the establishment of Sobic.001G385900 as a light-stress response gene in sorghum.

While accessions of divergent allele groups at SNP Chr01_76704821 (a significant locus for max NPQ in the joint model GWAS) did not tend to show great divergence in any of the four traits focused on in this study (Figure 4.7) and do not support rejection of the null hypothesis, it is still notable that the directional relationship of max NPQ was similar to that observed in the broader set of accessions in the 2017/2019 allele groups. This locus is still a strong candidate, as the SNP itself exhibited the lowest FDR-adjusted p-value in the entire GWAS trial, and is collocated within 20 kB of three other highly-enriched SNPs for max NPQ. As well, allelic segregation of accessions at those collocated SNPs tended to match closely with that of Chr01_76704821. However, this null confirmation result is

useful as well, signifying the importance of following up GWAS hits to weed out spurious, or strongly conditional, results.

In conclusion, this 2021 re-screen conducted from a genotype-first perspective improves confidence in SNP Chr01_67331530 underlying genetic control of photoprotection in dynamic light conditions in sorghum. Additionally, the null result at SNP Chr01_76704821 re-enforces the importance of validation of GWAS results in order to confirm genotype/phenotype associations. Further investigation via mutant segregation screening and RNA/expression analysis of Sobic.001G385900 and top genes provided in chapter three, either directly in sorghum or using Arabidopsis orthologues, would constitute a valuable next step toward uncovering genetic control of photoprotection and improving photosynthetic efficiency in sorghum.

5

Photoinhibition and C_4/C_3 cycle coordination in sorghum accessions with contrasting photoprotective capacity

5.1 Introduction

Several of the world's most important crops, including *Sorghum bicolor* (sorghum), *Zea mays* (maize), *Saccharum officinarum* (sugarcane) utilise C_4 photosynthesis to produce the food, fuel, and fibre required to sustain human life. The C_4 pathway has evolved as a naturally water-use efficient growth solution in high temperature and arid environments (Christin and Osborne, 2013). In the face of continued climate change and the associated increase in temperature and reduction in water availability in many crop production regions (Rahman et al., 2022), improving photosynthetic efficiency in these crops will be necessary in order to sustain production levels to meet future demand (Zhu, Long, et al., 2010). In order to enhance photosynthesis and water use efficiency, it is integral that we first mechanistically understand photosynthetic processes and their limitations in the dynamic environmental conditions in which crops are grown (Hatfield and Dold, 2019). Such an understanding will facilitate the targeted crop improvements necessary to ensure food and fuel security during this era of rapid climatic change.

The C_4 carbon concentrating mechanism (CCM) involves carboxylation of phosphoenolpyruvate (PEP) leading to four-carbon acids in mesophyll cells (MC). The resulting acids diffuse into physically separate bundle sheath cells (BSC) and are subsequently decarboxylated, increasing the CO_2 concentration around BSC-localised Ribulose-1,5-bisphosphate (RuBP) carboxylase/oxygenase (Rubisco) (Hatch, 1971). The CCM decreases RuBP oxygenation and subsequent photorespiration and generally results in improved photosynthetic efficiency compared to C_3 species (Ehleringer and Björkman, 1977; Ehleringer and Pearcy, 1983; Sage, 2014).

During stomatal diffusion and the aforementioned enzymatic carboxylation steps, the plant carbon pool becomes enriched in $^{12}CO_2$ due to small differences in reaction and diffusion rates compared to the minor $^{13}CO_2$ isotopologue– a process termed carbon isotope discrimination. If the BSC were impermeable to CO_2 diffusion, carbon isotope discrimination during C_4 photosynthesis would be limited to that observed between and within the atmospheric and mesophyll diffusional and enzymatic processes. BSC are not impermeable, however, and a portion of the highly-concentrated bundle sheath CO_2 "leaks" back into mesophyll cells (Farquhar, 1983).

This apparent leakiness (ϕ, the ratio of bundle sheath leak rate to PEP carboxylation rate) is relatively invariable in steady-state light conditions such as those experienced by plants grown in controlled environments, typically ranging from 0.1-0.3, and shows little acclimatory response to different growth light environments (Jaikumar et al., 2021). However, ϕ tends to increase transiently to 0.6-0.9 under low photosynthetic photon flux density (PPFD), potentially due to increased relative contribution of mitochondrial respiration or lack of photorespiratory suppression (Cousins et al., 2006; Henderson et al., 1992; Kromdijk, Griffiths, et al., 2010; Kromdijk, Schepers, et al., 2008; Kromdijk, Ubierna, et al., 2014; Tazoe et al., 2008). Assuming leaked CO_2 comes from prior C_4 acid decarboxylation, increased ϕ represents wasteful PEP overcycling and indicates a loss of photosynthetic efficiency, given the ATP cost of PEP regeneration (Henderson et al., 1992).

Dynamic light conditions, rather than steady-state, are the reality for field-grown crops. C_4 photosynthetic response to dynamic light conditions is complex, due to

the required dynamic coordination between the carboxylation and decarboxylation cycles in MC and BSC (Sage and McKown, 2005; Slattery et al., 2018; Von Caemmerer and Furbank, 1999). The CCM requires partitioning of light energy between regeneration of PEP in mesophyll cells and C_4 acid decarboxylation and subsequent RuBP carboxylation within BSC. Fluctuating light can upset the balance of energy partitioning, causing imbalances in MC/BSC metabolite pools and increasing the level of ϕ. This can result in increased photorespiration and decreased photosynthetic efficiency (Sage and McKown, 2005). Transient increases in ϕ have recently been recorded during photosynthetic induction (Wang, Stutz, et al., 2022), suggesting energy-use incoordination during the low-to-high portion of dynamic light fluctuation, though this incoordination could potentially be buffered in field conditions due to existing metabolite gradients (Cubas et al., 2023; Stitt and Zhu, 2014).

Photoinhibition, the sustained down-regulation of photosystem II (PSII) electron transport, can also increase in dynamic light conditions due to transient imbalances in photosynthetic energy supply and demand (Kubásek et al., 2013; Romanowska, Buczyńska, et al., 2017). BSC in sorghum are strongly depleted in PSII compared to their mesophyll cell counterparts (Hardt and Kok, 1978; Romanowska, Drożak, et al., 2006), thus the potential exists for photodamage to be manifested differentially between cells types, conceivably resulting in metabolic incoordination and increases in ϕ. This could be a frequent occurrence in the dynamic light conditions experienced by field crops. Indeed, medium-intensity dynamic light has been suggested to cause transient increases in ϕ (Kubásek et al., 2013) but clear evidence of sustained photoinhibition-induced increases in ϕ does not exist.

In the current study, it was hypothesised that sustained periods of high light would increase ϕ, more prominently in fluctuating rather than steady-state light. Additionally, it was hypothesised that a sorghum accession with lower capacity for photoprotection would be more negatively impacted by both high light treatments, resulting in increased post-treatment ϕ. Carbon isotope discrimination during photosynthesis was measured and used to calculate ϕ before, during, and after both

steady-state and fluctuating high light treatments. Because impacts on CCM efficiency could potentially affect the suppression of photorespiration, measurements were performed in both ambient (21%) and low (2%) O_2 conditions. In most cases ϕ decreased after treatment; however, the magnitude of effects of light treatment on carbon isotope discrimination differed by O_2 concentration, and sorghum accessions with contrasting photoprotective capacities appeared to be differentially affected by high light treatments.

5.2 Materials and methods

5.2.1 Plant material and growth

Two sorghum accessions (PI276818 and PI521057) were selected based on their contrasting NPQ phenotypes in the 2017/2019 field trials (chapter three). PI276818 was selected for its combination of high maximum NPQ and low rate constants of NPQ induction and relaxation (slower NPQ kinetics). PI521057 was selected for its combination of low maximum NPQ and high rate constants of NPQ induction and relaxation (faster NPQ kinetics).

Seeds of the two accessions were sown into Levington Advance Pot & Bedding M3 soil mixture (204/104/339 NPK) in 9 cm pots. Five to seven days after germination, seedlings were transferred to 2 l pots containing a mixture of 1:1:0.5 parts M3: Westland Top Soil: perlite, with additions of 2 tbsp l^{-1} Osmocote Smart Release Plant Food, 0.25 tbsp l^{-1} magnesium salt (Miracle-Gro, Evergreen Garden Care, Camberley, UK), and 0.5 tbsp l^{-1} ground lime. Plants were grown in two identical growth cabinets (Conviron, Winnipeg, Canada) fitted with LED lights providing approximately 500 μmol m^{-2} s^{-1} PPFD at pot level, with a 14:10 hour light:dark period. Light and dark-period temperatures were controlled at 28 and 20 °C, respectively, and relative humidity was controlled at 65%. Plants were grown in eight sets planted sequentially from early December 2022 through mid-February 2023 to provide a continuous supply of measurable samples. Plants were rotated sequentially within the cabinets three times per week and between the cabinets once per

week to mitigate potential heterogeneous lighting and environmental bias. Gas exchange and isotope measurements were made using the youngest fully expanded leaf with a visible ligule, four to five weeks after seedling emergence (generally the fifth leaf), with all plants from a growth set measured within a six day period.

5.2.2 Leaf gas exchange and carbon isotope measurement

Photosynthetic gas exchange measurements before, during, and after high-light treatments were made using LI-6800 Portable Photosynthesis Systems with 6800-01A Fluorometer chambers (LI-COR, Lincoln, NE, USA). Two LI-6800s were coupled to a tunable diode laser analyser (TDL, Thermo-Fisher Delta Ray IRIS, Bremen, Germany) to measure the stable carbon isotope ratio ($\delta^{13}C$) of CO_2 in air entering and exiting the leaf chamber in order to calculate online carbon isotope discrimination ($\Delta^{13}C$) during photosynthesis. A custom-built gas mixing and sampling system provided the LI-6800s and TDL with identical background gas at either 21% or 2% O_2 for calibrations and measurements.

Tanks of N_2 (99.998% purity, BOC, Guildford, UK), O_2 (99.5% purity, BOC), and a custom-blend 1% CO_2 in N_2 (BOC) were connected via stainless-steel tubing to a three-gas mixer (GMS_3CH, QCAL Messtechnik GmbH, Munich, Germany). The GMS_3CH uses mass flow controllers (MFCs) to provide a single outlet airstream with the desired gas composition. Another MFC (Bronkhorst F-201CB) was used downstream of the GMS_3CH to regulate flow output to the LI-6800 inlets and maintain pressure to the TDL carrier gas inlet. The TDL mixes CO_2 with a known $^{13}C/^{12}C$ isotopic composition with this CO_2-free carrier gas at a concentration matching that of the sample of interest. A custom Python script was used to monitor line pressure between the GMS_3CH and Bronkhorst MFC and adjust the Bronkhorst MFC flow to keep upstream pressure between 1.7 and 1.9 bar, as the TDL requires > 1 bar of carrier gas inlet pressure. Outlet flow to the LI-6800s was provided in excess of requirements and vented with an open split. The 1% CO_2 tank was only used during TDL concentration calibrations; during plant measurements the LI-6800 reference CO_2 was supplied via the LI-6800's 8 g cartridge. The TDL

was calibrated in accordance with manufacturer recommendations prior to starting measurement sets in either 2% or 21% O_2.

Prior to starting measurement campaigns at a given O_2 concentration, LI-6800s were range-matched for CO_2 and H_2O after running for at least two hours. Four plants were measured per day, using two LI-6800s– two plants in the morning, and two in the afternoon. Leaves of morning plants were dark adapted overnight, and afternoon leaves dark adapted for at least two hours, prior to being placed in the 6800-01A chamber (6 cm^2 aperture) with the actinic LEDs off and fluorometer measuring beam on. O_2 concentration in the LI-6800 was adjusted to the appropriate value prior to starting measurements. Gaps around the leaf midvein were sealed around the outside of the chamber with silicon grease (Dow Corning DC4 High Vacuum). Most leaves measured filled the chamber area; those that did not were photographed after measurement and leaf area subsequently calculated using Fiji (Schindelin et al., 2012). Sample CO_2 concentration was controlled at 420 μmol mol^{-1}, leaf-air VPD controlled at 1.5 kPa, and leaf temperature (T_{leaf}) controlled at 28° C. Prior to beginning the high-light portion of light treatments, temperature control was set to heat exchanger control at the steady-state value needed to maintain a T_{leaf} of 28 °C, to prevent excessive control loop swings during the fluctuating light treatment. Leaf temperature during high light periods did not exceed 29.4 °C. Sample chamber flow rate was controlled at 230 μmol s^{-1}. Chamber overpressure was controlled at 0.1 kPa and "Advance Polymer" (LI-COR) gaskets were used to reduce CO_2 diffusion between growth chamber and within-leaf chamber air. Before and during experiments the plants and measuring heads were kept in environmentally stable conditions inside a growth cabinet (E41-HO, Percival Scientific, Perry, IA, USA), set at 28°C and a light intensity of approximately 500 μmol m^{-2} s^{-1} PPFD at leaf level.

Once initial fluorescence was stable, a single datapoint was logged to record maximum photosystem II quantum efficiency (Fv/Fm). The 6800-01A actinic LEDs were then set to 500 μmol m^{-2} s^{-1} PPFD (90% red / 10% blue, up to a maximum 40 μmol m^{-2} s^{-1} PPFD blue), and CO_2 assimilation (A_{net}) and stomatal conductance to

water vapour g_{sw} monitored for stability (approximately 40 minutes) before starting measurements. The measurement routine consisted of 40 minutes of 500 μmol m^{-2} s^{-1} PPFD, followed by 160 minutes at either steady-state 2,000 μmol m^{-2} s^{-1} PPFD, or five-minute cyclic fluctuations of four minutes at 2,000 μmol m^{-2} s^{-1} PPFD and one minute at 50 μmol m^{-2} s^{-1} PPFD. The high-light treatment period was then followed by 500 μmol m^{-2} s^{-1} PPFD for 80 minutes. Gas exchange traits were logged at 10 second intervals and chlorophyll fluorescence at five minute intervals during the measurement routine. Fluorescence saturating flashes were scheduled using a LI-6800 background program to occur near the end of the high-light period of the fluctuating light cycle, outside of the TDL sampling window (described later). Multiphase flashes were used, with step and ramp durations calibrated prior to the experiment in accordance with Loriaux et al. (2013) and the LI-6800 manual, using sorghum accessions grown in the same environment as those used in experiments. Dynamic gas exchange calculations were used, with manufacturer-recommended "tuning" performed in advance of experiments, using the same chamber and flow conditions as used in experiments. LI-6800 point matches for CO_2 were performed manually two to three times during the measurement routine, only during periods when the TDL was not sampling from a photosynthesis system.

The TDL was programmed to sequentially sample from the LI-6800 sample and reference exhaust ports, using a custom designed manifold (LI-COR, (Figure 5.3)) controlled via the TDL's digital trigger outputs. Isotope standard referencing was performed after each LI-6800 sample, in accordance with manufacturer recommendations and internal testing. Long-term tank gas measurements and allan deviation analysis were performed previously in order to characterise TDL precision over different sample averaging intervals (Figure 5.2). Based on allan deviation precision analysis results, TDL data were collected at 1 Hz then averaged over 85 second sample periods, chosen as the most appropriate balance between sample throughput and precision. Two LI-6800s were operated simultaneously and sampled sequentially via a two-way three-port valve (Valco VICI, Schenkon, Switzerland)

controlled via the TDL's digital trigger outputs. Prior to sampling from the LI-6800s, 70 seconds of flush time was allowed to ensure steady-state conditions in the TDL. This timing was determined in advance based on the TDL optical cell flush time and the amount of time needed for step changes in CO_2 composition within the LI-6800 chamber to be reflected in the TDL signal. Prior to isotope reference sampling, 60 seconds of flush time was allowed (as the carrier gas inlet was under constant pressure, less time was needed). In aggregate, the sampling routine (a "measurement block") consisted of:

1. LI-6800(1) sample-side measurement ($\delta^{13}C_{sam}$) followed by TDL isotope reference
2. LI-6800(1) reference-side measurement ($\delta^{13}C_{ref}$) followed by TDL isotope reference

Repeat 1 and 2 (total: 20 minutes, four measurements)

3. LI-6800(2) $\delta^{13}C_{sam}$ followed by TDL isotope reference
4. LI-6800(2) $\delta^{13}C_{ref}$ followed by TDL isotope reference

Repeat 3 and 4 (total: 20 minutes, four measurements)

For each instrument, $d\delta^{13}C$ ($\delta^{13}C_{ref}$ - $\delta^{13}C_{sam}$, needed to calculate $\Delta^{13}C$) was calculated to provide two technical replicates per sample line by subtracting the first $\delta^{13}C_{sam}$ from the first and second $\delta^{13}C_{ref}$, then the second $\delta^{13}C_{sam}$ from the first and second $\delta^{13}C_{ref}$ (Figure 5.1).

High-light treatments from LI-6800 (2) were started 20 minutes later than LI-6800 (1), so that each plant received the same duration of treatment. LI-6800 and TDL clocks were manually synchronised at the beginning of each measurement day. The TDL program was coordinated to sample within the final 100 seconds of the high-light portion of the fluctuating period, in an effort to sample the most steady-state portion of the fluctuating light treatment. Data from the LI-6800s and TDL were combined by merging overlapping sampling periods using a custom script and R

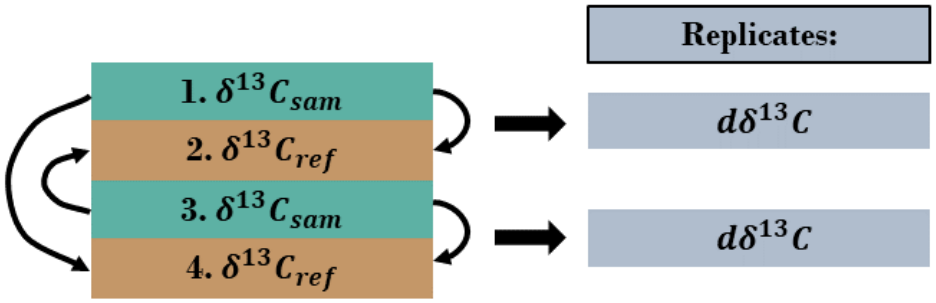

Figure 5.1: Schematic of sampling and averaging strategy for $\delta^{13}C$ measurement blocks from a single LI-6800 photosynthesis system coupled to a TDL.

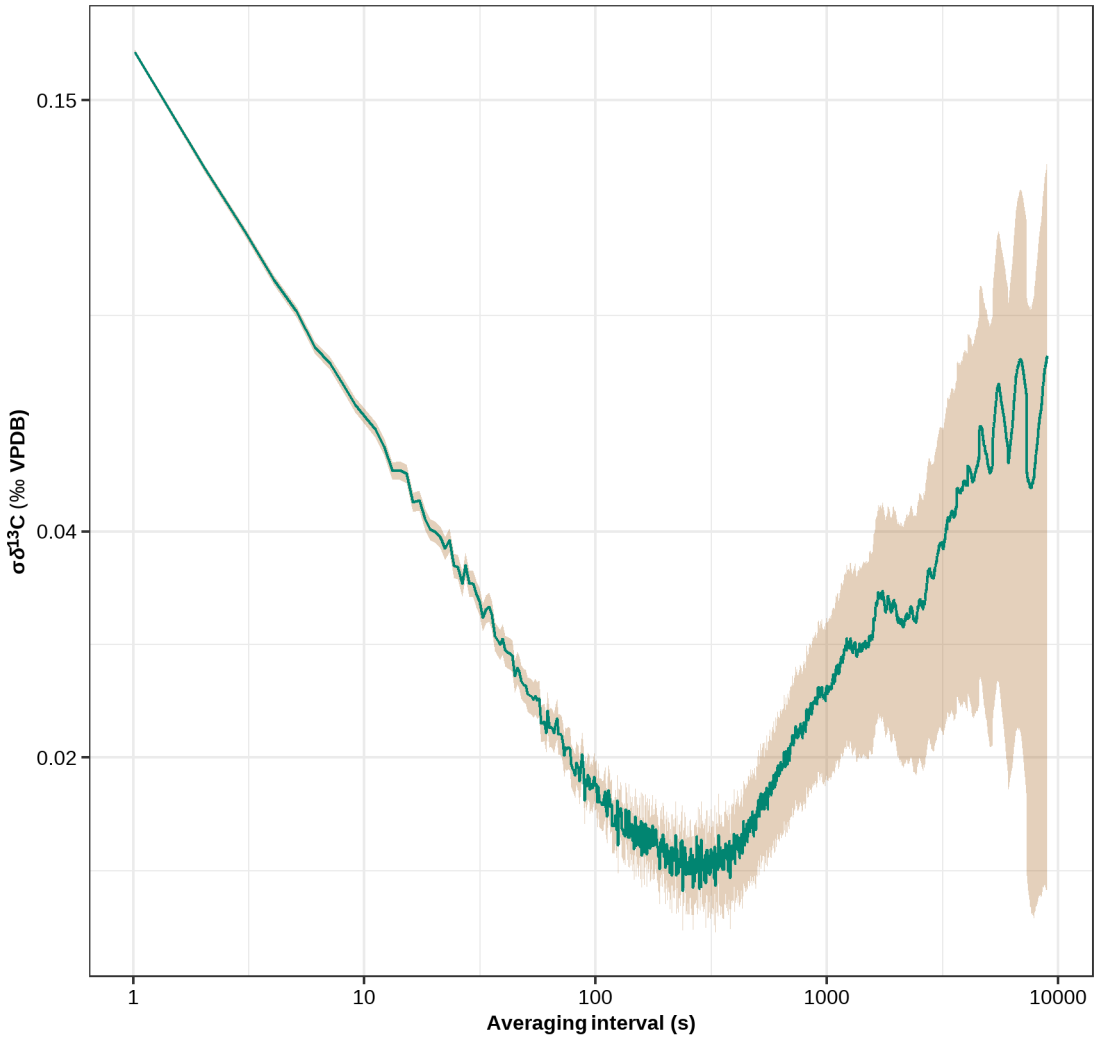

Figure 5.2: Allan deviation plot of tank CO_2 measured in TDL over 10 hours, showing precision at different averaging intervals. Shading is +/- two times the uncertainty of allan deviation value for a given averaging interval.

package "fuzzyjoin" (Robinson et al., 2015), thus eight LI-6800 log points collected during the TDL sampling interval were averaged as the gas exchange data for a single TDL sample. A delayed merge window was used to account for the 30 second delay between LI-6800s and the TDL (previously quantified by analysing step-changes in TDL CO_2 concentrations when switching between LI-6800 manifold sides). To account for isotope fractionation within the LI-6800 exhaust manifolds (as the reference/sample side exhaust bores were different diameters), empty-chamber measurements were collected at the end of each measurement day using the same conditions and background gas as was used for leaf measurements. The median apparent offset observed during the measurement campaign, tending towards a slightly higher $\delta^{13}C$ from the reference side of the manifold (Figure 5.4), was subtracted from reference side $\delta^{13}C$ values before computing further isotope discrimination values. Sorghum accessions and steady/fluctuating light treatments were structured evenly between instruments and morning/afternoon periods, to allow for accounting of possible structural variation in results analysis via mixed-effect modelling.

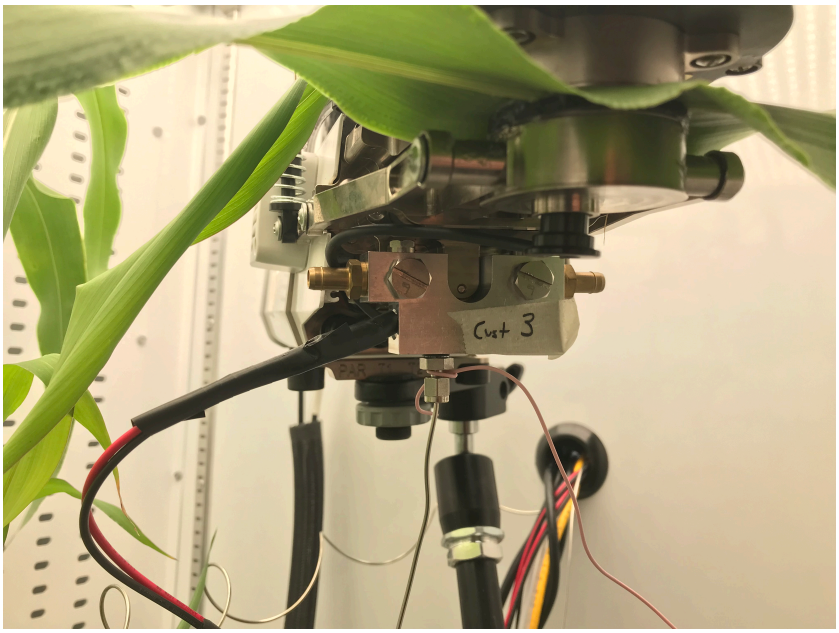

Figure 5.3: 6800-01A Fluorometer chamber and TDL sampling manifold during sorghum photosynthesis measurement

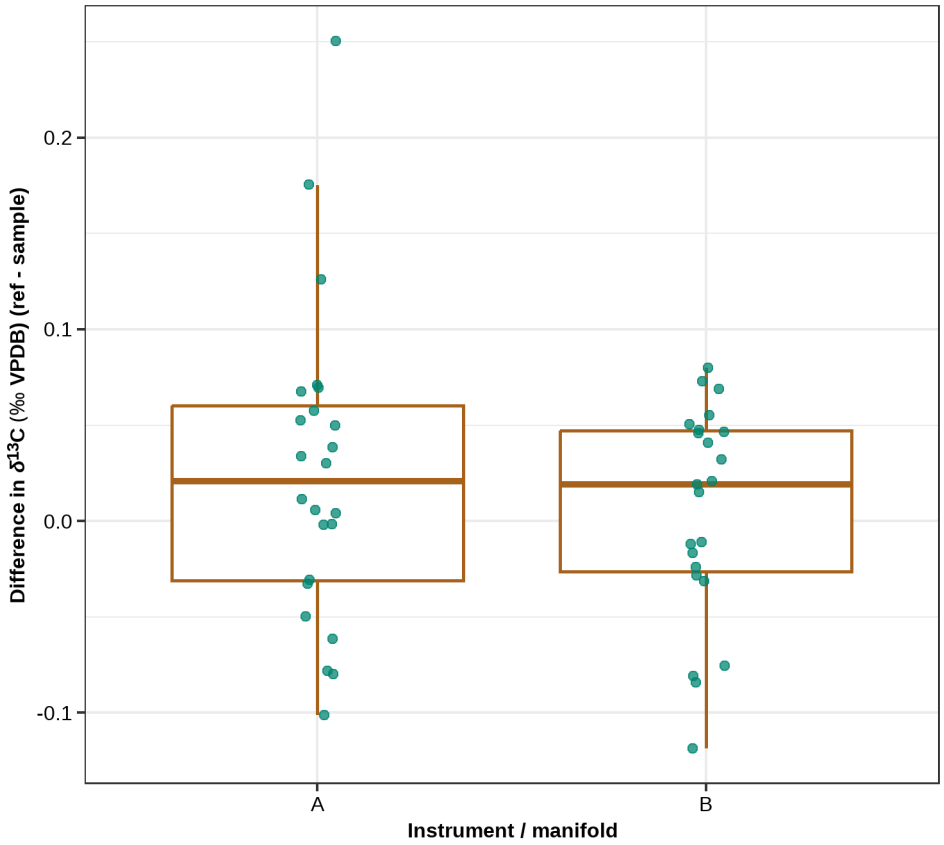

Figure 5.4: Difference between reference and sample side stable carbon isotope ($\delta^{13}C$) values of two LI-6800 exhaust port sampling manifolds when sampling empty gas exchange chambers. Points are 85 second sample means collected once per measurement day. Internal box plot edges represent first and third quartiles. The solid line within the boxes indicates the median.

5.2.3 Photosynthetic carbon isotope discrimination and bundle sheath leakiness

$\Delta^{13}C$ was calculated according to Evans et al. (1986):

$$\Delta^{13}C = \frac{\xi(\delta^{13}C_{sam} - \delta^{13}C_{ref})}{1000 + \delta^{13}C_{sam} - \xi(\delta^{13}C_{sam} - \delta^{13}C_{ref})} * 1000 \tag{5.1}$$

Where $\delta^{13}C_{sam}$ and $\delta^{13}C_{ref}$ are the $\delta^{13}C$ values from the LI-6800 sample and reference exhaust airstreams, respectively, and ξ a scaling term representing the magnitude of difference between LI-6800 reference (C_{ref}) and sample (C_{sam}) exhaust dry CO_2 concentrations:

$$\xi = \frac{C_{ref}}{C_{ref} - C_{sam}} \tag{5.2}$$

Electron transport rate was calculated and tested as a model parameter using three methods:

Method 1:

$$J_{6800} = \Phi PSII * Q_{abs} * p\frac{PSII}{PSI} \tag{5.3}$$

J_{6800} is the electron transport rate calculated from chlorophyll fluorescence from the LI-6800, where $\Phi PSII$ is PSII quantum efficiency at the current actinic light level, Q_{abs} the proportion of incident light absorbed by the leaf, and $p\frac{PSII}{PSI}$ the ratio of PSII/photosystem I (PSI), assumed to be 0.4. Q_{abs} was determined using an integrating sphere and spectrophotometer (LI-1800, LI-COR) at 475 and 625 nm, the blue and red LED peak wavelengths of the 6800-01A fluorometer reported in the instrument manual.

Method 2:

$$J_{atp} = s'Q_{inc}\Phi PSII/(1-x) \tag{5.4}$$

J_{atp} is the rate of ATP production driven by electron transport (Yin and Struik, 2009; Yin, Sun, et al., 2011). s' is a calibration factor calculated from the slope of A_{net} against $Q_{inc}\Phi PSII/3$ under non-photorespiratory conditions, Q_{inc} is PPFD incident on the leaf, and x the fraction of e^- or ATP partitioned to the C_4 cycle (assumed 0.4).

Method 3:

$$J_{et} = \frac{-II + \sqrt{II^2 - 4 * III * I}}{2 * III} \tag{5.5}$$

where

$$I = \left(1 + \frac{R_d}{A_{net}}\right)\left(R_m - g_{bs}C_m - \frac{7g_{bs}\gamma^* O_m}{3}\right) + (R_d + A_{net})\left(1 - \frac{7\alpha\gamma^*}{3 * 0.047}\right) \tag{5.6}$$

$$II = \frac{1-x}{3}\left[\frac{g_{bs}}{A_{net}}\left(C_m - \frac{R_m}{g_{bs}} - \gamma^* O_m\right) - 1 - \frac{\alpha\gamma^*}{0.047}\right] - \frac{x}{2}\left(1 + \frac{R_d}{A}\right) \tag{5.7}$$

$$III = \frac{x - x^2}{6A_{net}} \tag{5.8}$$

Derived from von Caemmerer (2000), Ubierna et al. (2013), and implemented as in Wang, Stutz, et al. (2022). R_d is total non-photorespiratory CO_2 respiration in the light, R_m is mesophyll non-photorespiratory CO_2 respiration in the light ($0.5R_d$), g_{bs} is bundle sheath CO_2 conductance (2.35 x 10^{-3} mol m^{-2} s^{-1}, Kromdijk, Griffiths, et al., 2010), C_m is mesophyll cell CO_2 concentration (assumed to equal to C_i, intercellular CO_2 concentration), γ^* is half the Rubisco specificity for CO_2 (1.93 x 10^{-4}, von Caemmerer, 2000; von Caemmerer et al., 1994), O_m is mesophyll cell O_2 concentration, and α is the fraction of PSII activity in the bundle sheath (0, von Caemmerer (2000)).

J_{et} was used moving forward, as it was the only method which did not lead to occasional calculated negative bundle-sheath CO_2 concentrations for a portion of sample lines. Phosphoenolpyruvate (PEP) carboxylation velocity V_p and bundle sheath O_2 concentration O_{bs} were then calculated to estimate bundle sheath CO_2 concentration C_{bs}, as follows:

$$V_p = xJ_{et}/2 \tag{5.9}$$

$$O_{bs} = \frac{\alpha A_{net}}{0.047 g_{bs}} + O_m \tag{5.10}$$

$$C_{bs} = \frac{\gamma^* O_{bs}\left[\frac{7}{3}(A_{net} + R_d) + \frac{(1-x)J_{et}}{3}\right]}{\frac{(1-x)J_{et}}{3} - A_{net} + R_d} \tag{5.11}$$

further used to estimate velocities of Rubisco carboxylation (V_c) and oxygenation (V_o), and b'_3, a term encompassing fractionation by Rubisco, respiratory, and photorespiratory fractionation (Farquhar, 1983; Pengelly et al., 2010):

$$V_c = \frac{A_{net} + R_d}{1 - \frac{\gamma^* O_{bs}}{C_{bs}}} \tag{5.12}$$

$$V_o = \frac{V_c - A_{net} - R_d}{0.5} \tag{5.13}$$

$$b'_3 = b_3 - \frac{e' R_d}{V_c} - \frac{f V_o}{V_c} \tag{5.14}$$

b_3 is fractionation by Rubisco (30‰), f is photorespiratory fractionation (11.6‰, Lanigan et al., 2008), and e' is an estimate of fractionation during decarboxylation, accounting for differences in instantaneous measurement and growth $\delta^{13}C$ ($\delta^{13}C_{gr}$):

$$e' = e + \delta^{13}C_{ref} - \delta^{13}C_{gr} \tag{5.15}$$

where e is fractionation during mitochondrial respiration (Gillon and Griffiths, 1997; Kromdijk, Griffiths, et al., 2010) and $\delta^{13}C_{gr}$ is taken as -8.85‰, near the average atmospheric $\delta^{13}C$ reported during the winter of 2021/22 at Mace Head Atmospheric Research Station in Galway, Ireland.

b'_4, net fractionation during CO_2 hydration and PEP carboxylation, was estimated as:

$$b'_4 = b_4 - e' \frac{0.5 R_d}{(A + 0.5 R_d)} \tag{5.16}$$

with the assumption that bicarbonate and CO_2 were in equilibrium (carbonic anhydrase was not limiting).

b_4 was calculated in accordance with Mook et al. (1974) using measured leaf temperature:

$$b_4 = \frac{-9.483 * 1000}{273 + (T_{leaf})} + 23.89 + 2.2 \tag{5.17}$$

ϕ can then be estimated, assuming infinite mesophyll conductance, by:

$$\phi = \frac{\frac{1-t}{1+t}\Delta - \frac{a'}{1+t} - (b'_4 - a')\frac{Ci}{Ca}}{(b'_3 - s)\frac{Ci}{Ca}} \tag{5.18}$$

where s is fractionation during bundle sheath leakage (1.8‰) and t is a ternary correction factor (Farquhar and Cernusak, 2012) accounting for the effect of the magnitude of leaf transpiration (E, from LI-6800) on CO_2 assimilation:

$$t = \frac{a_{ac}E}{2g_{tc}} \tag{5.19}$$

g_{tc} is combined boundary layer and stomatal conductance to CO_2, reported by the LI-6800, and a_{ac} is $1 + a' * 0.001$, where a' is the combined fractionation through the leaf boundary layer and stomata:

$$a' = \frac{a_s(C_a - C_i)}{C_a - C_i} \tag{5.20}$$

a_s is fractionation across the stomata (4.4‰) and C_i and C_a are, respectively, the leaf intercellular CO_2 concentration and the ambient CO_2 concentration surrounding the leaf, reported by the LI-6800. This formulation assumes that boundary layer conductance to CO_2 is infinite due to turbulence within the leaf chamber, thus C_a is equivalent to leaf surface CO_2 concentration (C_s).

Due to the error amplification in the equation by Evans et al. (1986) (Eq. (5.2)) The precision of the d13C determinations is the main determinant of D13C and leakiness estimation precision. As $\delta^{13}C_{sam}$ and $\delta^{13}C_{ref}$ were sampled sequentially over time, the possibility exists for different heirarchal averaging strategies to increase confidence in $\Delta^{13}C$ measurements. Several stepwise sample averaging methods were investigated in order to determine which provided the highest precision:

1. AV1: $d\delta^{13}C$ technical replicates and their associated e' values were averaged, then carried through to calculate two individual ϕ values per instrument, per measurement block.

2. AV2: $d\delta^{13}C$ technical replicates and their associated e' values multiplied to ξ values independently; ξ values were averaged, then carried through to calculate two individual ϕ values per instrument, per measurement block.

3. AV3: $d\delta^{13}C$ technical replicates and their associated e' values multiplied to ξ values independently, carried through to independent $\Delta^{13}C$ values, which were then averaged, then carried through to calculate two individual ϕ values per instrument, per measurement block.

4. Observation mean: $d\delta^{13}C$ technical replicates and their associated e' values were averaged, then downstream $\Delta^{13}C$ and gas exchange values were averaged within the measurement block, carrying forward single values through the isotope discrimination model calculations for each 20 minute measurement block.

Observation mean averaging was used for further analysis, as biological variance was large enough to obfuscate any substantial drawbacks or benefits of using any of the upstream averaging strategies. Measurement blocks of carbon isotope discrimination values were numbered one through seven, with block one corresponding to the 40 minutes of steady-state 500 μmol m^{-2} s^{-1} PPFD pre-treatment measurement, blocks two through five the 160 minutes of high light treatment, and blocks six and seven the 80 minute post- high light treatment 500 μmol m^{-2} s^{-1} PPFD period.

Table 5.1: List of symbols used in isotope discrimination and chlorophyll fluorescence calculations

Variable	Definition	Value
a_s	Fractionation accross the stomata	4.4‰ (Craig, 1953; Ubierna et al., 2013)
a'	Weighted fractionation through the leaf boundary layer and stomata	Eq. (5.20)
a_{ac}	Boundary layer / stomatal fractionation term for ternary correction	$1 + a' * 0.001$
A_{net}	Net CO_2 assimilation	Measured
b_3	Fractionation by Rubisco	30‰ (Roeske and O'Leary, 1984)
b'_3	Fractionation term including Rubisco, respiration, and photorespiration	Eq. (5.14), (Farquhar, 1983; Pengelly et al., 2010)
b_4	Fractionation during PEP carboxylation	Eq. (5.17), (Henderson et al., 1992; Mook et al., 1974)
b'_4	Net fractionation during CO_2 hydration and PEP carboxylation	Eq. (5.16)
C_a	Ambient CO_2 concentration surrounding leaf	Measured
C_{bs}	Bundle sheath CO_2 concentration	Eq. (5.11)
C_i	Leaf intercellular CO_2 concentration	Measured
C_m	Mesophyll cell CO_2 concentration	Assumed = C_i
C_{ref}	Dry LI-6800 reference CO_2 concentration	Measured
C_s	CO_2 concentration at leaf surface	Assumed = C_a
C_{sam}	Dry LI-6800 sample CO_2 concentration	Measured
e	Fractionation during mitochondrial respiration	-6‰ (Gillon and Griffiths, 1997; Kromdijk, Griffiths, et al., 2010)
e'	Respiratory fractionation corrected for growth substrate $\delta^{13}C$	Eq. (5.15)
E	Transpiration rate	Measured

Table 5.1: List of symbols used in isotope discrimination and chlorophyll fluorescence calculations *(continued)*

Variable	Definition	Value
f	Photorespiratory fractionation	11.6‰ (Lanigan et al., 2008)
Fv/Fm	Maximum PSII quantum efficiency	Measured
g_{bs}	Bundle sheath conductance to CO_2	2.35 x 10^{-3} mol m^{-2} s^{-1} (Kromdijk, Griffiths, et al., 2010)
g_{tc}	Total leaf conductance to CO_2	Measured
J_{6800}	Electron transport rate calculated via chlorophyll fluorescence	Measured Eq. (5.3)
J_{atp}	Rate of ATP production driven by electron transport	Eq. (5.4) (Yin and Struik, 2009; Yin, Sun, et al., 2011)
J_{et}	Electron transport rate calculated via gas exchange parameters	Eq. (5.5) (Ubierna et al., 2013; von Caemmerer, 2000; Wang, Stutz, et al., 2022)
O_{bs}	Bundle sheath cell O_2 concentration	Eq. (5.10), (von Caemmerer, 2000)
O_m	Mesophyll cell O_2 concentration	2,000 or 210,000 μmol m^{-2} s^{-1}
R_d	Total non-photorespiratory CO_2 respiration in the light	Intercept term from light response curve (Eq. 5.2.4) (Yin and Struik, 2009; Yin, Sun, et al., 2011)
R_m	Mesophyll non-photorespiratory CO_2 respiration in the light	$0.5R_d$
s	Fractionation during bundle sheath leakage	1.8‰ (Henderson et al., 1992)
s'	Calibration factor for J_{atp} calculation	Slope term from light response curve (Eq. 5.2.4) (Yin and Struik, 2009; Yin, Sun, et al., 2011)
t	Ternary term	Eq. (5.19)
V_c	Velocity of Rubisco carboxylation	Eq. (5.12)
V_o	Velocity of Rubisco oxygenation	Eq. (5.13)

Table 5.1: List of symbols used in isotope discrimination and chlorophyll fluorescence calculations *(continued)*

Variable	Definition	Value
V_p	Velocity of PEP carboxylation	Eq. (5.9)
α	Fraction of PSII activity in the bundle sheath	0 (von Caemmerer, 2000)
x	Portion of ATP allocated to C_4 cycle	0.4 (von Caemmerer, 2000)
$\delta^{13}C_{gr}$	Stable carbon isotope ratio, growth room	-8.85‰ (source: NOAA Global Monitoring Laboratory, Mace Head, Ireland– https://gml.noaa.gov/dv/site/index.php?stacode=MHD)
$\delta^{13}C_{ref}$	Stable carbon isotope ratio, reference	Measured
$\delta^{13}C_{sam}$	Stable carbon isotope ratio, sample	Measured
$\Delta^{13}C$	Online carbon isotope discrimination	Eq. (5.1)
γ^*	Half of reciprocal of Rubisco specificity for CO_2	1.93 x 10^{-4}, (von Caemmerer, 2000; von Caemmerer et al., 1994)
ξ	Ratio of dry reference CO_2 mole fraction to difference between reference and sample dry CO_2 mole fractions	Eq. (5.2)
ϕ	Bundle sheath leakiness	Eq. (5.18)
$\Phi PSII$	PSII operating quantum efficiency	Measured

5.2.4 Light response curves

For each sorghum accession, response of A_{net} to Q_{abs} was measured over a range of light intensities in both 21% and 2% O_2 to determine R_d using the Yin method (Yin and Struik, 2009; Yin, Sun, et al., 2011). Chamber flow rate, VPD, and leaf temperature conditions were the same as those used during isotope measurements. A_{net} and g_{sw} were allowed to stabilise at Q_{inc} of 500 μmol $m^{-2}s^{-1}$ PPFD and stability criteria based on values at this stage. Q_{inc} was gradually brought up to 1,800 μmol $m^{-2}s^{-1}$ PPFD, waiting there for stability for no more than 5 minutes to avoid causing pre-measurement photoinhibition. Gas exchange was then measured at steps of 1,800, 1,500, 1,200, 900, 750, 600, 500, 400, 300, 200, 120, 60, and 20 μmol $m^{-2}s^{-1}$ PPFD, with stability criteria enabled and a minimum/maximum step wait time of 60/240 seconds. Chlorophyll fluorescence was recorded during logging with a minimum of three minutes between flashes.

The y-intercept of the linear regression of A_{net} against $(I_{inc} * \Phi PSII)/3$ from the light response curves was used for R_d, using the lowest five Q_{inc} points (excluding the 30 μmol $m^{-2}s^{-1}$ point for 21% O_2 due to apparent Kok effect). Slopes at 2% O_2 were used as the *s'* calibration parameter (mol ATP (mol e^-)$^{-1}$) in J_{atp} e^- transport calculation (Eq. (5.4)).

5.2.5 Statistical analysis

In each O_2 level, differences between sorghum accessions at the first and final measurement blocks were tested using a Student's t-test. Additionally, analysis was focused on the changes in photosynthesis and isotope discrimination between the beginning and end of light treatments for each accession. Separately for each O_2 level, linear mixed-effects models were fit by restricted maximum likelihood to light treatment response data with accession, treatment (fluctuating or steady-state), and their interaction considered as fixed effects, using *R* packages *lme4* (Bates et al., 2015) and lmerTest (Kuznetsova et al., 2017). Growth set (sorghum seeds planted and grown together), day of measurement, LI-6800 of measurement, and

time of measurement (morning/afternoon) were considered as random effects. Models were run in full, then reduced by stepwise elimination based on Akaike information criteria using the R Stats "step" function. Day of measurement and LI-6800 of measurement did not contribute substantial structural variance and were dropped from all analyses. Estimated marginal means (emmeans, Lenth, 2021) were calculated for each accession/treatment combination to include shrinkage based on remaining random effects (typically only growth set or time of measurement).

5.3 Results

5.3.1 Sorghum accessions with contrasting photoprotective capacity show similar photosynthetic trait response to high light treatments

Prior to starting this experiment, NPQ screens were performed on these accessions grown in steady-state conditions, to verify conservation of NPQ phenotypes from the chapter three field screen in a controlled-growth environment. Similar relationships between the accessions' max NPQ and NPQ kinetics between field-grown plants (2017/2019) and growth room plants (Figure 5.5) were observed.

In the current study, the sorghum accession selected for low NPQ (PI521057) maintained higher A_{net} and g_{sw} than the high NPQ PI276818 throughout both light treatments and oxygen conditions (Figure 5.6 **A** and **B**). During the steady-state light treatment, both accessions exhibited a gradual reduction in A_{net} and g_{sw} from their values at the beginning through the high light period through the end of of the high light period. This trend was not evident in A_{net} during the fluctuating light treatments, and only slightly observable in fluctuating light g_{sw}, when considering the peaks of either trait during the "high" portion of light fluctuations.

Post-treatment values of both traits were lower than pre-treatment, but the magnitude of drop differed by oxygen level and accession, with 21% O_2 resulting in larger drops from pre-treatment values, when comparing values at two minutes prior to

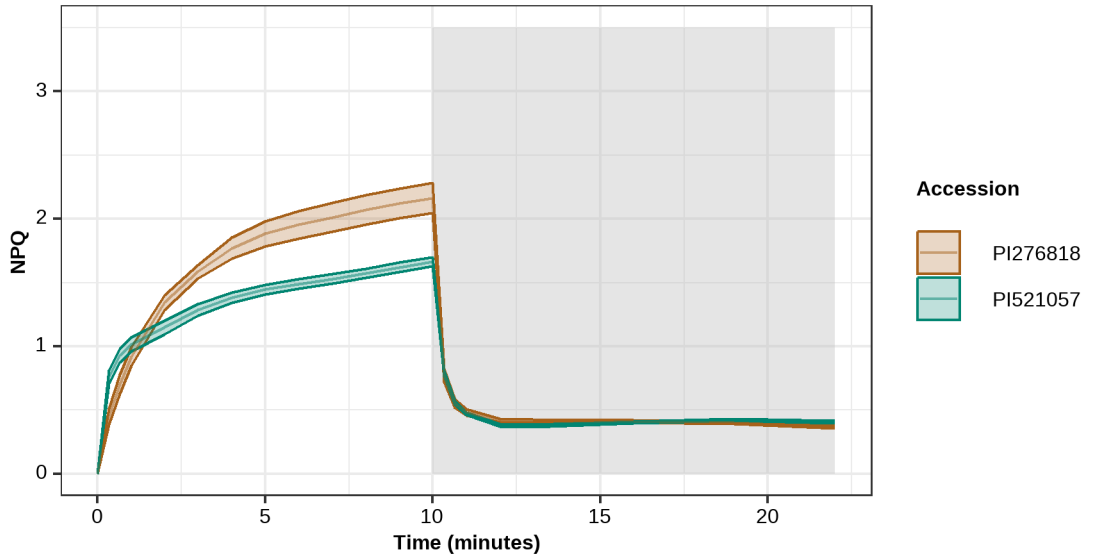

Figure 5.5: Nonphotochemical quenching (NPQ) kinetic traces of two *S. bicolor* accessions during a 10 minute high-light treatment, followed by 12 minutes in darkness (shaded region). Lines are accession means, shading +/- SE of the mean ($n = 6$), coloured by accession. Plants were grown in a controlled growth cabinet.

treatment start vs values at 210 minutes. In 2% O_2, steady-state rather than fluctuating light caused a greater decline in post-treatment A_{net} and g_{sw}, compared to the pre-treatment values for both accessions. A_{net} dropped by 11% in PI276818 vs 5% in PI521057 after steady state treatment, while after the fluctuating light treatment a drops of 6% in PI276818 and 5% PI521057 were observed. g_{sw} in 2% O_2 dropped after steady-state treatment by 14% in PI276818 and 8% in PI521057, compared to drops of 6% in PI276818 and 4% PI521057 after fluctuating. In 21% O_2 the effects of both light treatments on A_{net} were similar for each accession and led to a 15% drop in PI276818 compared to a 17% drop in PI521057. g_{sw} in 21% O_2 dropped after steady state by 16% in PI276818 and 18% in PI521057, compared to 10% in PI276818 and 14% in PI521057 after fluctuating light.

Trends in NPQ over the high light treatment were also similar between accessions, though accession differences were slightly more apparent during fluctuating light treatments (Figure 5.6 **C**). NPQ contrasted strongly between different O_2 environments. The relationship between maximum NPQ values of the high and low NPQ accessions was similar to that observed in the 2017/2019 field seasons, but

notably the low NPQ/fast inducing/fast relaxing accession (PI521057) did show slower NPQ induction upon the beginning of high light treatments, and very slightly slower post-treatment NPQ relaxation, compared to accession PI276818, which was chosen for exhibiting high NPQ and slow NPQ induction and relaxation during the field trials. Within each oxygen level, fluctuating and steady-state high light resulted in very similar NPQ values for both accessions. In 2% oxygen, NPQ tended to reach the maximum value observed during the treatment within 30 minutes of the beginning of the treatment. PI521057 returned to a NPQ post-treatment NPQ about 10% higher than observed pre-treatment, after both light treatments. PI276818 exhibited a similar level of NPQ after the fluctuating treatment, though NPQ after the steady-state treatment was notably higher.

Interestingly, the 21% O_2 environments tended to result in gradual increase in NPQ during the treatment period and a substantially higher post-treatment NPQ in both accessions, with an accession-pooled increase of 52.4% after fluctuating and 66.4% increase after the steady-state treatment.

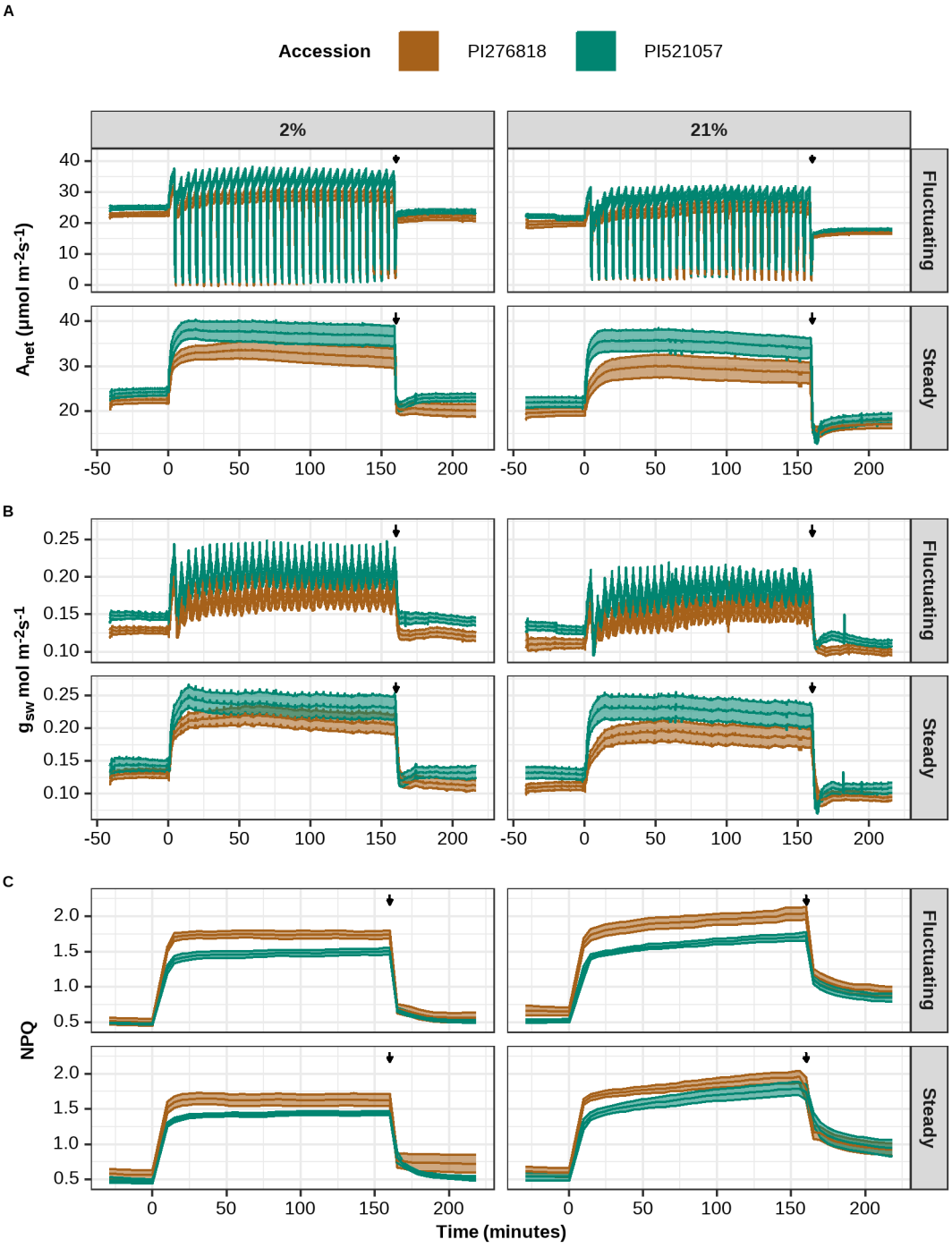

Figure 5.6: Photosynthetic parameters of two sorghum accessions before, during, and after fluctuating and steady-state high-light treatments, in 2% and 21% ambient O_2, measured with portable photosynthesis systems. **A**, net CO_2 assimilation (A_{net}); **B**, stomatal conductance to water vapour (g_{sw}); **C**, nonphotochemical quenching (NPQ). Time point 0 represents switch from 500 μmol m^{-2} s^{-1} PPFD to either 2,000 μmol m^{-2} s^{-1} PPFD (steady-state) or fluctuations of 2,000 μmol m^{-2} s^{-1} PPFD for four minutes followed by one minute at 50 μmol m^{-2} s^{-1} PPFD. Arrows mark return to steady-state 500 μmol m^{-2} s^{-1} PPFD after 160 minutes of treatment. Lines are the mean of n=8 plants. Shading is +/- standard error of the mean.

5.3.2 Sorghum bundle sheath leakiness is differentially affected by steady-state and fluctuating high light treatments

The level of instantaneous leaf carbon isotope discrimination ($\Delta^{13}C$) during photosynthesis in C_4 species is influenced primarily by changes in ϕ (due to the "opportunity" for expression of Rubisco fractionation via leaked CO_2) and the ratio of intercellular to ambient CO_2 concentrations (C_i/C_a). In both sorghum accessions, $\Delta^{13}C$ remained constant throughout steady-state high light treatments in both 2% and 21% O_2 (Figure 5.7 **A**). During the fluctuating light treatment, $\Delta^{13}C$ increased during the high-light portion of the measurement period, returning to a similar level upon return to 500 μmol m^{-2} s^{-1} PPFD. A similar pattern was observed for ϕ (Figure 5.7 **B**). Both $\Delta^{13}C$ and ϕ during the entire measurement period were slightly higher in 21% O_2, compared to 2% O_2. C_i/C_a tended to show the opposite trend, with a small increase over the duration of the measurement period in fluctuating light, but a large increase during steady-state treatment followed by a return to values similar to pre-treatment (Figure 5.7 **C**). Absolute values and trends in C_i/C_a were similar in both 2% and 21% O_2 concentrations.

To investigate the effects of high light treatments on these photosynthetic isotope discrimination parameters more closely, we can consider the change in these parameters between the pre- and post-treatment steady-state 500 μmol m^{-2} s^{-1} PPFD ($d\Delta^{13}C$, $d\phi$, and dC_i/C_a). This also facilitates the use of mixed-effect models to incorporate possible structural variation into results to produce estimated marginal means (adjusted means, Section 5.2.5) accounting for potential random effect bias. In 2% O_2, both accessions tended to show similar trends in response to light treatments ($p > 0.5$, linear mixed-effect model for Accession:treatment interaction, for all three parameters– see Tables 7.28, 7.26, and 7.30). The high NPQ accession (PI276818) was not appreciably affected by the fluctuating light treatment in any parameter (Figure 5.8 **A-C**). The steady-state light treatment, though, tended to cause a decrease in mean $\Delta^{13}C$ (-0.21‰), ϕ (-0.04), and C_i/C_a (-0.02). The low NPQ accession (PI521057) exhibited a slight reduction in $\Delta^{13}C$ (-0.15 ‰) and ϕ

(-0.02) in 2% O_2 fluctuating light, but C_i/C_a was similarly unaffected. Steady-state high light in 2% O_2, however, caused a notably larger drop in all three parameters in the low NPQ accession (-0.89 ‰ for $\Delta^{13}C$, -0.11 for ϕ, and -0.03 for C_i/C_a).

Intriguingly, in 21% O_2 the accessions tended to show divergent responses for $\Delta^{13}C$ ($p = 0.028$) and ϕ ($p = 0.045$), but not for C_i/C_a ($p = 0.47$, linear mixed-effect models– see Tables 7.27, 7.29, and 7.31). $\Delta^{13}C$ decreased in the high NPQ accession from beginning to end of both light treatments, with a drop of 0.55‰ after fluctuating and a more pronounced -0.83‰ after the steady-state treatment (Figure 5.8 **A**). The low NPQ accession, however, displayed increased $\Delta^{13}C$ after the fluctuating light treatment (0.59‰), but little change after the steady-state treatment (-0.11‰). The changes in ϕ (Figure 5.8 **B**) were quite similar between accessions/treatment combinations (-0.05 and -0.08 for high NPQ accession fluctuating and steady-state, respectively, and 0.05 and -0.02 for low NPQ fluctuating and steady-state, respectively), but were less consistent for C_i/C_a (Figure 5.8 **C**), suggesting that changes in ϕ might indeed explain the observed changes in $\Delta^{13}C$. Both accessions showed an increase in C_i/C_a after the fluctuating light treatment (increase of 0.02 in the low NPQ and a more profound 0.04 in the high NPQ accession), but C_i/C_a in both accessions decreased by 0.01 after the steady-state light treatment ($p = 0.0095$ for treatment effect, linear mixed effects model, Table 7.31).

As another indicator that changes in $\Delta^{13}C$ in this experiment were more clearly explained by changes in ϕ rather than Ci/Ca and Rubisco fractionation, the linear regression between measured points of $\Delta^{13}C$ and ϕ leads to a Pearson's $r > 0.97$, with p-values < 0.001 in both 2% and 21% O_2 (Figure 5.9 **A**). This starkly contrasts the relationship between $\Delta^{13}C$ and C_i/C_a (Figure 5.9 **B**) which resulted in a Pearson's r of -0.05 and -0.14 and $p = 0.427$ and 0.037 for 2% and 21% O_2, respectively.

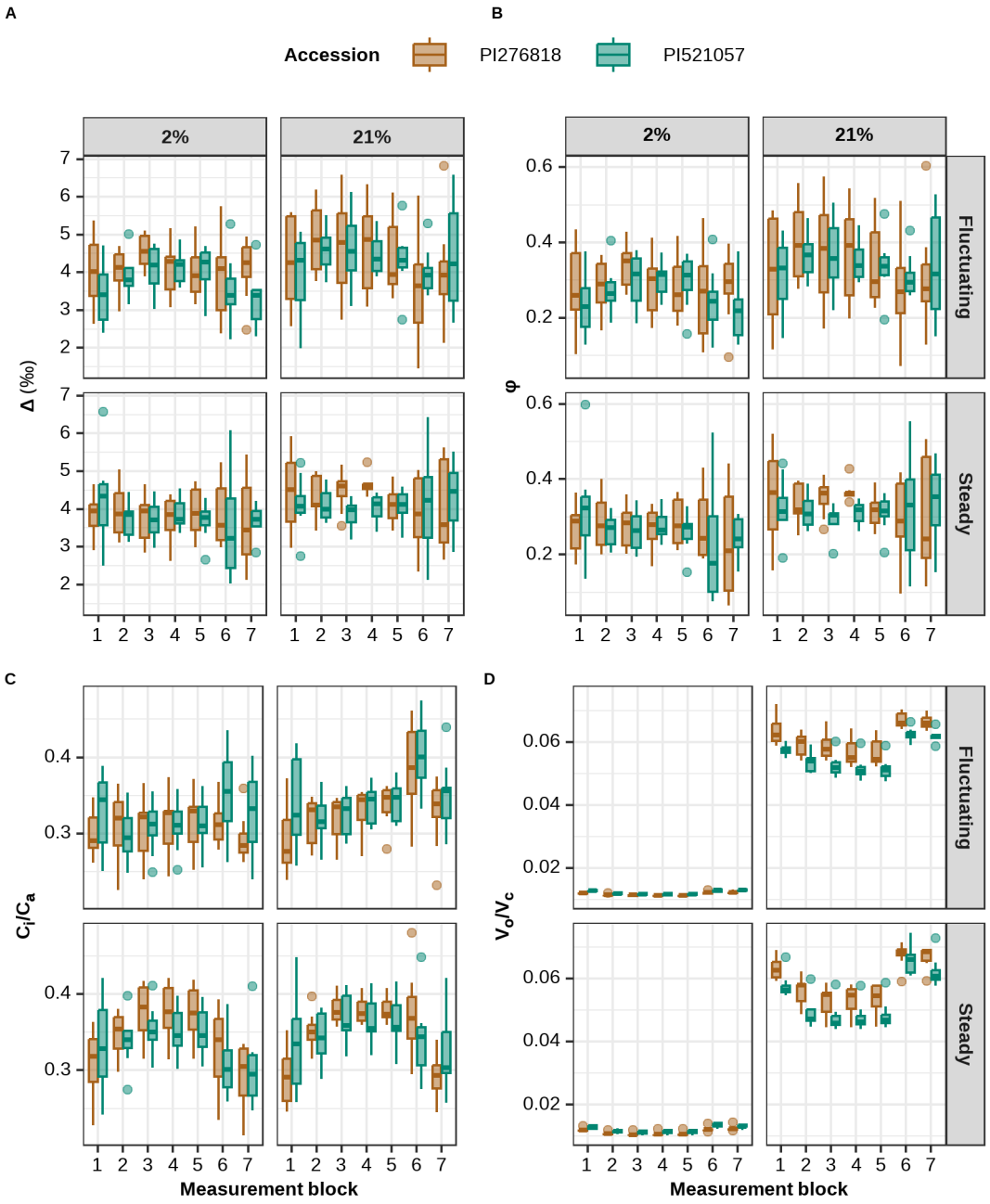

Figure 5.7: Carbon isotope discrimination parameters of two sorghum accessions before, during, and after fluctuating and steady-state high-light treatments, in 2% and 21% ambient O_2, measured with a photosynthesis system coupled to a tunable diode laser (TDL). **A**, carbon isotope discrimination (Δ); **B**, bundle sheath leakiness (ϕ); **C**, ratio of intercellular to ambient CO_2 mole fraction; **D**, Ratio of Rubisco oxygenase to carboxylase activity (V_o/V_c). Measurement block one corresponds to steady-state 500 μmol m^{-2} s^{-1} PPFD. Measurement blocks two through five represent either 2,000 μmol m^{-2} s^{-1} PPFD (steady-state) or fluctuations of 2,000 μmol m^{-2} s^{-1} PPFD for four minutes followed by one minute at 50 μmol m^{-2} s^{-1} PPFD. Measurement blocks six and seven correspond to steady-state 500 μmol m^{-2} s^{-1} PPFD after 160 minutes of treatment. Internal box plot edges represent first and third quartiles. Points represent outliers beyond 1.5 times the interquartile range. The solid line within the boxes indicates the median. n=8.

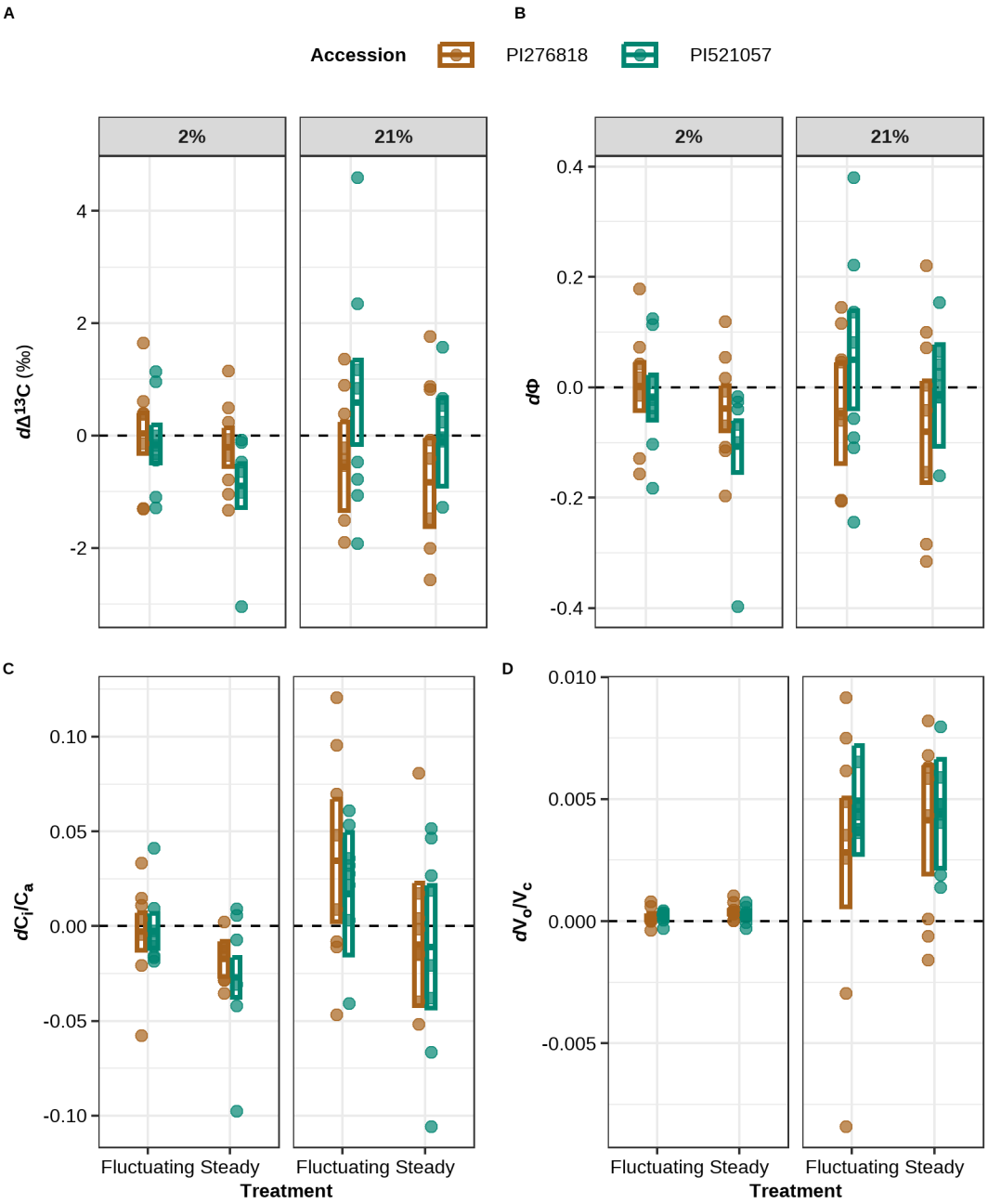

Figure 5.8: Difference (d) in carbon isotope discrimination parameters of two sorghum accessions at steady-state 500 μmol m^{-2} s^{-1} PPFD before and after fluctuating and steady-state high-light treatments, in 2% and 21% O_2, measured with a photosynthesis system coupled to a tunable laser diode (TDL). **A**, carbon isotope discrimination ($\Delta^{13}C$); **B**, bundle sheath leakiness (ϕ); **C**, ratio of intercellular to ambient CO_2 mole fraction (C_i/C_a). **D**, Ratio of Rubisco oxygenase to carboxylase activity (V_o/V_c). d represents the difference between the final and first measurement block (block seven - block one). Treatments were either 2,000 μmol m^{-2} s^{-1} PPFD (steady-state) or fluctuations of 2,000 μmol m^{-2} s^{-1} PPFD for four minutes followed by one minute at 50 μmol m^{-2} s^{-1} PPFD. Points represent values for individual plants (n=8). Crossbar box represents estimated marginal mean (EMM) +/- standard error of EMM.

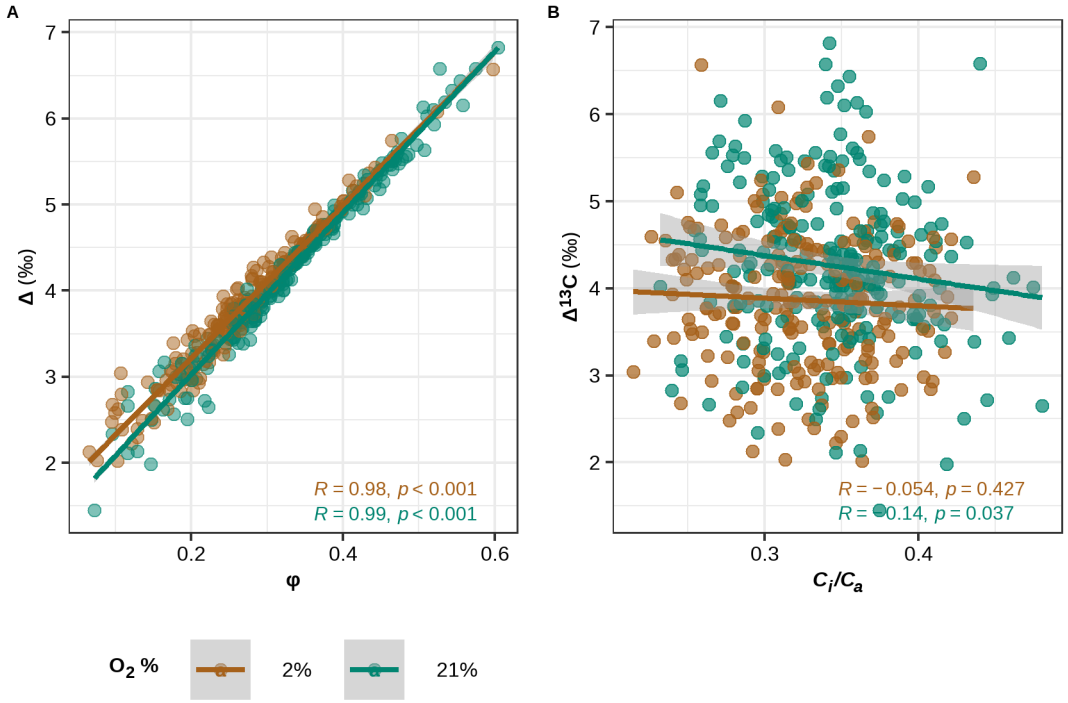

Figure 5.9: Online carbon isotope discrimination ($\Delta^{13}C$) plotted against bundle sheath leakiness (ϕ, **A**) and the ratio of leaf intercellular to ambient CO_2 concentration (C_i/C_a, **B**), coloured by measurement O_2 percentage. Lines are best-fit linear regression for each O_2 level; shading is the confidence interval of the regression.

5.4 Discussion

Understanding the response of C_4 photosynthesis to field-realistic dynamic light conditions is necessary in order to affect meaningful improvements in crop photosynthetic efficiency. Revealing the limitations, or lack thereof, to photosynthesis in high and fluctuating light can provide us with a clearer route forward when deciding where to best focus research efforts. This work has provided evidence that in sorghum, a species known for its high photosynthetic capacity and water-use efficiency, prolonged periods of steady-state or fluctuating high light may not substantially negatively impact BSC/MC metabolic coordination, even in leaves grown under low-to-medium intensity light levels, relative to light levels experienced in field conditions. Thus, it may be useful for future research efforts to focus on improvement of photosynthetic efficiency in low light environments (such as

lower canopy leaves) where increased ϕ and decreased quantum efficiency of CO_2 fixation have been previously observed (Jaikumar et al., 2021; Pignon, Jaiswal, et al., 2017; Sales et al., 2023).

5.4.1 Does photoinhibitory light treatment impact bundle sheath leakiness?

Both sorghum accessions in this study showed lower A_{net} and g_{sw} in 21% compared to 2% O_2 during the entire measurement period (Figures 5.6 **A & B**), possibly due to incomplete suppression of photorespiration as the modelled ratio of Rubisco oxygenase to carboxylase activity (V_o/V_c) was substantially higher in 21% O_2 (Figure 5.7 **D**). Modelled V_o/V_c during the 21% treatment was comparable with that of past reports for the closely related species maize and sugarcane (Bellasio et al., 2014). In both oxygen levels in the current study, the failure of post-treatment A_{net} and g_{sw} to return to pre-treatment levels, the increase in post-treatment V_o/V_c, and marked increase in post-treatment NPQ, suggests that some amount of photoinhibition and photodamage may have occurred during the light treatments, though it is not clear if this resulted in CCM incoordination resulting in heightened photorespiration. The differences between pre-treatment and residual A_{net}, g_{sw}, and NPQ were notably larger in the 21% O_2 environment, suggesting that photoinhibition and damage is increased under ambient, compared to low O_2, conditions in C_4 photosynthesis. In 2% O_2, while the accessions' A_{net} values dropped similarly between accessions during fluctuating light, the high NPQ accession experienced a notably larger drop after the steady-state light treatment. The high NPQ accession also exhibited larger drops in g_{sw} in after both light treatments. In 21% O_2, pre- to post-treatment drops in A_{net} and g_{sw} were similar in both light treatments, with the the low NPQ accession experiencing a slightly larger drop in both traits after either light condition. That the low NPQ capacity accession experienced more deleterious effects than the other accession after light treatments in 21% O_2 compared to 2% O_2 suggests that NPQ capacity may partially explain susceptibility to photoinhibition and evidence a potential photoinhibition/photorespiration connection.

NPQ immediately upon initiation of high-light treatments reached similar levels in both oxygen environments, but in 21% continued to climb with no sign of plateauing by the end of the 160 minute light treatments. Zulfugarov et al. (2019) observed similar reduced NPQ in rice in low O_2, though in that study after only 30 minutes there was a clear separation between control (presumably 21% O_2) and low (0% O_2) treatments, with the control substantially higher after 160 minutes at 700 μmol $m^{-2}s^{-1}$ PPFD. The utilisation of O_2-free instead of 2% O_2 in the oxygen treatment can lead to pleiotropic effects due to suppression of mitochondrial respiration as well (Forrester et al., 1966; Vialet-Chabrand et al., 2021; Zabalza et al., 2008), which was avoided by using 2% in the in the current study. Zulfugarov et al. (2019) used both wild-type and PsbS knockout rice lines, attributing the differences in NPQ potentially to effects of reduced stromal-lumenal pH gradient and thylakoid conformational changes, and suggested that longer term NPQ components such as qH, qI, and qZ might also be affected. The similar magnitude and timing of qE (the quickly inducing and relaxing form of NPQ) quenching between O_2 levels in the current study would suggest that indeed, longer-term NPQ is minimised under low O_2 conditions. It would be interesting to investigate whether this is in part explained by increased photoinhibition or photodamage in the 21% environment due to increased presence of O_2 as substrate for reactive oxygen species formation– increased prevalence of photoinhibition under 21% O_2 would speak against a role of photorespiration as a photoprotective electron sink (Busch, 2020).

5.4.2 Is C_4 CCM efficiency impacted by photoinhibition?

While sustained increases in NPQ in 21% O_2 are likely representative of a steady increase in photoinhibition (and potentially photodamage), the measurement in itself doesn't directly reflect potential photodamage in BSC as NPQ is derived from PSII fluorescence, which is assumed to be mostly localised to MC. Considering the metabolic flexibility conferred by the C_4 pathway (Stitt and Zhu, 2014), though, the effects of photoinhibition and damage on ATP and NADPH supply in either

cell type are likely manifested in changes to metabolic balances in the whole pathway. In most cases there was not a post-treatment increase in ϕ, which might have otherwise indicated preferential BSC photodamage and a loss of BSC carboxylation capacity which could lead to C_4 acid overcycling. Only the low-NPQ PI521057 in 21% fluctuating light exhibited increased post-treatment ϕ, which could reflect increased photorespiration due to energetic limitations in RuBP oxygenation suppression. This is supported by 21% fluctuating PI521057 also exhibiting the largest pre-to-post increase in V_o/V_c (Figure 5.8 **D**), though this relationship between ϕ and V_o/V_c did not hold true in every instance. Interestingly, in 21% the high NPQ capacity accession (PI276818) showed a smaller increase in V_o/V_c after the fluctuating light treatment than did PI521057, but the accessions displayed similar increases in V_o/V_c after the steady-state treatment. This may indicate that the lower-NPQ accession lacked the photoprotective capacity to cope with what might be expected to be the "most stressful" condition tested, but it appears photorespiration does not universally explain changes in ϕ in this work.

Despite the persistent differences in NPQ, both sorghum accessions examined in this chapter showed a reduced maximum NPQ compared to field grown sorghum (3.3.1, presumably due to developmental differences in growth light environment. Field-grown plants likely experience a larger discrepancy between absorbed energy and photochemical quenching capacity, and an increased maximum NPQ may represent acclimation to those more dynamic light conditions. If increases in ϕ are representative of metabolic incoordination, potentially exacerbated by imbalances in photochemical energy distribution between BSC and MC, then field-grown sorghum's enhanced capacity for NPQ may prove it to be even more resilient to high-light's potentially deleterious effects on CCM coordination.

This study provides additional evidence that C_4 bundle sheath leakiness is relatively imperturbable by stressful light treatments, in line with past reports suggesting similarly modest responses to light, temperature, CO_2, and C_4 subtype (Cousins et al., 2008; Henderson et al., 1992; Sonawane et al., 2017; Ubierna et al., 2013). The photoinhibitory light treatments in this study are not closely representative

of field-level dynamic light conditions, but these reductive experiments provide a useful guide for future study. Future improvements to C_4 photosynthetic efficiency are thus likely best directed toward improving CCM/C_3 cycle coordination and NPQ kinetics during transient low light events, such as sunflecks and cloudflecks.

6

General discussion

Photoprotection during dynamic light conditions is a key contributor to photosynthetic efficiency, and improvements in nonphotochemical quenching (NPQ) kinetics have been shown to increase potential plant biomass accumulation and yield in field conditions (De Souza et al., 2022; Kromdijk, Głowacka, Leonelli, et al., 2016). Natural genetic variation in photoprotective capacity within crop genomes is not well-described, with only a few species to date subjected to genome-wide studies to understand natural variation in photoprotection, only one of which (maize, Sahay et al., 2023) is a C_4 species. Characterising naturally occurring variation in crop photosynthetic traits is integral for driving crop improvement in the future (Lawson et al., 2012). This work has reported on the first genome-wide study of natural genetic variation in photoprotection within sorghum, a major crop species. Potential candidate genes underlying NPQ traits have been uncovered and sorghum's photoprotective response in comparison to other C_4 species has been contextualised. Additionally, a detailed study of C_4 photosynthetic and photoprotective response to dynamic light conditions, in sorghum accessions with contrasting photoprotective capacity, has led to improved mechanistic understanding of C_4 photosynthetic coordination during photosynthesis in dynamic light.

6.1 Principle chapter conclusions

6.1.1 Chapter two

Chapter two details the development and implementation of high-throughput methods and assays to apply variable high-intensity light conditions to several C_4 leaf samples and measure the resulting photodamage stress indicators of malondialdehyde accumulation, pigment breakdown, and electrolyte leakage. The methods were used to investigate sorghum's response to two, four, and six hours of continuous steady-state and fluctuating (dynamic) high-light, in comparison to that of the C_4 crops *Zea mays*, *Panicum miliaceum*, *Pennisetum glaucum*, and C_4 model *Setaria viridis*. In most cases sorghum's photodamage response was generally similar to the other species, neither more nor less sensitive to either light regime. Dynamic light, rather than steady-state light, generally caused more extreme photodamage in all species. Importantly, correlations observed between these photodamage assays and results from an NPQ photoprotective screen (using the screening method described in chapter three) suggests that the screen of photoprotection appears to be representative of susceptibility to photodamage.

6.1.2 Chapters three and four

Chapter three chronicles a large-scale NPQ kinetics screen of a genetically diverse panel of field-grown sorghum, over two years. Sizeable, heritable variation in NPQ traits was observed within the panel, facilitating the use of quantitative genetics methods to explore genetic variation associated with photoprotective trait variation. By combining genome-wide and transcriptome-wide association studies, candidate genomic regions were identified which are likely to underlie photoprotection in sorghum. Genes with relatively clear photoprotection-adjacent annotations in other species' orthologues were found, along with several more novel genes. Not all of these candidates may be directly involved in mechanistic photoprotective

regulation; some instead may be more likely to be associated with adjacent photosynthetic processes– the knowledge of all of which is important when considering genetic improvements in photosynthetic efficiency.

Chapter four recounts a re-screen of sorghum accessions selected based on their genotype at two candidate loci which were significantly associated with key NPQ traits during the chapter two screen. The field grown accessions which showed allelic variation at loci of interest showed divergent NPQ phenotypes for one, but not both loci. This provides a confirmation of the heritable genetic underpinning of NPQ of the divergent locus, while for the locus which did not show diverging NPQ phenotypes it is also a useful reminder that candidate genes uncovered in low-precision large-scale quantitative studies require further validation.

6.1.3 Chapter five

Chapter five details a comparative study of C_4 photosynthetic and photoprotective response to variable fluctuating and steady-state high light treatments, utilising two sorghum accessions with contrasting photoprotective capacities. Carbon isotope discrimination during leaf gas exchange was measured during the light treatments, in order to discern whether the C_4 photosynthetic apparatus was detrimentally affected by the high light treatments. Experiments were conducted in both 21% and 2% O_2 background air to better understand the role of photorespiration in observed responses.

The low NPQ capacity sorghum accession experienced more deleterious effects than the high NPQ accession in 21% O_2 compared to 2% O_2 in both light conditions, suggesting that NPQ capacity may partially explain susceptibility to photoinhibition and be evidence of a connection between photoinhibition and photorespiration.

The modelled ratio of Rubisco oxygenase to carboxylase activity (V_o/V_c) was lower under 2% O_2 in both sorghum accessions and light treatments, suggesting that incomplete suppression of photorespiration may have contributed to an observed larger drop in CO_2 assimilation and stomatal conductance to water vapour in the

21% O_2 experiments as compared to 2% O_2, suggesting also that less photoinhibition occurred in 2% O_2 conditions. Bundle sheath leakiness to CO_2, an indicator of mesophyll and bundle-sheath cell incoordination, did not increase substantially after more than two hours of high-light treatment, suggesting that C_4 photosynthesis is relatively robust under high light conditions.

6.2 Future directions

In conclusion, this work has revealed the scale of variation in photoprotective capacity within the sorghum genome and identified genomic regions associated with photoprotection under dynamic light conditions. The highest confidence candidate genomic regions from this study should be investigated further via mutant comparison or genome-editing to investigate whether or not the associations are causal. Causal identification of candidate regions will provide valuable background for photoprotection research in other C_4 grasses as well, with potential to inform photosynthetic efficiency improvements in important crops such as maize and sugarcane.

A more deleterious effect of fluctuating, compared to steady-state light, was evident in both chapters two and five. Considering the correlations observed in chapter two between photoprotection and photoinhibition/photodamage and the marked differences between sorghum accessions with contrasting NPQ capacity in chapter five, it appears that there could be scope for improvement in NPQ kinetics and capacity in fluctuating light conditions in C_4 crops. However, given the range of variation already present in NPQ kinetics within sorghum (and that being uncovered in other crops), it may be that improvements in C_4 NPQ kinetics won't provide massive benefits; evolution of C_4 grasses in an understorey environment likely has led to dynamic photosynthetic traits being better optimised for fluctuating light environments than C_3 species (Cubas et al., 2023; Hetherington and Woodward, 2003). Indeed, comparing several publications in the last decade, C_4 NPQ relaxation rate tends to be faster than that of C_3 species (Figure 6.1).

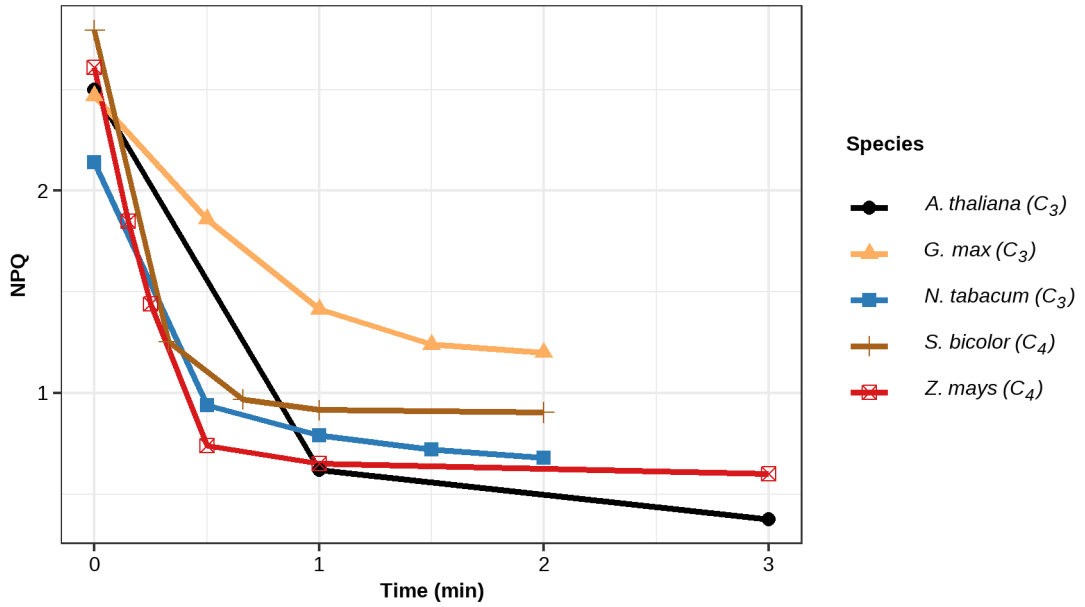

Figure 6.1: Line plots of NPQ relaxation of five different species. Time point "0" represents final light point of given study. *A. thaliana* data based on Li, Ahn, et al. (2009), Figure 5 (switch from 1,200 μmol m^{-2} s^{-1} photosynthetic photon flux density (PPFD) to dark). *G. max* data from De Souza et al. (2022) using averages of eight wildtype replicates provided in supplement (switch from 2,000 μmol m^{-2} s^{-1} PPFD to 200 PPFD). *N. tabacum* data from Kromdijk, Głowacka, Leonelli, et al. (2016), using averages of eighteen wildtype replicates provided in supplement (switch from 2,000 μmol m^{-2} s^{-1} PPFD to 200 PPFD). *S. bicolor* data from chapter three of current study, based on average joint model parameters of 861 accessions (switch from 2,000 μmol m^{-2} s^{-1} PPFD to dark). *Z. mays* data from Sahay et al. (2023), using averages of 751 accessions (four biological replicates) in 2020, provided in supplement (switch from 2,000 μmol m^{-2} s^{-1} PPFD to dark).

Instead, improvements may come through a focus on additional aspects of photosynthetic efficiency, effected through breeding or genomic-editing based approaches. For instance, modification of candidate genes such as Sobic.009G187300, involved in ATP synthase activation, may affect NPQ kinetics through changes in redox state. Or, this may represent a target for photosynthetic efficiency improvement through hastening of photosynthetic induction, which has been observed previously to be slower in C_4 species (Arce Cubas et al., 2023). Modifications to ATP synthase kinetics would have complex effects on upstream electron transport and NPQ (Kramer and Evans, 2010), but specific engineering of ATP synthase has the potential to confer flexibility in response to dynamic light conditions (Yamamoto et al., 2023).

The genes Sobic.003G418000 (strigaloactone biosynthesis) and Sobic.006G060100 (GRX-like protein encoding) may also offer potential targets given their role in antioxidant and redox regulation, particularly in plants already experiencing stressors such as drought or heat. Response to abiotic stress is a pressing concern for agricultural producers worldwide, with drought alone causing substantial annual yield losses in wheat and maize, among other crops (Daryanto et al., 2016). It may be the case that the relationship between dynamic-light photoprotection and photoinhibition is stronger in more stressful environments, perhaps due in part to redox-state mediated and shared antioxidant and photoprotective control and sensing mechanisms. Investigation of single genotypes' NPQ phenotypes in a variety of abiotic stress conditions, under similar light regimes, may help elucidate how photoprotection and photoinhibition scale up to affect plant productivity in the face of climate change-imposed stressors. While germplasm-focused enhancements in crop productivity will require a whole-plant focus (Lopes et al., 2011), improved photoprotective capacity in challenging stress conditions conferred through increased antioxidant capacity and photosynthetic control could play a role in development of crop germplasm better-suited to anticipated hotter, drier conditions in many crop growing regions, worldwide.

Progress in directing canopy-level specific gene expression, already occurring in traits such as leaf angle (Natukunda et al., 2022), could be critical in usefully modifying genes under photosynthetic control. This is particularly important for genes involved in light harvesting and energy transport, where reductions in top-of-canopy of light absorption may theoretically allow greater light use in lower-canopy leaves (Walter and Kromdijk, 2021), making more efficient use of the entire plant canopy. Ideally, these modifications could be controlled temporally as well through tissue (Sanchez-Bragado et al., 2020) and temporally-specific gene expression, allowing photosynthesis genes to be up-and-down regulated at the specific time and place needed to best optimise photosynthetic efficiency and improve yield.

The results of the carbon isotope discrimination during high dynamic light experiments support recent work by Cubas et al. (2023), suggesting that C_4 photosynthesis is likely well-primed for shorter-term fluctuating light conditions like those observed during sunflecks and cloudflecks, perhaps due in part to buffering capacity conferred by established mesophyll and bundle sheath cell metabolite gradients. Future research may be best directed toward improving carbon concentrating mechanism and C_3 cycle coordination and NPQ kinetics during photosynthetic induction to avoid damage and bundle sheath leakiness, already known to reduce C_4 photosynthetic efficiency (Arce Cubas et al., 2023; Wang, Stutz, et al., 2022). As sorghum is not an outlier in dynamic photoprotective response in comparison with other C_4 crops, future research results can quite possibly be extended to conclusions for other C_4 grasses as well. As these experiments were conducted on otherwise unstressed plants, it remains to be seen whether C_4/C_3 cycle metabolic control under dynamic light conditions or during photosynthetic induction is disrupted more strongly during longer-term field-realistic stress conditions. It may be the case that photoprotective capacity plays a larger role in maintaining photosynthetic efficiency when downstream photosynthetic sinks are limited by drought or heat stress.

Improvements to photosynthesis, whether accomplished transgenically or via directed breeding, will likely need to be accompanied by changes in agronomic practices. Potentially, improved canopy light distribution could allow for more densely planted fields, improving per-area yields. However, it may be that denser planting is only applicable in regions without substantial water limitation due to the likely increased water demand. Scaling photosynthetic efficiency improvements to the field has proven challenging (Grobbelaar, 2009). Quantification of potential yield improvement due to single plant and field-scale agronomic modifications is likely best approached by continued refinement of ecophysiological crop models (ECMs). Improvements in photosynthetic efficiency at the plant or canopy level can be tested in well-parametrised models to determine likely contributions under different yield scenarios. This is particularly important for sorghum, where genetic modifications are unlikely to be deployed at field scale due to outcrossing concerns;

directed breeding via model-assisted genomic prediction may be the only feasible method of rapid germplasm improvement. A coupling of quantitative genetics, such as that conducted in this work, with ECMs, allows for effective genomic prediction (Poudel et al., 2023). In combination with improved hydrological and climate modelling (Shahhosseini et al., 2021) and appropriate management practices, through implementation of genomic prediction it should be possible to consistently and accurately prescribe the most appropriate cultivar for a given location, for given anticipated climatic conditions. In parallel with cultivar and management practice improvements that reduce input requirements while improving nutritional quality and yield, this optimisation– facilitated in great part by leaf-level physiological research– is an integral step in the march toward more efficient agriculture and a future of food and fuel security across the globe.

7 Supplementary materials

7.1 Supplement for chapter two

Table 7.1: Monthly glasshouse conditions for photoinhibition experiment plants (see "Methods" Table 2.1 for growing dates)

	DLI	T_d	T_n	RH_d	RH_n
Oct 2019	13	20.2 - 23.3	18.4 - 21.2	35.6 - 61.3	43.2 - 63.8
Nov 2019	7	18.9 - 22.7	18.9 - 20.7	41.0 - 57.9	40.5 - 58.8
Dec 2019	5	19.9 - 21.8	18.3 - 20.6	39.0 - 58.2	42.1 - 61.2
Jan 2020	6	20.1 - 21.5	18.0 - 20.0	40.4 - 58.7	41.8 - 63.3
Feb 2020	12	20.2 - 23.3	18.2 - 20.2	32.2 - 57.0	39.4 - 58.6
Mar 2020	21	20.3 - 24.6	18.5 - 20.6	28.8 - 48.8	38.9 - 52.7
Mar 2021	27	24.3 - 27.1	21.3 - 23.5	45.0 - 51.0	58.3 - 65.2
Apr 2021	32	22.4 - 26.8	18.6 - 20.6	32.2 - 56.0	43.3 - 63.2
May 2021	32	22.7 - 27.5	19.2 - 21.4	37.9 - 57.6	51.4 - 69.6
Jun 2021	38	22.0 - 28.7	19.5 - 24.0	45.0 - 67.1	60.8 - 80.2

Note:
DLI, mean daily light integral ($mol\ m^{-2}\ day^{-1}$); T_d and T_n, indoor daytime and night-time temperature (^oC); RH_d and RH_n, indoor daytime and nighttime relative humidity (%). Light intensity measured above glasshouse at 1 Hz sampling frequency, logged seven times per hour. DLI integrated based on hourly mean PPFD flux, averaged over the month. RH and temperature averaged per hour, followed by day, and month. Daytime includes any hourly means where outdoor PPFD was greater than or equal to 2 $\mu mol\ m^{-2}\ s^{-1}$ and night-time includes all other records.

Table 7.2: ANOVA table of chlorophyll content response model parameters for five C_4 grass species, for zero-hour versus six-hour control (untreated) samples

Factor	DF_{num}	DF_{den}	F	p
Treatment	1	0.56	2.178	0.4890
Species	4	27.59	5.499	0.0022
Treatment:Time	2	50.00	0.741	0.4819
Treatment:Species	4	32.18	3.193	0.0257
Treatment:Time:Species	8	50.00	1.150	0.3477

Table 7.3: ANOVA table of carotenoid content response model parameters for five C_4 grass species, for zero-hour versus six-hour control (untreated) samples

Factor	DF_{num}	DF_{den}	F	p
Treatment	1	1.24	0.645	0.547
Species	4	46.49	9.317	<0.001
Treatment:Time	2	50.00	0.822	0.446
Treatment:Species	4	61.18	3.195	0.019
Treatment:Time:Species	8	50.00	1.336	0.248

Table 7.4: ANOVA table of chlorophyll a:b ratio response model parameters for five C_4 grass species, for zero-hour versus six-hour control (untreated) samples

Factor	DF_{num}	DF_{den}	F	p
Treatment	1	91.94	4.457	0.0375
Species	4	50.29	2.904	0.0308
Treatment:Time	2	49.99	5.394	0.0076
Treatment:Species	4	91.85	9.688	<0.001
Treatment:Time:Species	8	49.93	1.619	0.1432

Table 7.5: ANOVA table of chlorophyll to carotenoid response model parameters for five C_4 grass species, for zero-hour versus six-hour control (untreated) samples

Factor	DF_{num}	DF_{den}	F	p
Treatment	1	83.41	3.038	0.085
Species	4	50.00	7.194	<0.001
Treatment:Time	2	50.00	0.180	0.836
Treatment:Species	4	83.41	3.413	0.012
Treatment:Time:Species	8	50.00	2.847	0.011

Table 7.6: ANOVA table of malondialdehyde (MDA) response model parameters for five C_4 grass species, for zero-hour versus six-hour control (untreated) samples

Factor	DF_{num}	DF_{den}	F	p
Treatment	1	1.78	0.885	0.4564
Species	4	49.20	15.550	<0.001
Treatment:Time	2	50.00	2.067	0.1372
Treatment:Species	4	70.16	10.883	<0.001
Treatment:Time:Species	8	50.00	3.561	0.0024

Table 7.7: ANOVA table of relative injury model parameters for five C_4 grass species, for zero-hour versus six-hour control (untreated) samples

Factor	DF_{num}	DF_{den}	F	p
Treatment	1	80.65	1.442	0.233
Species	4	49.98	10.440	<0.001
Treatment:Time	2	49.48	2.843	0.068
Treatment:Species	4	80.68	1.392	0.244
Treatment:Time:Species	8	49.52	2.721	0.014

Table 7.8: ANOVA table of chlorophyll content light treatment response model parameters for five C_4 grass species

Factor	DF_{num}	DF_{den}	F	p
Treatment	1	0.38	4.326	0.5050
Species	4	18.54	8.440	<0.001
Treatment:Time	6	147.13	38.699	<0.001
Treatment:Species	4	25.22	4.718	0.0056
Treatment:Time:Species	24	147.12	1.267	0.1968

Table 7.9: ANOVA table of total carotenoid content light treatment response model parameters for five C_4 grass species

Factor	DF_{num}	DF_{den}	F	p
Treatment	1	1.07	1.118	0.4731
Species	4	42.57	13.357	<0.001
Treatment:Time	6	149.03	15.955	<0.001
Treatment:Species	4	62.81	4.669	0.0023
Treatment:Time:Species	24	149.04	1.401	0.1154

Table 7.10: ANOVA table of chlorophyll a:b ratio light treatment response model parameters for five C_4 grass species

Factor	DF_{num}	DF_{den}	F	p
Treatment	1	139.19	5.230	0.0237
Species	4	50.34	3.171	0.0212
Treatment:Time	6	148.65	6.946	<0.001
Treatment:Species	4	138.87	11.395	<0.001
Treatment:Time:Species	24	148.61	2.280	0.0015

Table 7.11: ANOVA table of chlorophyll to total carotenoid ratio light treatment response model parameters for five C_4 grass species

Factor	DF_{num}	DF_{den}	F	p
Treatment	1	83.12	5.603	0.02
Species	4	50.00	19.702	<0.001
Treatment:Time	6	149.07	34.763	<0.001
Treatment:Species	4	83.12	6.294	<0.001
Treatment:Time:Species	24	149.08	3.754	<0.001

Table 7.12: ANOVA table of malondialdehyde (MDA) abundance light treatment response model parameters for five C_4 grass species

Factor	DF_{num}	DF_{den}	F	p
Treatment	1	1.78	1.528	0.35
Species	4	50.08	16.755	<0.001
Treatment:Time	6	155.73	5.472	<0.001
Treatment:Species	4	110.88	10.215	<0.001
Treatment:Time:Species	24	151.80	2.779	<0.001

Table 7.13: ANOVA table of percent relative injury light treatment response model parameters for five C_4 grass species

Factor	DF_{num}	DF_{den}	F	p
Treatment	1	1.97	0.077	0.8078
Species	4	49.92	8.485	<0.001
Treatment:Time	6	147.44	8.959	<0.001
Treatment:Species	4	186.24	0.655	0.6241
Treatment:Time:Species	24	147.35	2.106	0.0038

Table 7.14: ANOVA table of NPQ kinetic trace selected model parameters for five C_4 grass species

Trait	DF_{num}	DF_{den}	F	p
NPQ relaxation rate constant	4	15	3.805	0.0250
Maximum NPQ	4	15	7.290	0.0018
Photoprotection index	4	15	17.725	<0.001
ΦPSII recovery rate constant	4	15	7.744	0.0014

Note:
Grouping factor is species. Post-hoc Tukey's HSD results shown in Fig. 7.16

Table 7.15: ANOVA table of A/Q_{inc} response model parameters for five C_4 grass species

Trait	DF_{num}	DF_{den}	F	p
A_{sat} ($\mu mol\ m^2\ s^1$)	4	13.24	2.186	0.13
ΦCO_2 ($mol\ mol^{-1}$)	4	13.37	1.147	0.38
θ	4	15.00	0.571	0.69
R ($\mu mol\ m^2 s^1$)	4	15.00	0.685	0.61

Note:
Grouping factor is species. A_{sat} and ΦCO_2 models are mixed-effect with day-of-measurement included as random effect.

Table 7.16: ANOVA table of specific leaf area for five C_4 grass species. Linear mixed-effect model included growth set as random effect.

Factor	DF_{num}	DF_{den}	F	p
Species	4	59.01	4.378	0.0036

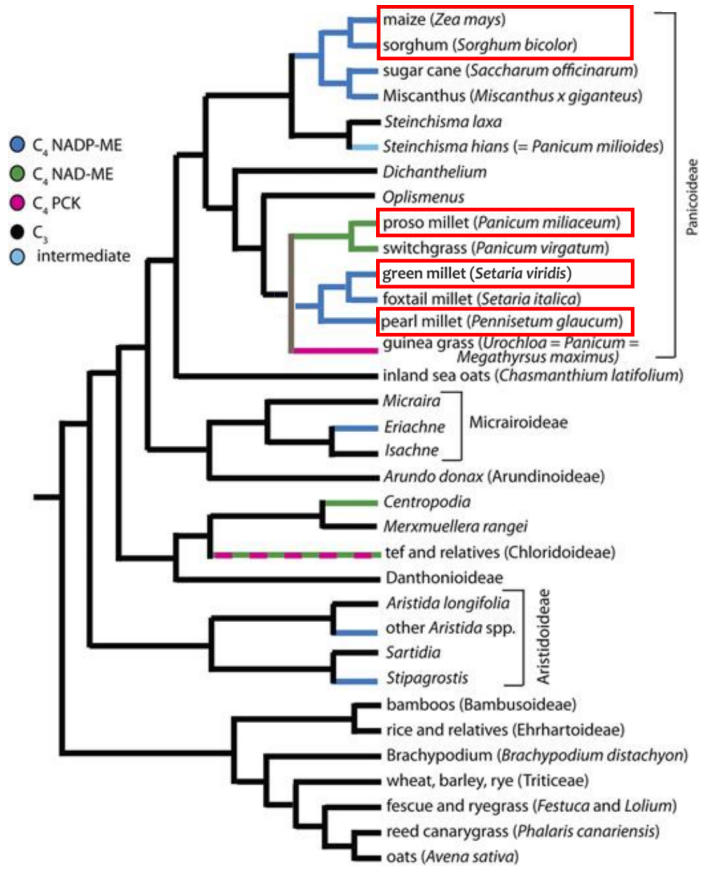

Figure 7.1: Phylogenetic summary of grasses. Modified from Brutnell et al. (2010), based on work by Vicentini et al. (2008) and Christin, Salamin, et al. (2009). Red boxes indicate species used in this study.

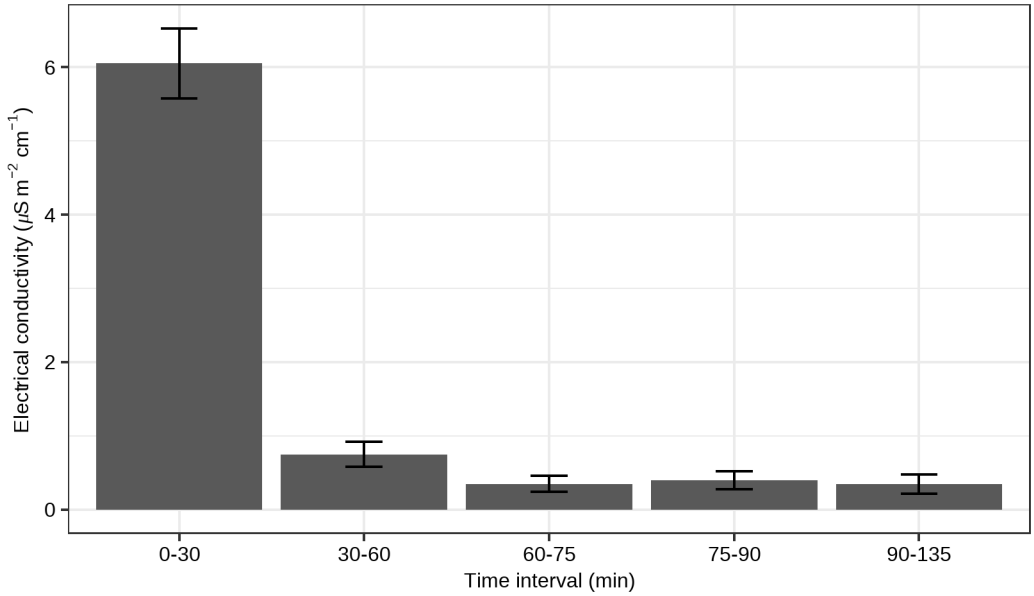

Figure 7.2: Electrical conductivity of *S. bicolor* leaf disc wash solution over time, used to determine appropriate wash time for relative injury assay (see 2.2.2 in methods). Error bars are +/- SE of the mean. $n = 10$ leaf discs, five from each of two plants.

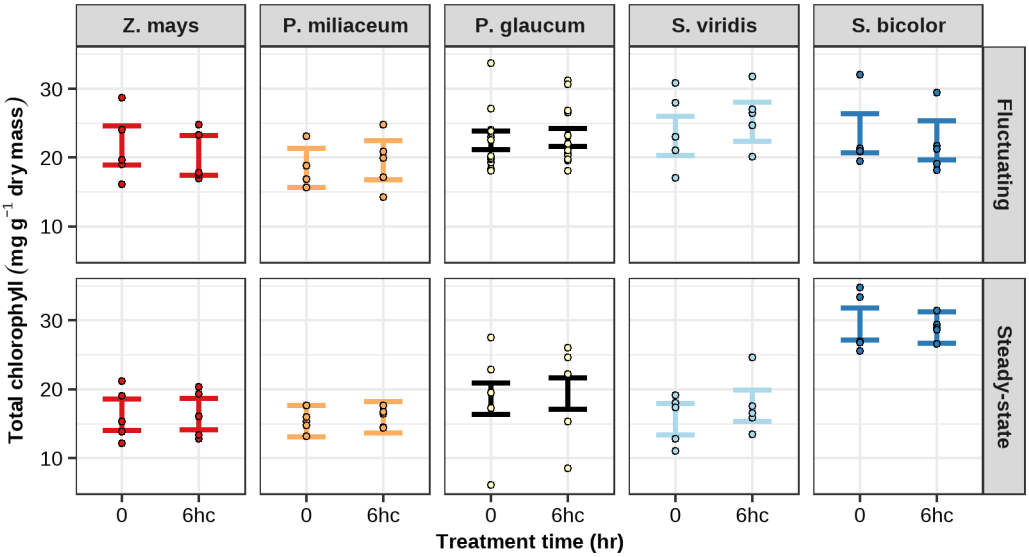

Figure 7.3: Estimated marginal means (EMM) of total chlorophyll content control measurements, produced by linear mixed-effect model which included individual plant and growth set as random effects. Whiskers indicate standard error of EMM. Original data points representing individual plants shown as dots. "6hc" refers to untreated control samples left for six hours under dim ambient light (<10 μmol m^{-2} s^{-1} PPFD).

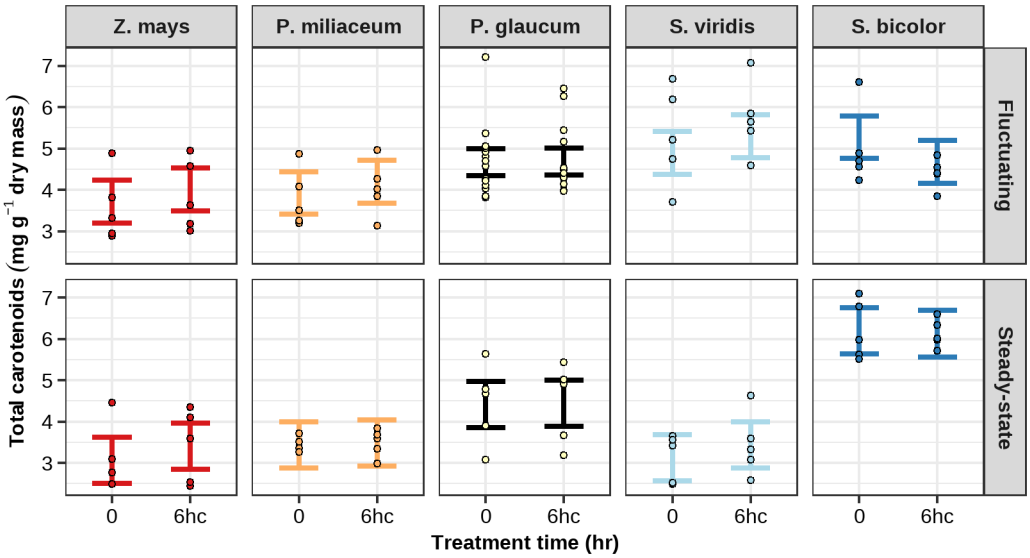

Figure 7.4: Estimated marginal means (EMM) of total carotenoid content control measurements, produced by linear mixed-effect model which included individual plant and growth set as random effects. Whiskers indicate standard error of EMM. Original data points representing individual plants shown as dots. "6hc" refers to untreated control samples left for six hours under dim ambient light (<10 μmol m^{-2} s^{-1} PPFD).

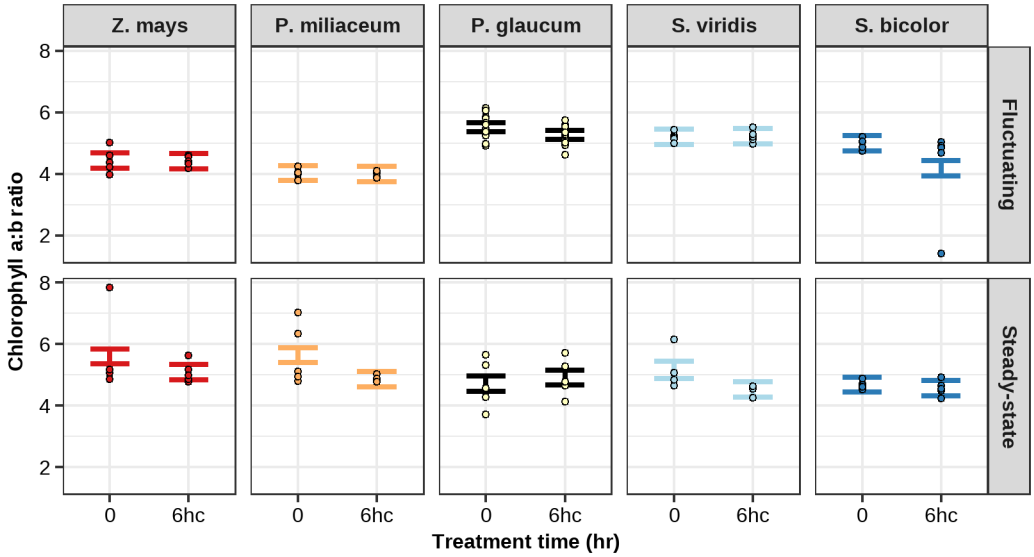

Figure 7.5: Estimated marginal means (EMM) of chlorophyll a:b ratio control measurements, produced by linear mixed-effect model which included individual plant as random effect. Whiskers indicate standard error of EMM. Original data points representing individual plants shown as dots. "6hc" refers to untreated control samples left for six hours under dim ambient light (<10 μmol m^{-2} s^{-1} PPFD).

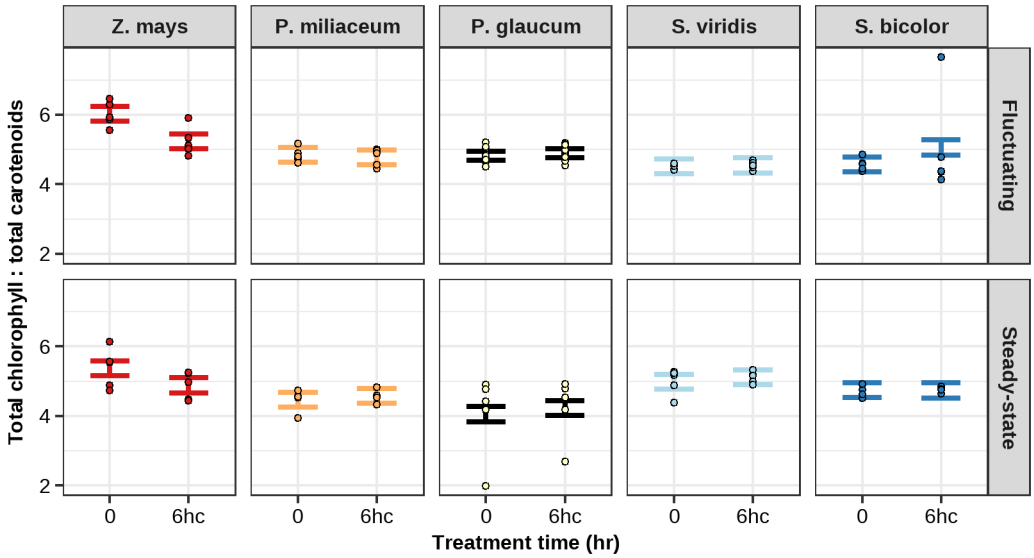

Figure 7.6: Estimated marginal means (EMM) of the ratio of chlorophyll to total carotenoids, produced by linear mixed-effect model which included individual plant as random effect. Whiskers indicate standard error of EMM. Original data points representing individual plants shown as dots. "6hc" refers to untreated control samples left for six hours under dim ambient light (<10 μmol m^{-2} s^{-1} PPFD).

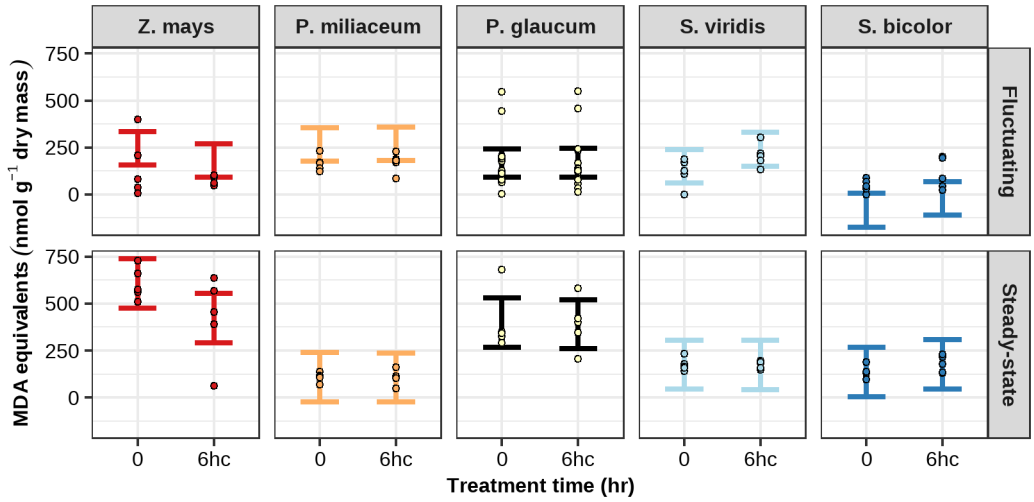

Figure 7.7: Estimated marginal means (EMM) of malondialdehyde (MDA) abundance control measurements, produced by linear mixed-effect model which included individual plant and growth set as random effects. Whiskers indicate standard error of EMM. Original data points representing individual plants shown as dots. "6hc" refers to untreated control samples left for six hours under dim ambient light (<10 μmol m^{-2} s^{-1} PPFD). Points at 0 nmol g^{-1} MDA had spectrophotometer absorbance values lower than measurement floor; the resulting negative MDA values were set to 0.

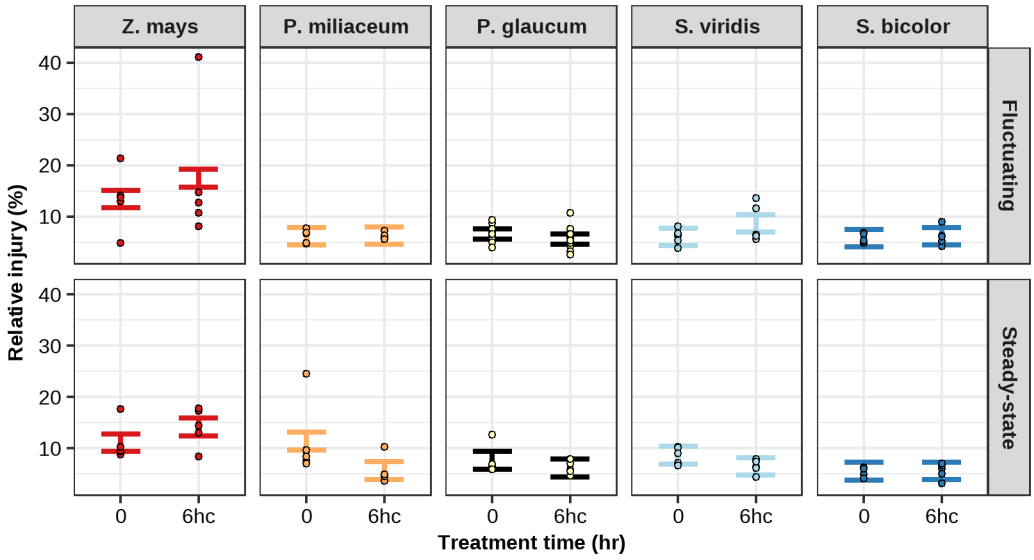

Figure 7.8: Estimated marginal means (EMM) of percent relative injury control measurements, produced by linear mixed-effect model which included individual plant and growth set as random effects. Whiskers indicate standard error of EMM. Original data points representing individual plants shown as dots. "6hc" refers to untreated control samples left for six hours under dim ambient light (<10 μmol m^{-2} s^{-1} PPFD).

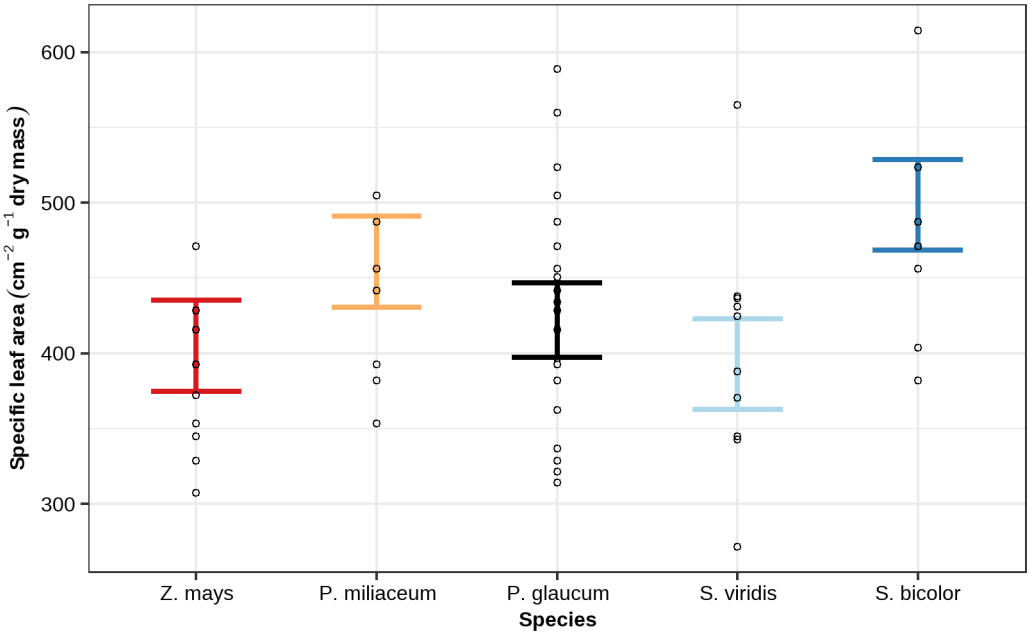

Figure 7.9: Estimated marginal means (EMM) of specific leaf area of plants grown in this study, produced by linear mixed-effect model which accounted for growth set (not shown on plot). Whiskers indicate standard error of EMM. Original data points representing individual plants shown as dots.

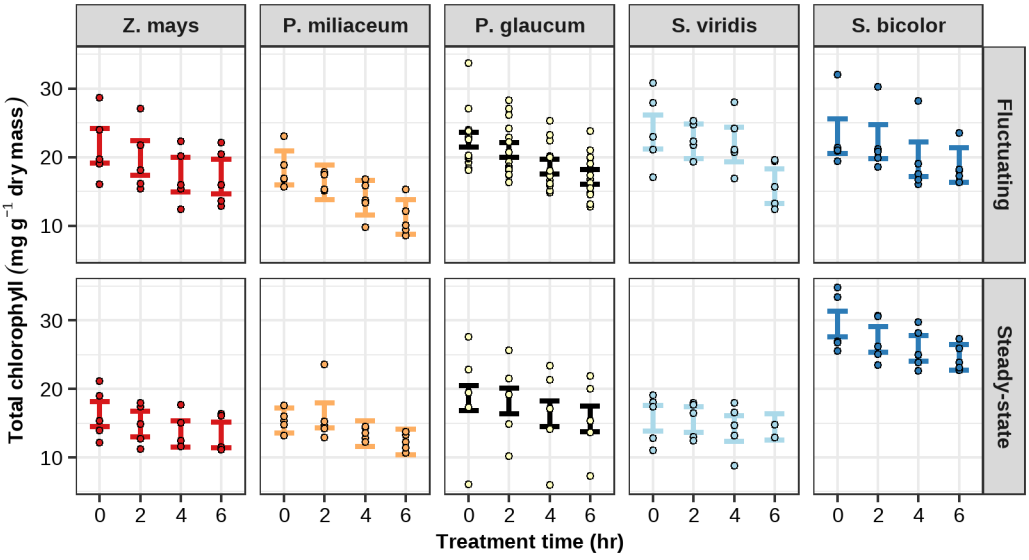

Figure 7.10: Estimated marginal means (EMM) of total chlorophyll content under fluctuating and steady-state light treatments, produced by linear mixed-effect model which included individual plant and growth set as random effects. Whiskers indicate standard error of EMM. Original data points representing individual plants shown as dots.

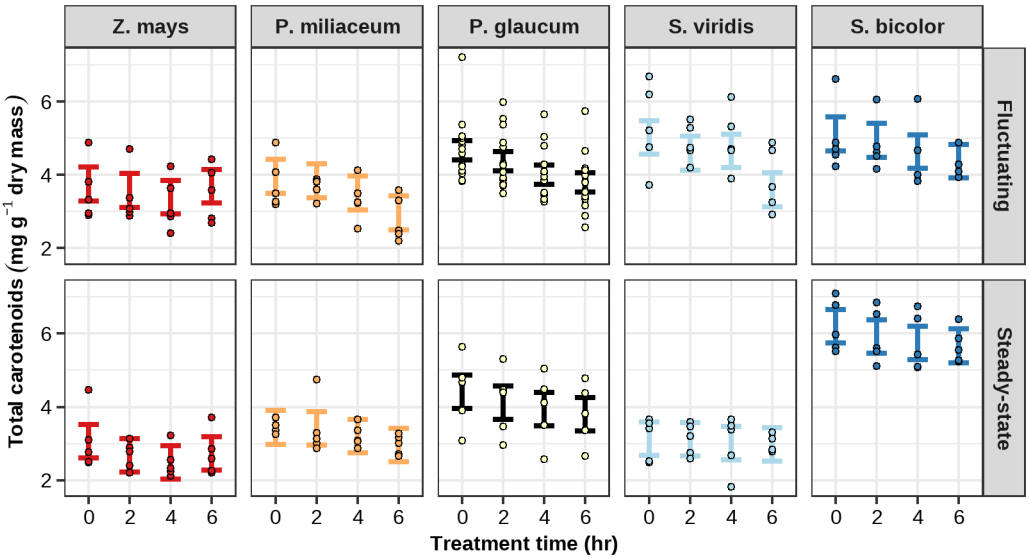

Figure 7.11: Estimated marginal means (EMM) of total carotenoid content under fluctuating and steady-state light treatments, produced by linear mixed-effect model which included individual plant and growth set as random effects. Whiskers indicate standard error of EMM. Original data points representing individual plants shown as dots.

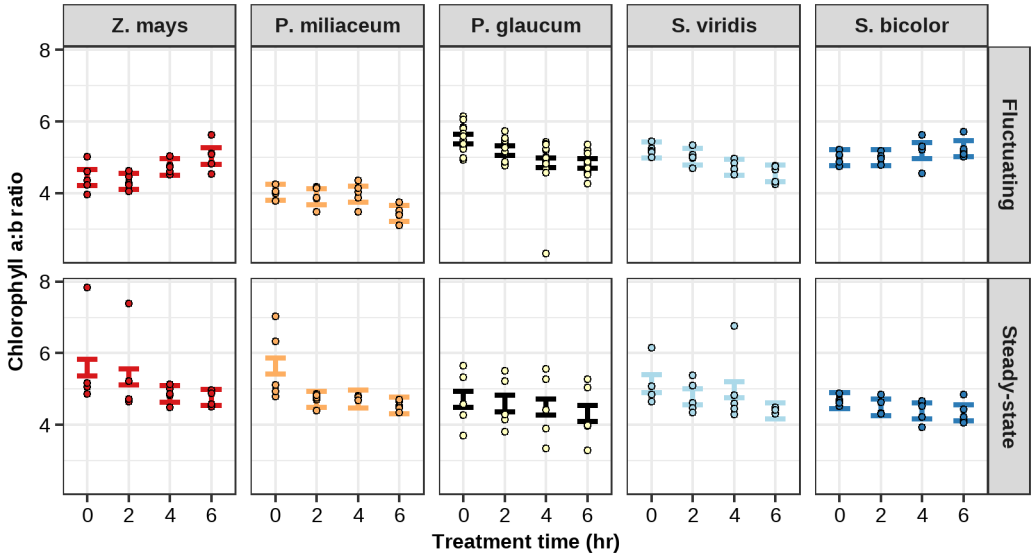

Figure 7.12: Estimated marginal means (EMM) of chlorophyll a:b ratio under fluctuating and steady-state light treatments, produced by linear mixed-effect model which included individual plant as random effect. Whiskers indicate standard error of EMM. Original data points representing individual plants shown as dots.

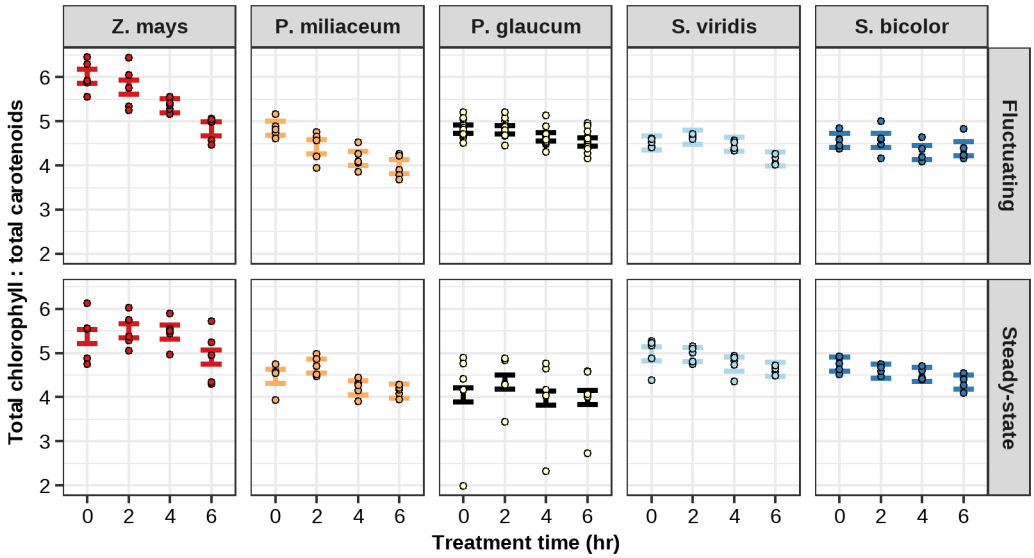

Figure 7.13: Estimated marginal means (EMM) of the ratio of total chlorophyll to total carotenoids under fluctuating and steady-state light treatments, produced by linear mixed-effect model which included individual plant as random effect. Whiskers indicate standard error of EMM. Original data points representing individual plants shown as dots.

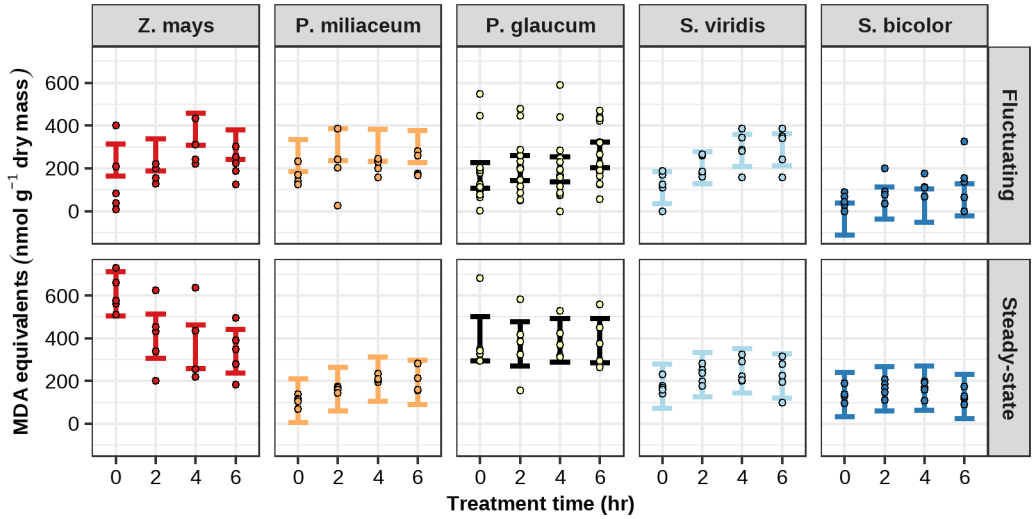

Figure 7.14: Estimated marginal means (EMM) of malondialdehyde (MDA) abundance ($nmol\ g^{-1}$) under fluctuating and steady-state light treatments, produced by linear mixed-effect model which included individual plant and growth set as random effects. Whiskers indicate standard error of EMM. Original data points representing individual plants shown as dots. Points at 0 nmol g^{-1} MDA had spectrophotometer absorbance values lower than measurement floor; the resulting negative MDA values were set to 0.

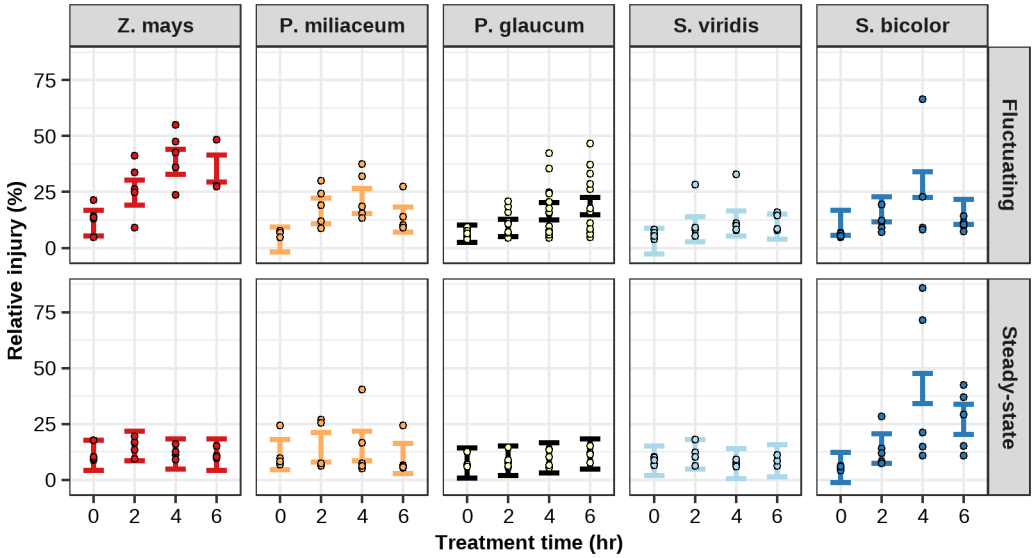

Figure 7.15: Estimated marginal means (EMM) of percent relative injury (Ri) under fluctuating and steady-state light treatments, produced by linear mixed-effect model which included individual plant and growth set as random effects. Whiskers indicate standard error of EMM. Original data points representing individual plants shown as dots.

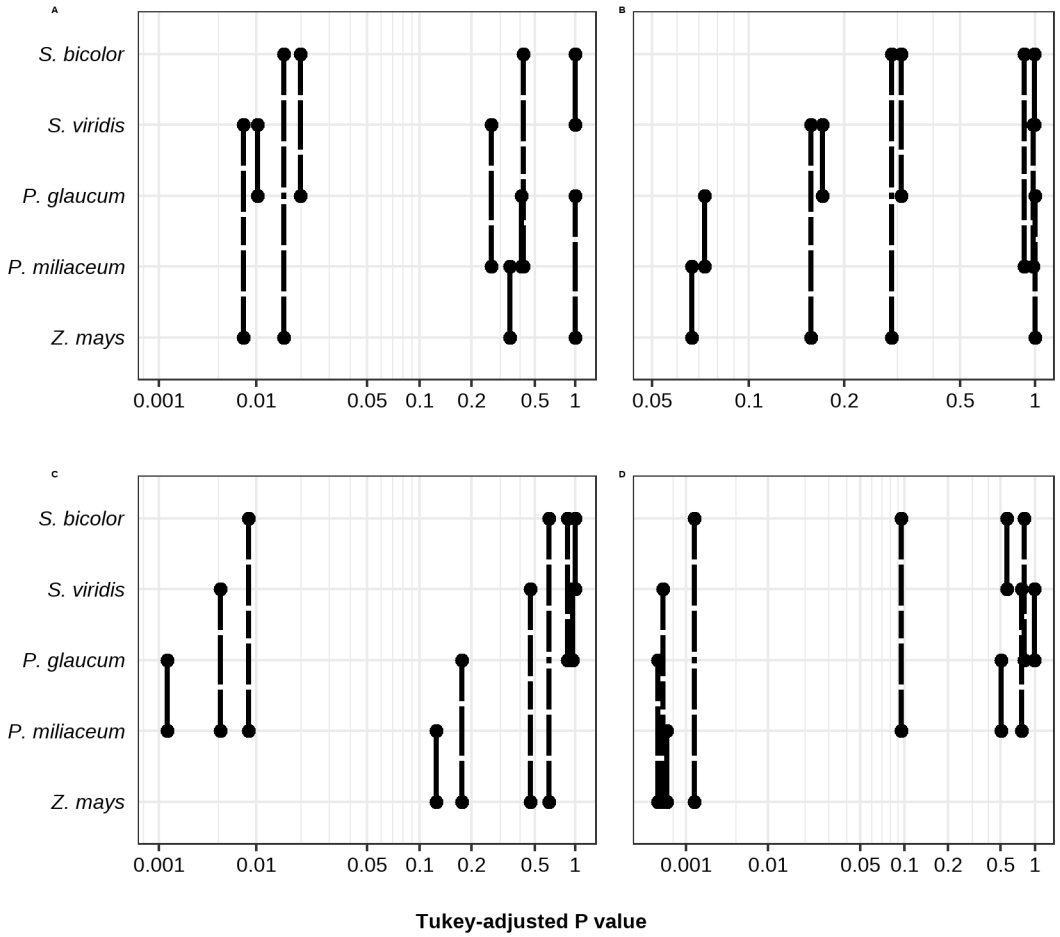

Figure 7.16: Pairwise p-value plots of selected NPQ kinetic trace model parameters. Estimated marginal means (EMM) of model parameters were compared between species via Tukey's HSD. EMM of species connected on vertical axis differ by the corresponding x-axis α (p) value. **A**) Maximum NPQ reached during trace; **B**) NPQ relaxation rate constant; **C**) $\Phi PSII$ recovery rate constant; **D**) Photoprotection index. NPQ induction k was not tested as data did not pass test of homogeneity of variances.

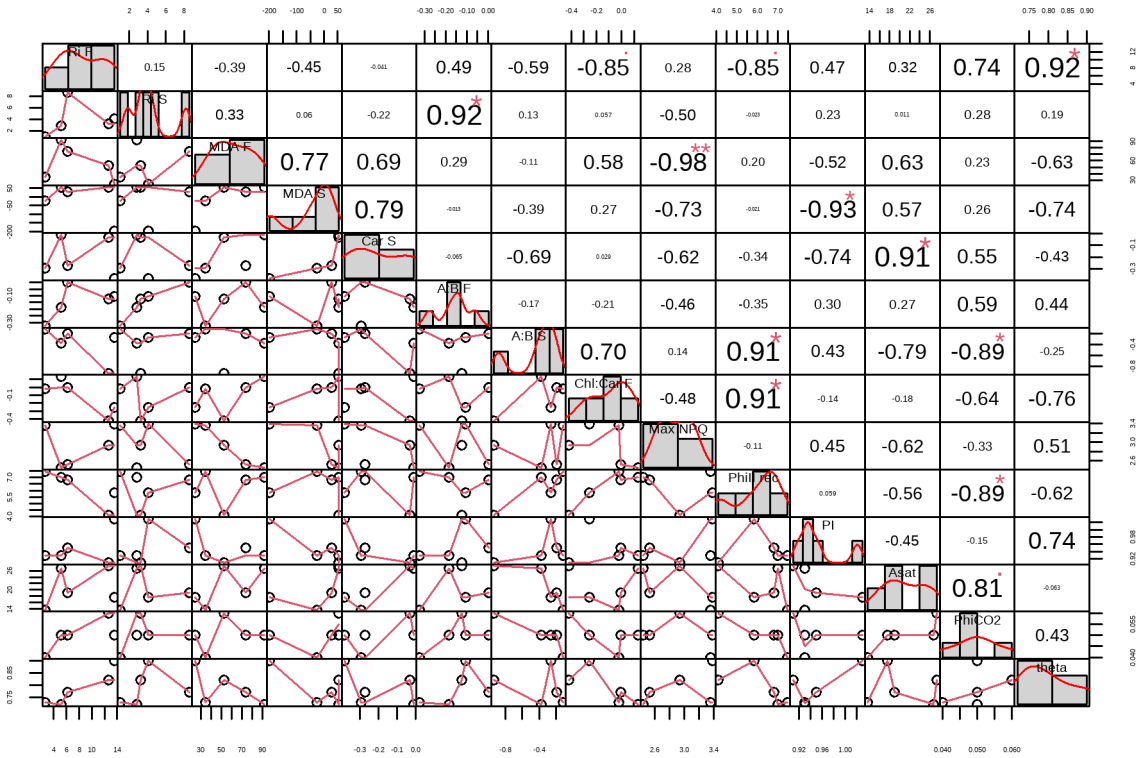

Figure 7.17: Scatterplot matrices of selected photodamage, photoprotection, and NPQ trace traits with significant correlations as noted in Fig. 2.8.

7.2 Supplement for chapter three

Chromosome mapping (physical location) for SNPs and genes associated with all trait and year combinations. **A**, GWAS; **B**, TWAS in GP tissue; **C**, TWAS in 3L tissue ; **D**, Fishers combined test from GP tissue; **E**, Fishers combined test from 3L tissue; Blue lines indicate threshold of SNPs in top 0.05% (**A**) or genes in top 1% (**B-E**) of -$\log_{10}$ p-values. 65% of SNPs below -log10 p-value of 2.5 have been randomly removed from each GWAS plot to reduce image size. TWAS and FCT gene positions plotted as midpoint of each gene. Followed by upset plot showing number of overlapping genes between top 1% of hits in FCT 3L and GP, TWAS 3L and GP, and top 0.05% of hits in GWAS analysis.

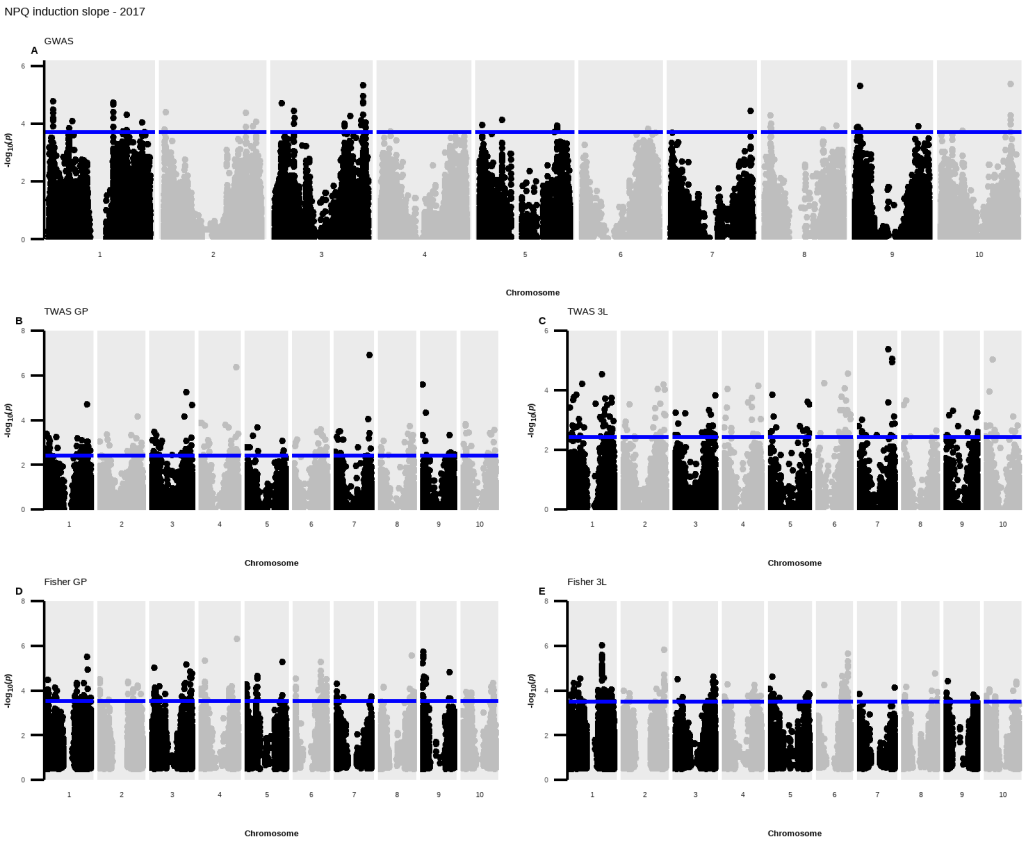

Figure 7.18: Chromosome mapping for SNPs and genes associated with NPQ induction slope, 2017 model

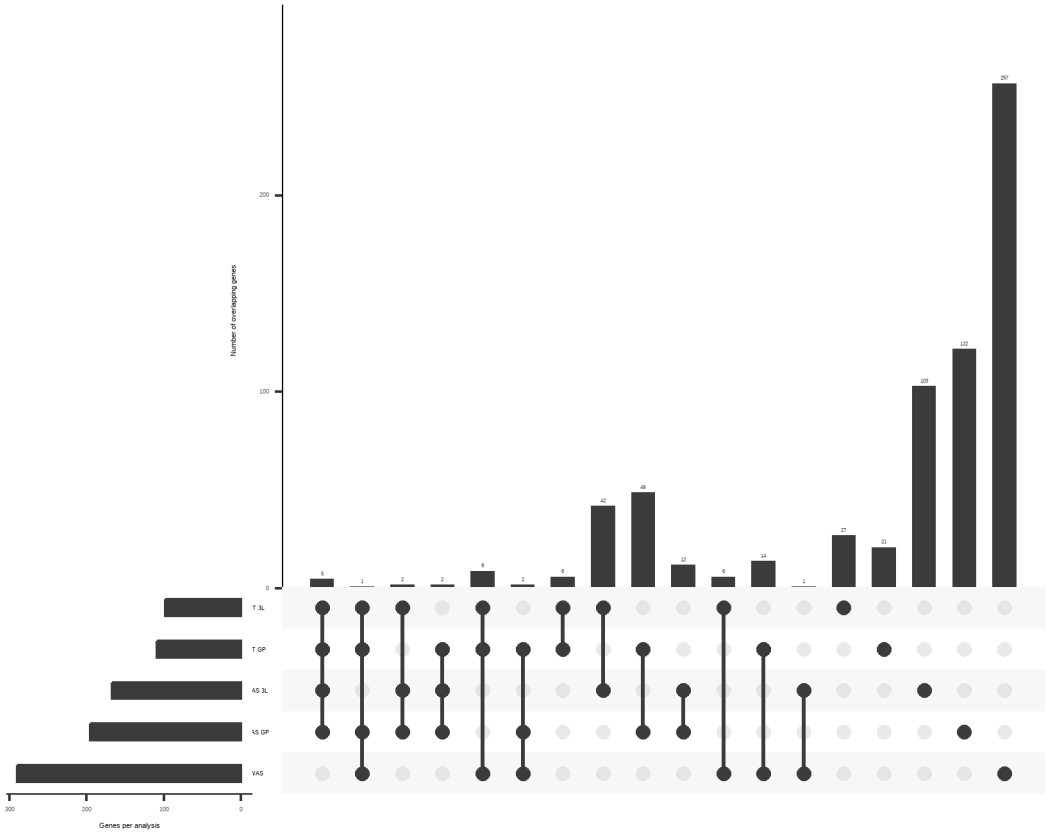

Figure 7.19: Upset plot for analyses associated with NPQ induction slope, 2017 model

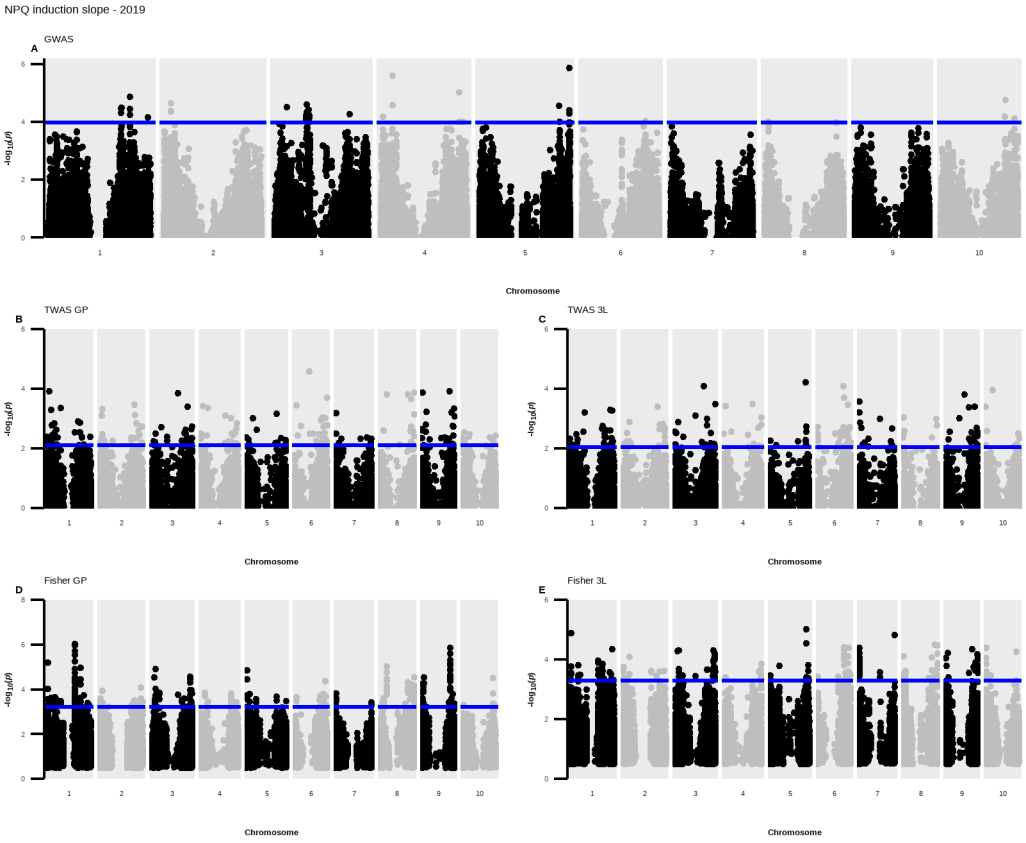

Figure 7.20: Chromosome mapping for SNPs and genes associated with NPQ induction slope, 2019 model

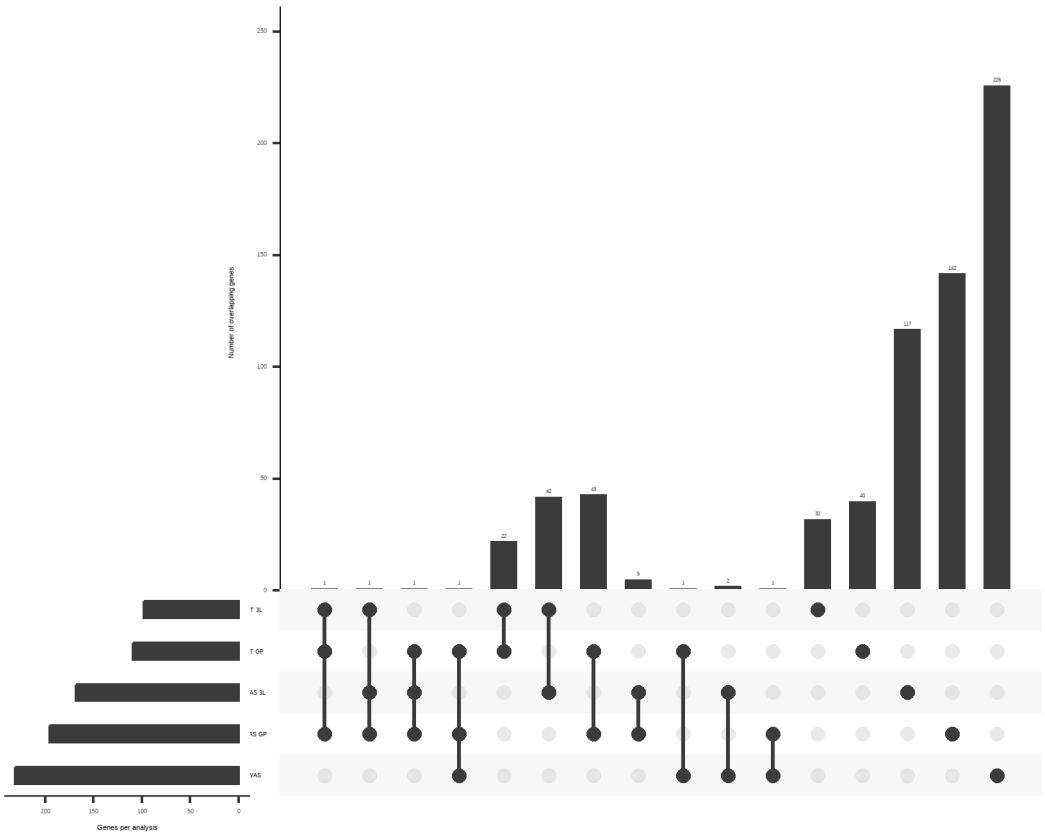

Figure 7.21: Upset plot for analyses associated with NPQ induction slope, 2019 model

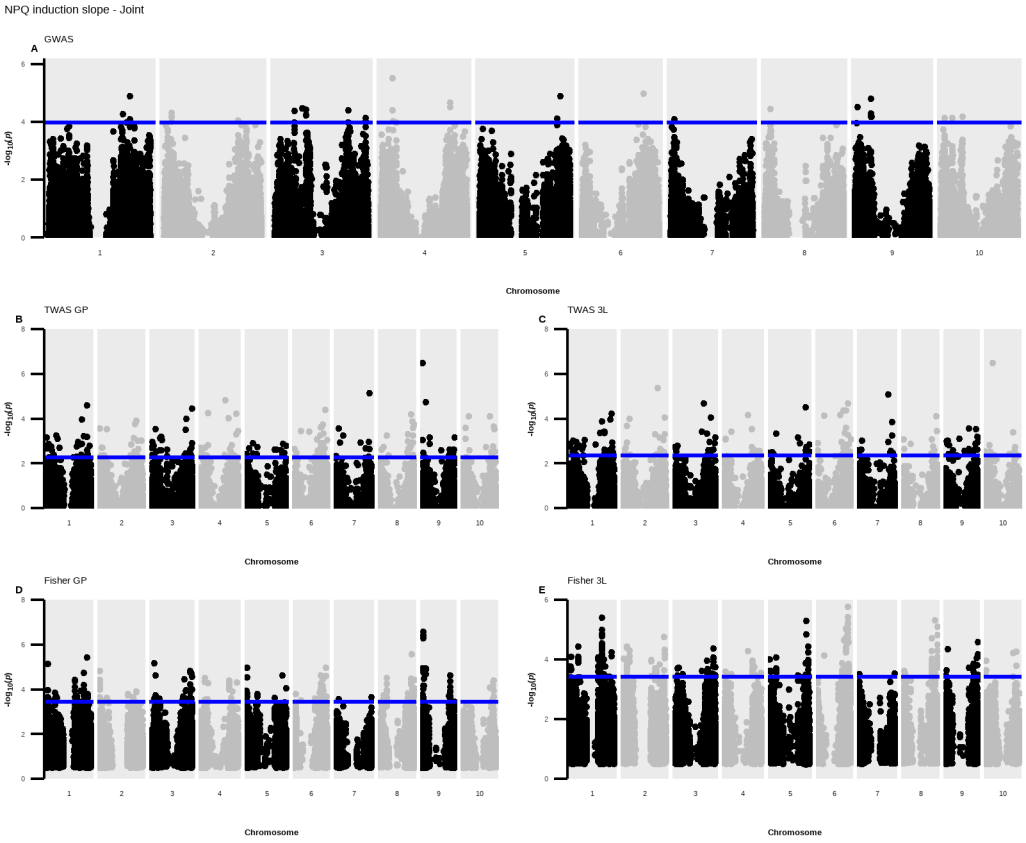

Figure 7.22: Chromosome mapping for SNPs and genes associated with NPQ induction slope, joint model

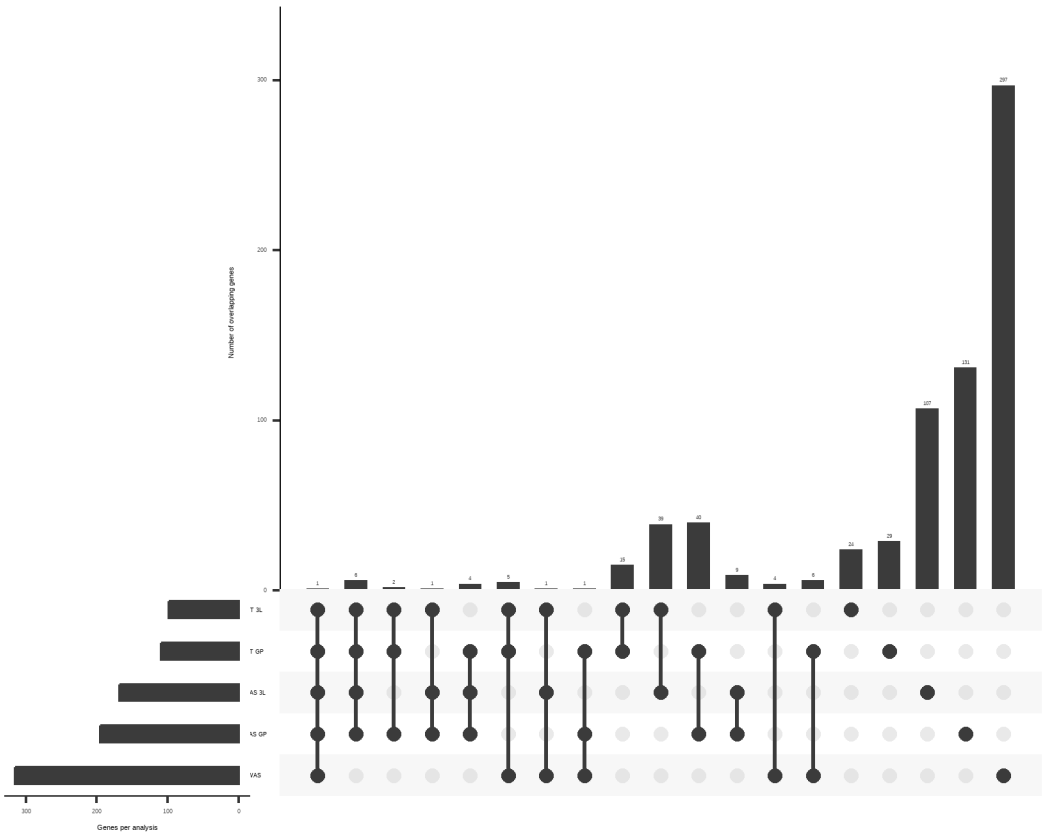

Figure 7.23: Upset plot for analyses associated with NPQ induction slope, joint model

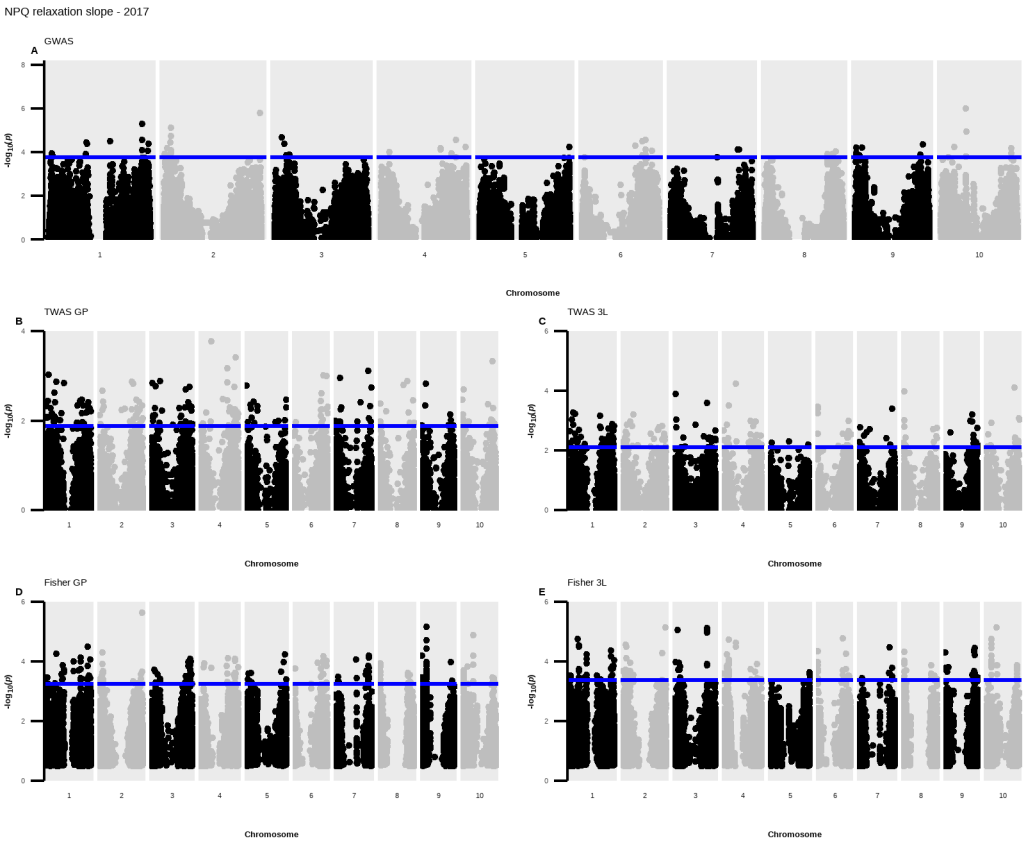

Figure 7.24: Chromosome mapping for SNPs and genes associated with NPQ relaxation slope, 2017 model

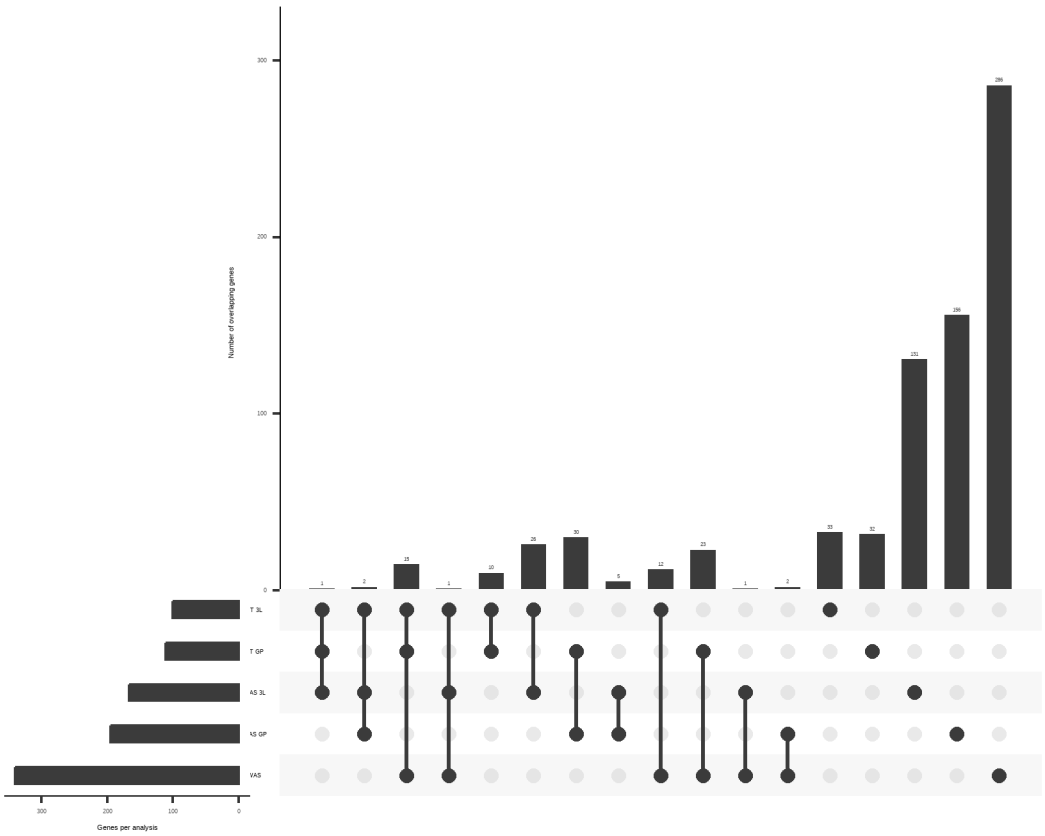

Figure 7.25: Upset plot for analyses associated with NPQ relaxation slope, 2017 model

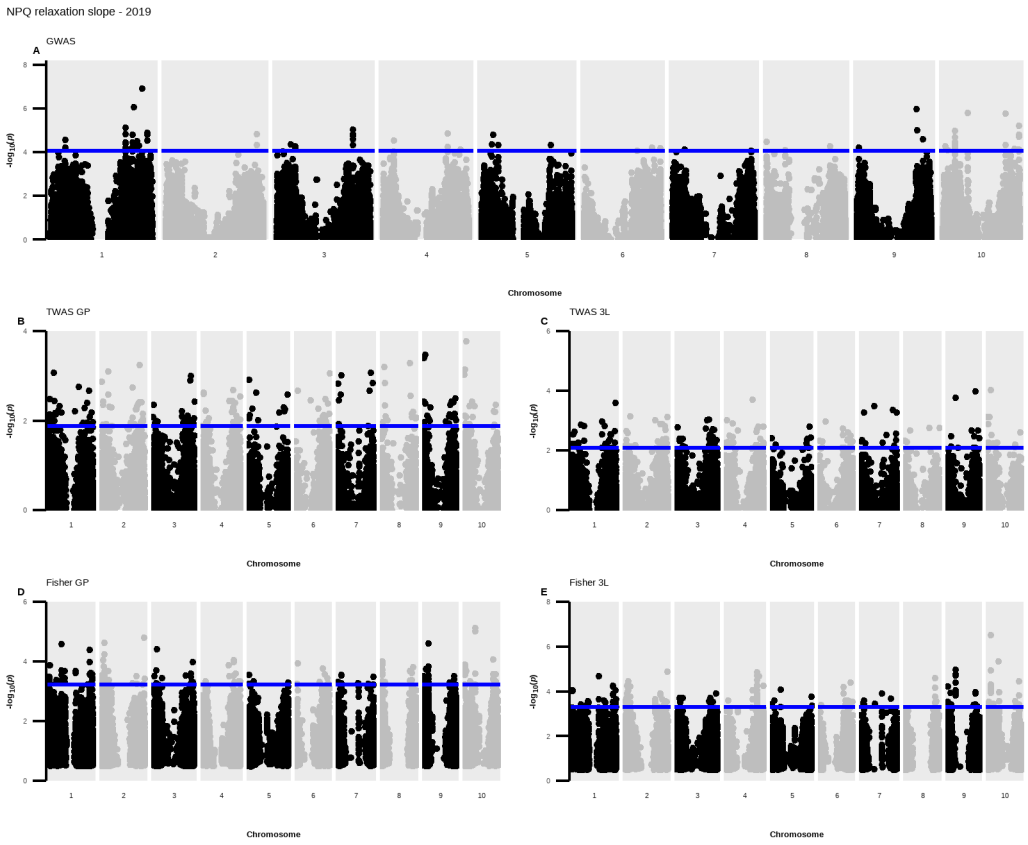

Figure 7.26: Chromosome mapping for SNPs and genes associated with NPQ relaxation slope, 2019 model

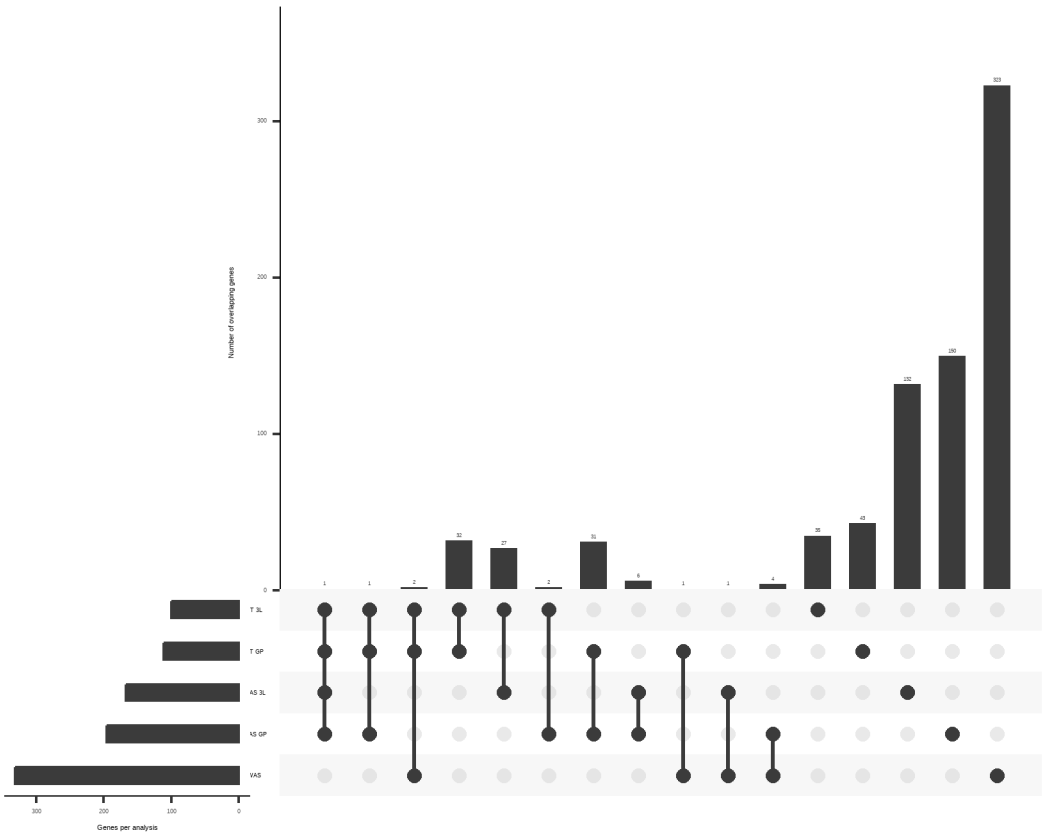

Figure 7.27: Upset plot for analyses associated with NPQ relaxation slope, 2019 model

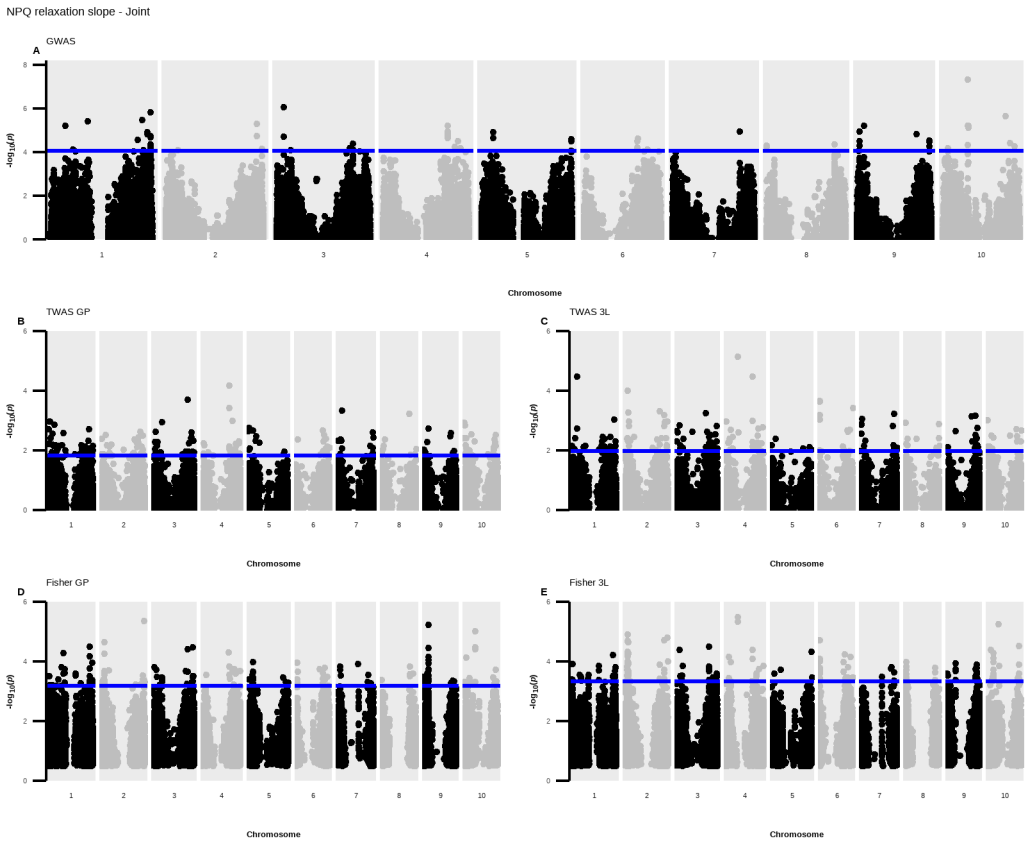

Figure 7.28: Chromosome mapping for SNPs and genes associated with NPQ relaxation slope, joint model

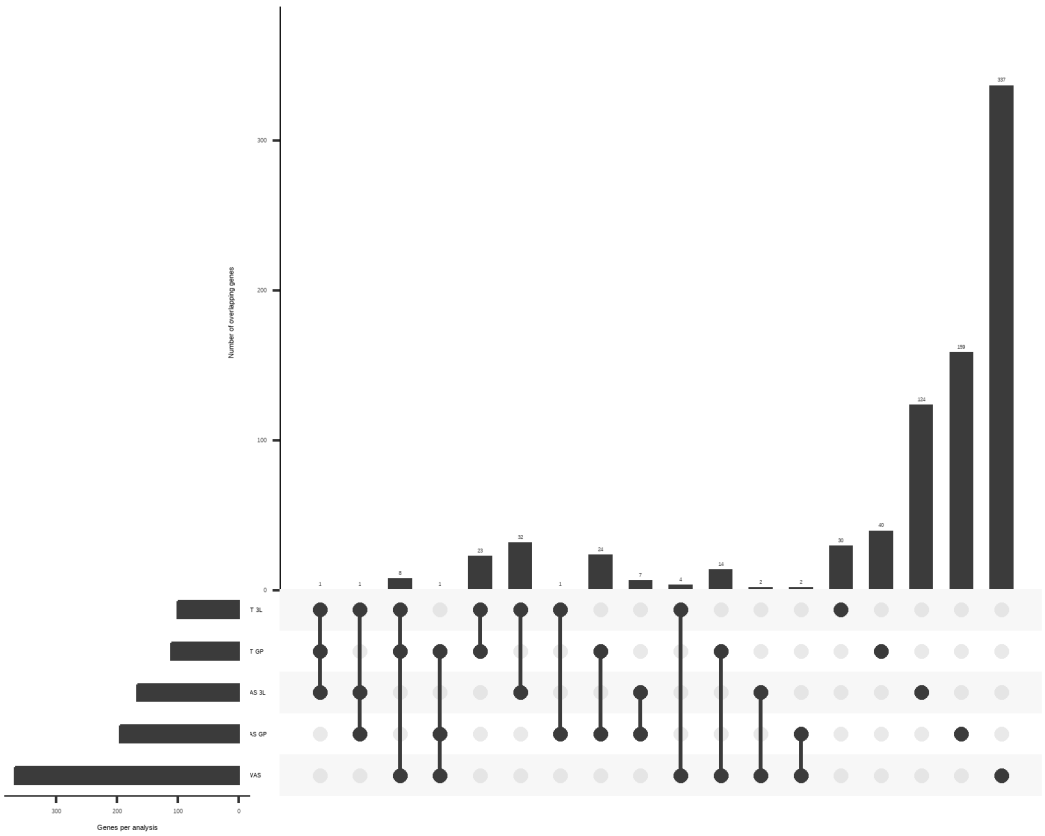

Figure 7.29: Upset plot for analyses associated with NPQ relaxation slope, joint model

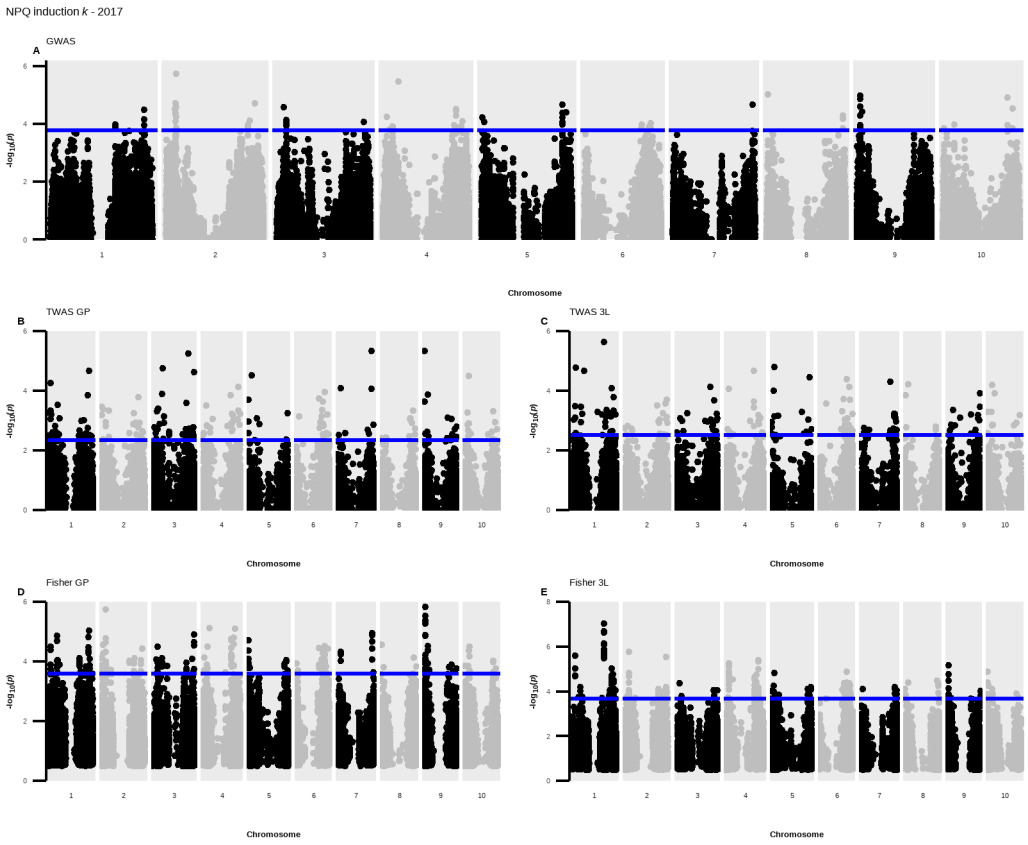

Figure 7.30: Chromosome mapping for SNPs and genes associated with NPQ induction rate constant, 2017 model

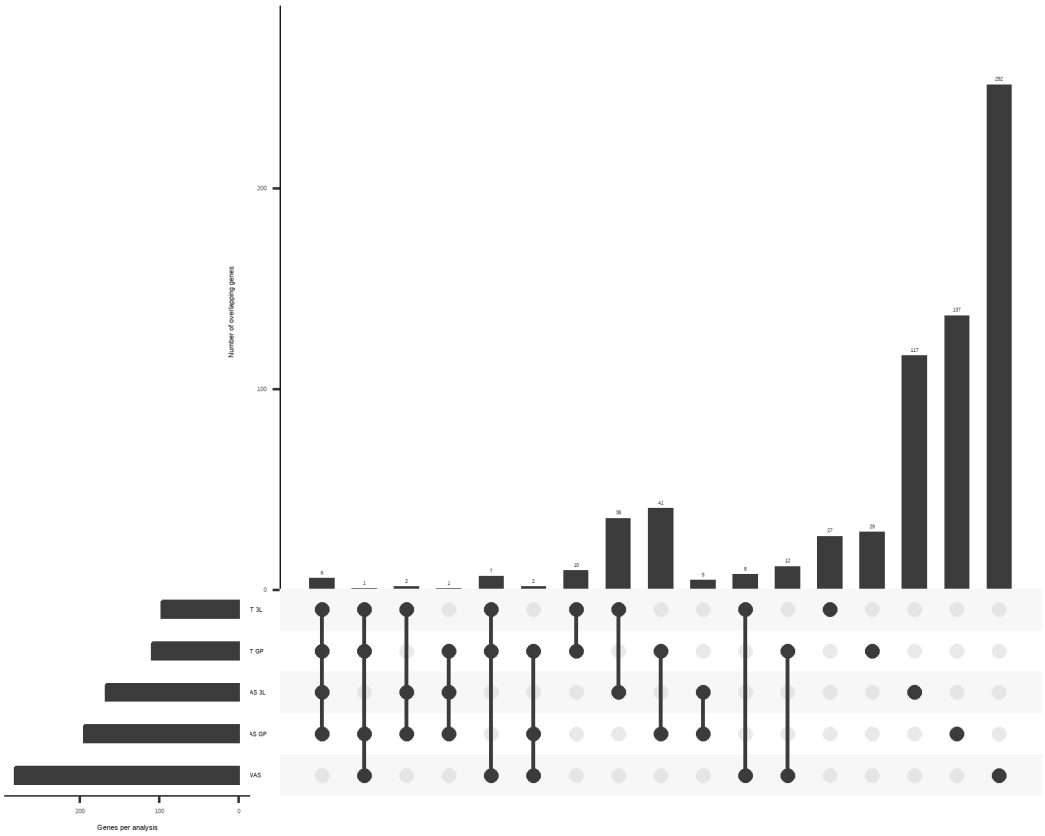

Figure 7.31: Upset plot for analyses associated with NPQ induction rate constant, 2017 model

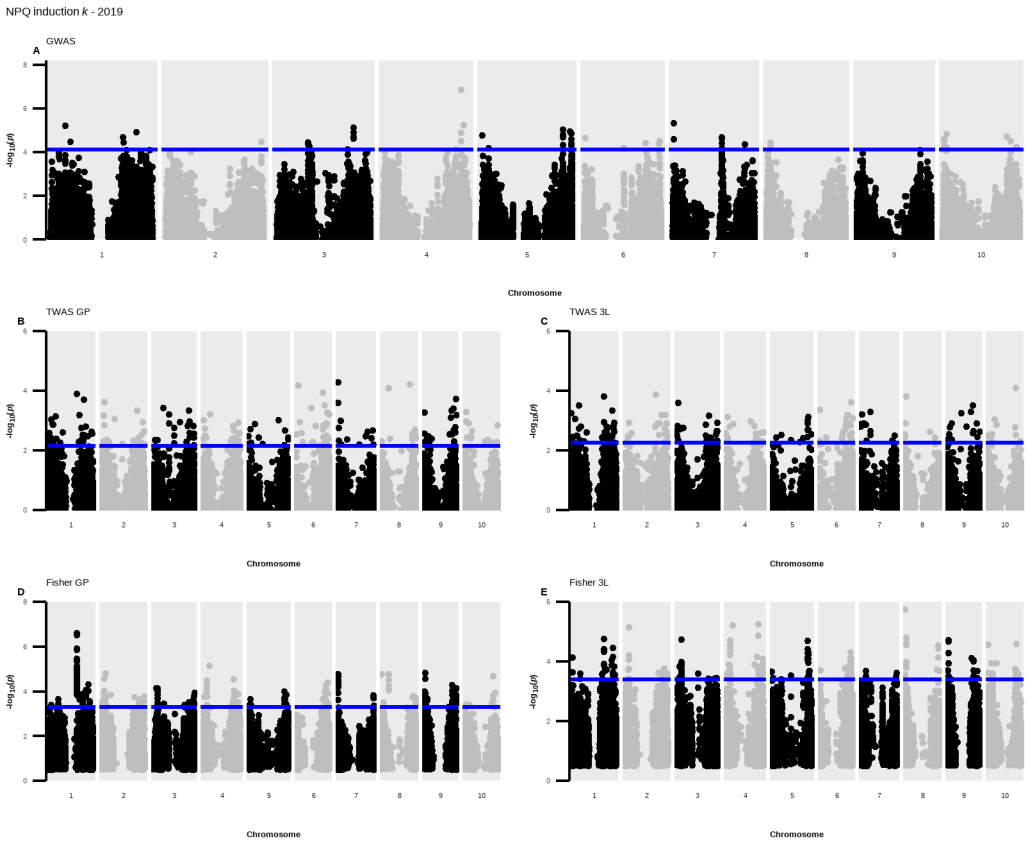

Figure 7.32: Chromosome mapping for SNPs and genes associated with NPQ induction rate constant, 2019 model

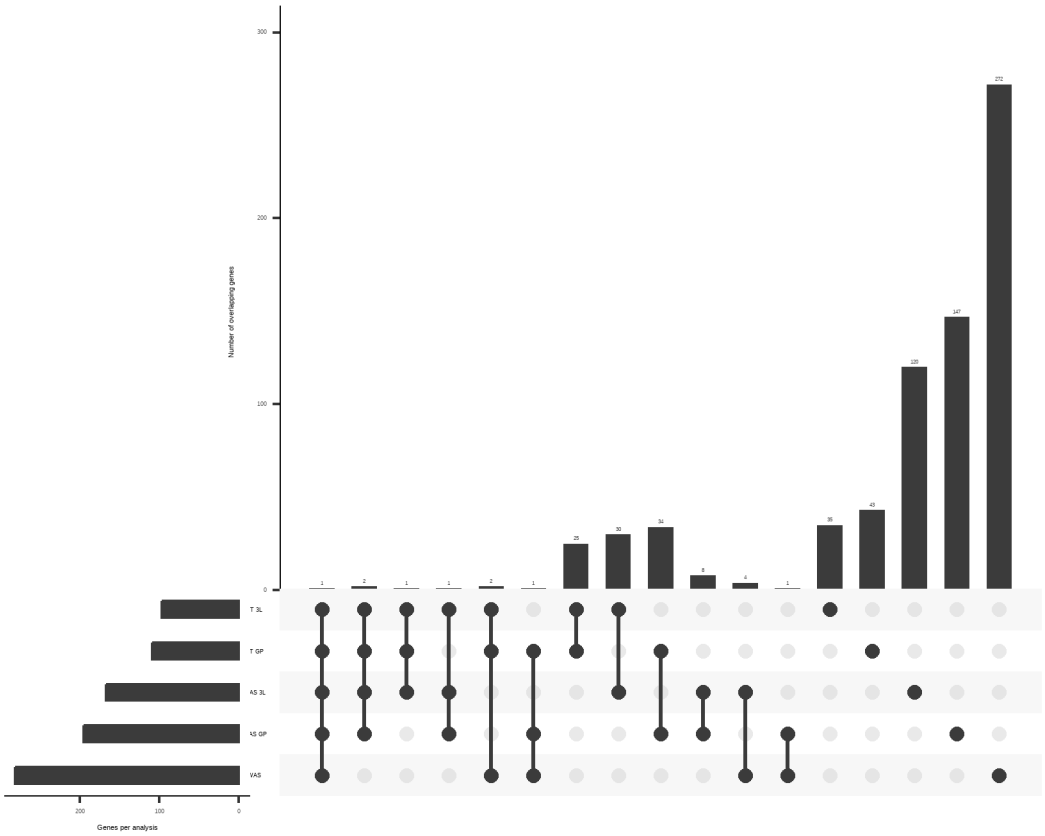

Figure 7.33: Upset plot for analyses associated with NPQ induction rate constant, 2019 model

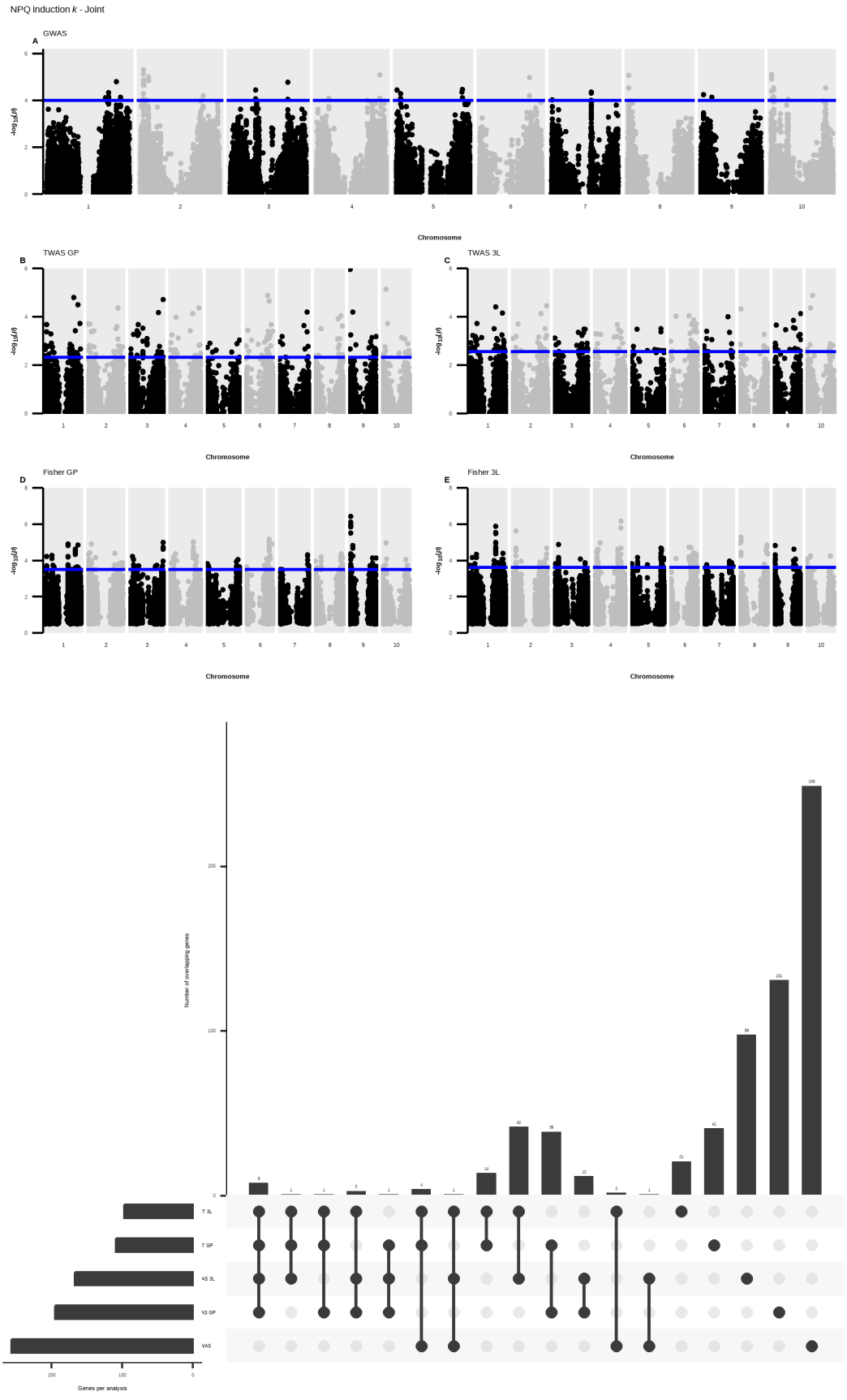
NPQ induction k - Joint
A
GWAS
B
TWAS GP
C
TWAS 3L
D
Fisher GP
E
Fisher 3L
Chromosome
Number of overlapping genes
Genes per analysis
T 3L
T GP
AS 3L
AS GP
VAS

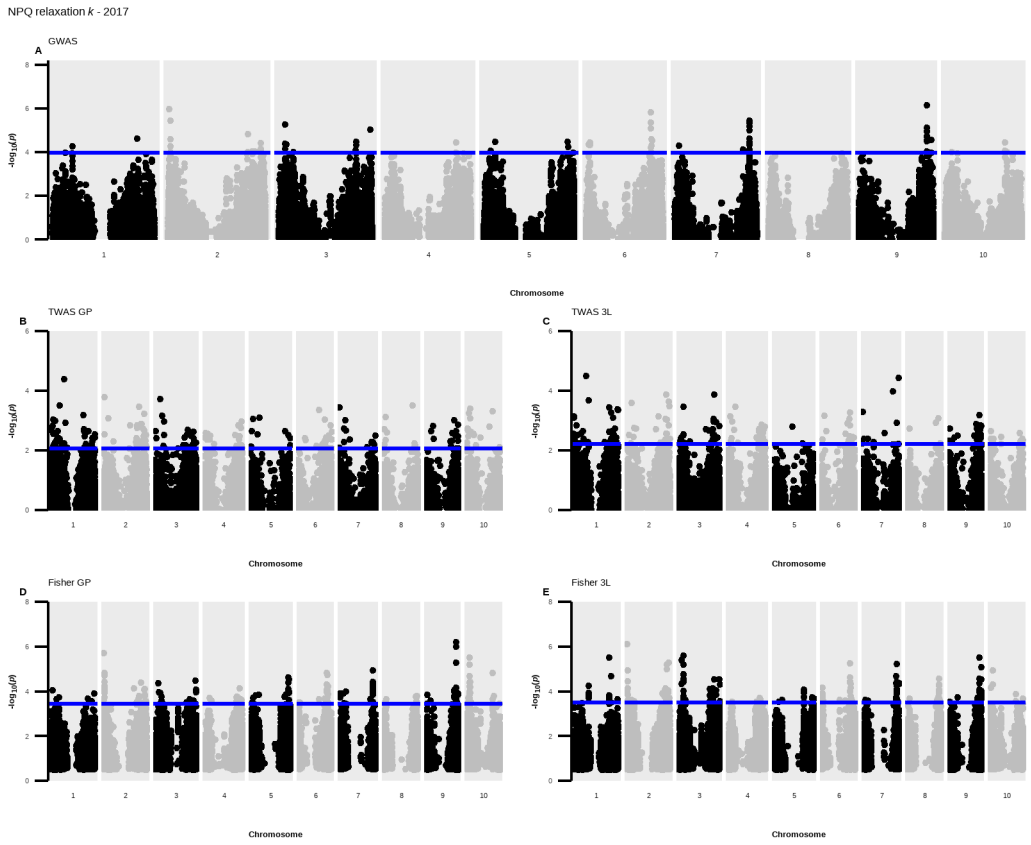

Figure 7.34: Chromosome mapping for SNPs and genes associated with NPQ relaxation rate constant, 2017 model

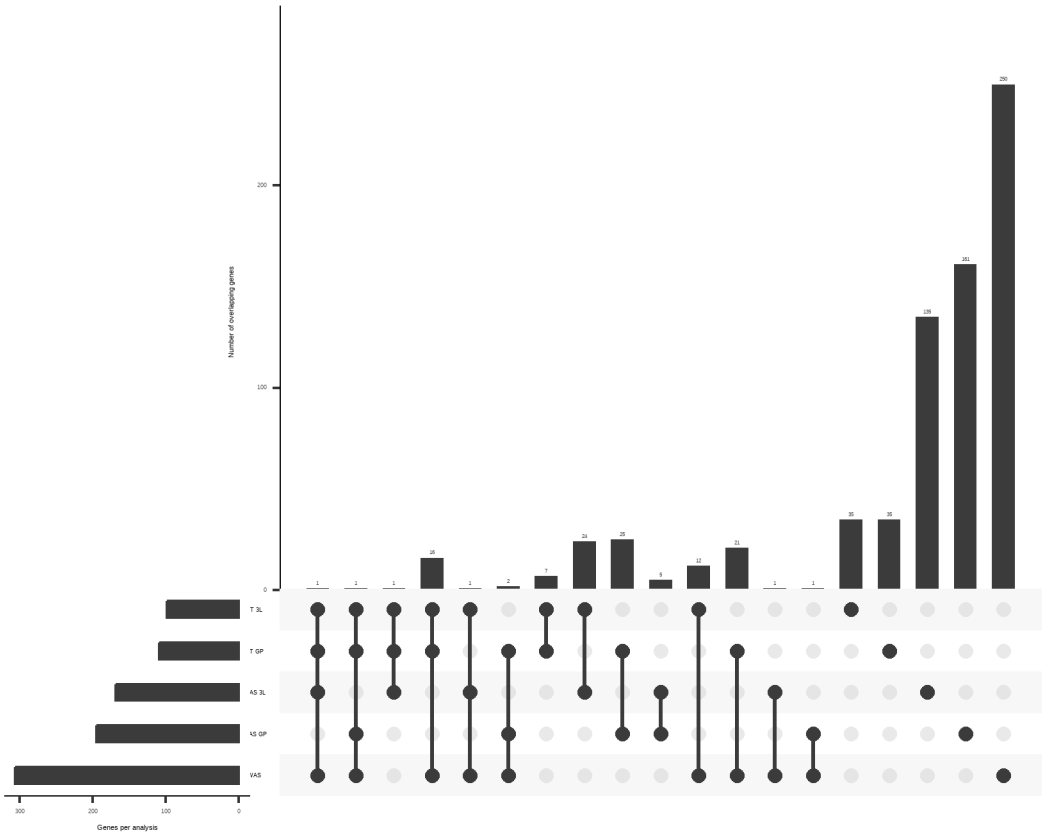

Figure 7.35: Upset plot for analyses associated with NPQ relaxation rate constant, 2017 model

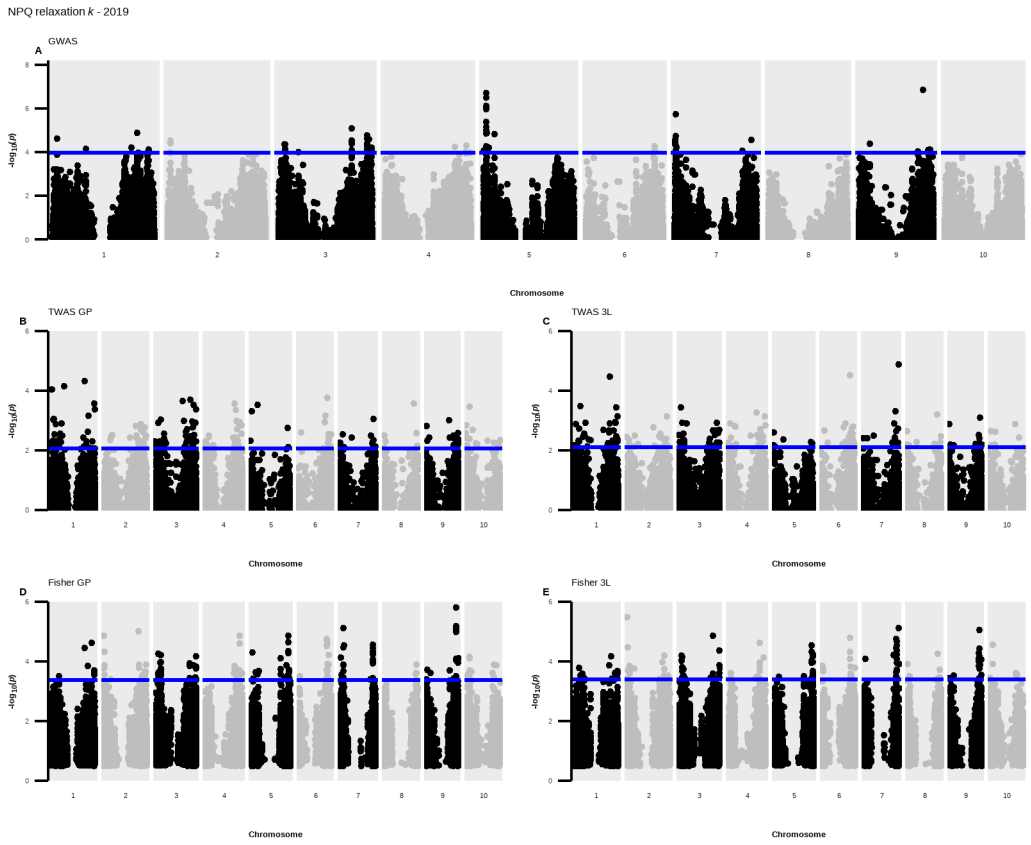

Figure 7.36: Chromosome mapping for SNPs and genes associated with NPQ relaxation rate constant, 2019 model

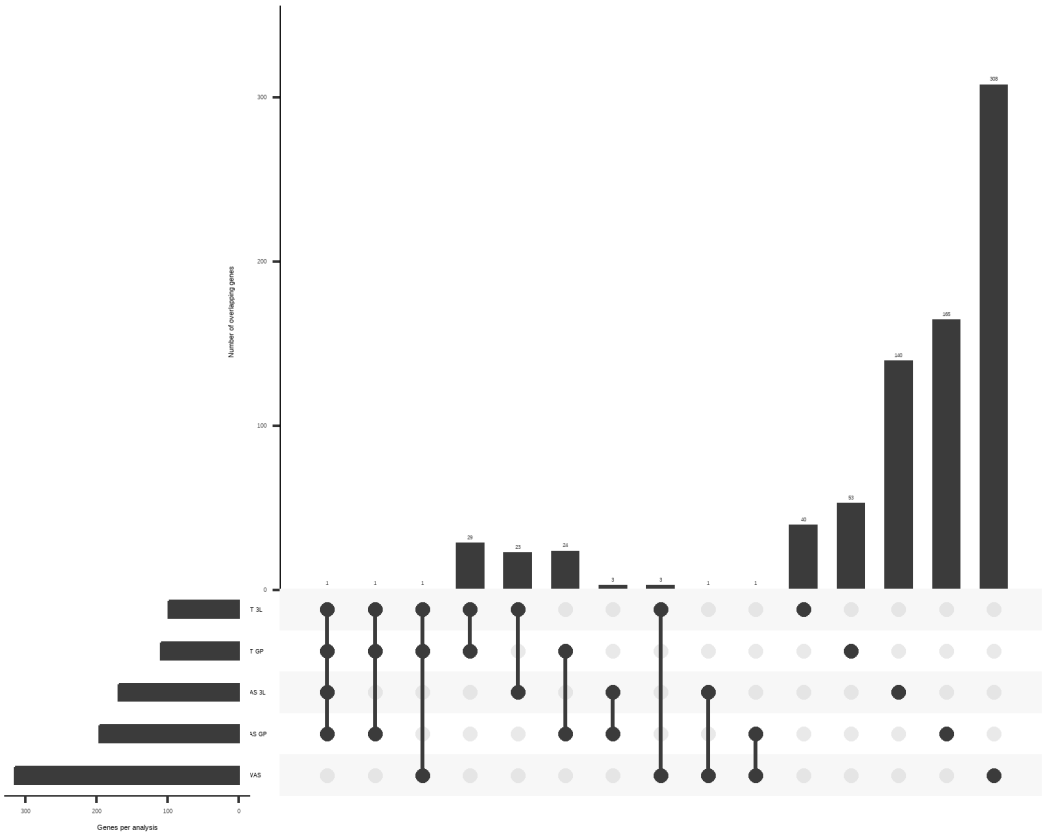

Figure 7.37: Upset plot for analyses associated with NPQ relaxation rate constant, 2019 model

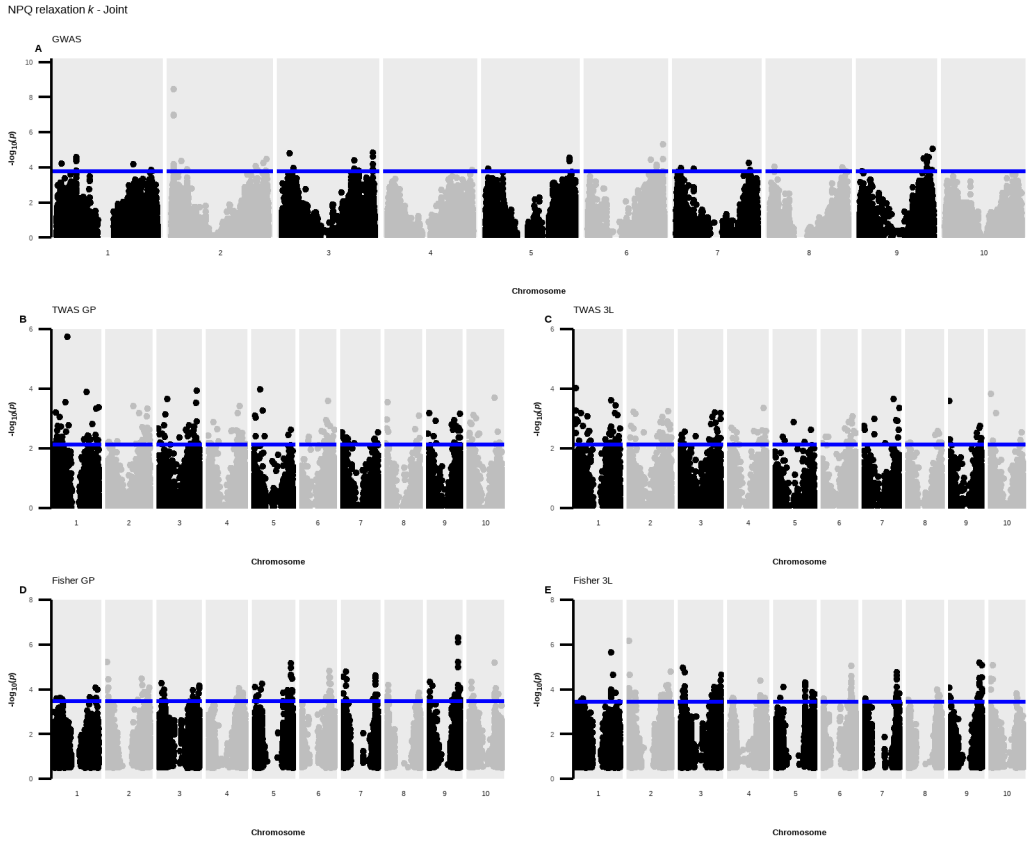

Figure 7.38: Chromosome mapping for SNPs and genes associated with NPQ relaxation rate constant, joint model

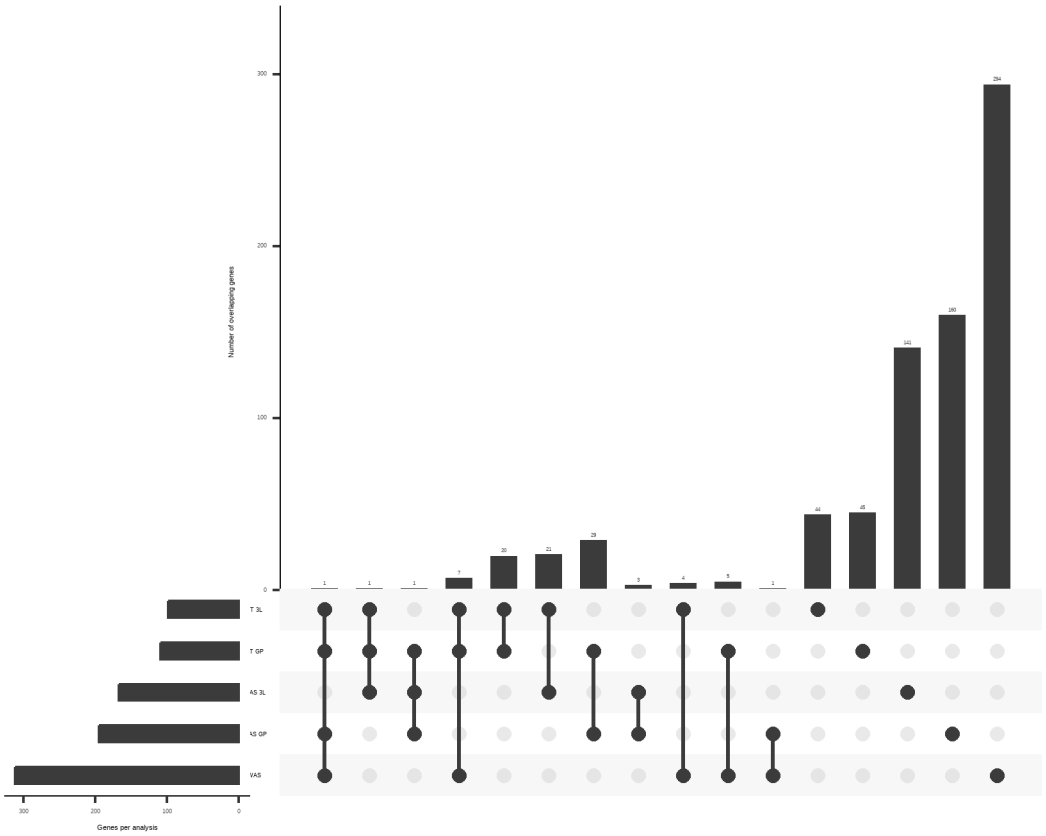

Figure 7.39: Upset plot for analyses associated with NPQ relaxation rate constant, joint model

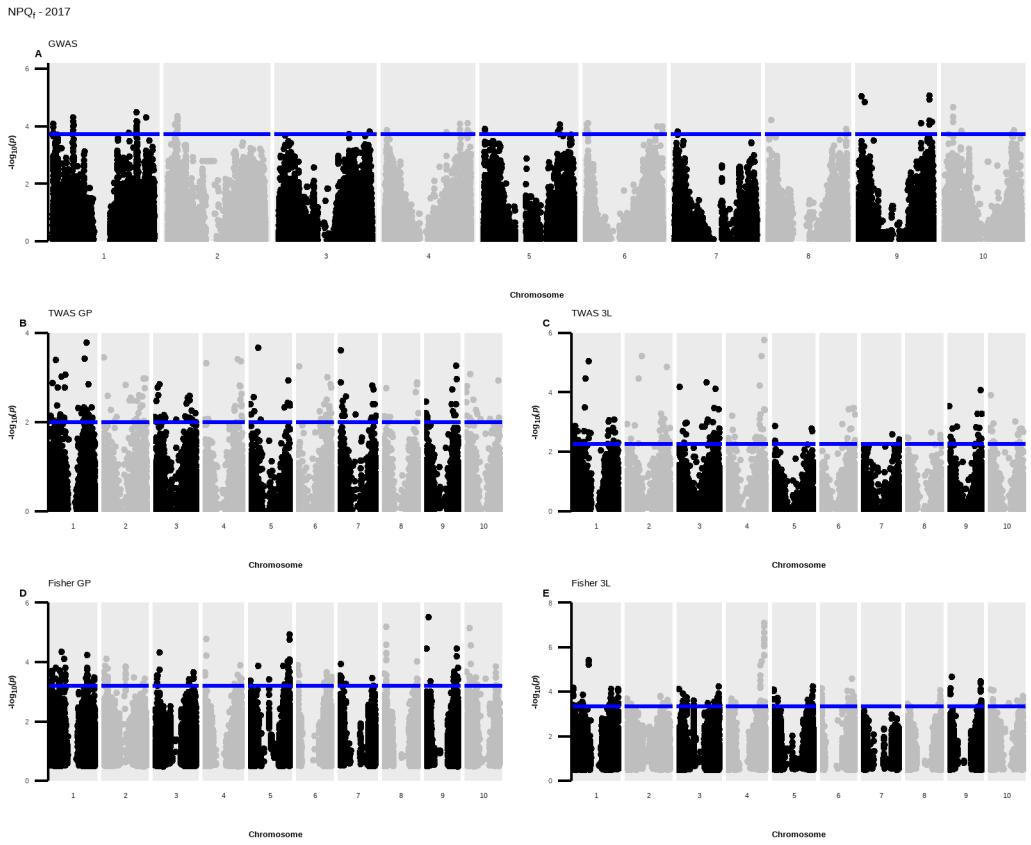

Figure 7.40: Chromosome mapping for SNPs and genes associated with final dark NPQ value, 2017 model

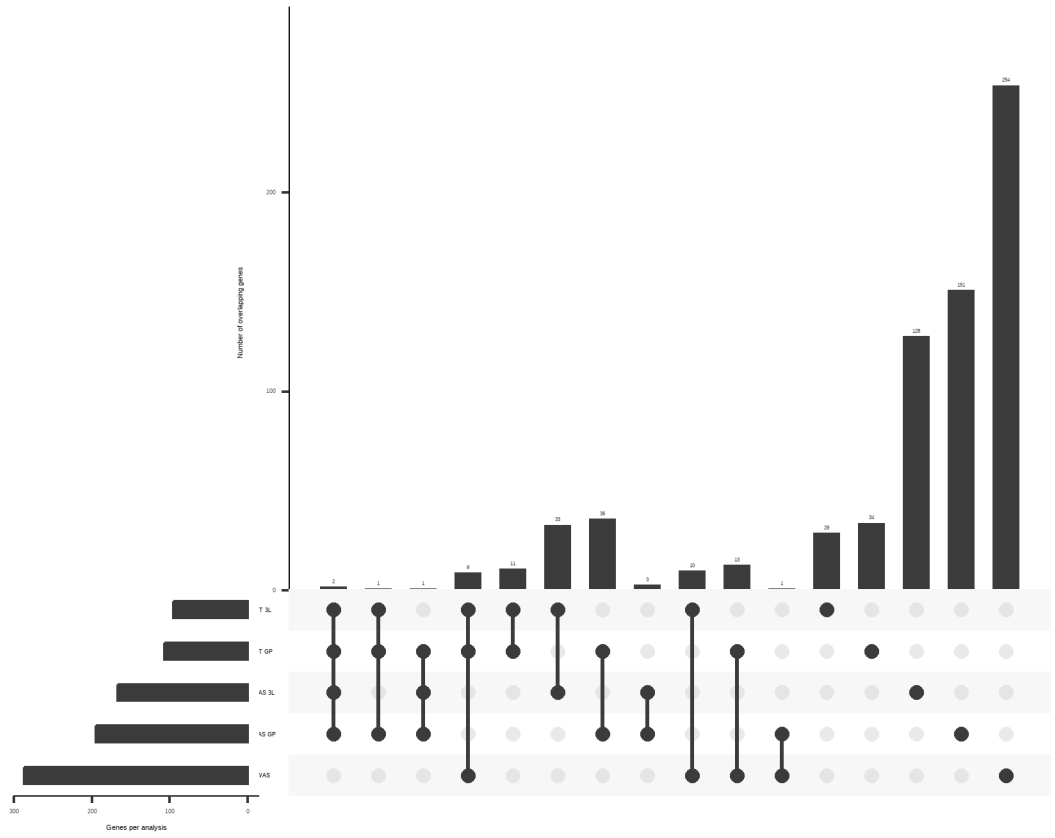

Figure 7.41: Upset plot for analyses associated with final dark NPQ value, 2017 model

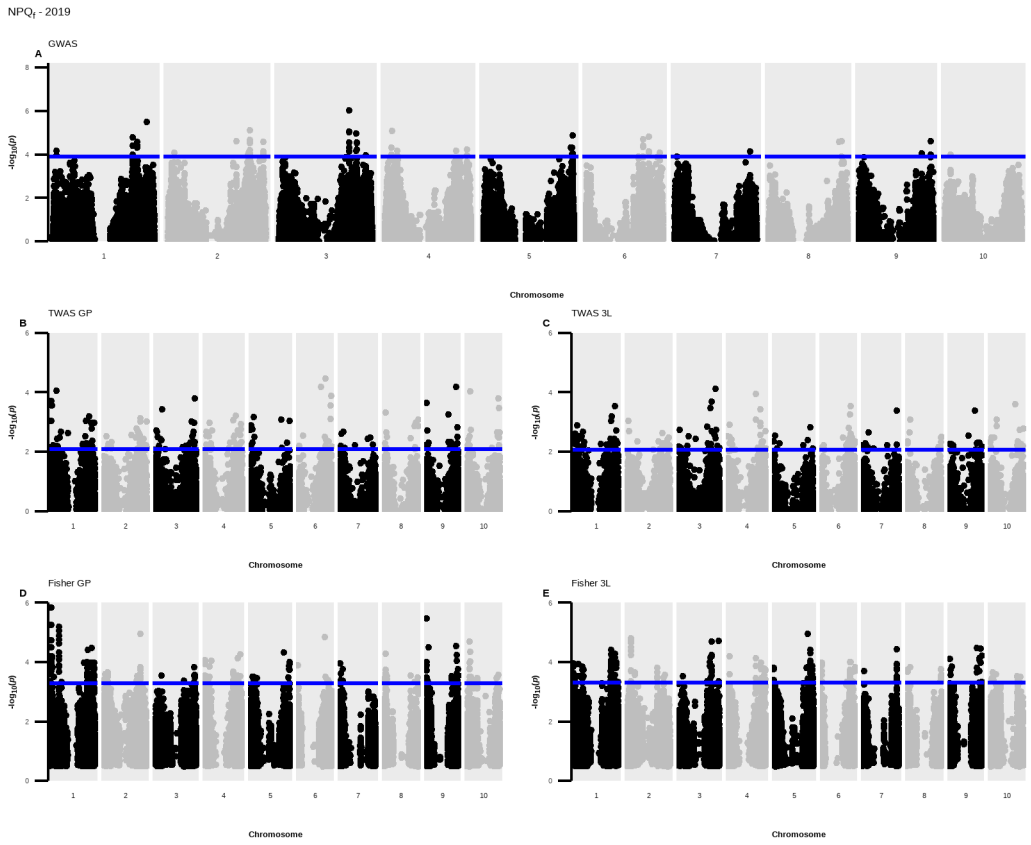

Figure 7.42: Chromosome mapping for SNPs and genes associated with final dark NPQ value, 2019 model

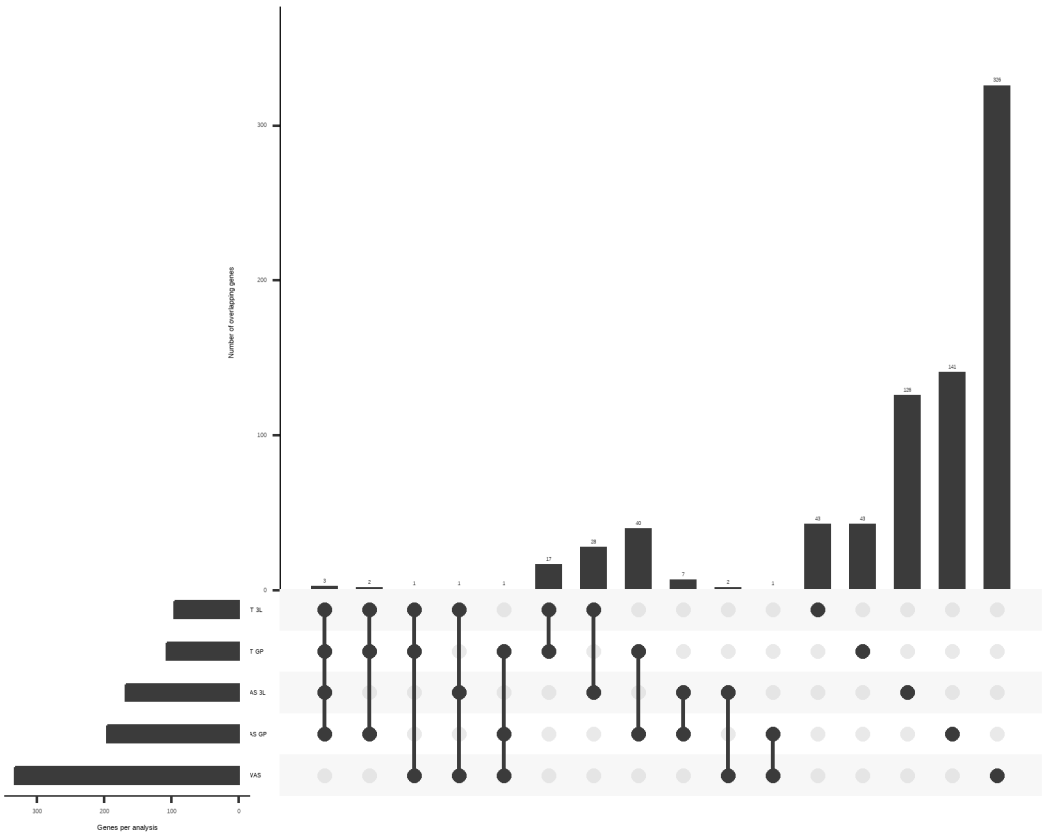

Figure 7.43: Upset plot for analyses associated with final dark NPQ value, 2019 model

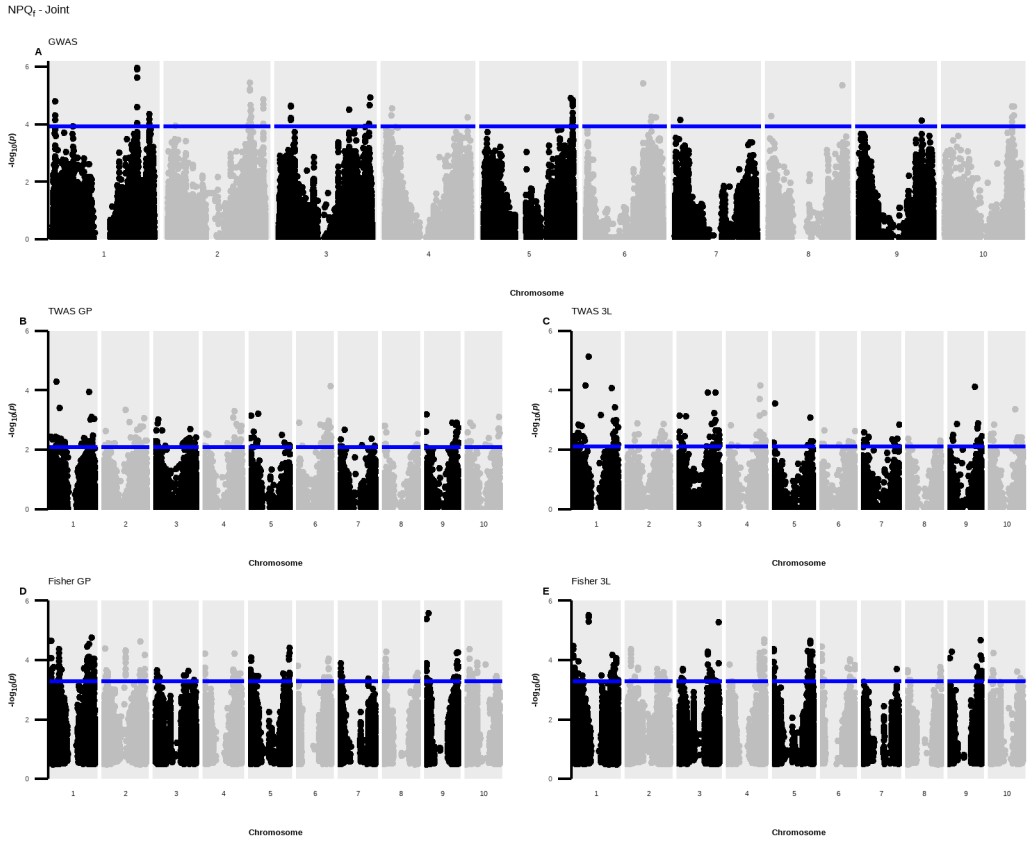

Figure 7.44: Chromosome mapping for SNPs and genes associated with final dark NPQ value, joint model

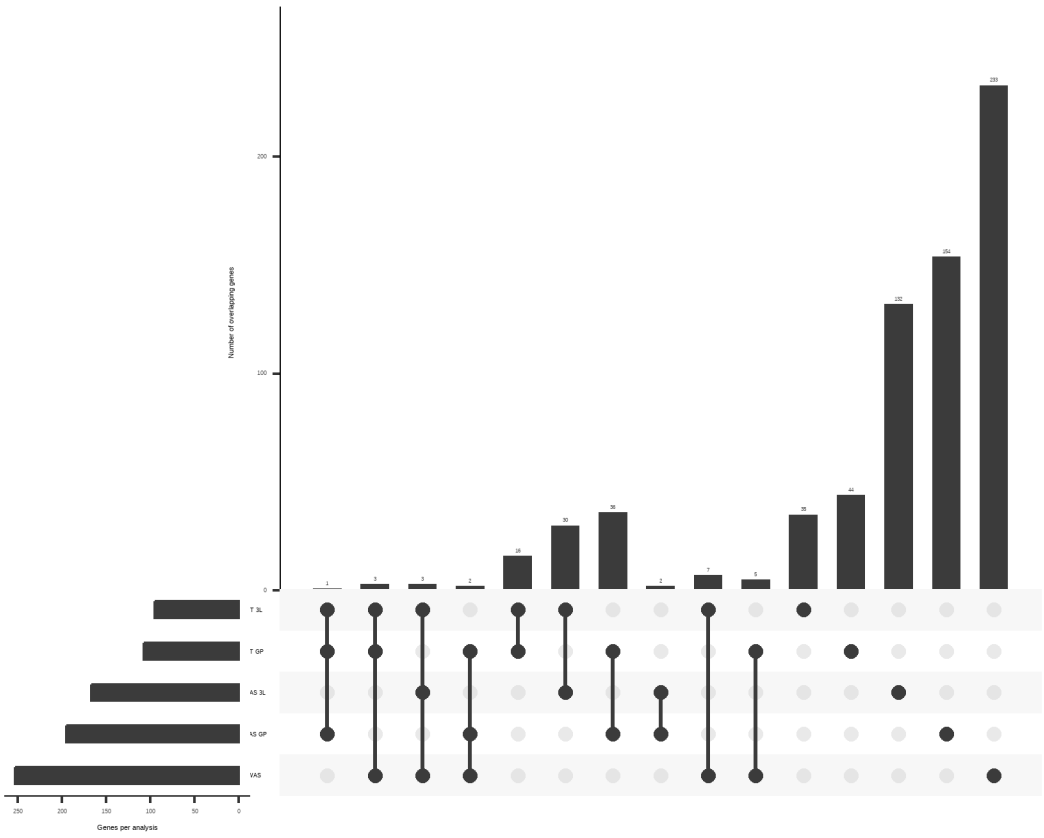

Figure 7.45: (ref:upjtnpq_endcap)

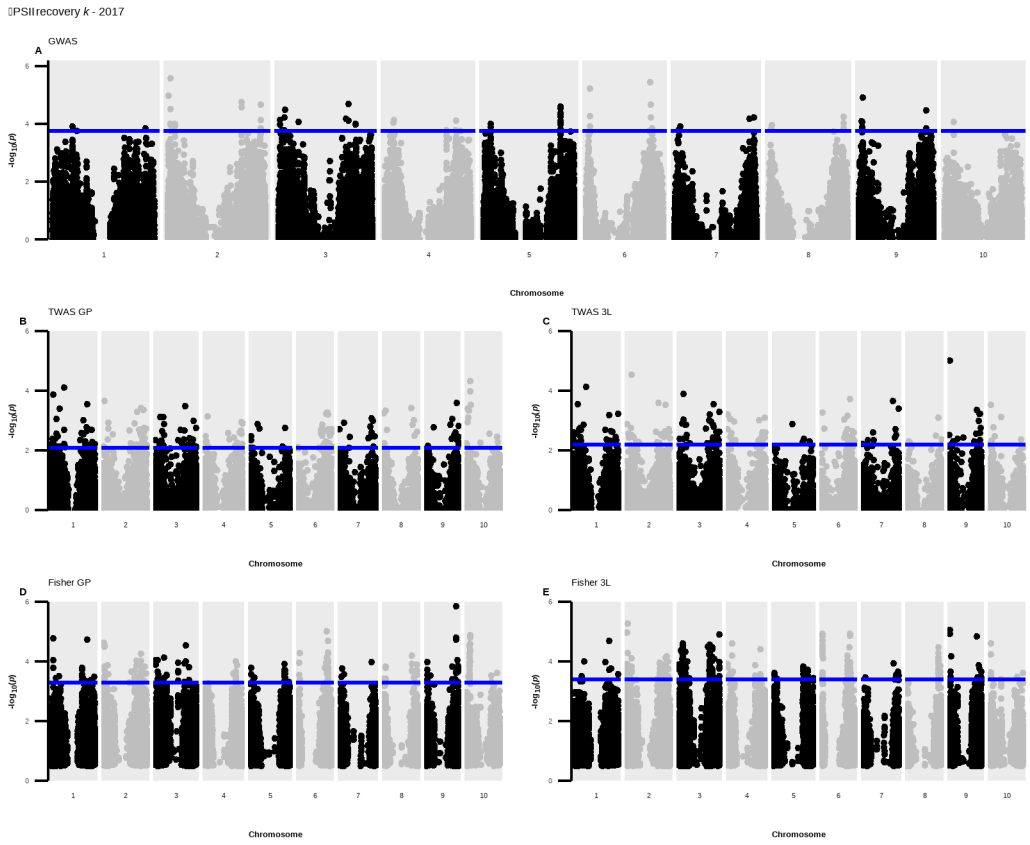

Figure 7.46: Chromosome mapping for SNPs and genes associated with ΦPSII recovery rate constant, 2017 model

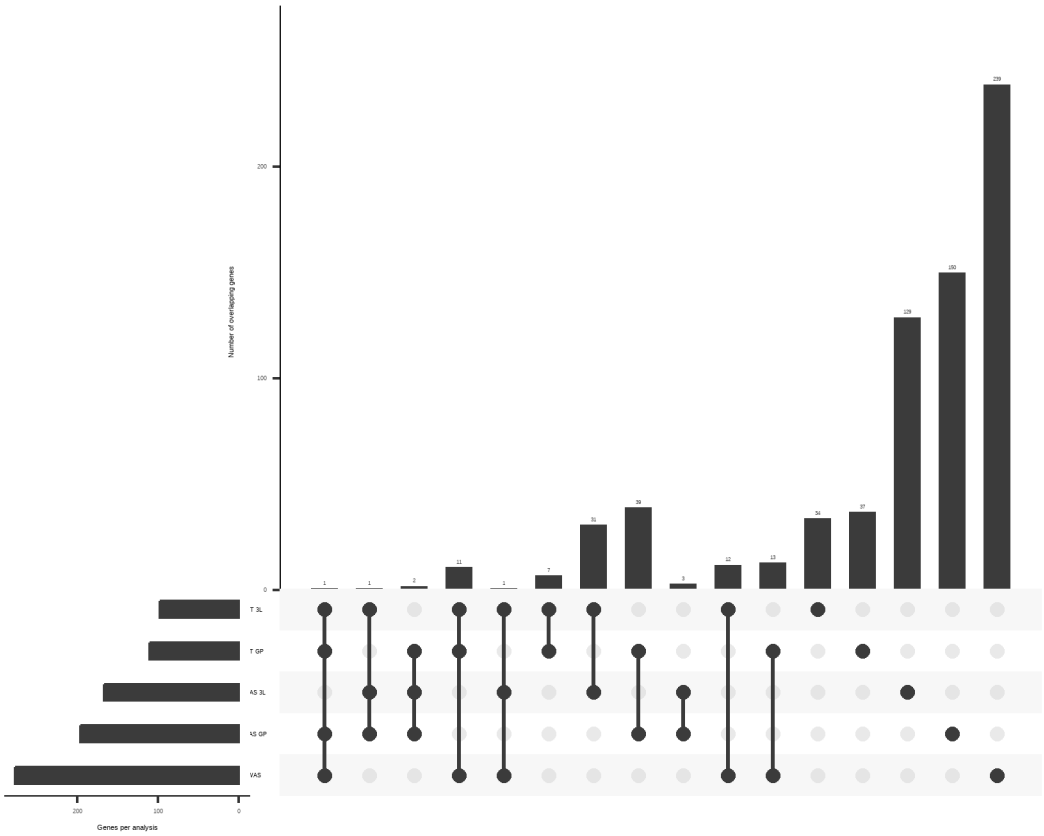

Figure 7.47: Upset plot for analyses associated with ΦPSII recovery rate constant, 2017 model

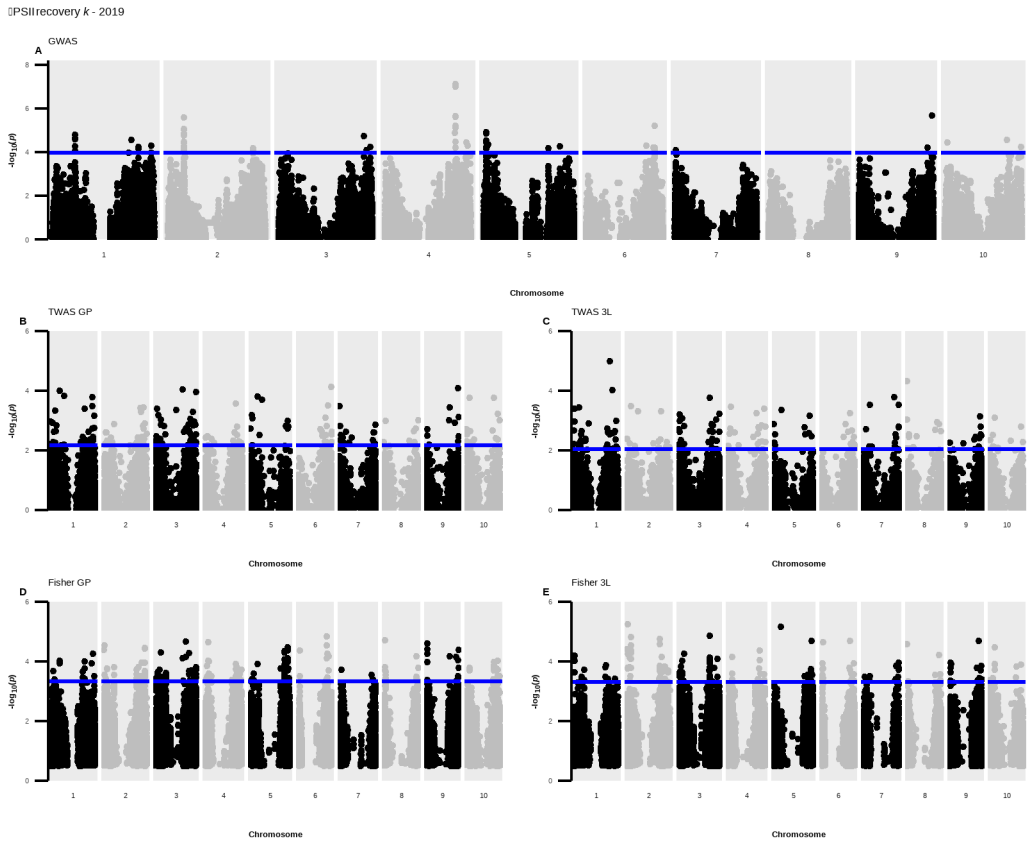

Figure 7.48: Chromosome mapping for SNPs and genes associated with ΦPSII recovery rate constant, 2019 model

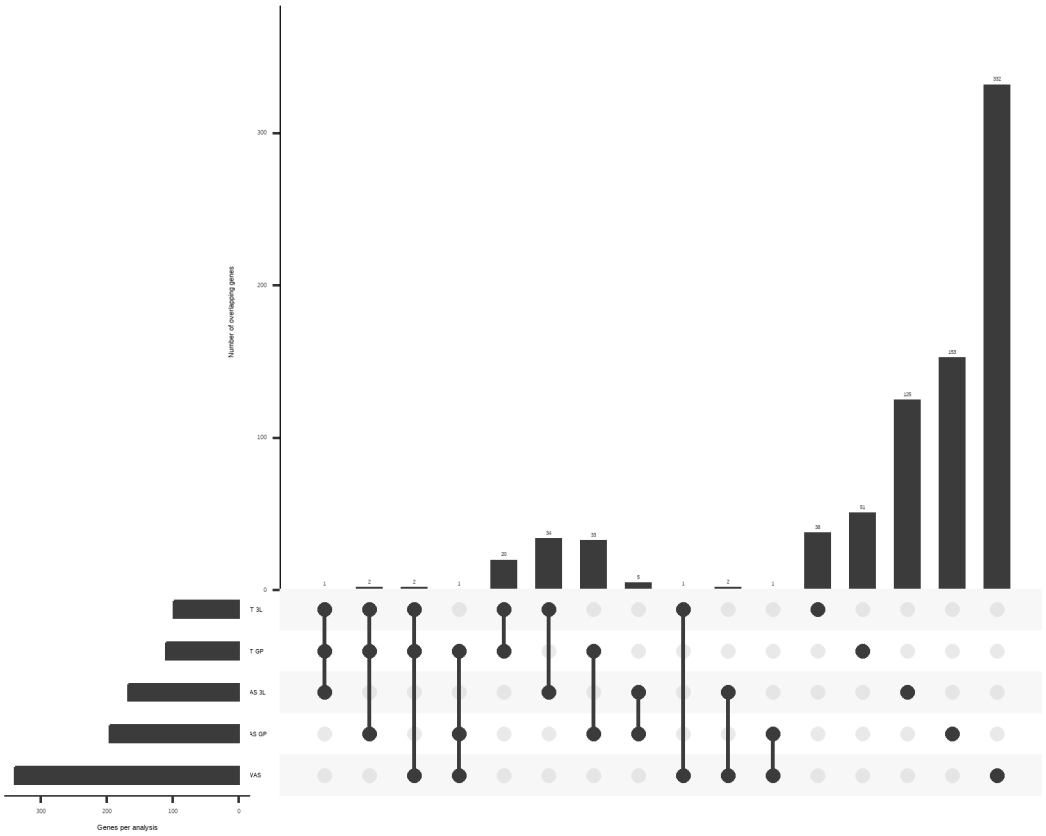

Figure 7.49: Upset plot for analyses associated with ΦPSII recovery rate constant, 2019 model

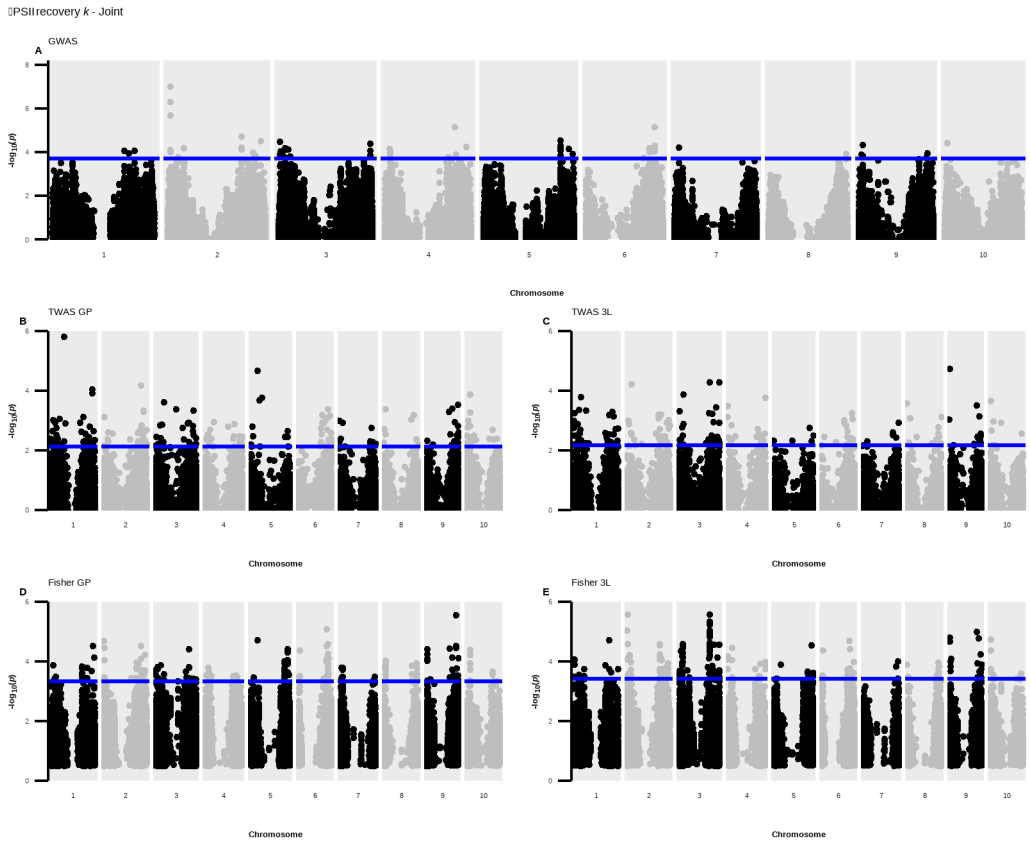

Figure 7.50: Chromosome mapping for SNPs and genes associated with ΦPSII recovery rate constant, joint model

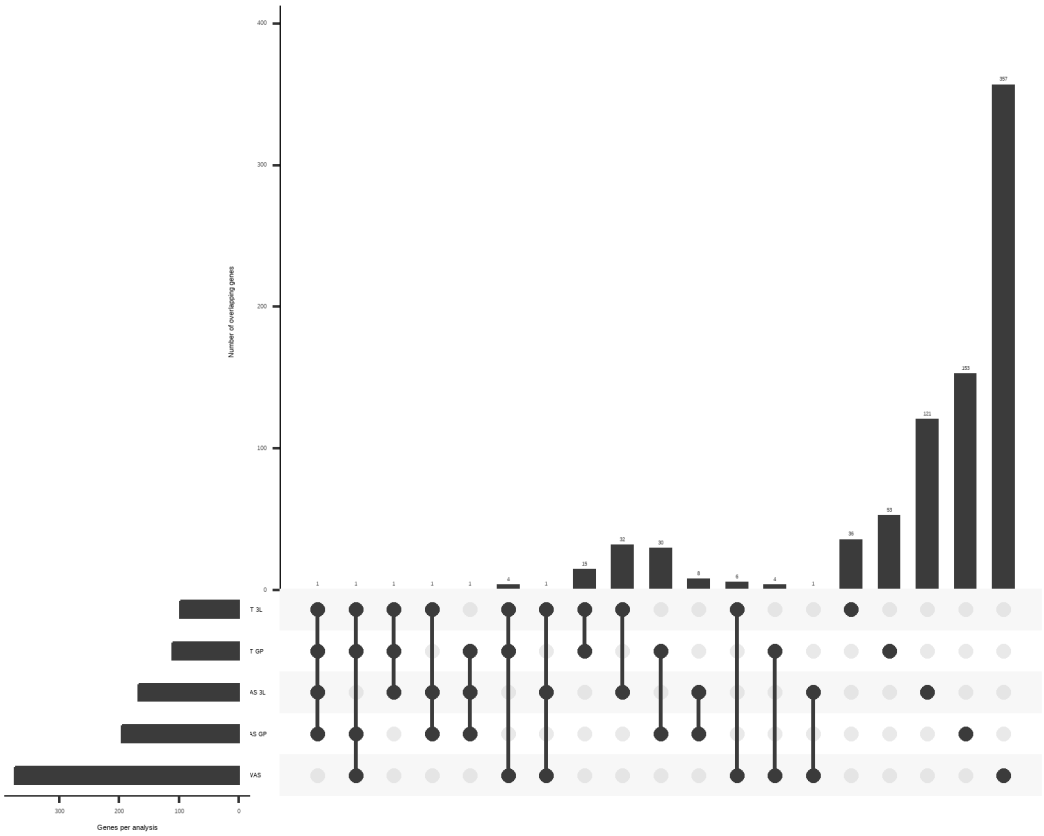

Figure 7.51: Upset plot for analyses associated with ΦPSII recovery rate constant, joint model

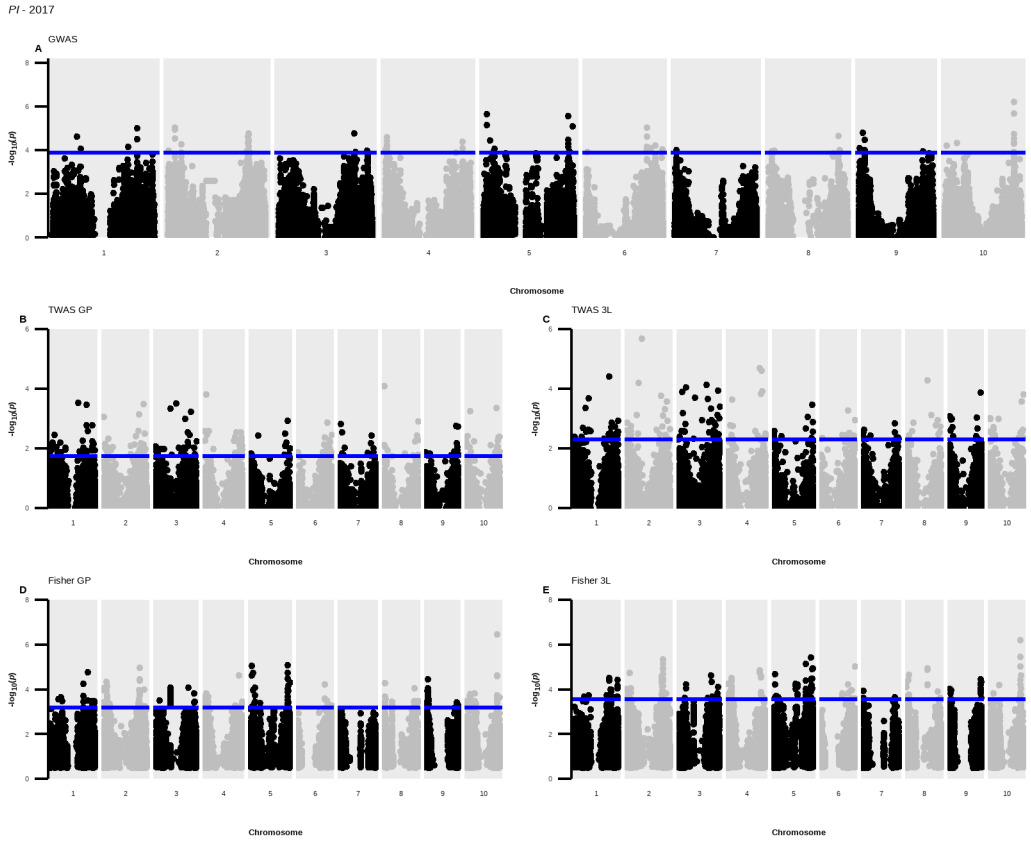

Figure 7.52: Chromosome mapping for SNPs and genes associated with photoprotection index, 2017 model

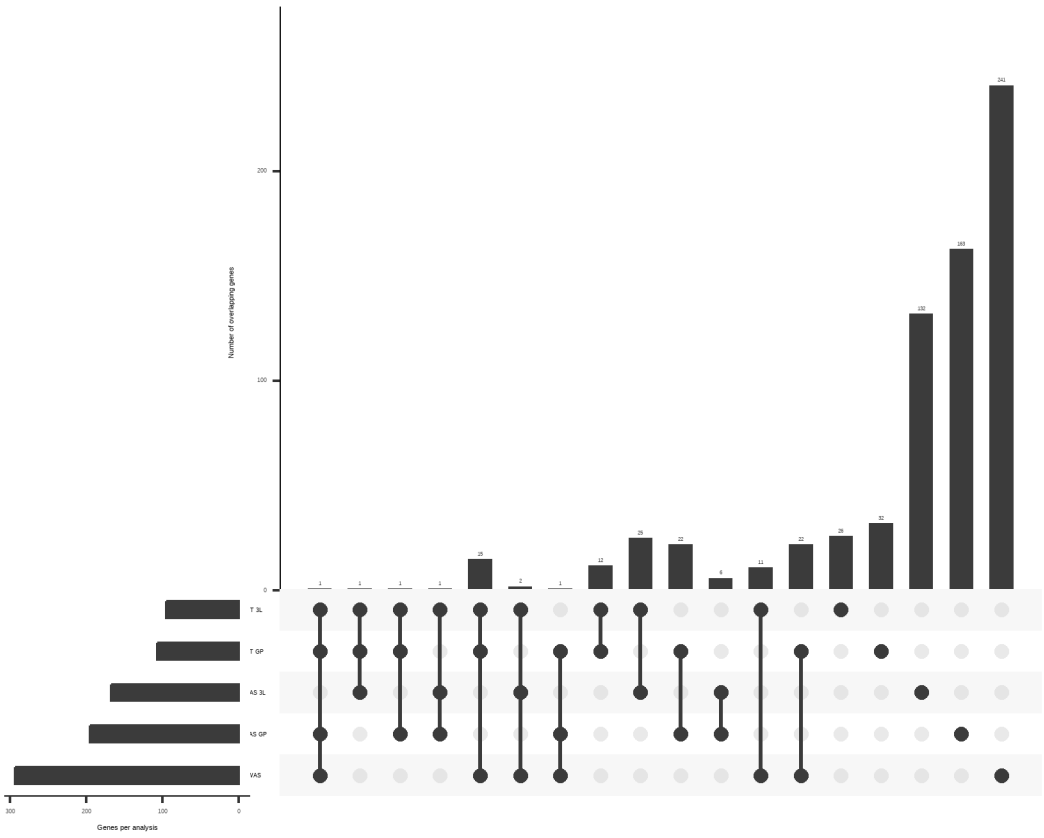

Figure 7.53: Upset plot for analyses associated with photoprotection index, 2017 model

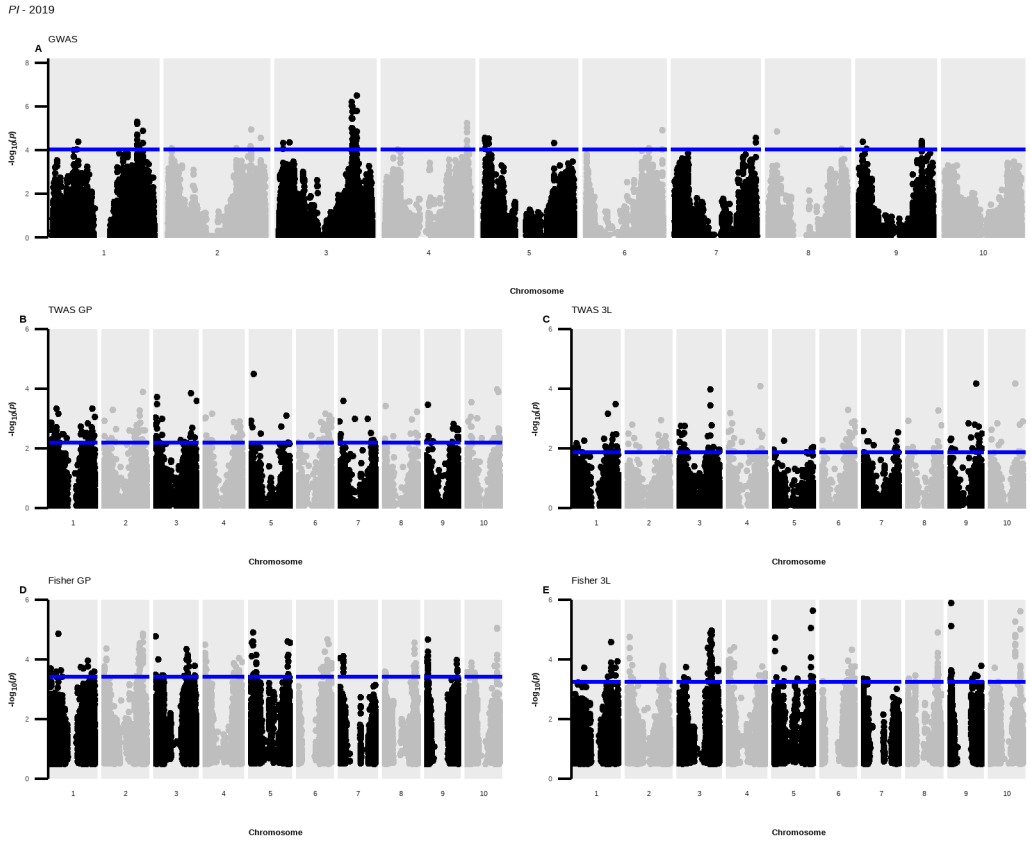

Figure 7.54: Chromosome mapping for SNPs and genes associated with photoprotection index, 2019 model

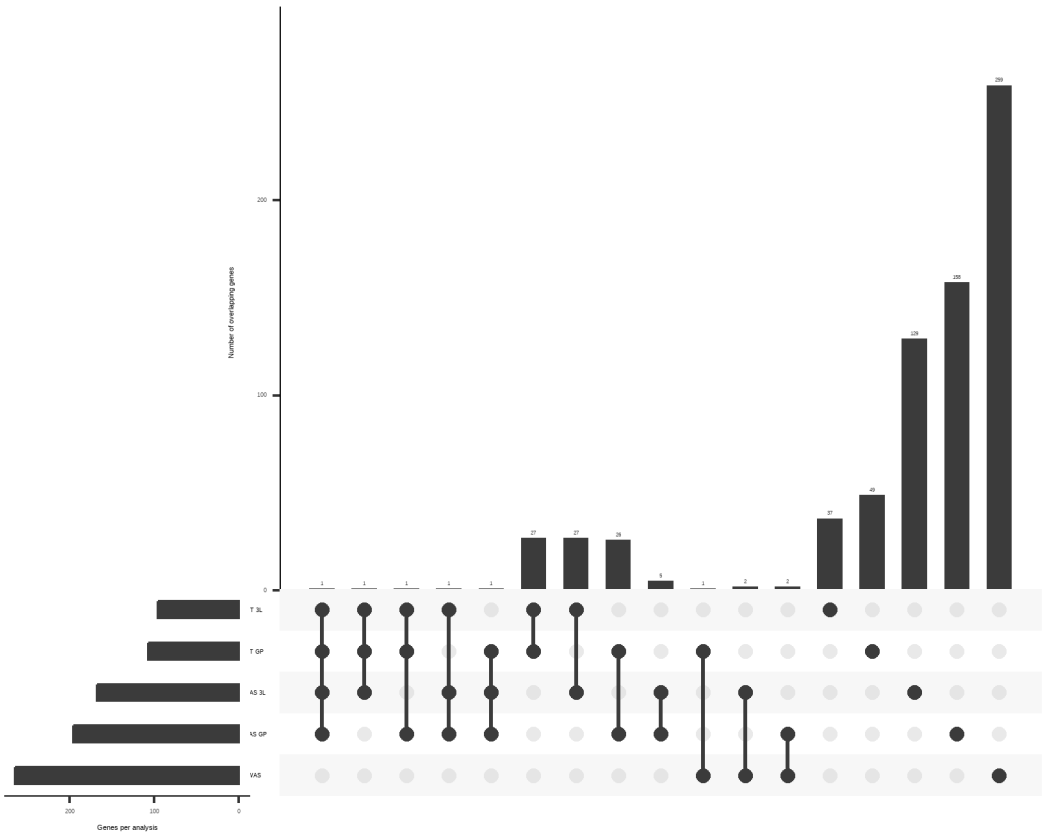

Figure 7.55: Upset plot for analyses associated with photoprotection index, 2019 model

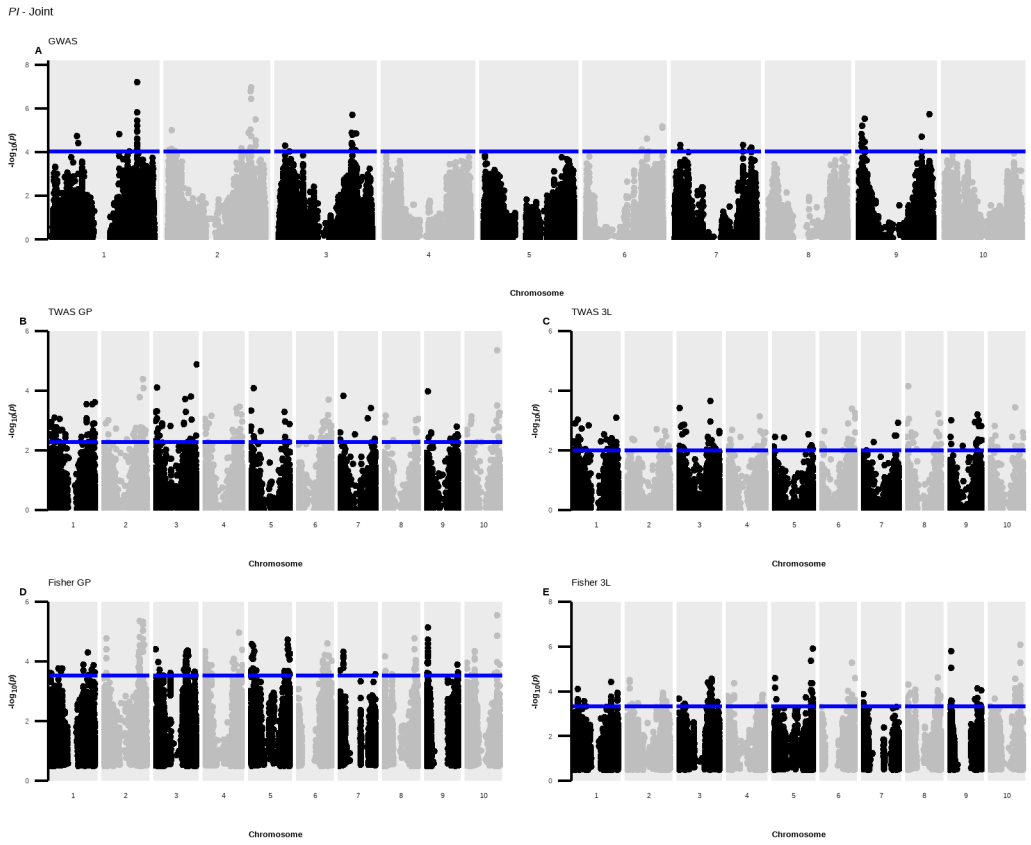

Figure 7.56: Chromosome mapping for SNPs and genes associated with photoprotection index, joint model

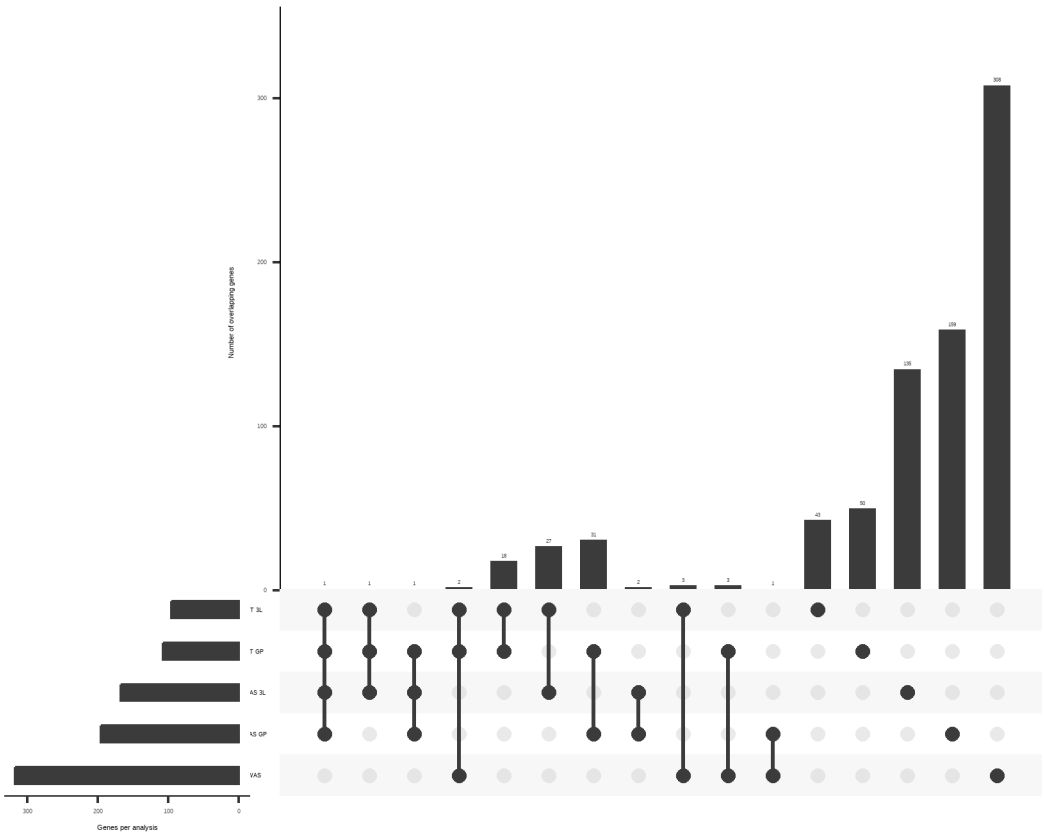

Figure 7.57: Upset plot for analyses associated with photoprotection index, joint model

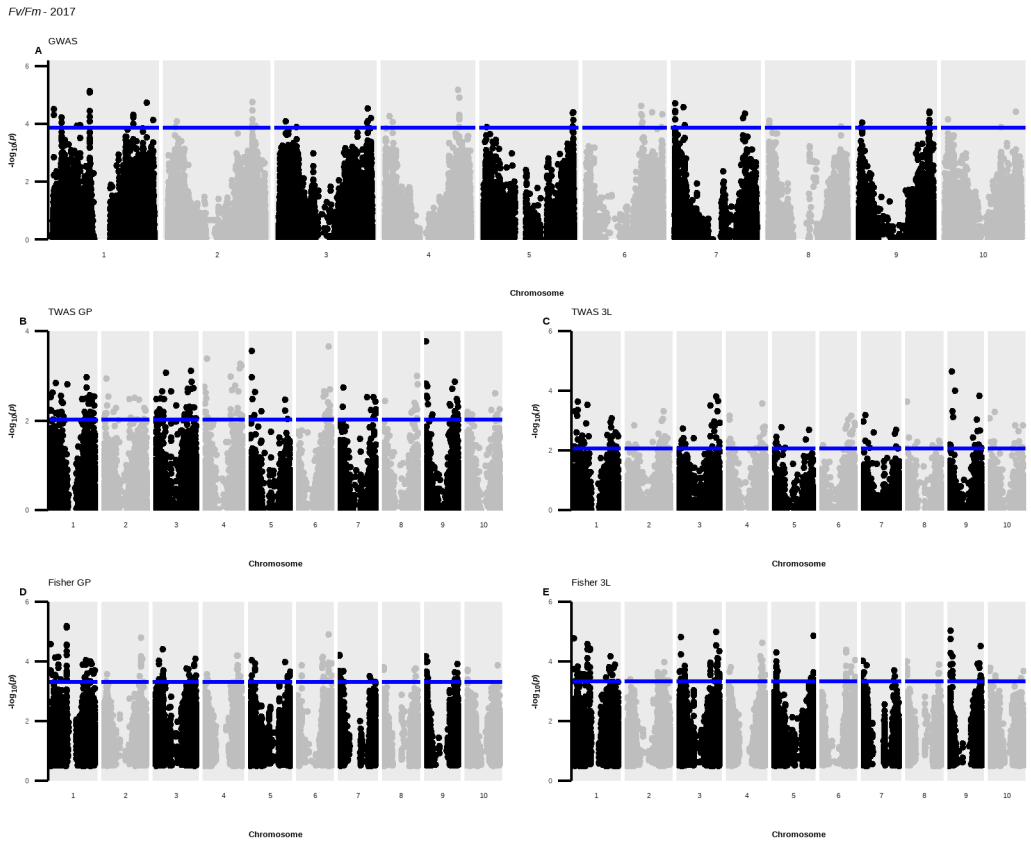

Figure 7.58: Chromosome mapping for SNPs and genes associated with Fv/Fm, 2017 model

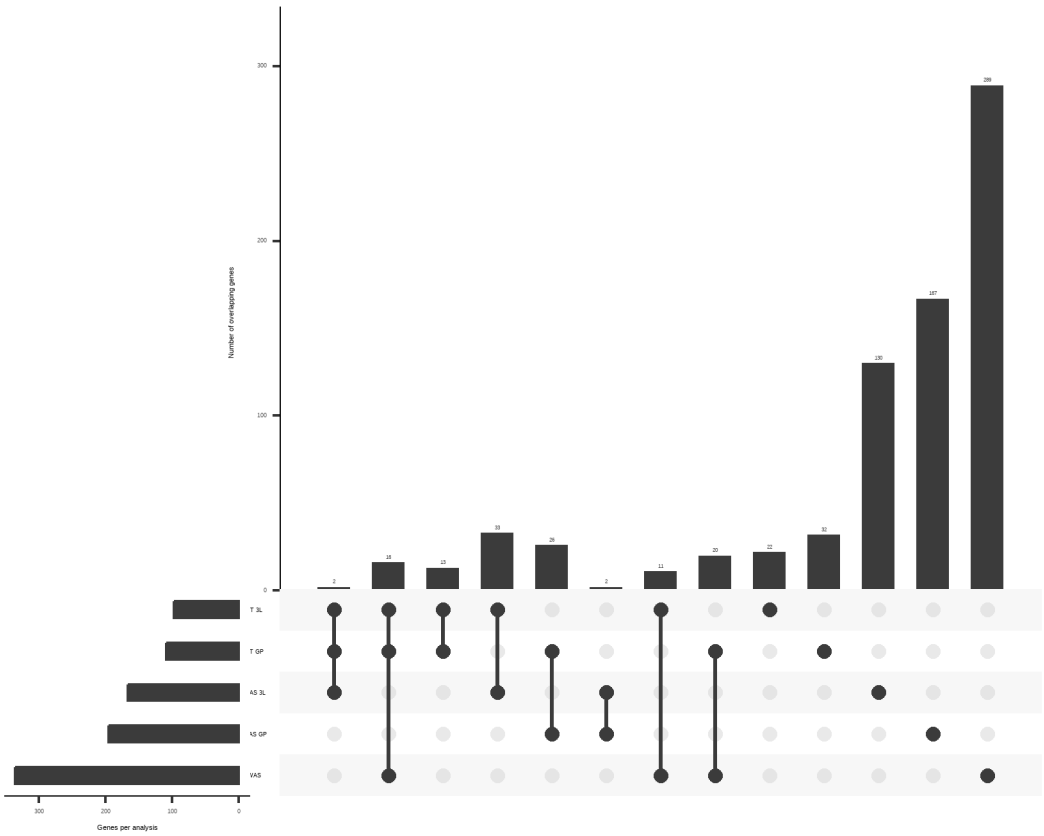

Figure 7.59: Upset plot for analyses associated with Fv/Fm, 2017 model

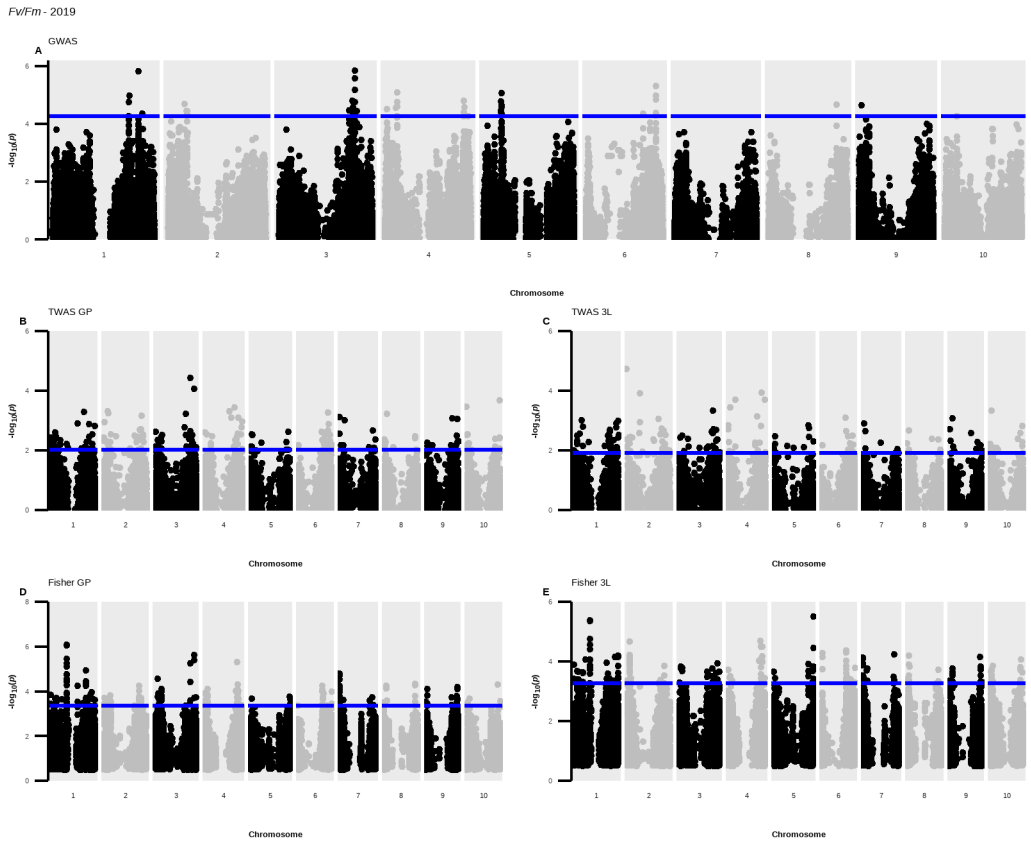

Figure 7.60: Chromosome mapping for SNPs and genes associated with Fv/Fm, 2019 model

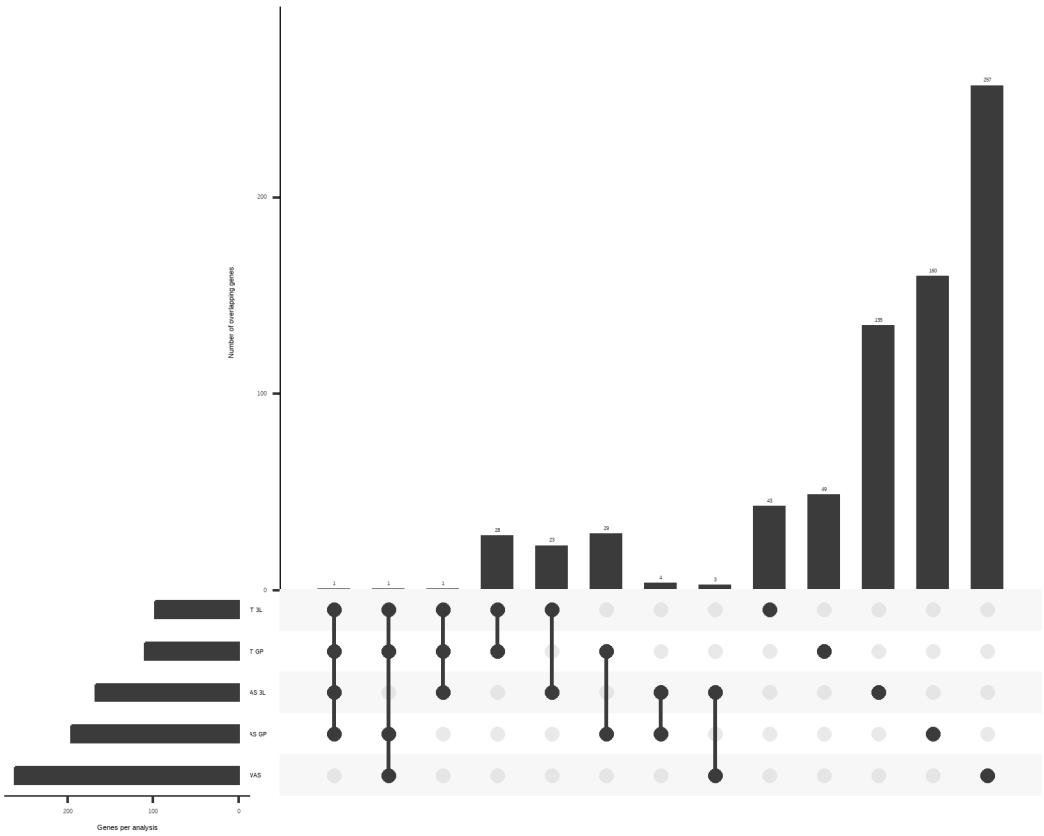

Figure 7.61: Upset plot for analyses associated with Fv/Fm, 2019 model

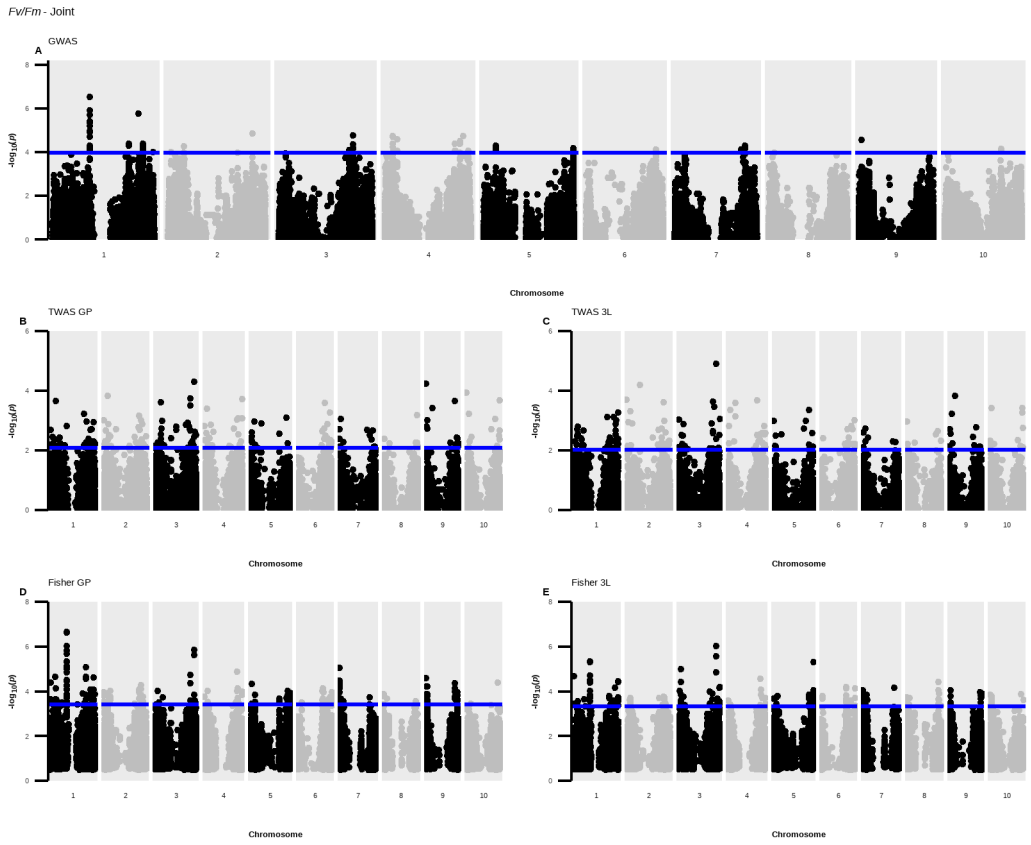

Figure 7.62: Chromosome mapping for SNPs and genes associated with Fv/Fm, joint model

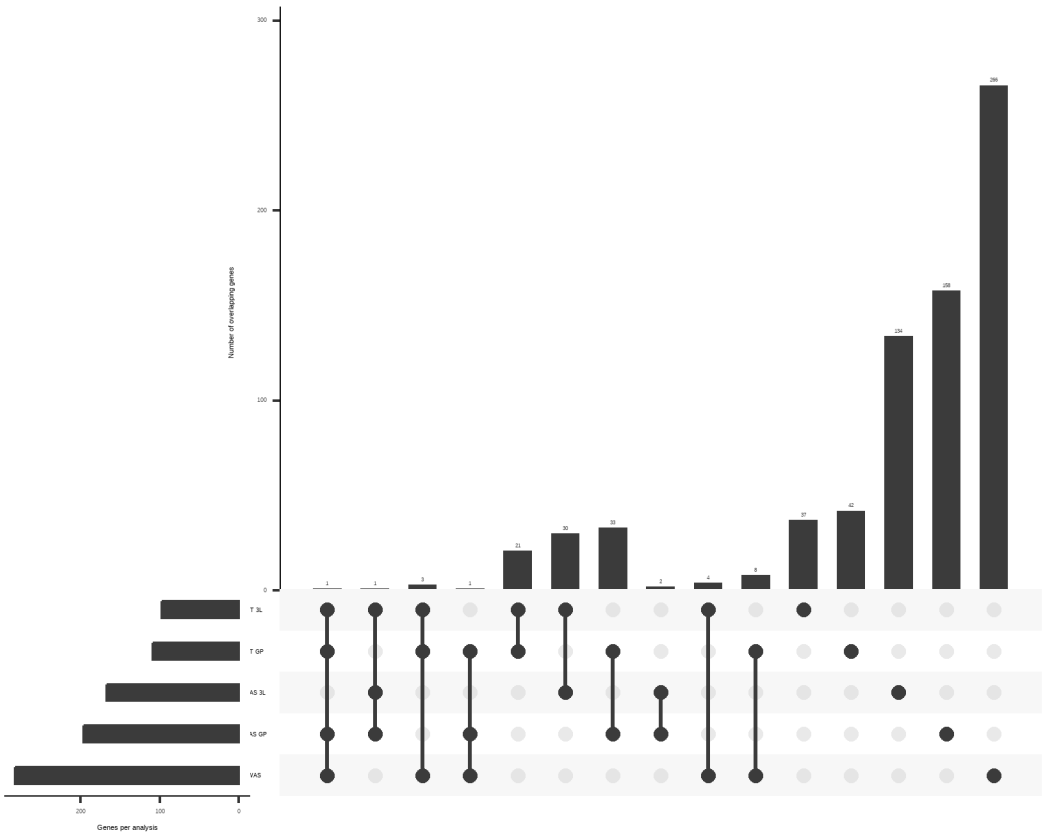

Figure 7.63: Upset plot for analyses associated with Fv/Fm, joint model

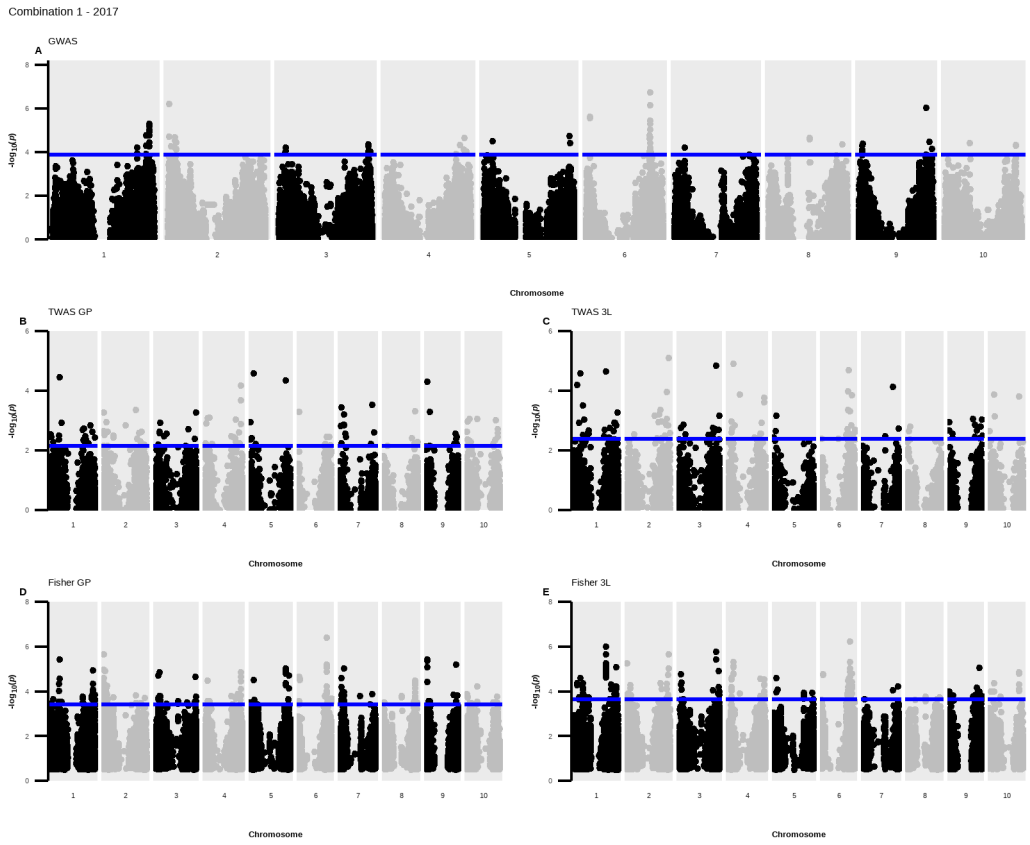

Figure 7.64: Chromosome mapping for SNPs and genes associated with combination trait 1, 2017 model

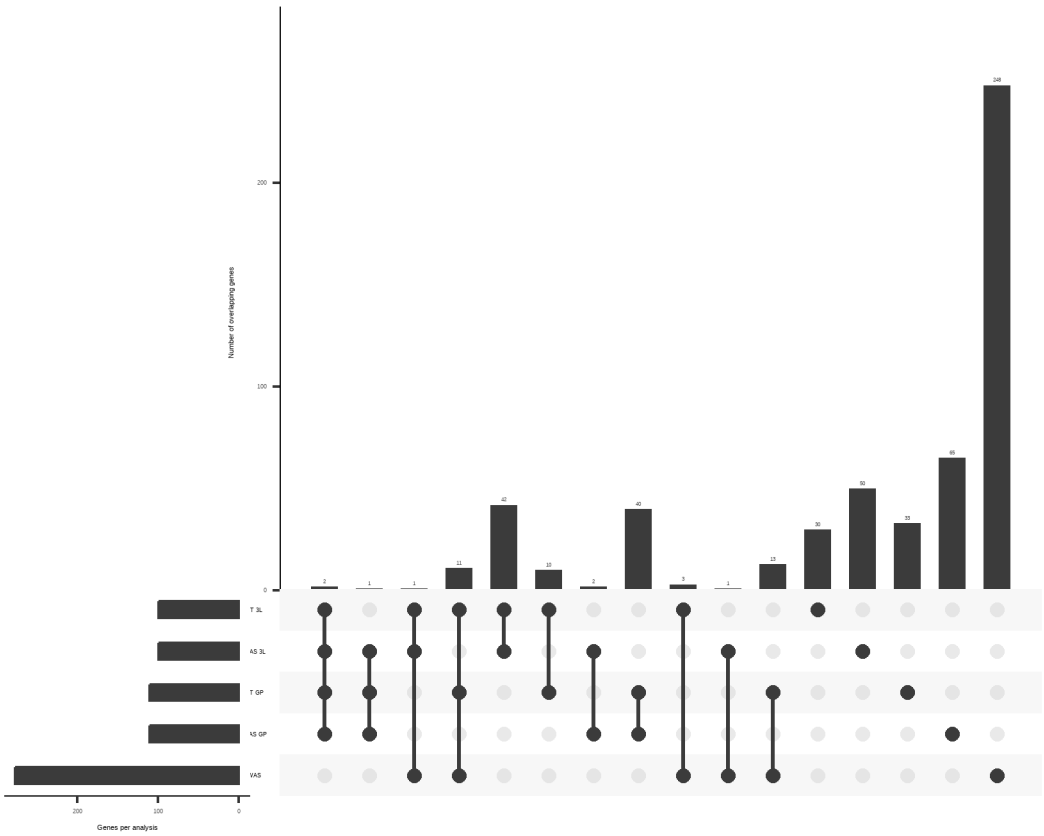

Figure 7.65: Upset plot for analyses associated with combination trait 1, 2017 model

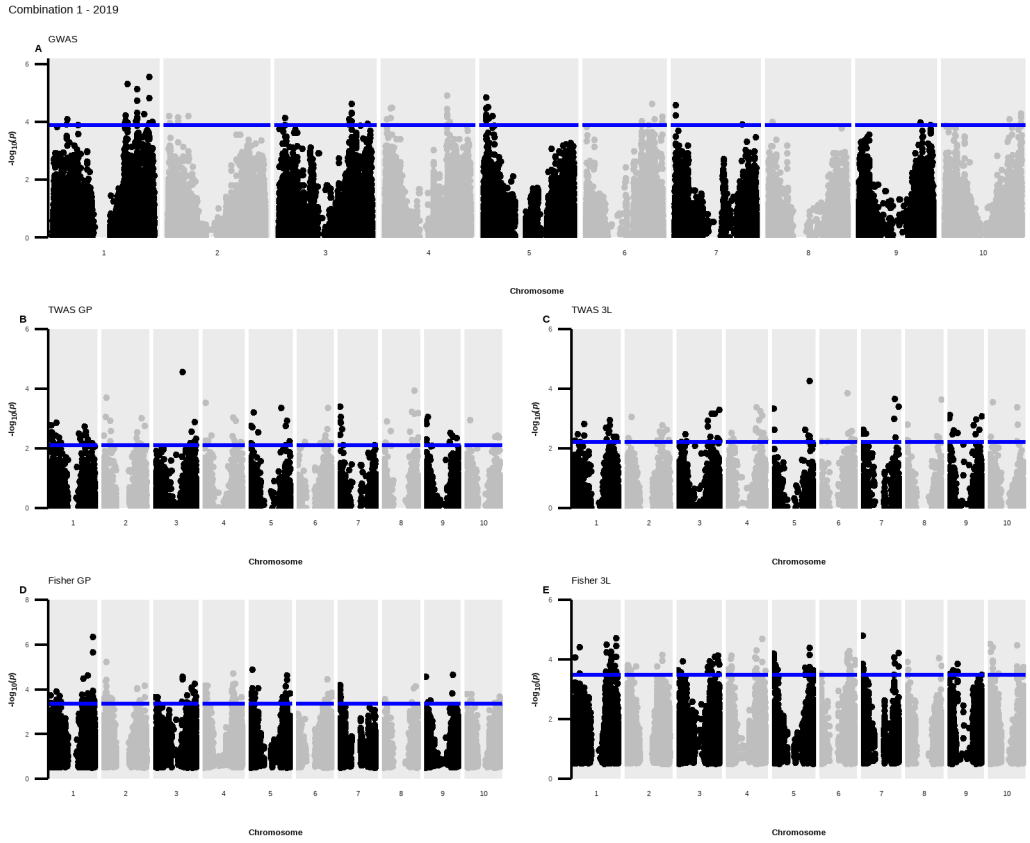

Figure 7.66: Chromosome mapping for SNPs and genes associated with combination trait 1, 2019 model

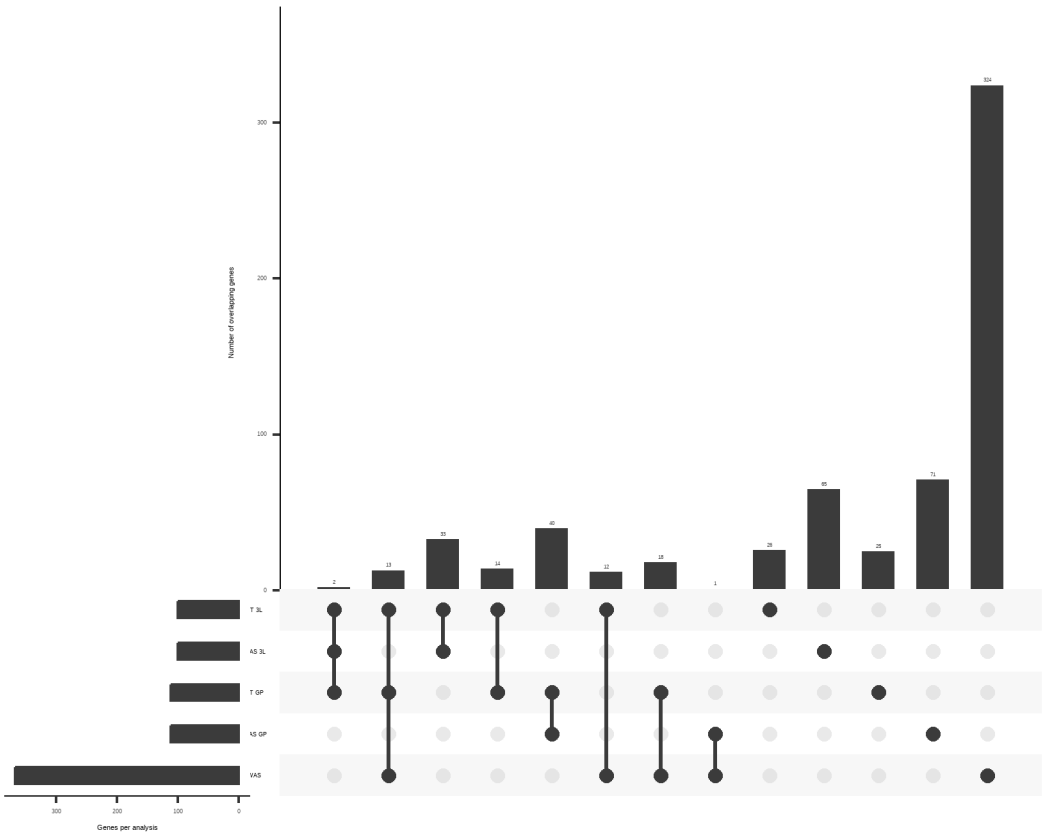

Figure 7.67: Upset plot for analyses associated with combination trait 1, 2019 model

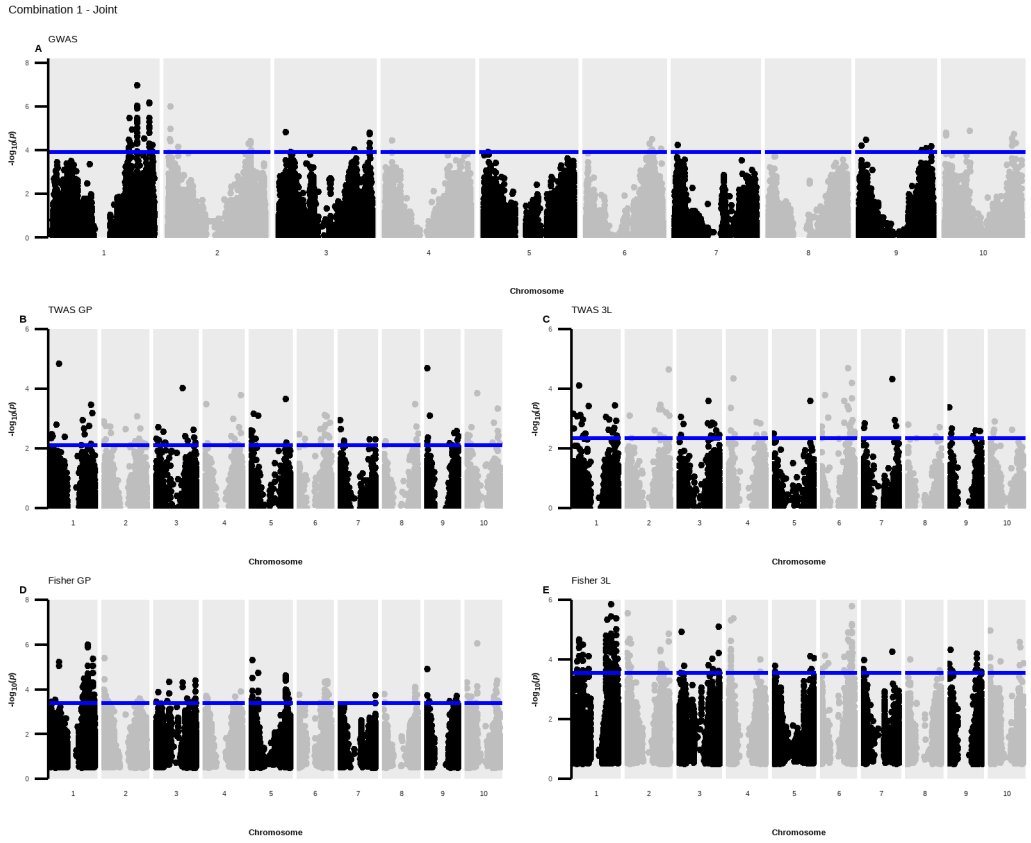

Figure 7.68: Chromosome mapping for SNPs and genes associated with combination trait 1, joint model

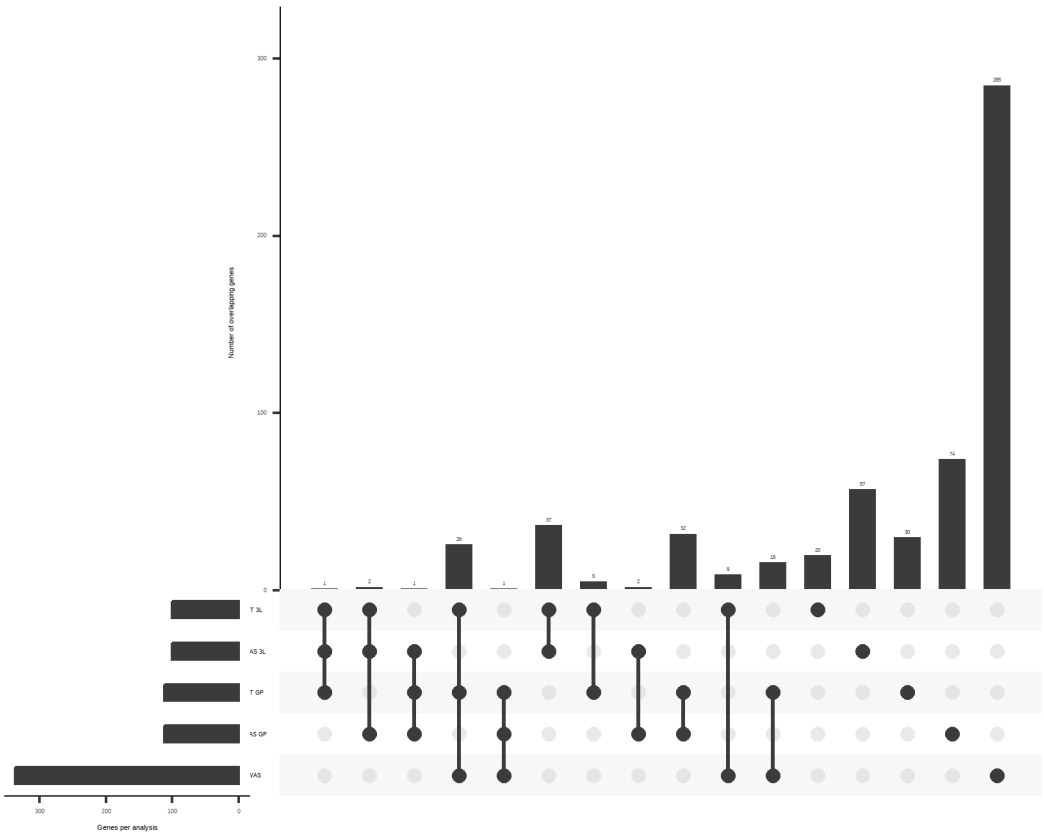

Figure 7.69: Upset plot for analyses associated with combination trait 1, joint model

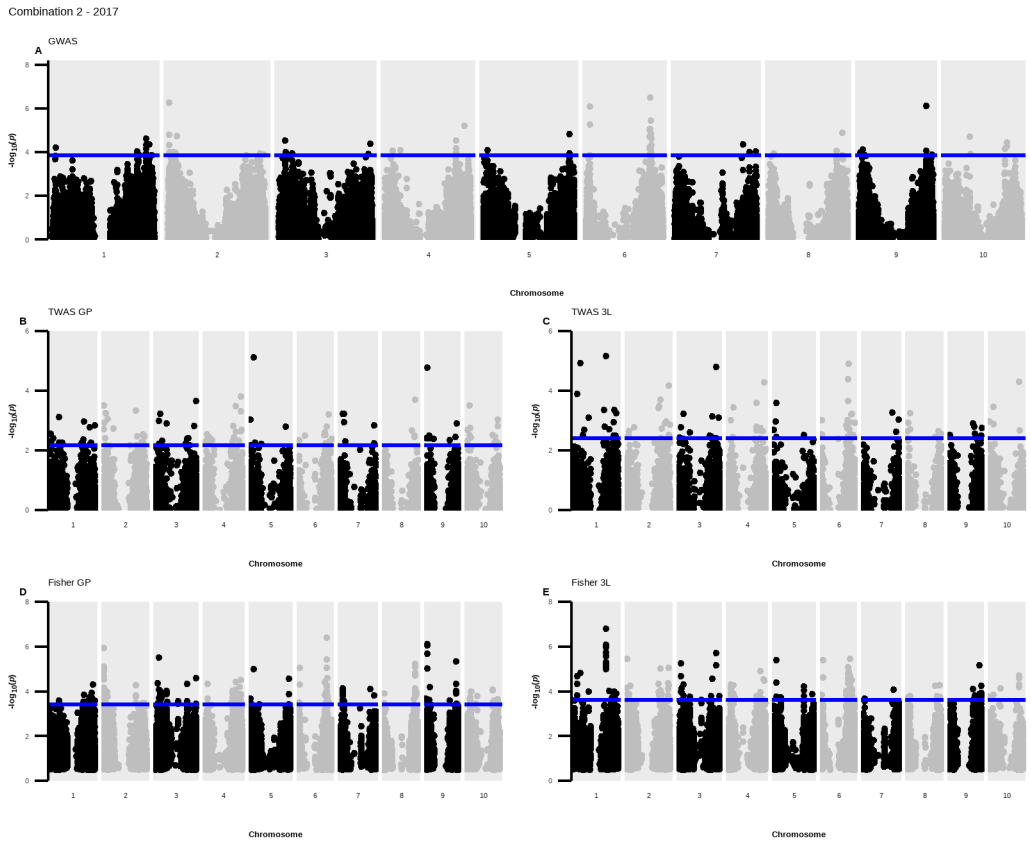

Figure 7.70: Chromosome mapping for SNPs and genes associated with combination trait 2, 2017 model

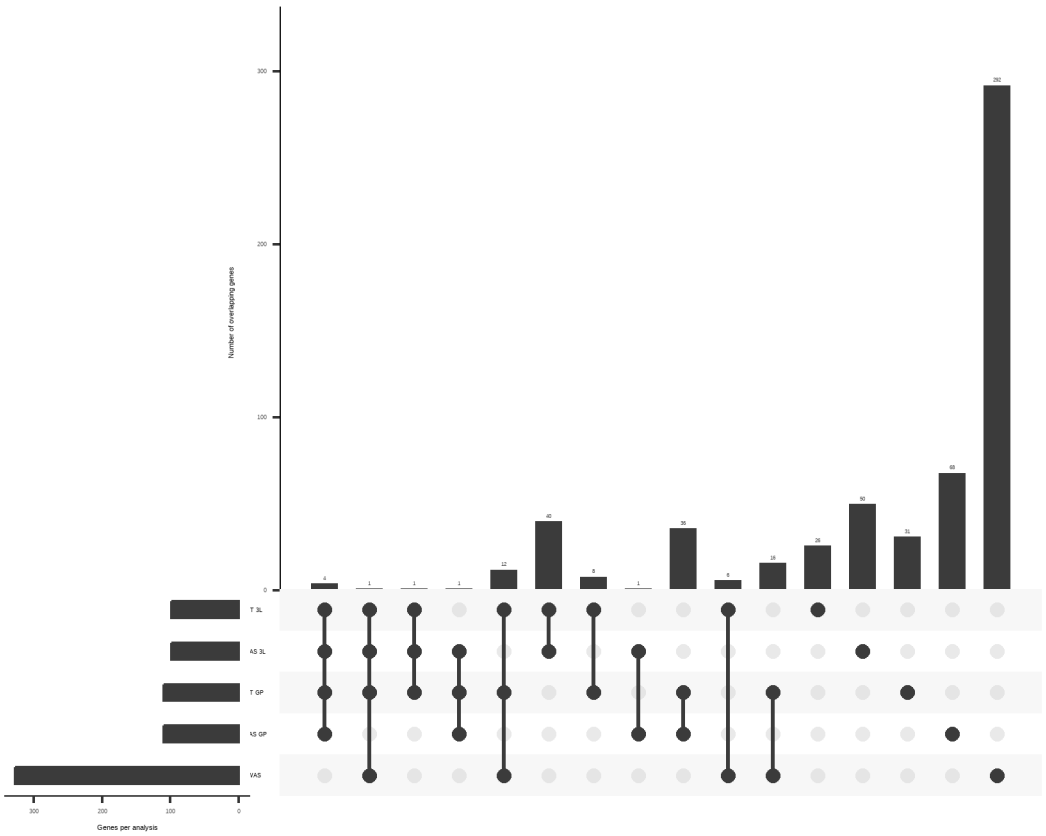

Figure 7.71: Upset plot for analyses associated with combination trait 2, 2017 model

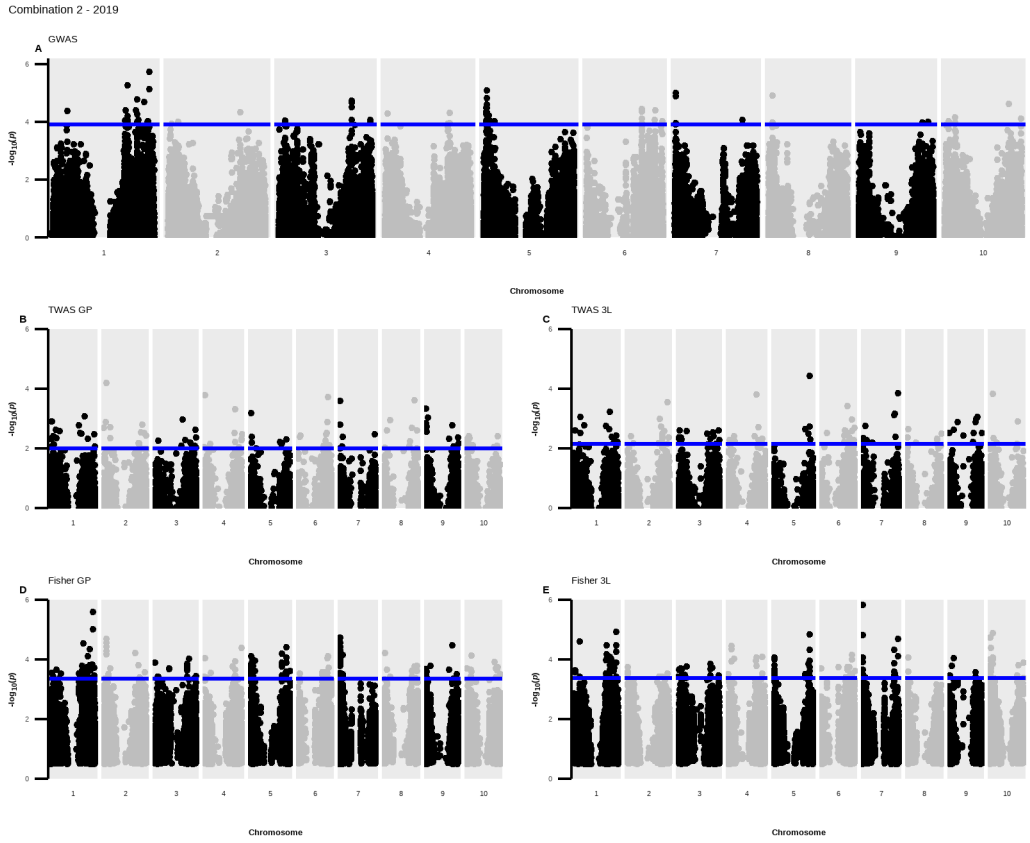

Figure 7.72: Chromosome mapping for SNPs and genes associated with combination trait 2, 2019 model

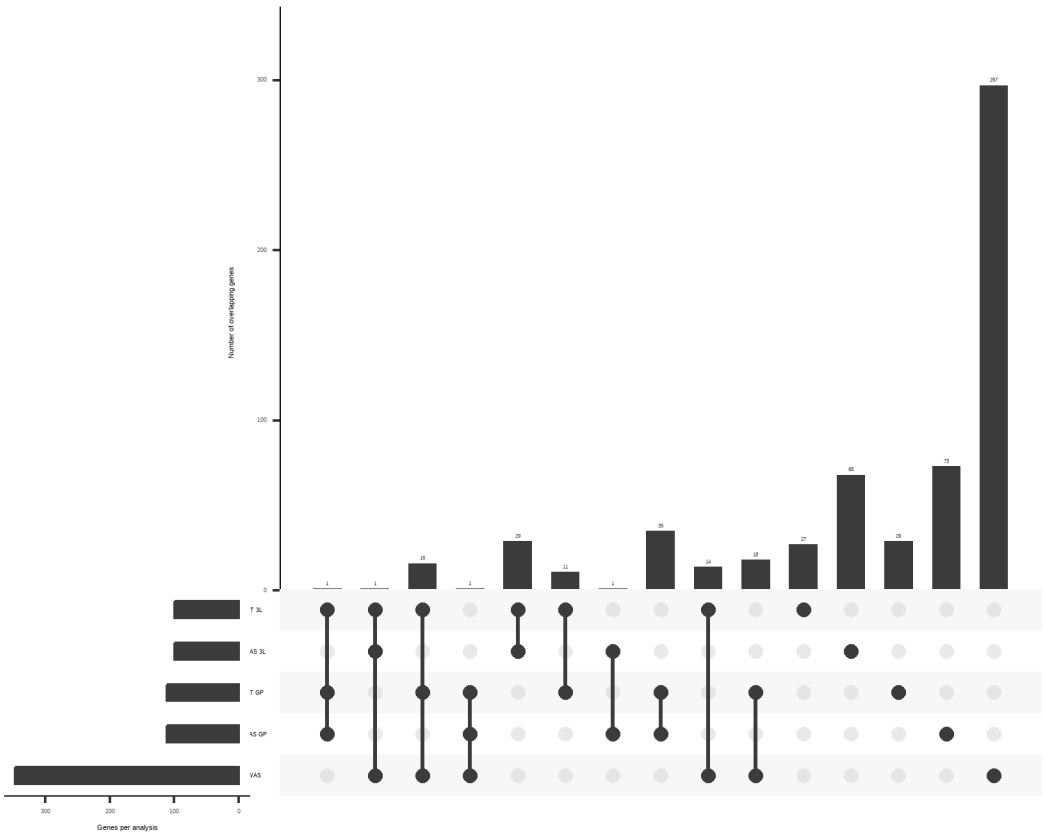

Figure 7.73: Upset plot for analyses associated with combination trait 2, 2019 model

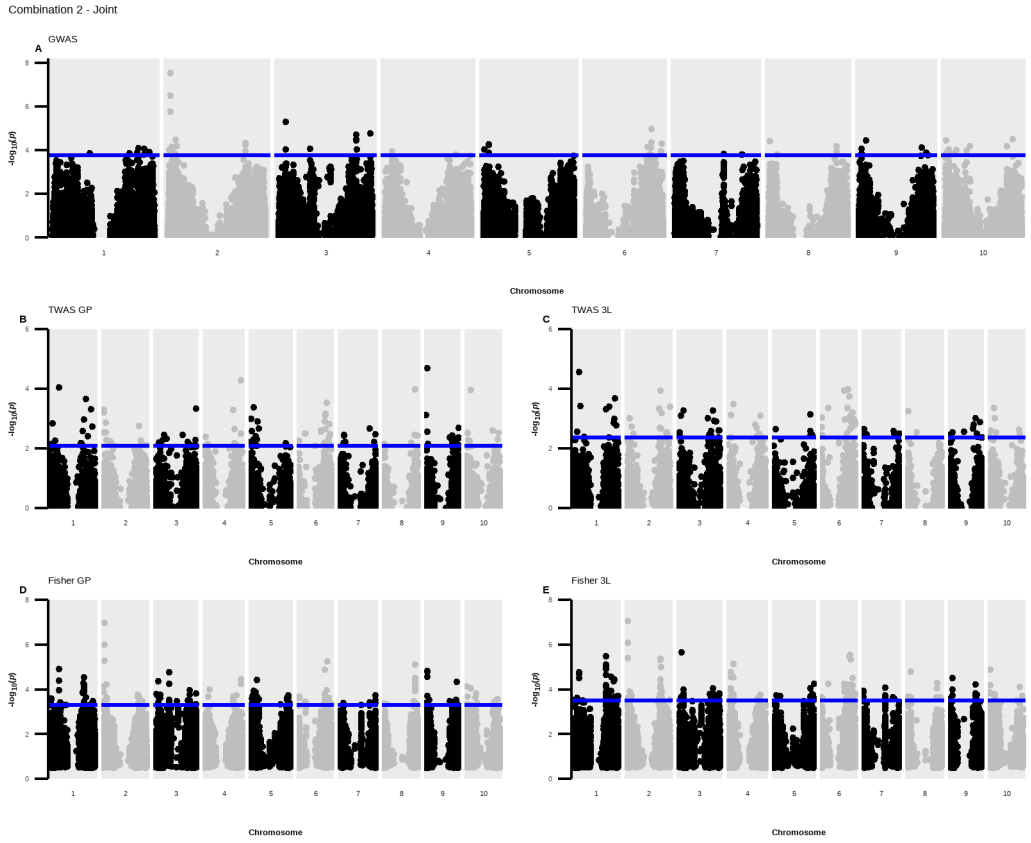

Figure 7.74: Chromosome mapping for SNPs and genes associated with combination trait 2, joint model

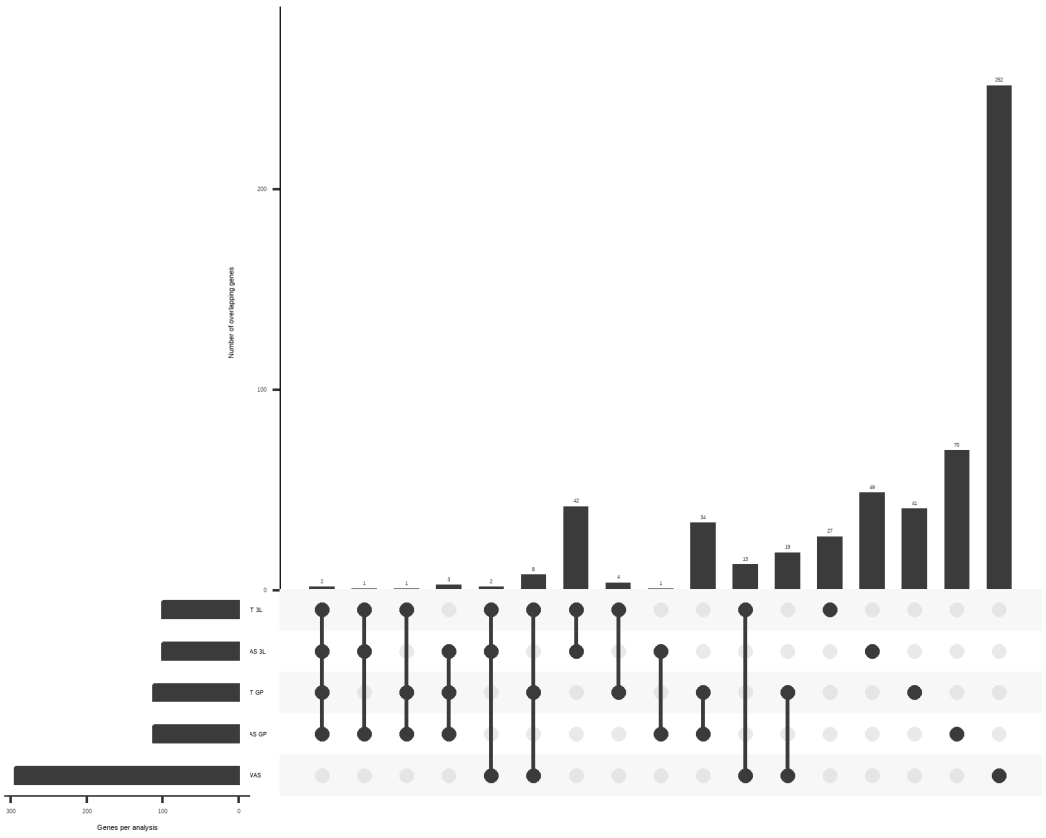

Figure 7.75: Upset plot for analyses associated with combination trait 2, joint model

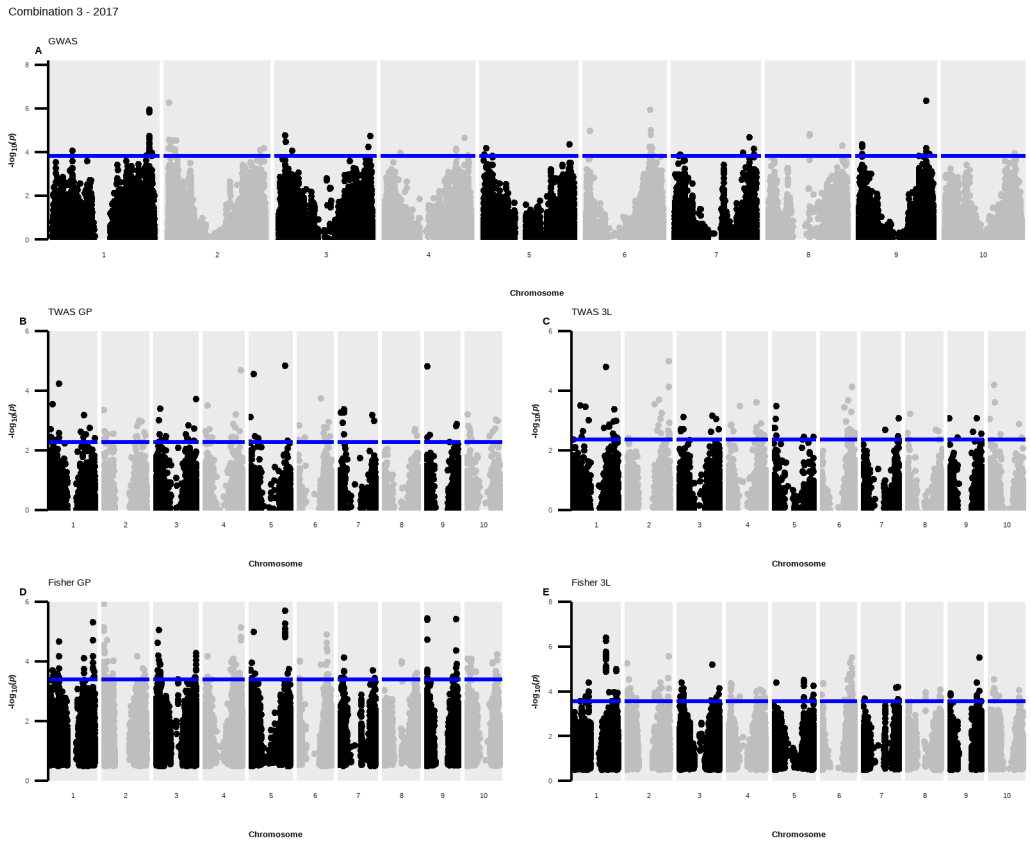

Figure 7.76: Chromosome mapping for SNPs and genes associated with combination trait 3, 2017 model

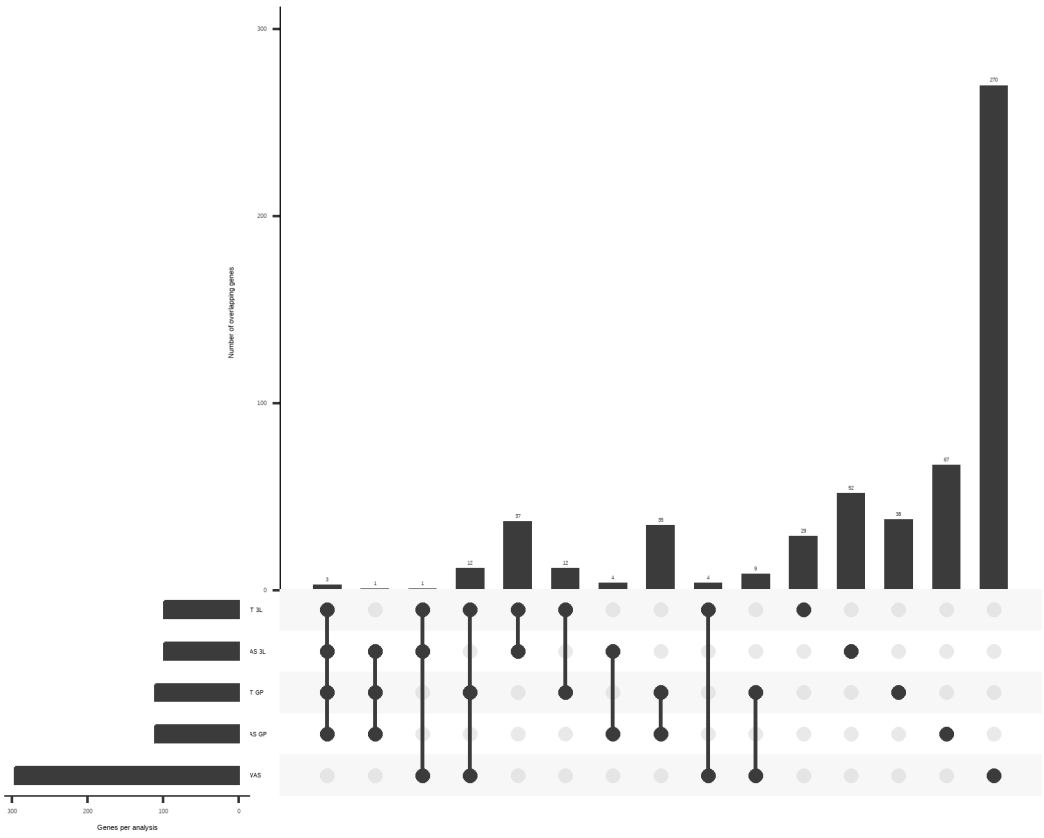

Figure 7.77: Upset plot for analyses associated with combination trait 3, 2017 model

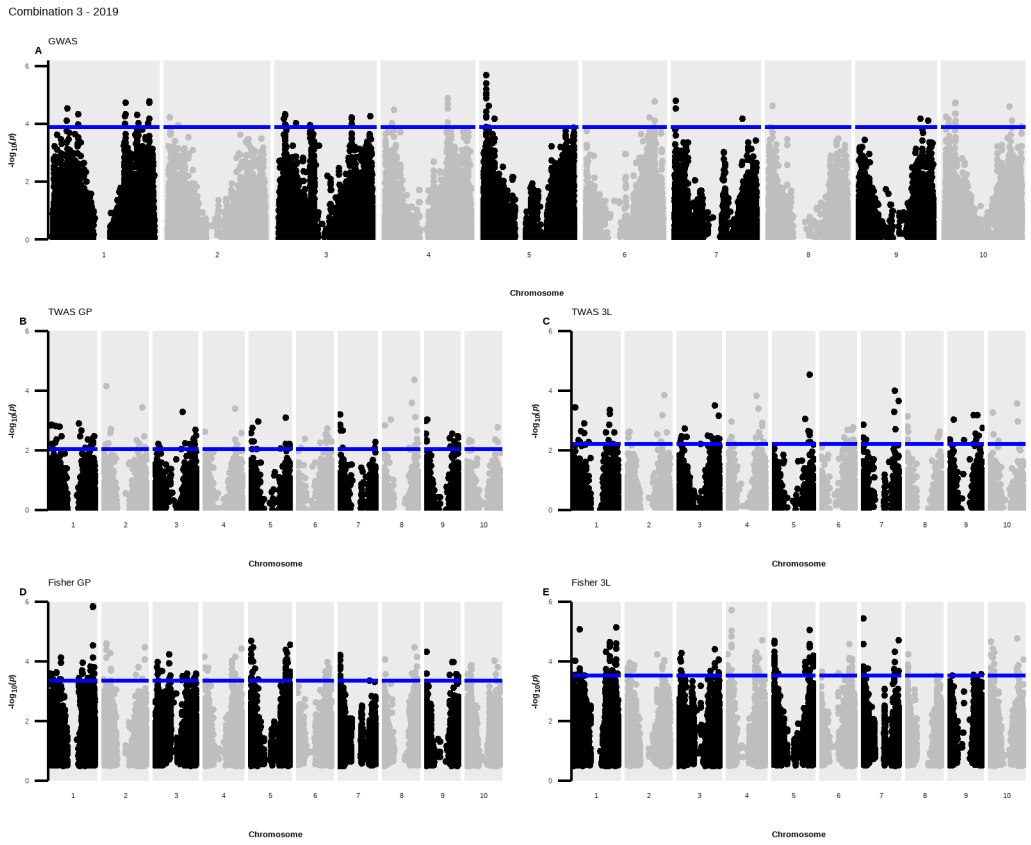

Figure 7.78: Chromosome mapping for SNPs and genes associated with combination trait 3, 2019 model

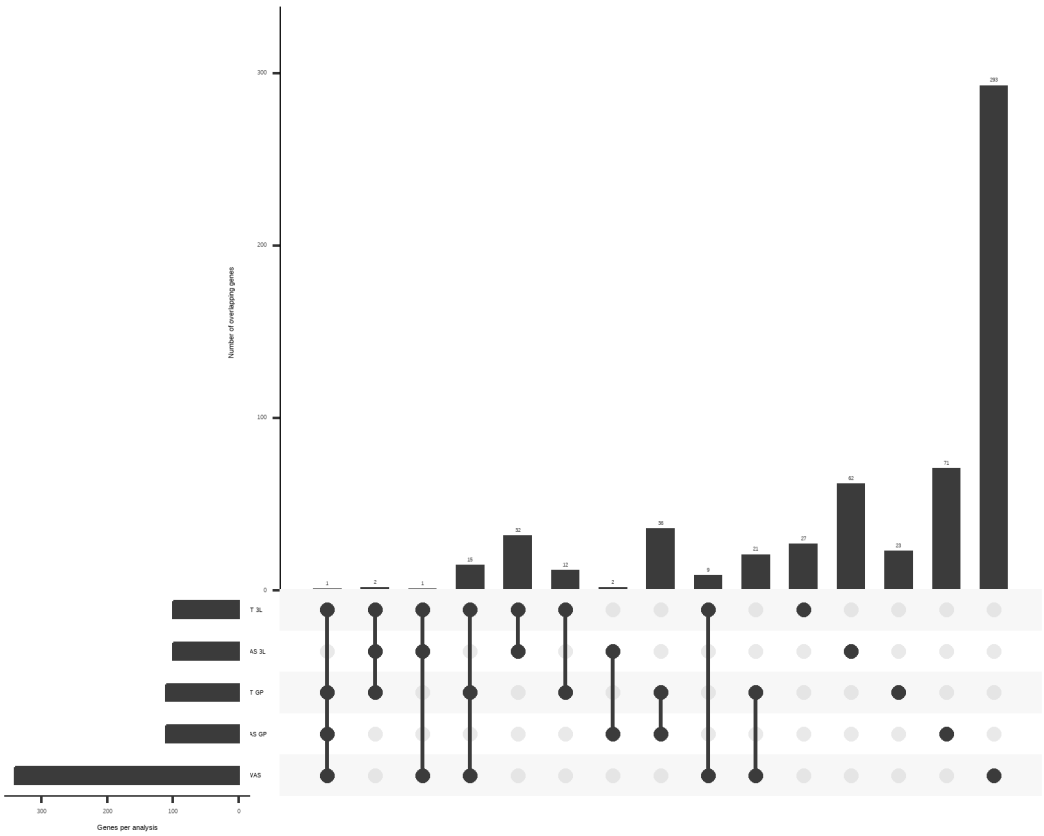

Figure 7.79: Upset plot for analyses associated with combination trait 3, 2019 model

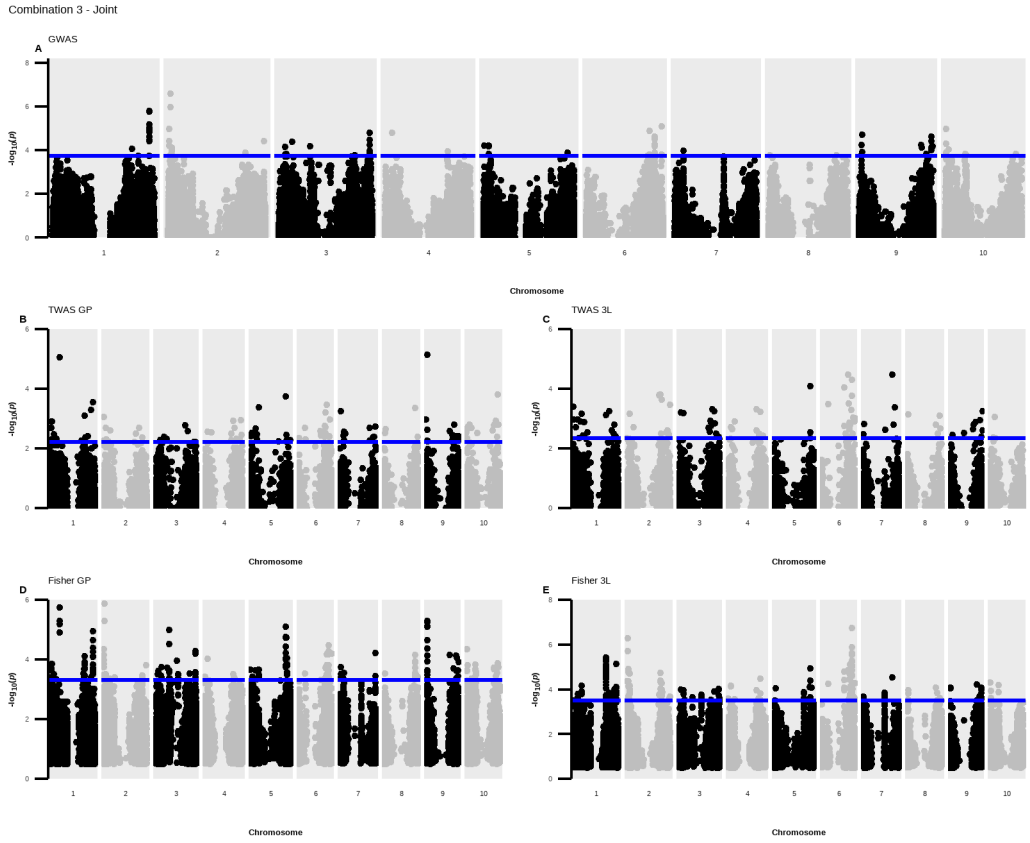

Figure 7.80: Chromosome mapping for SNPs and genes associated with combination trait 3, joint model

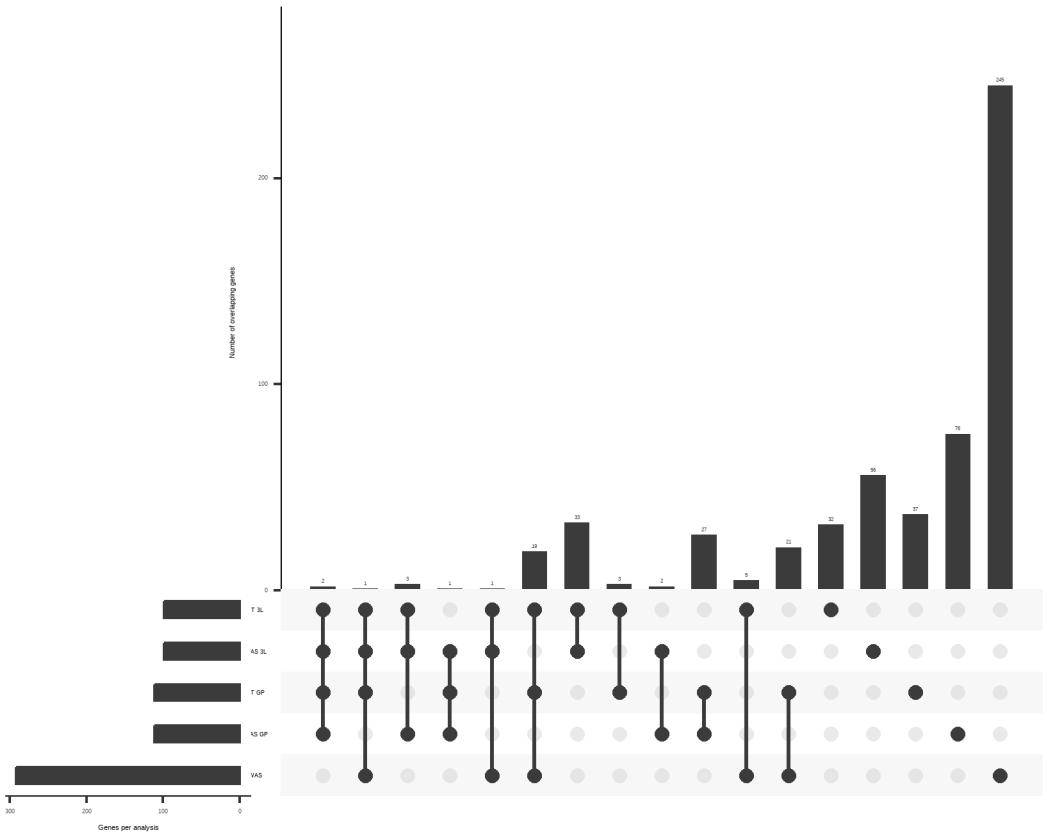

Figure 7.81: Upset plot for analyses associated with combination trait 3, joint model

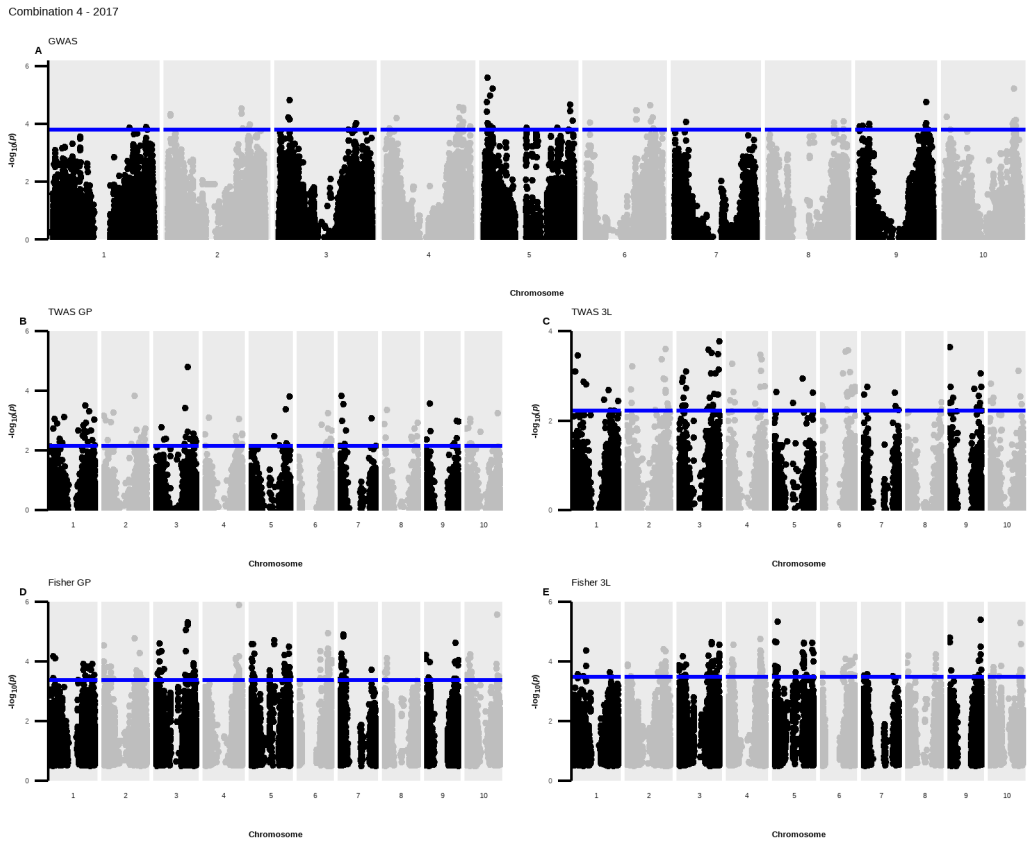

Figure 7.82: Chromosome mapping for SNPs and genes associated with combination trait 4, 2017 model

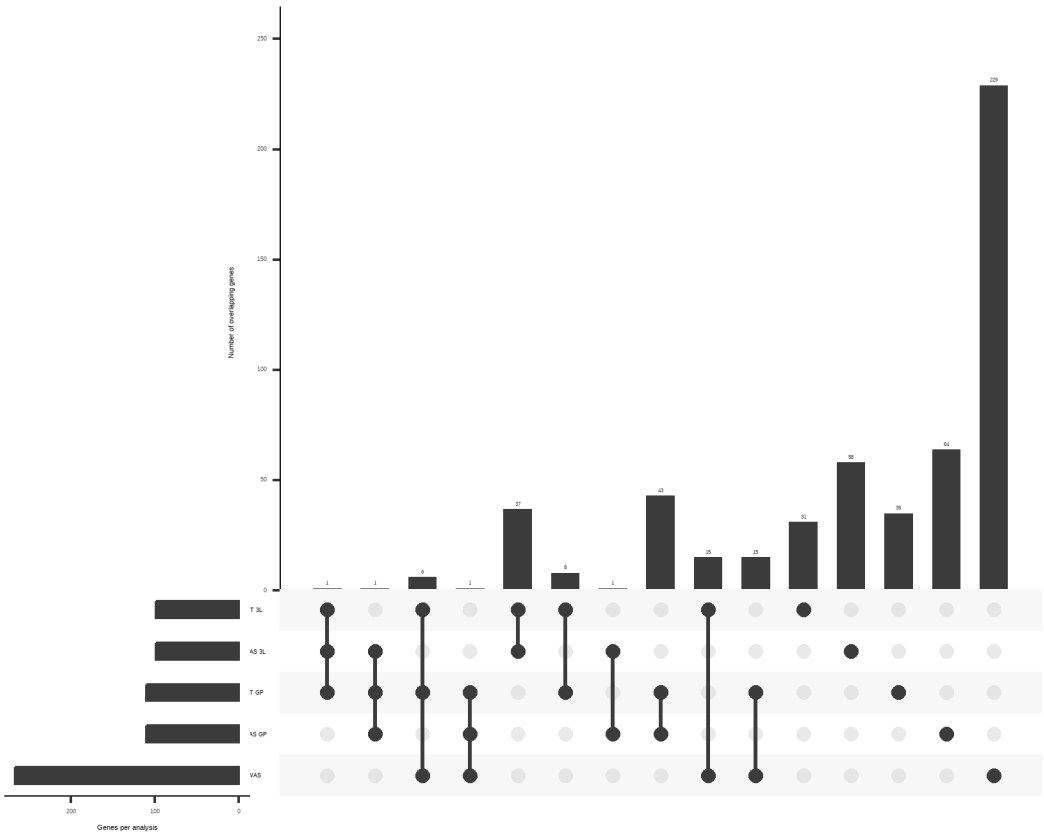

Figure 7.83: Upset plot for analyses associated with combination trait 4, 2017 model

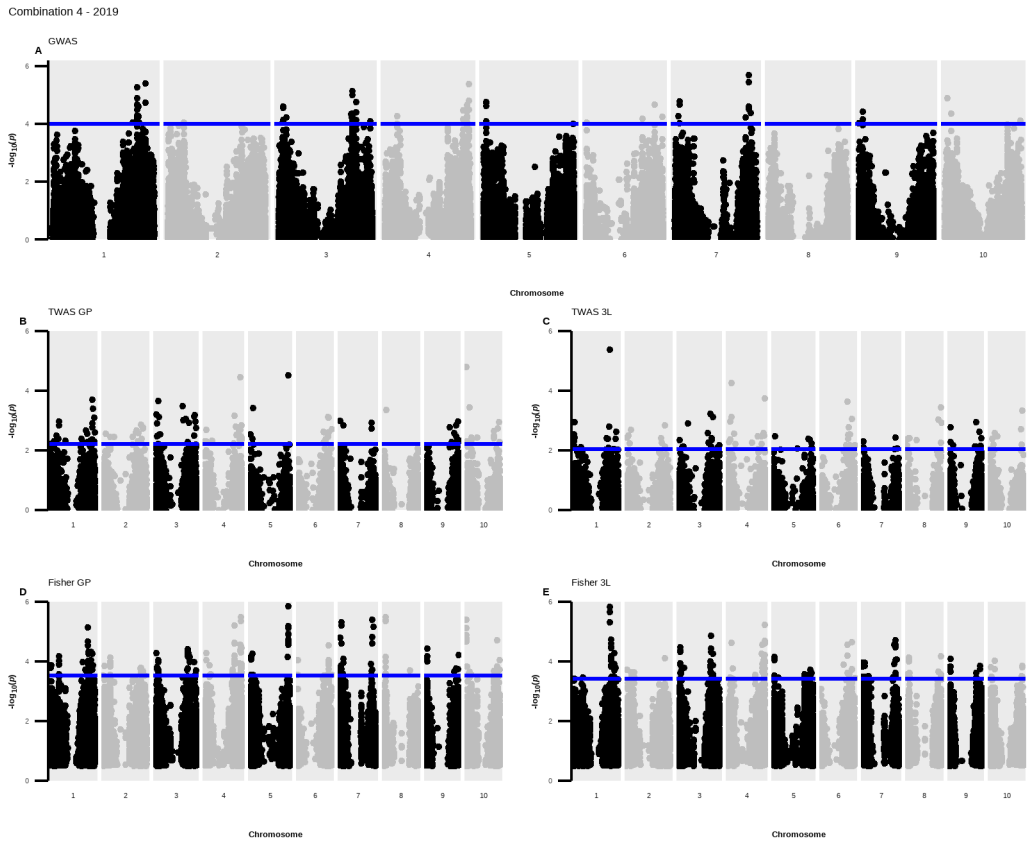

Figure 7.84: Chromosome mapping for SNPs and genes associated with combination trait 4, 2019 model

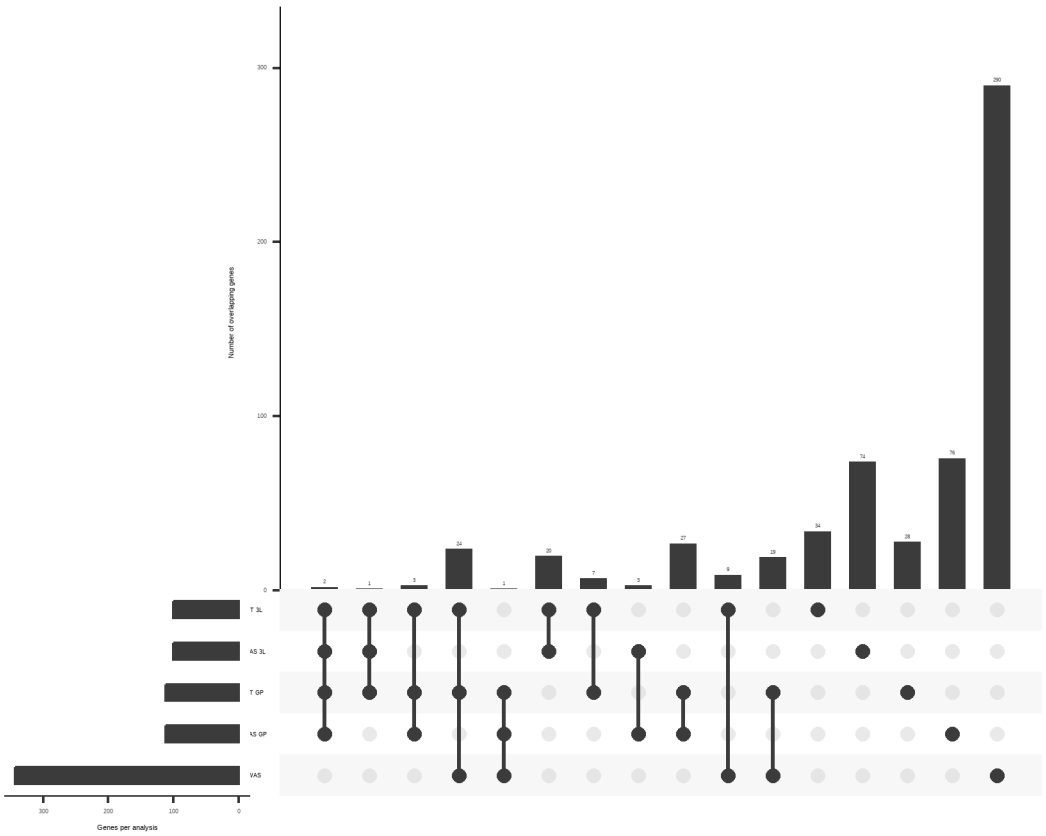

Figure 7.85: Upset plot for analyses associated with combination trait 4, 2019 model

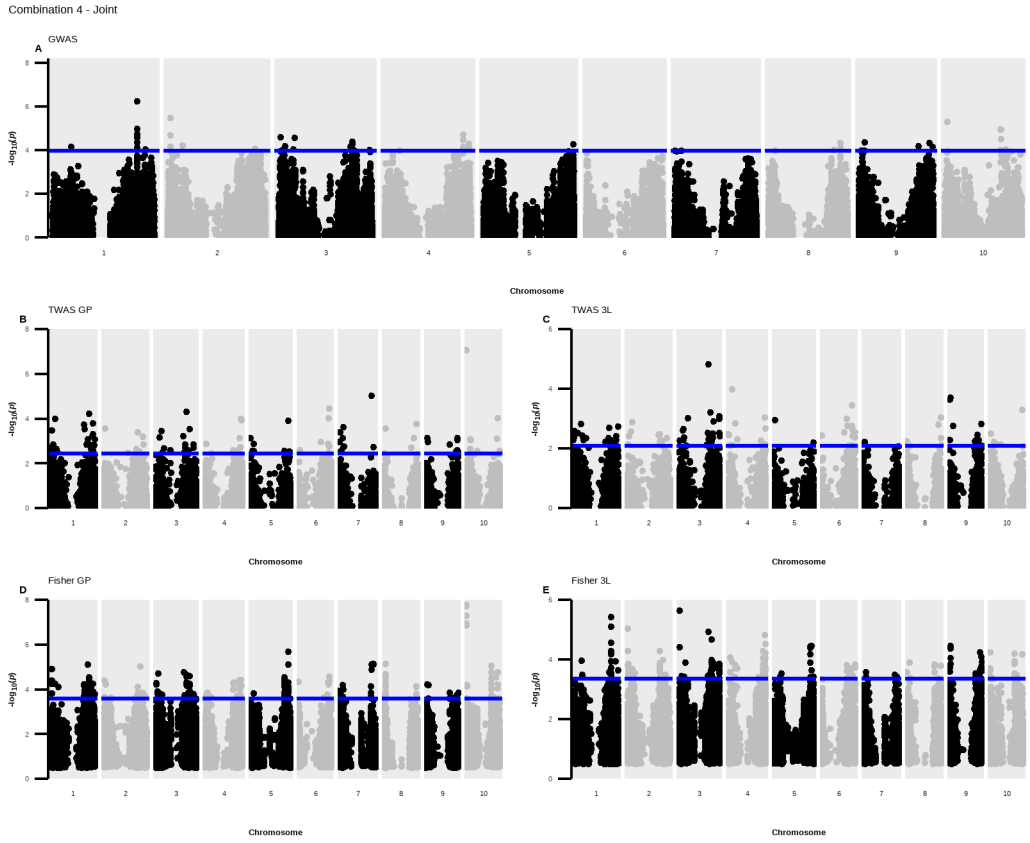

Figure 7.86: Chromosome mapping for SNPs and genes associated with combination trait 4, joint model

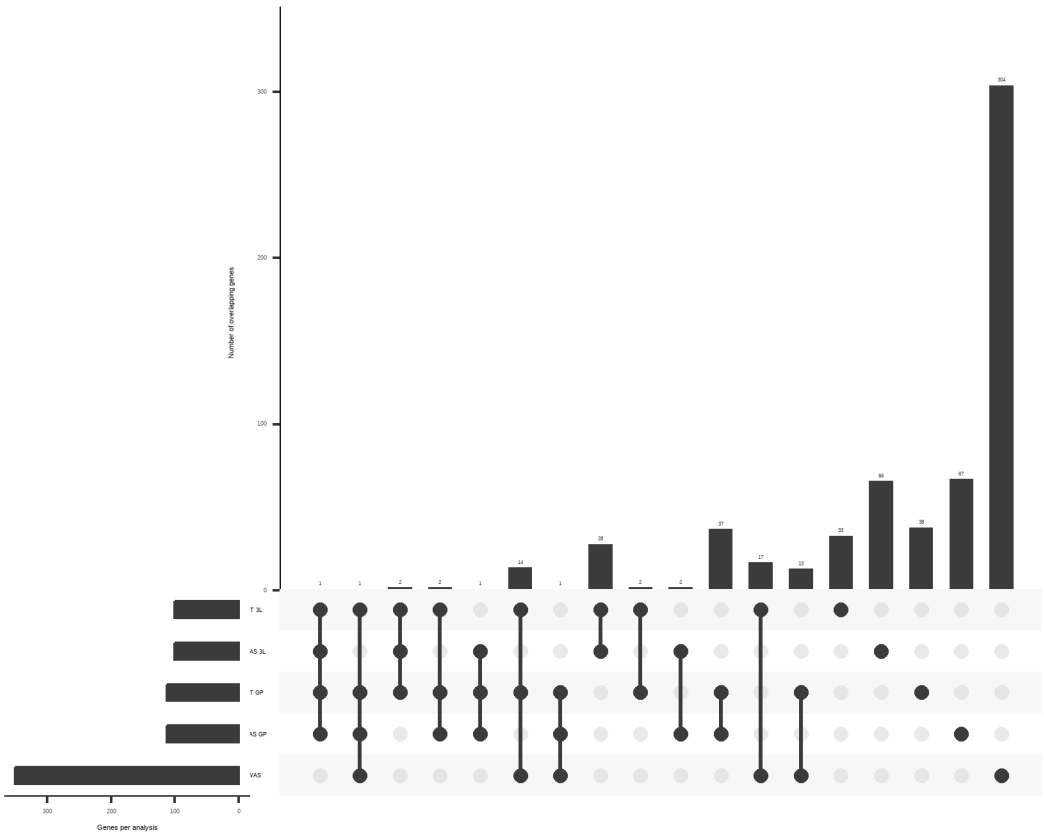

Figure 7.87: Upset plot for analyses associated with combination trait 4, joint model

7.3 Supplement for chapter four

Table 7.17: ANOVA table of max NPQ linear mixed effect model parameters for Chr01_67331530 accessions.

Factor	DF_{num}	DF_{den}	F	p
Allele value	1	14	0.064	0.8

Note:
Random effects included plate, accession, day, and replicate

Table 7.18: ANOVA table of PI linear mixed effect model parameters for Chr01_67331530 accessions.

Factor	DF_{num}	DF_{den}	F	p
Allele value	1	11.62	0	0.99

Note:
Random effects included plate, accession, subblock, and day

Table 7.19: ANOVA table of NPQ induction k linear mixed effect model paramters for Chr01_67331530 accessions.

Factor	DF_{num}	DF_{den}	F	p
Allele value	1	13.74	14.424	0.002

Note:
Random effects included accession, subblock, day, and sampler

Table 7.20: ANOVA table of NPQ relaxation k linear mixed effect model parameters for Chr01_67331530 accessions.

Factor	DF_{num}	DF_{den}	F	p
Allele value	1	13.96	7.63	0.015

Note:
Random effects included plate, accession, subblock, and sampler

Table 7.21: ANOVA table of max NPQ linear mixed effect model parameters for Chr01_76704821 accessions.

Factor	DF_{num}	DF_{den}	F	p
Allele value	1	14.12	1.065	0.32

Note:
Random effects included plate, accession, and day

Table 7.22: ANOVA table of PI linear mixed effect model parameters for Chr01_76704821 accessions.

Factor	DF_{num}	DF_{den}	F	p
Allele value	1	13.96	0.267	0.61

Note:
Random effects included plate, accession, sampler, and replicate

Table 7.23: ANOVA table of NPQ induction k linear mixed effect model parameters for Chr01_76704821 accessions.

Factor	DF_{num}	DF_{den}	F	p
Allele value	1	13.8	0.864	0.37

Note:
Random effects included plate, accession, subblock, and day

Table 7.24: ANOVA table of NPQ relaxation k linear mixed effect model parameters for Chr01_76704821 accessions.

Factor	DF_{num}	DF_{den}	F	p
Allele value	1	14.08	0.51	0.49

Note:
Random effects included plate, accession, day, and sampler

7.4 Supplement for chapter five

Table 7.25: Total day respiration (R_d) values used in C_4 photosynthesis modeling for two sorghum accessions at 2% and 21% O_2

Accession	O_2(%)	Slope	R_d ($\mu mol\ m^{-2}\ s^{-1}$)
PI276818	2	0.265	1.43
	21	0.249	1.01
PI521057	2	0.270	1.07
	21	0.264	1.38

Note:
Slope is linear regression of net CO_2 assimilation against $(I_{inc} * \Phi PSII)/3$ from light response curves, using the lowest five points (excluding the 30 μmol $m^{-2}s^{-1}$ point for 21% O_2 due to apparent Kok effect). Slopes at 2% O_2 used as *s'* calibration parameter (mol ATP (mol e^-)$^{-1}$) in J_{atp} e^- transport calculation.

Table 7.26: ANOVA table of $d\Delta^{13}C$ light treatment response model parameters at 2% O_2

Factor	DF_{num}	DF_{den}	F	p
Accession	1	25	1.109	0.30
Treatment	1	25	1.838	0.19
Accession:Treatment	1	25	0.469	0.50

Note:
No random effects included in model.

Table 7.27: ANOVA table of $d\Delta^{13}C$ light treatment response model parameters at 21% O_2

Factor	DF_{num}	DF_{den}	F	p
Accession	1	25.59	5.430	0.028
Treatment	1	25.59	1.529	0.228
Accession:Treatment	1	25.63	0.271	0.607

Note:
Random effects included growth set and measurement period (morning/afternoon)

Table 7.28: ANOVA table of $d\phi$ light treatment response model parameters at 2% O_2

Factor	DF_{num}	DF_{den}	F	p
Accession	1	25	0.748	0.40
Treatment	1	25	2.147	0.16
Accession:Treatment	1	25	0.318	0.58

Note:
No random effects included in model.

Table 7.29: ANOVA table of $d\phi$ light treatment response model parameters at 21% O_2

Factor	DF_{num}	DF_{den}	F	p
Accession	1	24.83	4.435	0.045
Treatment	1	24.83	1.651	0.211
Accession:Treatment	1	24.76	0.159	0.694

Note:
Random effects included growth set and measurement period (morning/afternoon)

Table 7.30: ANOVA table of C_i/C_a light treatment response model parameters at 2% O_2

Factor	DF_{num}	DF_{den}	F	p
Accession	1	25	0.069	0.794
Treatment	1	25	3.909	0.059
Accession:Treatment	1	25	0.264	0.612

Note:
No random effects included in model.

Table 7.31: ANOVA table of C_i/C_a light treatment response model parameters at 21% O_2

Factor	DF_{num}	DF_{den}	F	p
Accession	1	27.00	0.527	0.4741
Treatment	1	27.00	7.804	0.0095
Accession:Treatment	1	27.04	0.396	0.5346

Note:
Random effects included measurement period (morning/afternoon)

Table 7.32: ANOVA table of V_o/V_c light treatment response model parameters at 2% O_2

Factor	DF_{num}	DF_{den}	F	p
Accession	1	25	0.453	0.51
Treatment	1	25	1.564	0.22
Accession:Treatment	1	25	0.383	0.54

Note:
No random effects included in model.

Table 7.33: ANOVA table of V_o/V_c light treatment response model parameters at 21% O_2

Factor	DF_{num}	DF_{den}	F	p
Accession	1	27.00	1.238	0.28
Treatment	1	27.00	0.131	0.72
Accession:Treatment	1	27.06	0.768	0.39

Note:
Random effects included measurement period (morning/afternoon)

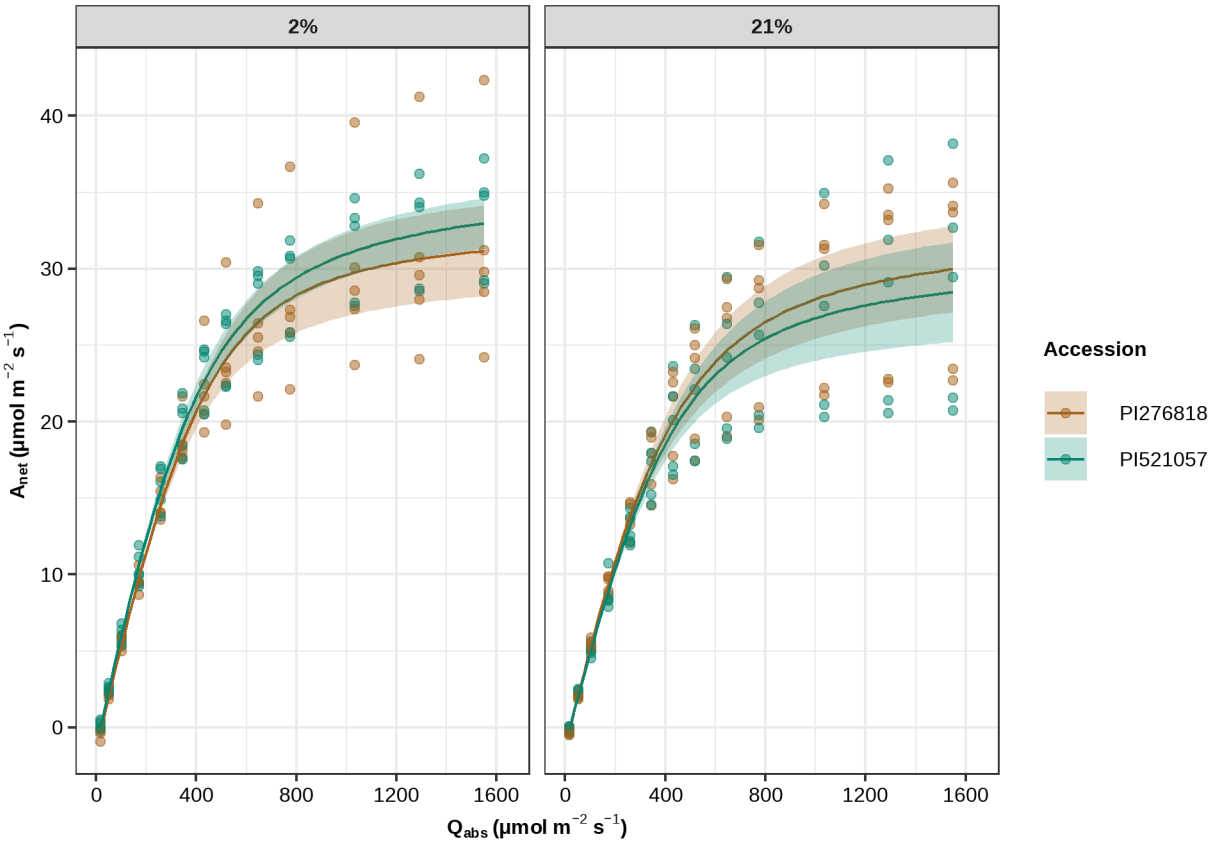

Figure 7.88: Steady-state response of net CO_2 assimilation (A_{net}) to absorbed photosynthetic photon flux density (Q_{abs}) at 420 μmol m^{-2}s^{-1} CO_2 in two sorghum accessions, in 2% and 21% O_2. Lines are the mean modelled fits of five replicates (n). Error shading is standard error of the mean modelled fit. Points are raw datapoints.

References

Al Atalah, B., De Vleesschauwer, D., Xu, J., Fouquaert, E., Höfte, M., and Van Damme, E.J., 2014. Transcriptional behavior of EUL-related rice lectins toward important abiotic and biotic stresses. *Journal of plant physiology* [Online], 171(12), pp.986–992. Available from: https://doi.org/10.1016/j.jplph.2014.04.004.

Allen, L.H., Kakani, V.G., Vu, J.C., and Boote, K.J., 2011. Elevated CO_2 increases water use efficiency by sustaining photosynthesis of water-limited maize and sorghum. *Journal of plant physiology* [Online], 168(16), pp.1909–1918. Available from: https://doi.org/10.1016/j.jplph.2011.05.005.

Arce Cubas, L., Vath, R.L., Bernardo, E.L., Sales, C.R.G., Burnett, A.C., and Kromdijk, J., 2023. Activation of CO_2 assimilation during photosynthetic induction is slower in C_4 than in C_3 photosynthesis in three phylogenetically controlled experiments. *Frontiers in plant science* [Online], 13. Available from: https://doi.org/10.3389/fpls.2022.1091115.

Arnon, D.I., 1949. Copper enzymes in isolated chloroplasts. polyphenoloxidase in *Beta vulgaris*. *Plant physiology* [Online], 24(1), pp.1–15. Available from: https://doi.org/10.1104/PP.24.1.1.

Assefa, Y., Staggenborg, S.A., and Prasad, V.P.V., 2010. Grain sorghum water requirement and responses to drought stress: A review. *Crop management* [Online], 9(1), pp.1–11. Available from: https://doi.org/10.1094/CM-2010-1109-01-RV.

Bajji, M., Kinet, J.M., and Lutts, S., 2002. The use of the electrolyte leakage method for assessing cell membrane stability as a water stress tolerance test in durum wheat. *Plant growth regulation* [Online], 36(1), pp.61–70. Available from: https://doi.org/10.1023/A:1014732714549.

Balevičius, V., Fox, K.F., Bricker, W.P., Jurinovich, S., Prandi, I.G., Mennucci, B., and Duffy, C.D.P., 2017. Fine control of chlorophyll-carotenoid interactions defines the functionality of light-harvesting proteins in plants. *Scientific reports* [Online], 7(1), p.13956. Available from: https://doi.org/10.1038/s41598-017-13720-6.

Barth, C. and Conklin, P.L., 2003. The lower cell density of leaf parenchyma in the *Arabidopsis thaliana* mutant *lcd1-1* is associated with increased sensitivity to ozone and virulent *Pseudomonas syringae*. *The plant journal* [Online], 35(2), pp.206–218. Available from: https://doi.org/10.1046/j.1365-313X.2003.01795.x.

Bassi, R., Pineau, B., Dainese, P., and Marquardt, J., 1993. Carotenoid-binding proteins of photosystem ii. *European journal of biochemistry* [Online], 212(2), pp.297–303. Available from: https://doi.org/10.1111/j.1432-1033.1993.tb17662.x.

Basu, A.K., O'Hara, S.M., Valladier, P., Stone, K., Mols, O., and Marnett, L.J., 1988. Identification of adducts formed by reaction of guanine nucleosides with malondialdehyde and structurally related aldehydes. *Chemical research in toxicology* [Online], 1, pp.5–59. Available from: https://doi.org/10.1021/tx00001a010.

Basu, U., Bajaj, D., Sharma, A., Malik, N., Daware, A., Narnoliya, L., Thakro, V., Upadhyaya, H.D., Kumar, R., Tripathi, S., Bharadwaj, C., Tyagi, A.K., and Parida, S.K., 2019. Genetic dissection of photosynthetic efficiency traits for enhancing seed yield in chickpea. *Plant, cell & environment* [Online], 42(1), pp.158–173. Available from: https://doi.org/10.1111/pce.13319.

Bates, D., Mächler, M., Bolker, B., and Walker, S., 2015. Fitting linear mixed-effects models using lme4. *Journal of statistical software* [Online], 67(1), pp.1–48. Available from: https://doi.org/10.18637/jss.v067.i01.

Baxter, A., Mittler, R., and Suzuki, N., 2014. ROS as key players in plant stress signalling. *Journal of experimental botany* [Online], 65(5), pp.1229–1240. Available from: https://doi.org/10.1093/JXB/ERT375.

Bazakos, C., Hanemian, M., Trontin, C., Jiménez-Gómez, J.M., and Loudet, O., 2017. New strategies and tools in quantitative genetics: how to go from the phenotype to the genotype. *Annual review of plant biology* [Online], 68(1), pp.435–455. Available from: https://doi.org/10.1146/annurev-arplant-042916-040820.

Bellasio, C., Burgess, S.J., Griffiths, H., and Hibberd, J.M., 2014. A high throughput gas exchange screen for determining rates of photorespiration or regulation of C_4 activity. *Journal of experimental botany* [Online], 65(13), pp.3769–3779. Available from: https://doi.org/10.1093/jxb/eru238.

Bellis, E.S., Kelly, E.A., Lorts, C.M., Gao, H., DeLeo, V.L., Rouhan, G., Budden, A., Bhaskara, G.B., Hu, Z., Muscarella, R., Timko, M.P., Nebie, B., Runo, S.M., Chilcoat, N.D., Juenger, T.E., Morris, G.P., dePamphilis, C.W., and Lasky, J.R., 2020. Genomics of sorghum local adaptation to a parasitic plant. *Proceedings of the national academy of sciences* [Online], 117(8), pp.4243–4251. Available from: https://doi.org/10.1073/pnas.1908707117.

Berardini, T.Z., Reiser, L., Li, D., Mezheritsky, Y., Muller, R., Strait, E., and Huala, E., 2015. The arabidopsis information resource: making and mining the "gold standard" annotated reference plant genome. *Genesis* [Online], 53(8), pp.474–485. Available from: https://doi.org/10.1002/dvg.22877.

Bernal-Vasquez, A.-M., Utz, H.F., and Piepho, H.-P., 2016. Outlier detection methods for generalized lattices: a case study on the transition from ANOVA to REML. *Theoretical and applied genetics* [Online], 129(4), pp.787–804. Available from: https://doi.org/10.1007/s00122-016-2666-6.

Bhattarai, B., Singh, S., West, C.P., and Saini, R., 2019. Forage potential of pearl millet and forage sorghum alternatives to corn under the water-limiting conditions of the texas high plains: a review. *Crop, forage & turfgrass management* [Online], 5(1), p.190058. Available from: https://doi.org/https://doi.org/10.2134/cftm2019.08.0058.

Boardman, N.K., 1977. Comparative photosynthesis of sun and shade plants. *Annual review of plant physiology* [Online], 28(1), pp.355–377. Available from: https://doi.org/10.1146/annurev.pp.28.060177.002035.

Bonsegna, S., Slocombe, S.P., Bellis, L.D., and Baker, A., 2005. AtLACS7 interacts with the TPR domains of the PTS1 receptor PEX5. *Archives of biochemistry and biophysics* [Online], 443(1), pp.74–81. Available from: https://doi.org/10.1016/j.abb.2005.09.003.

Boyles, R.E., Brenton, Z.W., and Kresovich, S., 2019. Genetic and genomic resources of sorghum to connect genotype with phenotype in contrasting environments. *The plant journal* [Online], 97(1), pp.19–39. Available from: https://doi.org/10.1111/tpj.14113.

Bradbury, P.J., Zhang, Z., Kroon, D.E., Casstevens, T.M., Ramdoss, Y., and Buckler, E.S., 2007. TASSEL: software for association mapping of complex traits in diverse samples. *Bioinformatics* [Online], 23(19), pp.2633–2635. Available from: https://doi.org/10.1093/bioinformatics/btm308.

Brewer, P.B., Yoneyama, K., Filardo, F., Meyers, E., Scaffidi, A., Frickey, T., Akiyama, K., Seto, Y., Dun, E.A., Cremer, J.E., Kerr, S.C., Waters, M.T., Flematti, G.R., Mason, M.G., Weiller, G., Yamaguchi, S., Nomura, T., Smith, S.M., Yoneyama, K., and Beveridge, C.A., 2016. *LATERAL BRANCHING OXIDOREDUCTASE* acts in the final stages of strigolactone biosynthesis in *Arabidopsis*. *Proceedings of the national academy of sciences* [Online], 113(22), pp.6301–6306. Available from: https://doi.org/10.1073/pnas.1601729113.

Browning, B.L. and Browning, S.R., 2016. Genotype imputation with millions of reference samples. *The american journal of human genetics* [Online], 98(1), pp.116–126. Available from: https://doi.org/10.1016/j.ajhg.2015.11.020.

Bru, P., Nanda, S., and Malnoë, A., 2020. A genetic screen to identify new molecular players involved in photoprotection qH in *Arabidopsis thaliana*. *Plants* [Online], 9(11). Available from: https://doi.org/10.3390/plants9111565.

Brugnoli, E., Scartazza, A., De Tullio, M.C., Monteverdi, M.C., Lauteri, M., and Augusti, A., 1998. Zeaxanthin and non-photochemical quenching in sun and shade leaves of C_3 and C_4 plants. *Physiologia plantarum* [Online], 104(4), pp.727–734. Available from: https://doi.org/10.1034/j.1399-3054.1998.1040430.x.

Brutnell, T.P., Wang, L., Swartwood, K., Goldschmidt, A., Jackson, D., Zhu, X.-G., Kellogg, E., and Van Eck, J., 2010. *Setaria viridis*: A model for C_4 photosynthesis. *The plant cell* [Online], 22(8), pp.2537–2544. Available from: https://doi.org/10.1105/TPC.110.075309.

Burkholder, P.R., 1936. The rôle of light in the life of plants. i. light and physiological processes. *Botanical review* [Online], 2(1), pp.1–52. Available from: http://www.jstor.org/stable/4353120.

Busch, F.A., 2014. Opinion: The red-light response of stomatal movement is sensed by the redox state of the photosynthetic electron transport chain. *Photosynthesis research* [Online], 119(1), pp.131–140. Available from: https://doi.org/10.1007/s11120-013-9805-6.

Busch, F.A., 2020. Photorespiration in the context of rubisco biochemistry, CO_2 diffusion and metabolism. *The plant journal* [Online], 101(4), pp.919–939. Available from: https://doi.org/10.1111/tpj.14674.

Butler, D., Cullis, B., Gilmour, B., and Thompson, R., 2017. *ASReml-R Reference Manual Version 4*. Hemel Hempstead, HP1 1ES, UK: VSN International Ltd.

Cai, J., Matheson, G., and Daniël, S.L., 2022. *Ggcorrplot2* [Online]. version 0.1.2. Available from: https://github.com/caijun/ggcorrplot2.

Campos, P.S., Quartin, V., Ramalho, J.C., and Nunes, M.A., 2003. Electrolyte leakage and lipid degradation account for cold sensitivity in leaves of *Coffea sp.* plants. *Journal of plant physiology* [Online], 160(3), pp.283–292. Available from: https://doi.org/10.1078/0176-1617-00833.

Chan, K.X., Phua, S.Y., Crisp, P., McQuinn, R., and Pogson, B.J., 2016. Learning the languages of the chloroplast: retrograde signaling and beyond. *Annual review of plant biology* [Online], 67(1), pp.25–53. Available from: https://doi.org/10.1146/annurev-arplant-043015-111854.

Chazdon, R.L. and Pearcy, R.W., 1991. The importance of sunflecks for forest understory plants: Photosynthetic machinery appears adapted to brief, unpredictable periods of radiation. *Bioscience* [Online], 41(11), pp.760–766. Available from: https://doi.org/10.2307/1311725.

Christin, P.-A. and Osborne, C.P., 2013. The recurrent assembly of C_4 photosynthesis, an evolutionary tale. *Photosynthesis research* [Online], 117(1), pp.163–175. Available from: https://doi.org/10.1007/s11120-013-9852-z.

Christin, P.-A., Salamin, N., Kellogg, E.A., Vicentini, A., and Besnard, G., 2009. Integrating phylogeny into studies of C_4 variation in the grasses. *Plant physiology* [Online], 149(1), pp.82–87. Available from: https://doi.org/10.1104/pp.108.128553.

Collison, R.F., Raven, E.C., Pignon, C.P., and Long, S.P., 2020. Light, not age, underlies the maladaptation of maize and miscanthus photosynthesis to self-shading. *Frontiers in plant science* [Online], 11. Available from: https://doi.org/10.3389/fpls.2020.00783.

Conway, J., Lex, A., and Gehlenborg, N., 2014. Upsetr: an r package for the visualization of intersecting sets and their properties. *Ieee transactions on visualization and computer graphics* [Online], 20(12), pp.1983–1992. Available from: https://doi.org/10.1109/TVCG.2014.2346248.

Correia, B., Hancock, R.D., Amaral, J., Gomez-Cadenas, A., Valledor, L., and Pinto, G., 2018. Combined drought and heat activates protective responses in eucalyptus globulus that are not activated when subjected to drought or heat stress alone. *Frontiers in plant science* [Online], 9, p.819. Available from: https://doi.org/10.3389/fpls.2018.00819.

Cousins, A.B., Badger, M.R., and von Caemmerer, S., 2006. Carbonic anhydrase and its influence on carbon isotope discrimination during C_4 photosynthesis. insights from antisense RNA in *Flaveria bidentis*. *Plant physiology* [Online], 141(1), pp.232–242. Available from: https://doi.org/10.1104/pp.106.077776.

Cousins, A.B., Badger, M.R., and von Caemmerer, S., 2008. C_4 photosynthetic isotope exchange in nad-me- and nadp-me-type grasses. *Journal of experimental botany* [Online], 59(7), pp.1695–1703. Available from: https://doi.org/10.1093/jxb/ern001.

Craig, H., 1953. The geochemistry of the stable carbon isotopes. *Geochimica et cosmochimica acta* [Online], 3(2), pp.53–92. Available from: https://doi.org/10.1016/0016-7037(53)90001-5.

Craufurd, P.Q. and Peacock, J.M., 1993. Effect of heat and drought stress on sorghum (*Sorghum Bicolor*). II. grain yield. *Experimental agriculture* [Online], 29(1), pp.77–86. Available from: https://doi.org/10.1017/S0014479700020421.

Cubas, L.A., Sales, C.R.G., Vath, R.L., Bernardo, E.L., Burnett, A.C., and Kromdijk, J., 2023. Lessons from relatives: C_4 photosynthesis enhances CO_2 assimilation during the low-light phase of fluctuations. *Biorxiv* [Online]. Available from: https://doi.org/10.1101/2023.04.03.535443.

Cullis, B.R., Smith, A.B., and Coombes, N.E., 2006. On the design of early generation variety trials with correlated data. *Journal of agricultural, biological, and environmental statistics* [Online], 11(4), p.381. Available from: https://doi.org/10.1198/108571106X154443.

D'Odorico, P., Emmel, C., Revill, A., Liebisch, F., Eugster, W., and Buchmann, N., 2019. Vertical patterns of photosynthesis and related leaf traits in two contrasting agricultural crops. *Functional plant biology* [Online], 46(3), pp.213–227. Available from: https://doi.org/10.1071/FP18061.

Darwin, C., 1880. *The power of movement in plants*. John Murray Publishers.

Daryanto, S., Wang, L., and Jacinthe, P.-A., 2016. Global synthesis of drought effects on maize and wheat production. *Plos one* [Online], 11(5), pp.1–15. Available from: https://doi.org/10.1371/journal.pone.0156362.

De Schutter, K., Tsaneva, M., Kulkarni, S.R., Rougé, P., Vandepoele, K., and Van Damme, E.J.M., 2017. Evolutionary relationships and expression analysis of EUL domain proteins in rice (*Oryza sativa*). *Rice* [Online], 10(1), p.26. Available from: https://doi.org/10.1186/s12284-017-0164-3.

De Souza, A.P., Burgess, S.J., Doran, L., Hansen, J., Manukyan, L., Maryn, N., Gotarkar, D., Leonelli, L., Niyogi, K.K., and Long, S.P., 2022. Soybean photosynthesis and crop yield are improved by accelerating recovery from photoprotection. *Science* [Online], 377(6608), pp.851–854. Available from: https://doi.org/10.1126/science.adc9831.

Demidchik, V., Straltsova, D., Medvedev, S.S., Pozhvanov, G.A., Sokolik, A., and Yurin, V., 2014. Stress-induced electrolyte leakage: the role of K+-permeable channels and involvement in programmed cell death and metabolic adjustment. *Journal of experimental botany* [Online], 65(5), pp.1259–1270. Available from: https://doi.org/10.1093/jxb/eru004.

Demmig, B., Winter, K., Krüger, A., and Czygan, F.-C., 1987. Photoinhibition and zeaxanthin formation in intact leaves: a possible role of the xanthophyll cycle in the dissipation of excess light energy. *Plant physiology* [Online], 84(2), pp.218–224. Available from: https://doi.org/10.1104/pp.84.2.218.

Demmig-Adams, B., 1990. Carotenoids and photoprotection in plants: A role for the xanthophyll zeaxanthin. *Biochimica et biophysica acta (bba) - bioenergetics* [Online], 1020(1), pp.1–24. Available from: https://doi.org/10.1016/0005-2728(90)90088-L.

Demmig-Adams, B., Adams, W.W., Barker, D.H., Logan, B.A., Bowling, D.R., and Verhoeven, A.S., 1996. Using chlorophyll fluorescence to assess the fraction of absorbed light allocated to thermal dissipation of excess excitation. *Physiologia plantarum* [Online], 98(2), pp.253–264. Available from: https://doi.org/10.1034/J.1399-3054.1996.980206.X.

Demmig-Adams, B., Winter, K., Krüger, A., and Czygan, F.-C., 1989. Zeaxanthin and the induction and relaxation kinetics of the dissipation of excess excitation energy in leaves in 2% O_2, 0% CO_2. *Plant physiology* [Online], 90(3), pp.887–893. Available from: https://doi.org/10.1104/pp.90.3.887.

De Souza Rodrigues, T., Lins, J.T., Cattem, M.V., Jardim, V.C., Buckeridge, M.S., Grossi-de-Sá, M.F., Reinert, F., and Alves-Ferreira, M., 2019. Evaluation of *Setaria viridis* physiological and gene expression responses to distinct water-deficit conditions. *Biotechnology research and innovation* [Online], 3, pp.42–58. Available from: https://doi.org/10.1016/j.biori.2020.03.001.

Devlin, B. and Roeder, K., 1999. Genomic control for association studies. *Biometrics* [Online], 55(4), pp.997–1004. eprint: https://onlinelibrary.wiley.com/doi/pdf/10.1111/j.0006-341X.1999.00997.x. Available from: https://doi.org/10.1111/j.0006-341X.1999.00997.x.

De Wet, J.M.J., 1978. Systematics and evolution of sorghum sect. sorghum (gramineae). *American journal of botany* [Online], 65(4), pp.477–484. Available from: http://www.jstor.org/stable/2442706.

Dewey, M., 2022. *metap: meta-analysis of significance values*. R package version 1.8.

Dos Santos, J.P., Fernandes, S.B., McCoy, S., Lozano, R., Brown, P.J., Leakey, A.D., Buckler, E.S., Garcia, A.A., and Gore, M.A., 2020. Novel bayesian networks for genomic prediction of developmental traits in biomass sorghum. *G3 genes/genomes/genetics* [Online], 10(2), pp.769–781. Available from: https://doi.org/10.1534/G3.119.400759.

Du, Z. and Bramlage, W.J., 1992. Modified thiobarbituric acid assay for measuring lipid oxidation in sugar-rich plant tissue extracts. *Journal of agricultural and food chemistry* [Online], 40(9), pp.1566–1570. Available from: https://doi.org/10.1021/jf00021a018.

Edwards, G. and Walker, D., 1983. Three C_4 subgroups: Biochemistry, photochemistry and taxonomy. In: *C_3, C_4: mechanisms, and cellular and environmental regulation, of photosynthesis*. Blackwell, pp.299–325.

Ehleringer, J. and Björkman, O., 1977. Quantum yields for co2 uptake in C_3 and C_4 plants: dependence on temperature, CO_2, and O_2 concentration. *Plant physiology* [Online], 59(1), pp.86–90. Available from: https://doi.org/10.1104/pp.59.1.86.

Ehleringer, J. and Pearcy, R.W., 1983. Variation in quantum yield for CO_2 among C_3 and C_4 plants. *Plant physiology* [Online], 73, pp.555–559. Available from: https://doi.org/10.1104/pp.73.3.555.

Ejeta, G. and Grenier, C., 2005. Sorghum and its weedy relatives. In: *Crop ferality and volunteerism*. Ed. by J. Gressel. CRC Press.

Elzhov, T.V., Mullen, K.M., Spiess, A.-N., and Bolker, B., 2016. *minpack.lm: R Interface to the Levenberg-Marquardt Nonlinear Least-Squares Algorithm Found in MINPACK, Plus Support for Bounds* [Online]. R package version 1.2-1. Available from: https://CRAN.R-project.org/package=minpack.lm.

Erickson, J.E., Woodard, K.R., and Sollenberger, L.E., 2012. Optimizing Sweet Sorghum Production for Biofuel in the Southeastern USA Through Nitrogen Fertilization and Top Removal. *Bioenergy research* [Online], 5(1), pp.86–94. Available from: https://doi.org/10.1007/s12155-011-9129-3.

Evans, J.R., Sharkey, T.D., Berry, J.A., and Farquhar, G.D., 1986. Carbon isotope discrimination measured concurrently with gas exchange to investigate CO_2 diffusion in leaves of higher plants. *Functional plant biology*, 13(2), pp.281–292.

Farquhar, G., 1983. On the Nature of Carbon Isotope Discrimination in C_4 Species. *Australian journal of plant physiology*, 10, pp.205–226.

Farquhar, G.D. and Cernusak, L.A., 2012. Ternary effects on the gas exchange of isotopologues of carbon dioxide. *Plant, cell & environment* [Online], 35(7), pp.1221–1231. Available from: https://doi.org/10.1111/j.1365-3040.2012.02484.x.

Ferguson, J.N., Fernandes, S.B., Monier, B., Miller, N.D., Allen, D., Dmitrieva, A., Schmuker, P., Lozano, R., Valluru, R., Buckler, E.S., Gore, M.A., Brown, P.J., Spalding, E.P., and Leakey, A.D.B., 2021. Machine learning-enabled phenotyping for GWAS and TWAS of WUE traits in 869 field-grown sorghum accessions. *Plant physiology* [Online], 187(3), pp.1481–1500. Available from: https://doi.org/10.1093/plphys/kiab346.

Fernie, A.R., Tadmor, Y., and Zamir, D., 2006. Natural genetic variation for improving crop quality. *Current opinion in plant biology* [Online], 9(2), pp.196–202. Available from: https://doi.org/10.1016/j.pbi.2006.01.010.

Flood, P.J., Harbinson, J., and Aarts, M.G., 2011. Natural genetic variation in plant photosynthesis. *Trends in plant science* [Online], 16(6), pp.327–335. Available from: https://doi.org/10.1016/j.tplants.2011.02.005.

Food and Agriculture Organization of the United Nations, 2017. *The future of food and agriculture - Trends and challenges* [Online]. (technical report). FAO. Available from: https://www.fao.org/3/i6583e/i6583e.pdf.

Forrester, M.L., Krotkov, G., and Nelson, C.D., 1966. Effect of oxygen on photosynthesis, photorespiration and respiration in detached leaves. i. soybean. *Plant physiology* [Online], 41(3), pp.422–427. Available from: https://doi.org/10.1104/pp.41.3.422.

Fouquaert, E., Peumans, W.J., Vandekerckhove, T.T.M., Ongenaert, M., and Van Damme, E.J.M., 2009. Proteins with an Euonymus lectin-like domain are ubiquitous in Embryophyta. *Bmc plant biology* [Online], 9(1), p.136. Available from: https://doi.org/10.1186/1471-2229-9-136.

Foyer, C., Furbank, R., Harbinson, J., and Horton, P., 1990. The mechanisms contributing to photosynthetic control of electron transport by carbon assimilation in leaves. *Photosynthesis research* [Online], 25(2), pp.83–100. Available from: https://doi.org/10.1007/BF00035457.

Foyer, C.H., Neukermans, J., Queval, G., Noctor, G., and Harbinson, J., 2012. Photosynthetic control of electron transport and the regulation of gene expression. *Journal of experimental botany* [Online], 63(4), pp.1637–1661. Available from: https://doi.org/10.1093/jxb/ers013.

Franck, J. and Rosenberg, J., 1964. A theory of light utilization in plant photosynthesis. *Journal of theoretical biology* [Online], 7(2), pp.276–301. Available from: https://doi.org/https://doi.org/10.1016/0022-5193(64)90073-6.

Frank, H.A. and Cogdell, R.J., 1996. Carotenoids in photosynthesis. *Photochemistry and photobiology* [Online], 63(3), pp.257–264. Available from: https://doi.org/https://doi.org/10.1111/j.1751-1097.1996.tb03022.x.

Gabriel, S.B., Schaffner, S.F., Nguyen, H., Moore, J.M., Roy, J., Blumenstiel, B., Higgins, J., DeFelice, M., Lochner, A., Faggart, M., Liu-Cordero, S.N., Rotimi, C., Adeyemo, A., Cooper, R., Ward, R., Lander, E.S., Daly, M.J., and Altshuler, D., 2002. The structure of haplotype blocks in the human genome. *Science* [Online], 296(5576), pp.2225–2229. Available from: https://doi.org/10.1126/science.1069424.

Garcia-Molina, A. and Leister, D., 2020. Accelerated relaxation of photoprotection impairs biomass accumulation in arabidopsis. *Nature plants* [Online], 6(1), pp.9–12. Available from: https://doi.org/10.1038/s41477-019-0572-z.

Gillon, J. and Griffiths, H., 1997. The influence of (photo)respiration on carbon isotope discrimination in plants. *Plant, cell & environment* [Online], 20(10), pp.1217–1230. Available from: https://doi.org/https://doi.org/10.1046/j.1365-3040.1997.d01-24.x.

Głowacka, K., Kromdijk, J., Kucera, K., Xie, J., Cavanagh, A.P., Leonelli, L., Leakey, A.D.B., Ort, D.R., Niyogi, K.K., and Long, S.P., 2018. Photosystem II Subunit S overexpression increases the efficiency of water use in a field-grown crop. *Nature communications* [Online], 9(1), p.868. Available from: https://doi.org/10.1038/s41467-018-03231-x.

Gómez, S.M., Park, J.J., Zhu, J., Whitelegge, J.P., and Thornbee, J.P., 1998. Isolation and characterization of a novel xanthophyll-rich pigmentprotein complex from spinach. In: *Photosynthesis: mechanisms and effects: volume I–V: proceedings of the XIth international congress on photosynthesis, budapest, hungary, august 17–22, 1998* [Online]. Ed. by G. Garab. Dordrecht: Springer Netherlands, pp.353–356. Available from: https://doi.org/10.1007/978-94-011-3953-3_83.

Gong, P., Wu, G., and Ort, D.R., 2006. Slow dark deactivation of Arabidopsis chloroplast ATP synthase caused by a mutation in a nonplastidic SAC domain protein. *Photosynthesis research* [Online], 88(2), pp.133–142. Available from: https://doi.org/10.1007/s11120-006-9041-4.

Gotarkar, D., Doran, L., Burns, M., Hinkle, A., Kromdijk, J., and Burgess, S.J., 2022. High-throughput analysis of non-photochemical quenching in crops using pulse amplitude modulated chlorophyll fluorometry. *Jove* [Online], (185), e63485. Available from: https://doi.org/doi:10.3791/63485.

Grivet, L. and Arruda, P., 2002. Sugarcane genomics: depicting the complex genome of an important tropical crop. *Current opinion in plant biology* [Online], 5(2), pp.122–127. Available from: https://doi.org/https://doi.org/10.1016/S1369-5266(02)00234-0.

Grobbelaar, J.U., 2009. Upper limits of photosynthetic productivity and problems of scaling. *Journal of applied phycology* [Online], 21(5), pp.519–522. Available from: https://doi.org/10.1007/s10811-008-9372-y.

Gui, S., Martinez-Rivas, F.J., Wen, W., Meng, M., Yan, J., Usadel, B., and Fernie, A.R., 2023. Going broad and deep: sequencing-driven insights into plant physiology, evolution, and crop domestication. *The plant journal* [Online], 113, pp.446–459. Available from: https://doi.org/10.1111/tpj.16070.

Hadebe, S.T., Modi, A.T., and Mabhaudhi, T., 2017. Drought tolerance and water use of cereal crops: a focus on sorghum as a food security crop in sub-saharan africa. *Journal of agronomy and crop science* [Online], 203(3), pp.177–191. Available from: https://doi.org/10.1111/jac.12191.

Hao, H., Li, Z., Leng, C., Lu, C., Luo, H., Liu, Y., Wu, X., Liu, Z., Shang, L., and Jing, H.-C., 2021. Sorghum breeding in the genomic era: opportunities and challenges. *Theoretical and applied genetics* [Online], 134(7), pp.1899–1924. Available from: https://doi.org/10.1007/s00122-021-03789-z.

Hardt, H. and Kok, B., 1978. Comparison of photosynthetic activities of spinach chloroplasts with those of corn mesophyll and corn bundle sheath tissue. *Plant physiology* [Online], 62(1), pp.59–63. Available from: https://doi.org/10.1104/pp.62.1.59.

Hariprasanna, K. and Rakshit, S., 2016. Economic importance of sorghum. In: S. Rakshit and Y.-H. Wang, eds. *The sorghum genome* [Online]. Cham: Springer, pp.1–25. Available from: https://doi.org/10.1007/978-3-319-47789-3_1.

Hatch, M.D., 1971. Mechanism and function of the c4 pathway of photosynthesis. In: *Photosynthesis and photorespiration*. Wiley-Interscience, pp.139–152.

Hatch, M.D., Kagawa, T., and Craig, S., 1975. Subdivision of C_4-Pathway Species Based on Differing C_4 Acid Decarboxylating Systems and Ultrastructural Features. *Functional plant biology* [Online], 2(2), pp.111–128. Available from: https://doi.org/10.1071/PP9750111.

Hatch, M.D., 1987. C_4 photosynthesis: a unique blend of modified biochemistry, anatomy and ultrastructure. *Biochimica et biophysica acta (bba) - reviews on bioenergetics* [Online], 895(2), pp.81–106. Available from: https://doi.org/10.1016/S0304-4173(87)80009-5.

Hatch, M. and Slack, C., 1966. Photosynthesis by sugar-cane leaves. a new carboxylation reaction and the pathway of sugar formation. *Biochemical journal* [Online], 101(1), pp.103–111. Available from: https://doi.org/10.1042/bj1010103.

Hatfield, J.L. and Dold, C., 2019. Water-use efficiency: advances and challenges in a changing climate. *Frontiers in plant science* [Online], 10. Available from: https://doi.org/10.3389/fpls.2019.00103.

Heath, R.L. and Packer, L., 1968. Photoperoxidation in isolated chloroplasts: I. Kinetics and stoichiometry of fatty acid peroxidation. *Archives of biochemistry and biophysics* [Online], 125(1), pp.189–198. Available from: https://doi.org/10.1016/0003-9861(68)90654-1.

Henderson, S.A., Von Caemmerer, S., and Farquhar, G.D., 1992. Short-term measurements of carbon isotope discrimination in several C_4 species. *Functional plant biology* [Online], 19(3), pp.263–285. Available from: https://doi.org/10.1071/PP9920263.

Herritt, M., Dhanapal, A.P., and Fritschi, F.B., 2016. Identification of genomic loci associated with the photochemical reflectance index by genome-wide association study in soybean. *The plant genome* [Online], 9(2), plantgenome2015.08.0072. Available from: https://doi.org/10.3835/plantgenome2015.08.0072.

Hetherington, A.M. and Woodward, F.I., 2003. The role of stomata in sensing and driving environmental change. *Nature* [Online], 424(6951), pp.901–908. Available from: https://doi.org/10.1038/nature01843.

Hirschberg, J., 2001. Carotenoid biosynthesis in flowering plants. *Current opinion in plant biology* [Online], 4(3), pp.210–218. Available from: https://doi.org/10.1016/S1369-5266(00)00163-1.

Hodges, D.M., DeLong, J.M., Forney, C.F., and Prange, R.K., 1999. Improving the thiobarbituric acid-reactive-substances assay for estimating lipid peroxidation in plant tissues containing anthocyanin and other interfering compounds. *Planta* [Online], 207(4), pp.604–611. Available from: https://doi.org/10.1007/s004250050524.

Holland, J.J., Roberts, D., and Liscum, E., 2009. Understanding phototropism: from Darwin to today. *Journal of experimental botany* [Online], 60(7), pp.1969–1978. Available from: https://doi.org/10.1093/jxb/erp113.

Holm, S., 1979. A simple sequentially rejective multiple test procedure. *Scandinavian journal of statistics* [Online], 6(2), pp.65–70. Available from: http://www.jstor.org/stable/4615733.

Huang, Q., Hu, R., Hui zhu, Peng, C., and Chen, L., 2021. Expression of multi-domain type III antifreeze proteins from the antarctic eelpout (*Lycodichths dearborni*) in transgenic tobacco plants improves cold resistance. *Aquaculture and fisheries* [Online], 6(2), pp.186–191. Available from: https://doi.org/10.1016/j.aaf.2019.11.006.

Jaikumar, N.S., Stutz, S.S., Fernandes, S.B., Leakey, A.D.B., Bernacchi, C.J., Brown, P.J., and Long, S.P., 2021. Can improved canopy light transmission ameliorate loss of photosynthetic efficiency in the shade? an investigation of natural variation in *Sorghum bicolor*. *Journal of experimental botany* [Online], 72(13), pp.4965–4980. Available from: https://doi.org/10.1093/jxb/erab176.

Janero, D.R., 1990. Malondialdehyde and thiobarbituric acid-reactivity as diagnostic indices of lipid peroxidation and peroxidative tissue injury. *Free radical biology and medicine* [Online], 9(6), pp.515–540. Available from: https://doi.org/10.1016/0891-5849(90)90131-2.

Jiao, Q., Niu, G., Wang, F., Dong, J., Chen, T., Zhou, C., Hong, Z., et al., 2020. N-glycosylation regulates photosynthetic efficiency of *Arabidopsis thaliana*. *Photosynthetica*, 58, pp.72–79.

Jung, H.-S. and Niyogi, K.K., 2010. Mutations in Arabidopsis YCF20-like genes affect thermal dissipation of excess absorbed light energy. *Planta* [Online], 231(4), pp.923–937. Available from: https://doi.org/10.1007/s00425-010-1098-9.

Kaiser, E., Morales, A., and Harbinson, J., 2017. Fluctuating light takes crop photosynthesis on a rollercoaster ride. *Plant physiology* [Online], 176(2), pp.977–989. Available from: https://doi.org/10.1104/pp.17.01250.

Kasajima, I., Ebana, K., Yamamoto, T., Takahara, K., Yano, M., Kawai-Yamada, M., and Uchimiya, H., 2011. Molecular distinction in genetic regulation of nonphotochemical quenching in rice. *Proceedings of the national academy of sciences* [Online], 108(33), pp.13835–13840. Available from: https://doi.org/10.1073/pnas.1104809108.

Khoury, C.K., Brush, S., Costich, D.E., Curry, H.A., de Haan, S., Engels, J.M.M., Guarino, L., Hoban, S., Mercer, K.L., Miller, A.J., Nabhan, G.P., Perales, H.R., Richards, C., Riggins, C., and Thormann, I., 2022. Crop genetic erosion: understanding and responding to loss of crop diversity. *New phytologist* [Online], 233(1), pp.84–118. Available from: https://doi.org/https://doi.org/10.1111/nph.17733.

Kok, B., Gassner, E.S., and Rurainski, H.J., 1965. Photoinhibition of chloroplast reactions. *Photochemistry and photobiology* [Online], 4(2), pp.215–227. Available from: https://doi.org/https://doi.org/10.1111/j.1751-1097.1965.tb05739.x.

Kolberg, L., Raudvere, U., Kuzmin, I., Vilo, J., and Peterson, H., 2020. gprofiler2– an R package for gene list functional enrichment analysis and namespace conversion toolset g:Profiler. *F1000research*, 9 (ELIXIR)(709). R package version 0.2.1.

Kramer, D.M. and Evans, J.R., 2010. The importance of energy balance in improving photosynthetic productivity. *Plant physiology* [Online], 155(1), pp.70–78. Available from: https://doi.org/10.1104/pp.110.166652.

Kremling, K.A.G., Diepenbrock, C.H., Gore, M.A., Buckler, E.S., and Bandillo, N.B., 2019. Transcriptome-wide association supplements genome-wide association in *Zea mays*. *G3 genes|genomes|genetics* [Online], 9(9), pp.3023–3033. Available from: https://doi.org/10.1534/g3.119.400549.

Krieger-Liszkay, A., 2004. Singlet oxygen production in photosynthesis. *Journal of experimental botany* [Online], 56(411), pp.337–346. Available from: https://doi.org/10.1093/jxb/erh237.

Kromdijk, J., Głowacka, K., Leonelli, L., Gabilly, S.T., Iwai, M., Niyogi, K.K., and Long, S.P., 2016. Improving photosynthesis and crop productivity by accelerating recovery from photoprotection. *Science* [Online], 354(6314), pp.857–861. Available from: https://doi.org/10.1126/science.aai8878.

Kromdijk, J., Głowacka, K., and Long, S.P., 2019. Predicting light-induced stomatal movements based on the redox state of plastoquinone: theory and validation. *Photosynthesis research* [Online], 141(1), pp.83–97. Available from: https://doi.org/10.1007/s11120-019-00632-x.

Kromdijk, J., Griffiths, H., and Schepers, H.E., 2010. Can the progressive increase of CO_2 bundle sheath leakiness at low pfd be explained by incomplete suppression of photorespiration? *Plant, cell & environment* [Online], 33(11), pp.1935–1948. Available from: https://doi.org/10.1111/j.1365-3040.2010.02196.x.

Kromdijk, J., Schepers, H.E., Albanito, F., Fitton, N., Carroll, F., Jones, M.B., Finnan, J., Lanigan, G.J., and Griffiths, H., 2008. Bundle sheath leakiness and light limitation during C_4 leaf and canopy CO_2 uptake. *Plant physiology* [Online], 148(4), pp.2144–2155. Available from: https://doi.org/10.1104/pp.108.129890.

Kromdijk, J., Ubierna, N., Cousins, A.B., and Griffiths, H., 2014. Bundle-sheath leakiness in C_4 photosynthesis: a careful balancing act between CO_2 concentration and assimilation. *Journal of experimental botany* [Online], 65(13), pp.3443–3457. Available from: https://doi.org/10.1093/jxb/eru157.

Kubásek, J., Urban, O., and Santrůček, J., 2013. C_4 plants use fluctuating light less efficiently than do C_3 plants: a study of growth, photosynthesis and carbon isotope discrimination. *Physiologia planatarum* [Online], 149, pp.528–539. Available from: https://doi.org/10.1111/ppl.12057.

Kuznetsova, A., Brockhoff, P.B., and Christensen, R.H.B., 2017. lmerTest package: tests in linear mixed effects models. *Journal of statistical software* [Online], 82(13), pp.1–26. Available from: https://doi.org/10.18637/jss.v082.i13.

Lambrev, P.H., Miloslavina, Y., Jahns, P., and Holzwarth, A.R., 2012. On the relationship between non-photochemical quenching and photoprotection of photosystem II. *Biochimica et biophysica acta (bba) - bioenergetics* [Online], 1817(5), pp.760–769. Available from: https://doi.org/10.1016/j.bbabio.2012.02.002.

Landi, M., 2017. Commentary to: "Improving the thiobarbituric acid-reactive-substances assay for estimating lipid peroxidation in plant tissues containing anthocyanin and other interfering compounds" by Hodges et al., Planta (1999) 207:604–611. *Planta* [Online], 245(6), pp.1067–1067. Available from: https://doi.org/10.1007/s00425-017-2699-3.

Lanigan, G.J., Betson, N., Griffiths, H., and Seibt, U., 2008. Carbon isotope fractionation during photorespiration and carboxylation in *Senecio*. *Plant physiology* [Online], 148(4), pp.2013–2020. Available from: https://doi.org/10.1104/pp.108.130153.

Lawson, T., Kramer, D.M., and Raines, C.A., 2012. Improving yield by exploiting mechanisms underlying natural variation of photosynthesis. *Current opinion in biotechnology* [Online], 23(2). Food biotechnology - Plant biotechnology, pp.215–220. Available from: https://doi.org/10.1016/j.copbio.2011.12.012.

Lê, S., Josse, J., and Husson, F., 2008. FactoMineR: An R package for multivariate analysis. *Journal of statistical software* [Online], 25(1), pp.1–18. Available from: https://doi.org/10.18637/jss.v025.i01.

Lee, M.S., Boyd, R.A., and Ort, D.R., 2022. The photosynthetic response of C_3 and C_4 bioenergy grass species to fluctuating light. *Gcb bioenergy* [Online], 14(1), pp.37–53. Available from: https://doi.org/10.1111/GCBB.12899.

Leegood, R.C., 2002. C_4 photosynthesis: principles of CO_2 concentration and prospects for its introduction into C_3 plants. *Journal of experimental botany* [Online], 53(369), pp.581–590. Available from: https://doi.org/10.1093/jexbot/53.369.581.

Lehretz, G.G., Schneider, A., Leister, D., and Sonnewald, U., 2022. High non-photochemical quenching of VPZ transgenic potato plants limits CO_2 assimilation under high light conditions and reduces tuber yield under fluctuating light. *Journal of integrative plant biology* [Online], 64(9), pp.1821–1832. Available from: https://doi.org/10.1111/jipb.13320.

Lenth, R.V., 2021. *Emmeans: Estimated marginal means, aka least-squares means* [Online]. R package version 1.6.3. Available from: https://CRAN.R-project.org/package=emmeans.

Léonard, R., Costa, G., Darrambide, E., Lhernould, S., Fleurat-Lessard, P., Carlué, M., Gomord, V., Faye, L., and Maftah, A., 2002. The presence of lewis a epitopes in arabidopsis thaliana glycoconjugates depends on an active 4-fucosyltransferase gene. *Glycobiology* [Online], 12(5), pp.299–306. Available from: https://doi.org/10.1093/glycob/12.5.299.

Levchuk, A.N., Voitovich, E.N., and Lyakh, V.A., 2013. Lectins of oil-seed flax plants exposed to abiotic stress. *Russian journal of plant physiology* [Online], 60(1), pp.77–83. Available from: https://doi.org/10.1134/S1021443712060106.

Lewis, S.C. and King, A.D., 2017. Evolution of mean, variance and extremes in 21st century temperatures. *Weather and climate extremes* [Online], 15, pp.1–10. Available from: https://doi.org/10.1016/j.wace.2016.11.002.

Lex, A., Gehlenborg, N., Strobelt, H., Vuillemot, R., and Pfister, H., 2014. Upset: visualization of intersecting sets. *Ieee transactions on visualization and computer graphics* [Online], 20(12), pp.1983–1992. Available from: https://doi.org/10.1109/TVCG.2014.2346248.

Li, J., Ye, X., An, B., Du, L., and Xu, H., 2012. Genetic transformation of wheat: current status and future prospects. *Plant biotechnology reports* [Online], 6(3), pp.183–193. Available from: https://doi.org/10.1007/s11816-011-0213-0.

Li, X.-P., Björkman, O., Shih, C., Grossman, A.R., Rosenquist, M., Jansson, S., and Niyogi, K.K., 2000. A pigment-binding protein essential for regulation of photosynthetic light harvesting. *Nature* [Online], 403(6768), pp.391–395. Available from: https://doi.org/10.1038/35000131.

Li, X.-P., Müller-Moulé, P., Gilmore, A.M., and Niyogi, K.K., 2002. PsbS-dependent enhancement of feedback de-excitation protects photosystem II from photoinhibition. *Proceedings of the national academy of sciences* [Online], 99(23), pp.15222–15227. Available from: https://doi.org/10.1073/pnas.232447699.

Li, Z., Ahn, T.K., Avenson, T.J., Ballottari, M., Cruz, J.A., Kramer, D.M., Bassi, R., Fleming, G.R., Keasling, J.D., and Niyogi, K.K., 2009. Lutein accumulation in the absence of zeaxanthin restores nonphotochemical quenching in the *Arabidopsis thaliana npq1* mutant. *The plant cell* [Online], 21(6), pp.1798–1812. Available from: https://doi.org/10.1105/tpc.109.066571.

Liang, Y., Liu, H.-J., Yan, J., and Tian, F., 2021. Natural variation in crops: realized understanding, continuing promise. *Annual review of plant biology* [Online], 72(1), pp.357–385. Available from: https://doi.org/10.1146/annurev-arplant-080720-090632.

Lichtenthaler, H. and Buschmann, C., 2001. Chlorophylls and carotenoids: Measurement and characterization by UV-VIS spectroscopy. *Current protocols in food analytical chemistry* [Online], 1(1), F4.3.1–F4.3.8. Available from: https://doi.org/10.1002/0471142913.faf0403s01.

Lichtenthaler, H.K., 1987. Chlorophylls and carotenoids: Pigments of photosynthetic biomembranes. In: *Methods in enzymology* [Online]. Vol. 148. Academic Press, pp.350–382. Available from: https://doi.org/10.1016/0076-6879(87)48036-1.

Liepman, A.H., Nairn, C.J., Willats, W.G., Sørensen, I., Roberts, A.W., and Keegstra, K., 2007. Functional genomic analysis supports conservation of function among cellulose synthase-like a gene family members and suggests diverse roles of mannans in plants. *Plant physiology* [Online], 143(4), pp.1881–1893. Available from: https://doi.org/10.1104/pp.106.093989.

Liguori, N., Xu, P., van Stokkum, I.H.M., van Oort, B., Lu, Y., Karcher, D., Bock, R., and Croce, R., 2017. Different carotenoid conformations have distinct functions in light-harvesting regulation in plants. *Nature communications* [Online], 8(1), p.1994. Available from: https://doi.org/10.1038/s41467-017-02239-z.

Lin, M., Qiao, P., Matschi, S., Vasquez, M., Ramstein, G.P., Bourgault, R., Mohammadi, M., Scanlon, M.J., Molina, I., Smith, L.G., and Gore, M.A., 2022. Integrating GWAS and TWAS to elucidate the genetic architecture of maize leaf cuticular conductance. *Plant physiology* [Online], 189(4), pp.2144–2158. Available from: https://doi.org/10.1093/plphys/kiac198.

Lipka, A.E., Kandianis, C.B., Hudson, M.E., Yu, J., Drnevich, J., Bradbury, P.J., and Gore, M.A., 2015. From association to prediction: statistical methods for the dissection and selection of complex traits in plants. *Current opinion in plant biology* [Online], 24, pp.110–118. Available from: https://doi.org/10.1016/j.pbi.2015.02.010.

Lopes, M.S., Araus, J.L., van Heerden, P.D.R., and Foyer, C.H., 2011. Enhancing drought tolerance in C_4 crops. *Journal of experimental botany* [Online], 62(9), pp.3135–3153. Available from: https://doi.org/10.1093/jxb/err105.

Loriaux, S.D., Avenson, T.J., Welles, J.M., McDermitt, D.K., Eckles, R.D., Riensche, B., and Genty, B., 2013. Closing in on maximum yield of chlorophyll fluorescence using a single multiphase flash of sub-saturating intensity. *Plant, cell & environment* [Online], 36(10), pp.1755–1770. Available from: https://doi.org/https://doi.org/10.1111/pce.12115.

Lozano, R., Gazave, E., dos Santos, J.P.R., Stetter, M.G., Valluru, R., Bandillo, N., Fernandes, S.B., Brown, P.J., Shakoor, N., Mockler, T.C., Cooper, E.A., Taylor Perkins, M., Buckler, E.S., Ross-Ibarra, J., and Gore, M.A., 2021. Comparative evolutionary genetics of deleterious load in sorghum and maize. *Nature plants* [Online], 7(1), pp.17–24. Available from: https://doi.org/10.1038/s41477-020-00834-5.

Ma, L., Gao, Y., Qu, L., Chen, Z., Li, J., Zhao, H., and Deng, X.W., 2002. Genomic Evidence for COP1 as a Repressor of Light-Regulated Gene Expression and Development in Arabidopsis. *The plant cell* [Online], 14(10), pp.2383–2398. Available from: https://doi.org/10.1105/tpc.004416.

Maai, E., Nishimura, K., Takisawa, R., and Nakazaki, T., 2020. Light stress-induced chloroplast movement and midday depression of photosynthesis in sorghum leaves. *Plant production science* [Online], 23(2), pp.172–181. Available from: https://doi.org/10.1080/1343943X.2019.1673666.

Malnoë, A., 2018. Photoinhibition or photoprotection of photosynthesis? update on the (newly termed) sustained quenching component qH. *Environmental and experimental botany* [Online], 154. An Integrative Approach to Photoinhibition and Photoprotection of Photosynthesis, pp.123–133. Available from: https://doi.org/https://doi.org/10.1016/j.envexpbot.2018.05.005.

Malnoë, A., Schultink, A., Shahrasbi, S., Rumeau, D., Havaux, M., and Niyogi, K.K., 2017. The plastid lipocalin LCNP is required for sustained photoprotective energy dissipation in arabidopsis. *The plant cell* [Online], 30(1), pp.196–208. Available from: https://doi.org/10.1105/tpc.17.00536.

Maman, N., Lyon, D.J., Mason, S.C., Galusha, T.D., and Higgins, R., 2003. Pearl millet and grain sorghum yield response to water supply in nebraska. *Agronomy journal* [Online], 95(6), pp.1618–1624. Available from: https://doi.org/10.2134/agronj2003.1618.

Marshall, B. and Biscoe, P., 1980. A model for C_3 leaves describing the dependence of net photosynthesis on irradiance. *Journal of experimental botany* [Online], 31(120), pp.29–39. Available from: http://www.jstor.org/stable/23689820.

Martínez-Fortún, J., Phillips, D.W., and Jones, H.D., 2022. Natural and artificial sources of genetic variation used in crop breeding: a baseline comparator for genome editing. *Frontiers in genome editing* [Online], 4. Available from: https://doi.org/10.3389/fgeed.2022.937853.

Massel, K., Lam, Y., Hintzsche, J., Lester, N., Botella, J.R., and Godwin, I.D., 2022. Endogenous U6 promoters improve CRISPR/Cas9 editing efficiencies in Sorghum bicolor and show potential for applications in other cereals. *Plant cell reports* [Online], 41(2), pp.489–492. Available from: https://doi.org/10.1007/s00299-021-02816-z.

MATLAB, 2020. *version 9.8.0.1721703 (R2020a) Update 7*. Natick, Massachusetts: The MathWorks Inc.

McAusland, L., Vialet-Chabrand, S., Davey, P., Baker, N.R., Brendel, O., and Lawson, T., 2016. Effects of kinetics of light-induced stomatal responses on photosynthesis and water-use efficiency. *The new phytologist* [Online], 211(4), pp.1209–1220. Available from: https://doi.org/10.1111/nph.14000.

McCormick, R.F., Truong, S.K., Sreedasyam, A., Jenkins, J., Shu, S., Sims, D., Kennedy, M., Amirebrahimi, M., Weers, B.D., McKinley, B., Mattison, A., Morishige, D.T., Grimwood, J., Schmutz, J., and Mullet, J.E., 2018. The sorghum bicolor reference genome: improved assembly, gene annotations, a transcriptome atlas, and signatures of genome organization. *The plant journal* [Online], 93(2), pp.338–354. Available from: https://doi.org/10.1111/tpj.13781.

Meier, H. and Reid, J.S.G., 1982. Reserve polysaccharides other than starch in higher plants. In: *Plant carbohydrates I: intracellular carbohydrates* [Online]. Ed. by F.A. Loewus and W. Tanner. Berlin, Heidelberg: Springer Berlin Heidelberg, pp.418–471. Available from: https://doi.org/10.1007/978-3-642-68275-9_11.

Meierhoff, K. and Westhoff, P., 1993. Differential biogenesis of photosystem II in mesophyll and bundle-sheath cells of monocotyledonous NADP-malic enzyme-type C_4 plants: the non-stoichiometric abundance of the subunits of photosystem II in the bundle-sheath chloroplasts and the translational activity of the plastome-encoded genes. *Planta* [Online], 191(1), pp.23–33. Available from: https://doi.org/10.1007/BF00240892.

Mohammadi, M., Xavier, A., Beckett, T., Beyer, S., Chen, L., Chikssa, H., Cross, V., Freitas Moreira, F., French, E., Gaire, R., Griebel, S., Lopez, M.A., Prather, S., Russell, B., and Wang, W., 2020. Identification, deployment, and transferability of quantitative trait loci from genome-wide association studies in plants. *Current plant biology* [Online], 24, p.100145. Available from: https://doi.org/10.1016/j.cpb.2020.100145.

Monier, B., Casstevens, T.M., Bradbury, P.J., and Buckler, E.S., 2022. rTASSEL: An R interface to TASSEL for analyzing genomic diversity. *Journal of open source software* [Online], 7(76), p.4530. Available from: https://doi.org/10.21105/joss.04530.

Mook, W., Bommerson, J., and Staverman, W., 1974. Carbon isotope fractionation between dissolved bicarbonate and gaseous carbon dioxide. *Earth and planetary science letters* [Online], 22(2), pp.169–176. Available from: https://doi.org/10.1016/0012-821X(74)90078-8.

Morales, A. and Kaiser, E., 2020. Photosynthetic acclimation to fluctuating irradiance in plants. *Frontiers in plant science* [Online], 11. Available from: https://doi.org/10.3389/fpls.2020.00268.

Moussa, H.R. and Abdel-Aziz, S.M., 2008. Comparative response of drought tolerant and drought sensitive maize genotypes to water stress. *Australian journal of crop science* [Online], 1(1), pp.31–36. Available from: https://www.cabdirect.org/cabdirect/abstract/20083194806.

Müller-Moulé, P., Conklin, P.L., and Niyogi, K.K., 2002. Ascorbate deficiency can limit violaxanthin de-epoxidase activity in vivo. *Plant physiology* [Online], 128(3), pp.970–977. Available from: https://doi.org/10.1104/pp.010924.

Mundia, C.W., Secchi, S., Akamani, K., and Wang, G., 2019. A regional comparison of factors affecting global sorghum production: The case of North America, Asia and Africa's Sahel. *Sustainability* [Online], 11(7), p.2135. Available from: https://doi.org/10.3390/su11072135.

Munné-Bosch, S., 2005. The role of a-tocopherol in plant stress tolerance. *Journal of plant physiology* [Online], 162(7), pp.743–748. Available from: https://doi.org/https://doi.org/10.1016/j.jplph.2005.04.022.

Murata, N., Takahashi, S., Nishiyama, Y., and Allakhverdiev, S.I., 2007. Photoinhibition of photosystem II under environmental stress. *Biochimica et biophysica acta (bba) - bioenergetics* [Online], 1767(6), pp.414–421. Available from: https://doi.org/10.1016/j.bbabio.2006.11.019.

Murchie, E.H., Pinto, M., and Horton, P., 2009. Agriculture and the new challenges for photosynthesis research. *New phytologist* [Online], 181(3), pp.532–552. Available from: https://doi.org/10.1111/j.1469-8137.2008.02705.x.

Murchie, E.H. and Burgess, A.J., 2022. Casting light on the architecture of crop yield. *Crop and environment* [Online], 1(1), pp.74–85. Available from: https://doi.org/10.1016/j.crope.2022.03.009.

Murchie, E.H. and Ruban, A.V., 2020. Dynamic non-photochemical quenching in plants: from molecular mechanism to productivity. *The Plant Journal* [Online], 101(4), pp.885–896. Available from: https://doi.org/10.1111/tpj.14601.

Nagy, Z., Tuba, Z., Zsoldos, F., and Erdei, L., 1995. CO_2-exchange and water relation responses of sorghum and maize during water and salt stress. *Journal of plant physiology* [Online], 145(4), pp.539–544. Available from: https://doi.org/10.1016/S0176-1617(11)81785-2.

Natukunda, M.I., Mantilla-Perez, M.B., Graham, M.A., Liu, P., and Salas-Fernandez, M.G., 2022. Dissection of canopy layer-specific genetic control of leaf angle in sorghum bicolor by rna sequencing. *Bmc genomics* [Online], 23(1), p.95. Available from: https://doi.org/10.1186/s12864-021-08251-4.

Ng, P.C. and Henikoff, S., 2003. SIFT: predicting amino acid changes that affect protein function. *Nucleic acids research* [Online], 31(13), pp.3812–3814. Available from: https://doi.org/10.1093/nar/gkg509.

Nguyen, C.T., Singh, V., van Oosterom, E.J., Chapman, S.C., Jordan, D.R., and Hammer, G.L., 2013. Genetic variability in high temperature effects on seed-set in sorghum. *Functional plant biology* [Online], 40(5), pp.439–448. Available from: https://doi.org/10.1071/FP12264.

Nicol, L., Nawrocki, W.J., and Croce, R., 2019. Disentangling the sites of non-photochemical quenching in vascular plants. *Nature plants* [Online], 5(11), pp.1177–1183. Available from: https://doi.org/10.1038/s41477-019-0526-5.

Nilkens, M., Kress, E., Lambrev, P., Miloslavina, Y., Müller, M., Holzwarth, A.R., and Jahns, P., 2010. Identification of a slowly inducible zeaxanthin-dependent component of non-photochemical quenching of chlorophyll fluorescence generated under steady-state conditions in arabidopsis. *Biochimica et biophysica acta (bba) - bioenergetics* [Online], 1797(4), pp.466–475. Available from: https://doi.org/https://doi.org/10.1016/j.bbabio.2010.01.001.

Nishiyama, Y., Allakhverdiev, S.I., and Murata, N., 2011. Protein synthesis is the primary target of reactive oxygen species in the photoinhibition of photosystem ii. *Physiologia plantarum* [Online], 142(1), pp.35–46. Available from: https://doi.org/https://doi.org/10.1111/j.1399-3054.2011.01457.x.

Office of the Gene Technology Regulator, 2017. *The biology of sorghum bicolor (l.) moench subsp. bicolor (sorghum)*. Australian Government Department of Health.

Ögren, E. and Evans, J.R., 1993. Photosynthetic light-response curves. *Planta* [Online], 189(2), pp.182–190. Available from: https://doi.org/10.1007/BF00195075.

Ohnishi, N., Allakhverdiev, S.I., Takahashi, S., Higashi, S., Watanabe, M., Nishiyama, Y., and Murata, N., 2005. Two-step mechanism of photodamage to photosystem II: Step 1 occurs at the oxygen-evolving complex and step 2 occurs at the photochemical reaction center. *Biochemistry* [Online], 44(23), pp.8494–8499. Available from: https://doi.org/10.1021/bi047518q.

Oquist, G., Samuelsson, G., and Bishop, N.I., 1980. On the role of ß-carotene in the reaction center chlorophyll a antennae of photosystem i. *Physiologia plantarum* [Online], 50(1), pp.63–70. Available from: https://doi.org/10.1111/j.1399-3054.1980.tb02685.x.

Ort, D.R. and Yocum, C.F., 1996. *Oxygenic photosynthesis: the light reactions*. Vol. 4. Springer Science & Business Media.

Ortiz, D., Hu, J., and Salas Fernandez, M.G., 2017. Genetic architecture of photosynthesis in *Sorghum bicolor* under non-stress and cold stress conditions. *Journal of experimental botany* [Online], 68(16), pp.4545–4557. Available from: https://doi.org/10.1093/jxb/erx276.

Osman, M.E.-f.M., Dirar, A.I., and Konozy, E.H.E., 2022. Genome-wide screening of lectin putative genes from *Sorghum bicolor* l., distribution in QTLs and a probable implications of lectins in abiotic stress tolerance. *Bmc plant biology* [Online], 22(1), p.397. Available from: https://doi.org/10.1186/s12870-022-03792-6.

Parikh, A., Brant, E.J., Baloglu, M.C., and Altpeter, F., 2021. CRISPR/Cas-mediated genome editing in sorghum — recent progress, challenges and prospects. *In vitro cellular & developmental biology - plant* [Online], 57(4), pp.720–730. Available from: https://doi.org/10.1007/s11627-021-10215-y.

Pearcy, R.W., 1990. Sunflecks and photosynthesis in plant canopies. *Annual review of plant physiology and plant molecular biology* [Online], 41(1), pp.421–53. Available from: https://doi.org/10.1146/annurev.pp.41.060190.002225.

Pendergrass, A.G., Knutti, R., Lehner, F., Deser, C., and Sanderson, B.M., 2017. Precipitation variability increases in a warmer climate. *Scientific reports* [Online], 7(1), p.17966. Available from: https://doi.org/10.1038/s41598-017-17966-y.

Pengelly, J.J.L., Sirault, X.R.R., Tazoe, Y., Evans, J.R., Furbank, R.T., and von Caemmerer, S., 2010. Growth of the C_4 dicot *Flaveria bidentis*: photosynthetic acclimation to low light through shifts in leaf anatomy and biochemistry. *Journal of experimental botany* [Online], 61(14), pp.4109–4122. Available from: https://doi.org/10.1093/jxb/erq226.

Pfündel, E. and Neubohn, B., 1999. Assessing photosystem I and II distribution in leaves from C_4 plants using confocal laser scanning microscopy. *Plant, cell & environment* [Online], 22(12), pp.1569–1577. Available from: https://doi.org/10.1046/j.1365-3040.1999.00521.x.

Pfündel, E., 1998. Estimating the contribution of photosystem I to total leaf chlorophyll fluorescence. *Photosynthesis research* [Online], 56(2), pp.185–195. Available from: https://doi.org/10.1023/A:1006032804606.

Piepho, H.-P. and Möhring, J., 2007. Computing heritability and selection response from unbalanced plant breeding trials. *Genetics* [Online], 177(3), p.1881. Available from: https://doi.org/10.1534/GENETICS.107.074229.

Pignon, C.P., Fernandes, S.B., Valluru, R., Bandillo, N., Lozano, R., Buckler, E., Gore, M.A., Long, S.P., Brown, P.J., and Leakey, A.D.B., 2021. Phenotyping stomatal closure by thermal imaging for GWAS and TWAS of water use efficiency-related genes. *Plant physiology* [Online], 187(4), pp.2544–2562. Available from: https://doi.org/10.1093/plphys/kiab395.

Pignon, C.P., Jaiswal, D., McGrath, J.M., and Long, S.P., 2017. Loss of photosynthetic efficiency in the shade. an achilles heel for the dense modern stands of our most productive C_4 crops? *Journal of experimental botany* [Online], 68(2), pp.335–345. Available from: https://doi.org/10.1093/jxb/erw456.

Pixley, K.V., Falck-Zepeda, J.B., Paarlberg, R.L., Phillips, P.W.B., Slamet-Loedin, I.H., Dhugga, K.S., Campos, H., and Gutterson, N., 2022. Genome-edited crops for improved food security of smallholder farmers. *Nature genetics* [Online], 54(4), pp.364–367. Available from: https://doi.org/10.1038/s41588-022-01046-7.

Plumb, W., Townsend, A.J., Rasool, B., Alomrani, S., Razak, N., Karpinska, B., Ruban, A.V., and Foyer, C.H., 2018. Ascorbate-mediated regulation of growth, photoprotection, and photoinhibition in *Arabidopsis thaliana*. *Journal of experimental botany* [Online], 69(11), pp.2823–2835. Available from: https://doi.org/10.1093/JXB/ERY170.

Porra, R., Thompson, W., and Kriedemann, P., 1989. Determination of accurate extinction coefficients and simultaneous equations for assaying chlorophylls *a* and *b* extracted with four different solvents: verification of the concentration of chlorophyll standards by atomic absorption spectroscopy. *Biochimica et biophysica acta (BBA) - bioenergetics* [Online], 975(3), pp.384–394. Available from: https://doi.org/10.1016/S0005-2728(89)80347-0.

Poudel, P., Naidenov, B., Chen, C., Alderman, P.D., and Welch, S.M., 2023. Integrating genomic prediction and genotype specific parameter estimation in ecophysiological models: overview and perspectives. *In silico plants* [Online], 5(1). Available from: https://doi.org/10.1093/insilicoplants/diad007.

Prášil, I. and Zámečník, J., 1998. The use of a conductivity measurement method for assessing freezing injury: I. Influence of leakage time, segment number, size and shape in a sample on evaluation of the degree of injury. *Environmental and experimental botany* [Online], 40(1), pp.1–10. Available from: https://doi.org/10.1016/S0098-8472(98)00010-0.

Purcell, S., Neale, B., Todd-Brown, K., Thomas, L., Ferreira, M.A., Bender, D., Maller, J., Sklar, P., de Bakker, P.I., Daly, M.J., and Sham, P.C., 2007. PLINK: a tool set for whole-genome association and population-based linkage analyses. *The american journal of human genetics* [Online], 81(3), pp.559–575. Available from: https://doi.org/https://doi.org/10.1086/519795.

Qu, M.N., Bunce, J.A., and Shi, Z.S., 2014. Does elevated CO_2 protect photosynthesis from damage by high temperature via modifying leaf water status in maize seedlings? *Photosynthetica* [Online], 52(2), pp.211–216. Available from: https://doi.org/10.1007/s11099-014-0022-0.

Quero, G., Bonnecarrère, V., Simondi, S., Santos, J., Fernández, S., Gutierrez, L., Garaycochea, S., and Borsani, O., 2021. Genetic architecture of photosynthesis energy partitioning as revealed by a genome-wide association approach. *Photosynthesis research* [Online], 150(1), pp.97–115. Available from: https://doi.org/10.1007/s11120-020-00721-2.

R Core Team, 2022. *R: A language and environment for statistical computing* [Online]. Vienna, Austria: R Foundation for Statistical Computing. Available from: https://www.R-project.org/.

Rahman, S., Anik, A.R., and Sarker, J.R., 2022. Climate, environment and socio-economic drivers of global agricultural productivity growth. *Land* [Online], 11(4). Available from: https://doi.org/10.3390/land11040512.

Ray, D.K., Mueller, N.D., West, P.C., and Foley, J.A., 2013. Yield trends are insufficient to double global crop production by 2050. *Plos one* [Online], 8(6), pp.1–8. Available from: https://doi.org/10.1371/journal.pone.0066428.

Rees, D., Young, A., Noctor, G., Britton, G., and Horton, P., 1989. Enhancement of the Δph-dependent dissipation of excitation energy in spinach chloroplasts by light-activation: correlation with the synthesis of zeaxanthin. *Febs letters* [Online], 256(1), pp.85–90. Available from: https://doi.org/https://doi.org/10.1016/0014-5793(89)81723-5.

Revelle, W., 2022. *psych: Procedures for Psychological, Psychometric, and Personality Research* [Online]. R package version 2.2.9. Evanston, Illinois: Northwestern University. Available from: https://CRAN.R-project.org/package=psych.

Rezwani, M., Pourfathollah, A.A., and Noorbakhsh, F., 2022. rbioapi: user-friendly r interface to biologic web services' api. *Bioinformatics* [Online], 38(10), pp.2952–2953. Available from: https://doi.org/10.1093/bioinformatics/btac172.

Ridley, S.M., 1977. Interaction of chloroplasts with inhibitors: induction of chlorosis by diuron during prolonged illumination in vitro. *Plant physiology* [Online], 59(4), pp.724–732. Available from: https://doi.org/10.1104/pp.59.4.724.

Ritchie, R.J., 2006. Consistent sets of spectrophotometric chlorophyll equations for acetone, methanol and ethanol solvents. *Photosynthesis research* [Online], 89(1), pp.27–41. Available from: https://doi.org/10.1007/s11120-006-9065-9.

Robinson, D., Bryan, J., and Elias, J., 2015. *Fuzzyjoin: join tables together on inexact matching* [Online]. R package version 0.1.6. Available from: https://cran.r-project.org/web/packages/fuzzyjoin/index.html.

Rodrigues Castro, F.M., Bruzi, A.T., Rodrigues Nunes, J.A., Costa Parrella, R.A., Romeiro Lombardi, G.M., Brant Albuquerque, C.J., and Lopes, M., 2015. Agronomic and energetic potential of biomass sorghum genotypes. *American journal of plant sciences* [Online], (6), pp.1862–1873. Available from: https://doi.org/10.4236/ajps.2015.611187.

Roeske, C. and O'Leary, M.H., 1984. Carbon isotope effects on the enzyme-catalyzed carboxylation of ribulose bisphosphate. *Biochemistry*, 23, pp.6275–6284.

Rolny, N., Costa, L., Carrión, C., and Guiamet, J.J., 2011. Is the electrolyte leakage assay an unequivocal test of membrane deterioration during leaf senescence? *Plant physiology and biochemistry* [Online], 49(10), pp.1220–1227. Available from: https://doi.org/10.1016/j.plaphy.2011.06.010.

Romanowska, E., Buczyńska, A., Wasilewska, W., Krupnik, T., Drożak, A., Rogowski, P., Parys, E., and Zienkiewicz, M., 2017. Differences in photosynthetic responses of NADP-ME type C_4 species to high light. *Planta* [Online], 245(3), pp.641–657. Available from: https://doi.org/10.1007/s00425-016-2632-1.

Romanowska, E., Drożak, A., Pokorska, B., Shiell, B.J., and Michalski, W.P., 2006. Organization and activity of photosystems in the mesophyll and bundle sheath chloroplasts of maize. *Journal of plant physiology* [Online], 163(6), pp.607–618. Available from: https://doi.org/https://doi.org/10.1016/j.jplph.2005.06.007.

Rosenzweig, C., Elliott, J., Deryng, D., Ruane, A.C., Müller, C., Arneth, A., Boote, K.J., Folberth, C., Glotter, M., Khabarov, N., Neumann, K., Piontek, F., Pugh, T.A.M., Schmid, E., Stehfest, E., Yang, H., and Jones, J.W., 2014. Assessing agricultural risks of climate change in the 21st century in a global gridded crop model intercomparison. *Proceedings of the national academy of sciences* [Online], 111(9), pp.3268–3273. Available from: https://doi.org/10.1073/pnas.1222463110.

Rouhier, N., Lemaire, S.D., and Jacquot, J.-P., 2008. The role of glutathione in photosynthetic organisms: emerging functions for glutaredoxins and glutathionylation. *Annual review of plant biology* [Online], 59(1), pp.143–166. Available from: https://doi.org/10.1146/annurev.arplant.59.032607.092811.

Ruban, A.V., 2017. Crops on the fast track for light. *Nature* [Online], 541(7635), pp.36–37. Available from: https://doi.org/10.1038/541036a.

Ruban, A.V. and Murchie, E.H., 2012. Assessing the photoprotective effectiveness of non-photochemical chlorophyll fluorescence quenching: A new approach. *Biochimica et biophysica acta - bioenergetics* [Online], 1817(7), pp.977–982. Available from: https://doi.org/10.1016/j.bbabio.2012.03.026.

Ruban, A.V. and Wilson, S., 2021. The mechanism of non-photochemical quenching in plants: Localization and driving forces. *Plant and cell physiology* [Online], 62(7), pp.1063–1072. Available from: https://doi.org/10.1093/PCP/PCAA155.

Rungrat, T., Almonte, A.A., Cheng, R., Gollan, P.J., Stuart, T., Aro, E.-M., Borevitz, J.O., Pogson, B., and Wilson, P.B., 2019. A genome-wide association study of non-photochemical quenching in response to local seasonal climates in arabidopsis thaliana. *Plant direct* [Online], 3(5), e00138. Available from: https://doi.org/10.1002/pld3.138.

Ryu, C., 2021. *Dlookr: Tools for data diagnosis, exploration, transformation* [Online]. R package version 0.5.1. Available from: https://CRAN.R-project.org/package=dlookr.

Sage, R.F., 2014. Photosynthetic efficiency and carbon concentration in terrestrial plants: the C_4 and cam solutions. *Journal of experimental botany* [Online], 65(13), pp.3323–3325. eprint: https://academic.oup.com/jxb/article-pdf/65/13/3323/9569865/eru262.pdf. Available from: https://doi.org/10.1093/jxb/eru262.

Sage, R.F. and McKown, A.D., 2005. Is C_4 photosynthesis less phenotypically plastic than C_3 photosynthesis? *Journal of experimental botany* [Online], 57(2), pp.303–317. eprint: https://academic.oup.com/jxb/article-pdf/57/2/303/1323718/erj040.pdf. Available from: https://doi.org/10.1093/jxb/erj040.

Sahay, S., Grzybowski, M., Schnable, J.C., and Głowacka, K., 2023. Genetic control of photoprotection and photosystem II operating efficiency in plants. *New phytologist* [Online]. Available from: https://doi.org/10.1111/nph.18980.

Salas Fernandez, M.G., Strand, K., Hamblin, M.T., Westgate, M., Heaton, E., and Kresovich, S., 2015. Genetic analysis and phenotypic characterization of leaf photosynthetic capacity in a sorghum (*Sorghum* spp.) diversity panel. *Genetic resources and crop evolution* [Online], 62(6), pp.939–950. Available from: https://doi.org/10.1007/s10722-014-0202-6.

Sales, C.R., Ribeiro, R.V., Marchiori, P.E., Kromdijk, J., and Machado, E.C., 2023. The negative impact of shade on photosynthetic efficiency in sugarcane may reflect a metabolic bottleneck. *Environmental and experimental botany* [Online], 211, p.105351. Available from: https://doi.org/10.1016/j.envexpbot.2023.105351.

Sanchez-Bragado, R., Vicente, R., Molero, G., Serret, M.D., Maydup, M.L., and Araus, J.L., 2020. New avenues for increasing yield and stability in c3 cereals: exploring ear photosynthesis. *Current opinion in plant biology* [Online], 56. Biotic interactions AGRI 2019, pp.223–234. Available from: https://doi.org/https://doi.org/10.1016/j.pbi.2020.01.001.

Sandmann, G., 2019. Antioxidant protection from UV- and light-stress related to carotenoid structures. *Antioxidants 2019, vol. 8, page 219* [Online], 8(7), p.219. Available from: https://doi.org/10.3390/ANTIOX8070219.

Sarvikas, P., Hakala, M., Pätsikkä, E., Tyystjärvi, T., and Tyystjärvi, E., 2006. Action spectrum of photoinhibition in leaves of wild type and *npq1-2* and *npq4-1* mutants of *Arabidopsis thaliana*. *Plant and cell physiology* [Online], 47(3), pp.391–400. Available from: https://doi.org/10.1093/PCP/PCJ006.

Schindelin, J., Arganda-Carreras, I., Frise, E., Kaynig, V., Longair, M., Pietzsch, T., Preibisch, S., Rueden, C., Saalfeld, S., Schmid, B., Tinevez, J.-Y., White, D.J., Hartenstein, V., Eliceiri, K., Tomancak, P., and Cardona, A., 2012. Fiji: an open-source platform for biological-image analysis. *Nature methods* [Online], 9(7), pp.676–682. Available from: https://doi.org/10.1038/nmeth.2019.

Schmid-Siegert, E., Stepushenko, O., Glauser, G., and Farmer, E.E., 2016. Membranes as structural antioxidants: Recycling of malondialdehyde to its source in oxidation-sensitive chloroplast fatty acids. *Journal of biological chemistry* [Online], 291(25), pp.13005–13013. Available from: https://doi.org/10.1074/jbc.M116.729921.

Schnable, J.C. and Freeling, M., 2011. Genes identified by visible mutant phenotypes show increased bias toward one of two subgenomes of maize. *Plos one* [Online], 6(3), pp.1–6. Available from: https://doi.org/10.1371/journal.pone.0017855.

Shahhosseini, M., Hu, G., Huber, I., and Archontoulis, S.V., 2021. Coupling machine learning and crop modeling improves crop yield prediction in the us corn belt. *Scientific reports* [Online], 11(1), p.1606. Available from: https://doi.org/10.1038/s41598-020-80820-1.

Sharma, P., Jha, A.B., Dubey, R.S., and Pessarakli, M., 2012. Reactive oxygen species, oxidative damage, and antioxidative defense mechanism in plants under stressful conditions. *Journal of botany* [Online], 2012, pp.1–26. Available from: https://doi.org/10.1155/2012/217037.

Silva, T.N., Thomas, J.B., Dahlberg, J., Rhee, S.Y., and Mortimer, J.C., 2021. Progress and challenges in sorghum biotechnology, a multipurpose feedstock for the bioeconomy. *Journal of experimental botany* [Online]. Available from: https://doi.org/10.1093/JXB/ERAB450.

Singh, B. and Singh, D., 1995. Agronomic and physiological responses of sorghum, maize and pearl millet to irrigation. *Field crops research* [Online], 42(2), pp.57–67. Available from: https://doi.org/10.1016/0378-4290(95)00025-L.

Slattery, R.A., Walker, B.J., Weber, A.P.M., and Ort, D.R., 2018. The impacts of fluctuating light on crop performance. *Plant physiology* [Online], 176(2), pp.990–1003. Available from: https://doi.org/10.1104/pp.17.01234.

Sonawane, B.V., Sharwood, R.E., von Caemmerer, S., Whitney, S.M., and Ghannoum, O., 2017. Short-term thermal photosynthetic responses of C_4 grasses are independent of the biochemical subtype. *Journal of experimental botany* [Online], 68(20), pp.5583–5597. Available from: https://doi.org/10.1093/jxb/erx350.

Springer, N.M. and Schmitz, R.J., 2017. Exploiting induced and natural epigenetic variation for crop improvement. *Nature reviews genetics* [Online], 18(9), pp.563–575. Available from: https://doi.org/10.1038/nrg.2017.45.

Stefanov, M.A., Rashkov, G.D., Yotsova, E.K., Borisova, P.B., Dobrikova, A.G., and Apostolova, E.L., 2021. Different sensitivity levels of the photosynthetic apparatus in *Zea mays* L. and *Sorghum bicolor* L. under salt stress. *Plants* [Online], 10(7). Available from: https://doi.org/10.3390/plants10071469.

Stefanowicz, K., Lannoo, N., Proost, P., and Van Damme, E.J., 2012. Arabidopsis f-box protein containing a nictaba-related lectin domain interacts with n-acetyllactosamine structures. *Febs open bio* [Online], 2, pp.151–158. Available from: https://doi.org/https://doi.org/10.1016/j.fob.2012.06.002.

Stegle, O., Parts, L., Piipari, M., Winn, J., and Durbin, R., 2012. Using probabilistic estimation of expression residuals (PEER) to obtain increased power and interpretability of gene expression analyses. *Nature protocols* [Online], 7(3), pp.500–507. Available from: https://doi.org/10.1038/nprot.2011.457.

Stinziano, J.R., Roback, C., Gamble, D., Murphy, B., Hudson, P., and Muir, C.D., 2020. *Photosynthesis: tools for plant ecophysiology & modeling* [Online]. R package version 2.0.1. Available from: https://CRAN.R-project.org/package=photosynthesis.

Stitt, M. and Zhu, X.G., 2014. The large pools of metabolites involved in intercellular metabolite shuttles in C_4 photosynthesis provide enormous flexibility and robustness in a fluctuating light environment. *Plant, cell & environment* [Online], 37(9), pp.1985–1988. Available from: https://doi.org/10.1111/pce.12290.

Stone, K., Ksebati, M.B., and Marnett, L.J., 1990. Investigation of the adducts formed by reaction of malondialdehyde with adenosine. *Chemical research in toxicology* [Online], 3(1), pp.33–38. Available from: https://doi.org/10.1021/tx00013a006.

Strasser, R., 2022. Recent developments in deciphering the biological role of plant complex n-glycans. *Frontiers in plant science* [Online], 13. Available from: https://doi.org/10.3389/fpls.2022.897549.

Strasser, R., Schoberer, J., Jin, C., Glössl, J., Mach, L., and Steinkellner, H., 2006. Molecular cloning and characterization of arabidopsis thaliana golgi -mannosidase ii, a key enzyme in the formation of complex n-glycans in plants. *The plant journal* [Online], 45(5), pp.789–803. Available from: https://doi.org/https://doi.org/10.1111/j.1365-313X.2005.02648.x.

Tack, J., Lingenfelser, J., and Jagadish, S.K., 2017. Disaggregating sorghum yield reductions under warming scenarios exposes narrow genetic diversity in us breeding programs. *Proceedings of the national academy of sciences* [Online], 114(35), pp.9296–9301. Available from: https://doi.org/10.1073/pnas.1706383114.

Takagi, D., Amako, K., Hashiguchi, M., Fukaki, H., Ishizaki, K., Goh, T., Fukao, Y., Sano, R., Kurata, T., Demura, T., Sawa, S., and Miyake, C., 2017. Chloroplastic ATP synthase builds up a proton motive force preventing production of reactive oxygen species in photosystem I. *The plant journal* [Online], 91(2), pp.306–324. Available from: https://doi.org/10.1111/tpj.13566.

Takagi, D., Takumi, S., Hashiguchi, M., Sejima, T., and Miyake, C., 2016. Superoxide and singlet oxygen produced within the thylakoid membranes both cause photosystem I photoinhibition. *Plant physiology* [Online], 171(3), pp.1626–1634. Available from: https://doi.org/10.1104/pp.16.00246.

Talbott, L.D., Shmayevich, I.J., Chung, Y., Hammad, J.W., and Zeiger, E., 2003. Blue light and phytochrome-mediated stomatal opening in the npq1 and phot1 phot2 mutants of arabidopsis. *Plant physiology* [Online], 133(4), pp.1522–1529. Available from: https://doi.org/10.1104/pp.103.029587.

Tam, V., Patel, N., Turcotte, M., Bossé, Y., Paré, G., and Meyre, D., 2019. Benefits and limitations of genome-wide association studies. *Nature reviews genetics* [Online], 20(8), pp.467–484. Available from: https://doi.org/10.1038/s41576-019-0127-1.

Tazoe, Y., Hanba, Y.T., Furumoto, T., Noguchi, K., and Terashima, I., 2008. Relationships between quantum yield for CO_2 assimilation, activity of key enzymes and CO_2 leakiness in amaranthus cruentus, a C_4 dicot, grown in high or low light. *Plant and cell physiology* [Online], 49(1), pp.19–29. Available from: https://doi.org/10.1093/pcp/pcm160.

Thula, S., Moturu, T.R., Salava, H., Balakhonova, V., Berka, M., Kerchev, P., Mishra, K.B., Nodzynski, T., and Simon, S., 2022. Strigolactones stimulate high light stress adaptation by modulating photosynthesis rate in arabidopsis. *Journal of plant growth regulation* [Online]. Available from: https://doi.org/10.1007/s00344-022-10764-5.

Tibbs Cortes, L., Zhang, Z., and Yu, J., 2021. Status and prospects of genome-wide association studies in plants. *The plant genome* [Online], 14(1), e20077. Available from: https://doi.org/10.1002/tpg2.20077.

Travassos-Lins, J., de Oliveira Rocha, C.C., de Souza Rodrigues, T., and Alves-Ferreira, M., 2021. Evaluation of the molecular and physiological response to dehydration of two accessions of the model plant *Setaria viridis*. *Plant physiology and biochemistry* [Online], 169, pp.211–223. Available from: https://doi.org/10.1016/j.plaphy.2021.11.015.

Trebst, A., Depka, B., and Holländer-Czytko, H., 2002. A specific role for tocopherol and of chemical singlet oxygen quenchers in the maintenance of photosystem II structure and function in *Chlamydomonas reinhardtii*. *Febs letters* [Online], 516(1-3), pp.156–160. Available from: https://doi.org/10.1016/S0014-5793(02)02526-7.

Ubierna, N., Sun, W., Kramer, D.M., and Cousins, A.B., 2013. The efficiency of C_4 photosynthesis under low light conditions in *Zea mays*, *Miscanthus x giganteus* and *Flaveria bidentis*. *Plant, cell & environment* [Online], 36(2), pp.365–381. Available from: https://doi.org/https://doi.org/10.1111/j.1365-3040.2012.02579.x.

UN Department of Economic and Social Affairs, 2019. *World population prospects 2019, online edition* [Online]. (technical report Rev. 1). United Nations. Available from: https://population.un.org/wpp/Download/Standard/Population/.

Valluru, R., Gazave, E.E., Fernandes, S.B., Ferguson, J.N., Lozano, R., Hirannaiah, P., Zuo, T., Brown, P.J., Leakey, A.D.B., Gore, M.A., Buckler, E.S., and Bandillo, N., 2019. Deleterious mutation burden and its association with complex traits in sorghum (*Sorghum bicolor*). *Genetics* [Online], 211(3), pp.1075–1087. Available from: https://doi.org/10.1534/GENETICS.118.301742.

Van Hove, J., De Jaeger, G., De Winne, N., Guisez, Y., and Van Damme, E.J., 2015. The arabidopsis lectin euls3 is involved in stomatal closure. *Plant science* [Online], 238, pp.312–322. Available from: https://doi.org/10.1016/j.plantsci.2015.07.005.

Van Bezouw, R.F.H.M., Keurentjes, J.J.B., Harbinson, J., and Aarts, M.G.M., 2019. Converging phenomics and genomics to study natural variation in plant photosynthetic efficiency. *The plant journal* [Online], 97(1), pp.112–133. Available from: https://doi.org/10.1111/tpj.14190.

Van Rooijen, R., Kruijer, W., Boesten, R., van Eeuwijk, F.A., Harbinson, J., and Aarts, M.G.M., 2017. Natural variation of YELLOW SEEDLING1 affects photosynthetic acclimation of *Arabidopsis thaliana*. *Nature communications* [Online], 8(1), p.1421. Available from: https://doi.org/10.1038/s41467-017-01576-3.

Vass, I., 2012. Molecular mechanisms of photodamage in the photosystem ii complex. *Biochimica et biophysica acta (bba) - bioenergetics* [Online], 1817(1). Photosystem II, pp.209–217. Available from: https://doi.org/10.1016/j.bbabio.2011.04.014.

Velitchkova, M. and Picorel, R., 2004. Photobleaching of photosynthetic pigments in spinach thylakoid membranes. Effect of temperature, oxygen and DCMU. *Biophysical chemistry* [Online], 107(1), pp.25–32. Available from: https://doi.org/10.1016/S0301-4622(03)00217-5.

Vialet-Chabrand, S., Matthews, J.S.A., and Lawson, T., 2021. Light, power, action! interaction of respiratory energy- and blue light-induced stomatal movements. *New phytologist* [Online], 231(6), pp.2231–2246. Available from: https://doi.org/10.1111/nph.17538.

Vicentini, A., Barber, J.C., Aliscioni, S.S., Giussani, L.M., and Kellogg, E.A., 2008. The age of the grasses and clusters of origins of C_4 photosynthesis. *Global change biology* [Online], 14(12), pp.2963–2977. Available from: https://doi.org/10.1111/j.1365-2486.2008.01688.x.

Visarada, K. and Aruna, C., 2019. Sorghum: a bundle of opportunities in the 21st century. In: C. Aruna, K. Visarada, B.V. Bhat, and V.A. Tonapi, eds. *Breeding sorghum for diverse end uses* [Online], Woodhead publishing series in food science, technology and nutrition. Woodhead Publishing, pp.1–14. Available from: https://doi.org/doi.org/10.1016/B978-0-08-101879-8.00001-2.

Von Caemmerer, S. and Furbank, R.T., 1999. Modeling c4 photosynthesis. *C4 plant biology*, pp.173–211.

Von Caemmerer, S., 2000. *Biochemical models of leaf photosynthesis* [Online]. CSIRO Publishing, p.176. Available from: https://doi.org/10.1071/9780643103405.

Von Caemmerer, S., Evans, J.R., Hudson, G.S., and Andrews, T.J., 1994. The kinetics of ribulose-1,5-bisphosphate carboxylase/oxygenase in vivo inferred from measurements of photosynthesis in leaves of transgenic tobacco. *Planta* [Online], 195(1), pp.88–97. Available from: https://doi.org/10.1007/BF00206296.

Walter, J. and Kromdijk, J., 2021. Here comes the sun: How optimization of photosynthetic light reactions can boost crop yields. *Journal of integrative plant biology* [Online]. Available from: https://doi.org/10.1111/jipb.13206.

Walters, R.G., Ruban, A.V., and Horton, P., 1994. Higher plant light-harvesting complexes LHCIIa and LHCIIc are bound by dicyclohexylcarbodiimide during inhibition of energy dissipation. *European journal of biochemistry* [Online], 226(3), pp.1063–1069. Available from: https://doi.org/https://doi.org/10.1111/j.1432-1033.1994.01063.x.

Wang, K., Riaz, B., and Ye, X., 2018. Wheat genome editing expedited by efficient transformation techniques: progress and perspectives. *The crop journal* [Online], 6(1). Wheat Functional Genomics in China, pp.22–31. Available from: https://doi.org/10.1016/j.cj.2017.09.009.

Wang, N., Fang, W., Han, H., Sui, N., Li, B., and Meng, Q.-W., 2008. Overexpression of zeaxanthin epoxidase gene enhances the sensitivity of tomato PSII photoinhibition to high light and chilling stress. *Physiologia plantarum* [Online], 132(3), pp.384–396. Available from: https://doi.org/10.1111/j.1399-3054.2007.01016.x.

Wang, Q., Zhao, H., Jiang, J., Xu, J., Xie, W., Fu, X., Liu, C., He, Y., and Wang, G., 2017. Genetic architecture of natural variation in rice nonphotochemical quenching capacity revealed by genome-wide association study. *Frontiers in plant science* [Online], 8. Available from: https://doi.org/10.3389/fpls.2017.01773.

Wang, Y., Stutz, S.S., Bernacchi, C.J., Boyd, R.A., Ort, D.R., and Long, S.P., 2022. Increased bundle-sheath leakiness of CO_2 during photosynthetic induction shows a lack of coordination between the C_4 and C_3 cycles. *New phytologist* [Online], 236(5), pp.1661–1675. Available from: https://doi.org/10.1111/nph.18485.

Warren, G., McKown, R., Marin, A.L., and Teutonico, R., 1996. Isolation of mutations affecting the development of freezing tolerance in *Arabidopsis thaliana* (L.) Heynh. *Plant physiology* [Online], 111(4), pp.1011–9. Available from: https://doi.org/10.1104/pp.111.4.1011.

Wei, T. and Simko, V., 2021. *R package 'corrplot': Visualization of a Correlation Matrix* [Online]. (Version 0.92). Available from: https://github.com/taiyun/corrplot.

Wei, Y., Liu, S., Xiong, D., Xiong, Z., Zhang, Z., Wang, F., and Huang, J., 2022. Genome-wide association study for non-photochemical quenching traits in *Oryza sativa* l. *Agronomy* [Online], 12(12). Available from: https://doi.org/10.3390/agronomy12123216.

Whippo, C.W. and Hangarter, R.P., 2006. Phototropism: bending towards enlightenment. *The plant cell* [Online], 18(5), pp.1110–1119. Available from: https://doi.org/10.1105/tpc.105.039669.

Witt, H.T., Müller, A., and Rumberg, B., 1963. Electron-Transport System in Photosynthesis of Green Plants Analysed by Sensitive Flash Photometry. *Nature* [Online], 197(4871), pp.987–991. Available from: https://doi.org/10.1038/197987a0.

Wraight, C.A. and Crofts, A.R., 1970. Energy-dependent quenching of chlorophyll a fluorescence in isolated chloroplasts. *European journal of biochemistry* [Online], 17(2), pp.319–327. Available from: https://doi.org/https://doi.org/10.1111/j.1432-1033.1970.tb01169.x.

Yamada, M., Kawasaki, M., Sugiyama, T., Miyake, H., and Taniguchi, M., 2009. Differential positioning of C_4 mesophyll and bundle sheath chloroplasts: Aggregative movement of C_4 mesophyll chloroplasts in response to environmental stresses. *Plant and cell physiology* [Online], 50(10), pp.1736–1749. Available from: https://doi.org/10.1093/pcp/pcp116.

Yamamoto, H., Cheuk, A., Shearman, J., Nixon, P.J., Meier, T., and Shikanai, T., 2023. Impact of engineering the atp synthase rotor ring on photosynthesis in tobacco chloroplasts. *Plant physiology* [Online], 192(2), pp.1221–1233. Available from: https://doi.org/10.1093/plphys/kiad043.

Yamauchi, R. and Matsushita, S., 1979. Light-induced lipid peroxidation in isolated chloroplasts and role of a-tocopherol. *Agricultural and biological chemistry* [Online], 43(10), pp.2157–2161. Available from: https://doi.org/10.1271/bbb1961.43.2157.

Yamori, W., Kusumi, K., Iba, K., and Terashima, I., 2020. Increased stomatal conductance induces rapid changes to photosynthetic rate in response to naturally fluctuating light conditions in rice. *Plant, cell & environment* [Online], 43(5), pp.1230–1240. Available from: https://doi.org/10.1111/pce.13725.

Yamori, W., Makino, A., and Shikanai, T., 2016. A physiological role of cyclic electron transport around photosystem I in sustaining photosynthesis under fluctuating light in rice. *Scientific reports* [Online], 6(1), p.20147. Available from: https://doi.org/10.1038/srep20147.

Yamori, W., Masumoto, C., Fukayama, H., and Makino, A., 2012. Rubisco activase is a key regulator of non-steady-state photosynthesis at any leaf temperature and, to a lesser extent, of steady-state photosynthesis at high temperature. *Plant journal* [Online], 71(6), pp.871–880. Available from: https://doi.org/10.1111/j.1365-313X.2012.05041.x.

Yan, J., Tsuichihara, N., Etoh, T., and Iwai, S., 2007. Reactive oxygen species and nitric oxide are involved in ABA inhibition of stomatal opening. *Plant, cell & environment* [Online], 30(10), pp.1320–1325. Available from: https://doi.org/10.1111/j.1365-3040.2007.01711.x.

Yang, Y.-J., Ding, X.-X., and Huang, W., 2019. Stimulation of cyclic electron flow around photosystem i upon a sudden transition from low to high light in two angiosperms *Arabidopsis thaliana* and *Bletilla striata*. *Plant science* [Online], 287, p.110166. Available from: https://doi.org/10.1016/j.plantsci.2019.110166.

Yang, Y., Zhu, X., Cui, R., Wang, R., Li, H., Wang, J., Chen, H., and Zhang, D., 2021. Identification of soybean phosphorous efficiency QTLs and genes using chlorophyll fluorescence parameters through GWAS and RNA-seq. *Planta* [Online], 254(6), p.110. Available from: https://doi.org/10.1007/s00425-021-03760-8.

Yin, X. and Struik, P.C., 2009. Theoretical reconsiderations when estimating the mesophyll conductance to CO_2 diffusion in leaves of C_3 plants by analysis of combined gas exchange and chlorophyll fluorescence measurements. *Plant, cell & environment* [Online], 32(11), pp.1513–1524. Available from: https://doi.org/10.1111/j.1365-3040.2009.02016.x.

Yin, X., Sun, Z., Struik, P.C., Van Der Putten, P.E.L., Van Iiperen, W., and Harbinson, J., 2011. Using a biochemical C_4 photosynthesis model and combined gas exchange and chlorophyll fluorescence measurements to estimate bundle-sheath conductance of maize leaves differing in age and nitrogen content. *Plant, cell & environment* [Online], 34(12), pp.2183–2199. Available from: https://doi.org/10.1111/j.1365-3040.2011.02414.x.

Zabalza, A., van Dongen, J.T., Froehlich, A., Oliver, S.N., Faix, B., Gupta, K.J., Schmälzlin, E., Igal, M., Orcaray, L., Royuela, M., and Geigenberger, P., 2008. Regulation of respiration and fermentation to control the plant internal oxygen concentration. *Plant physiology* [Online], 149(2), pp.1087–1098. Available from: https://doi.org/10.1104/pp.108.129288.

Zhang, W., Dai, X., Wang, Q., Xu, S., and Zhao, P.X., 2016. Pepis: a pipeline for estimating epistatic effects in quantitative trait locus mapping and genome-wide association studies. *Plos computational biology* [Online], 12(5), pp.1–16. Available from: https://doi.org/10.1371/journal.pcbi.1004925.

Zheng, X., Levine, D., Shen, J., Gogarten, S.M., Laurie, C., and Weir, B.S., 2012. A high-performance computing toolset for relatedness and principal component analysis of snp data. *Bioinformatics* [Online], 28(24), pp.3326–3328. Available from: https://doi.org/10.1093/bioinformatics/bts606.

Zhou, X. and Stephens, M., 2012. Genome-wide efficient mixed-model analysis for association studies. *Nature genetics* [Online], 44(7), pp.821–824. Available from: https://doi.org/10.1038/ng.2310.

Zhu, X.-G., Long, S.P., and Ort, D.R., 2010. Improving photosynthetic efficiency for greater yield. *Annual review of plant biology* [Online], 61(1), pp.235–261. Available from: https://doi.org/10.1146/annurev-arplant-042809-112206.

Zhu, X.-G., Ort, D.R., Whitmarsh, J., and Long, S.P., 2004. The slow reversibility of photosystem II thermal energy dissipation on transfer from high to low light may cause large losses in carbon gain by crop canopies: a theoretical analysis. *Journal of experimental botany* [Online], 55(400), pp.1167–1175. Available from: https://doi.org/10.1093/jxb/erh141.

Zulfugarov, I.S., Wu, G., Tovuu, A., and Lee, C.-H., 2019. Effect of oxygen on the non-photochemical quenching of vascular plants and potential oxygen deficiency in the stroma of PsbS-knock-out rice. *Plant science* [Online], 286, pp.1–6. Available from: https://doi.org/https://doi.org/10.1016/j.plantsci.2019.05.015.